UNIVERSITY OF CATANIA
Faculty of Engineering
Department of Civil and Enviromental Engineering

Doctoral Program in Structural and Geotechnical Engineering
Cycle XXV

PhD Dissertation

Advanced Seismic Design *of* *Innovative Precast Systems* *for* *Structural Response Control*

Giovanni De Francesco

Giuseppe Oliveto
Professor, UniCt Advisor

José I. Restrepo
Professor, UCSD Advisor

Mario Granata
Engineer, S.A.P. Srl

Agesilao Marinetti
Professor, UniCt

Salvatore Porto
Engineer, SICEP Spa

October 27, 2012

For the precious contribution to my growth.

To my Advisors.

La furberia è una qualità italiana
potente, però *ci ha rovinato*...

Roberto Benigni

Abstract

Emerging Design Philosophy In current design philosophy a key concept is *ductility*, a parameter that reflect intrinsic energy dissipation capacity of structural elements. The key concept is the reduction of the structural cost, from the point of view of the initial cost, for design under moderate or important earthquake levels assuming possible damages at structural and non structural elements but ensuring the *Life Safety*. However, when the ductility of the elements is activated damage is introduced. Since, the described philosophy has been introduced, a lot of buildings have been designed and constructed. They have been subjected to various earthquakes and the obtained performances make evident the limits of this design philosophy.

The considered arguments require the development of structural systems able to realize higher structural performances under level of the earthquakes moderate or severe. The most serious obstruction is the increase in cost. If substantial increase in cost is not required, compared with those required in ordinary buildings then, it is rational to design buildings characterized by absence of damage even for very rare earthquakes and a such design will be accepted by the society. Therefore, we should changeover the direction of technology development from cost reduction keeping same performance level to higher performance level without cost increase.

Advanced Seismic Design Methodologies and Procedures The characterization of systems with higher structural performances calls for the introduction of design methodologies able to define the structural response in a more efficient and detailed. In the cost analysis, costs related to Non Structural component and contents (NCs) are usually dominant, especially for buildings with relevant impact for society. The response of NCs must be carefully characterized, and must be taken into account. In particular, the interaction between structural and non structural components must be properly investigated. Evidently, Performance based seismic Design Methodologies largely developed in the research field, are necessary and should be apply, even by practitioners engineers.

In the comparison with Strength Based Seismic Design Procedures, Displacement Based Seismic Design Procedures appear to be more appropriate to better achieved the performance objectives. A displacement Based Seismic Design Procedure via Inelastic Displacement Ratio is highlighted and an analysis of Inelastic Displacement Ratio-key aspect in the mentioned procedure-is developed.

Passive Structural Control The achievement of the prescribed higher performance levels without relevant additional costs makes evident the need to introduce new technologies. Techniques of passive structural control are beginning to be prominently applied and them appear to be useful to reach the previous goal. In both the design of new structures and the retrofit of existing structures, Hysteretic Metallic and Friction Dampers, Linear Viscous and Viscous Elastic Dampers, Non Linear Elastic Dampers, Rocking Systems, Tuned Mass Damper, and Isolation techniques have shown to be an efficient way to improve seismic performances.

Structural Systems for Seismic Response Control In ductile moment-resisting frames many plastic mechanisms are suitable to be developed during seismic events based both on structural system features and on seismic excitation peculiarities. The control of the plastic mechanism of a structural system is very important because it is closely related to the ductility demands for different components of a structures and, consequently, to the energy dissipation capacity. Substantially, Capacity Design procedures are introduced to avoid non-desirable mechanisms.

Taking account the large seismic action variability, systems with a reliable, and convenient, kinematic mechanism-subjected to be activated-are introduced. This is obtained introducing a global kinematic mechanism characterized by a particular deformability and this can be achieved in two ways. In same cases, it is obtained increasing the stiffness, and maybe the strength, of non-desirable mechanisms as, for instance, in the retrofit of structures by hinged walls where, the chosen mechanism is characterized by a constant demand distribution, in terms of inter-story drift, to optimize ductility demand and dissipation capacity. In other cases, it is obtained decreasing the stiffness of a particular mechanism and it is possible for the particular compatibility between mass and stiffness distributions as, for instance, in base isolated structures where the mechanism is the global horizontal translation of the structure on top of the isolation system and the reduction in the seismic demand is achieved thanks to the frequency isolation between the fundamental frequency content of the structure and of the seismic excitation.

For one story buildings where the mass is mainly concentrate at the top, the kinematic can be introduced, as for base isolated building, decreasing the stiffness of the sway mechanism. The reduction of the stiffness is obtained introducing boundaries at the base and beam-column connections able to develop the mentioned mechanism where structural elements are supposed undergo rigid motion and post-tensioned strands and dissipators are introduced to give respectively the necessary global stiffness and strength, and dissipation capacity.

Main advantages achieved are the increase in displacement capacity with structural elements still in elastic range and the noticeable improve in reliability and effectiveness of the energy dissipation. The increased displacement capacity involves the period elongation and this, generally, a reduction of the seismic demand. The reliability of the activated mechanism, makes *reliable* the *dissipation capacity activation* whether related to the develop of ductility/damage in structural elements or to the activation of suitable external energy dissipators. The effectiveness of energy dissipators, to avoid damages at structural elements, depends on the displacement capacity before that damages are activated.

Therefore the introduced systems, other than make more probable the dissipators activation-avoiding uncertainty in the developed mechanism-increases the amount of energy dissipated by dampers thanks to the increased displacement capacity. Given the energy dissipation demand, the concentration of energy dissipation in dampers reduces the energy dissipation demand on structural elements making the reduction in the seismic response, due to the introduction of energy dissipators, relevant.

Innovative Systems applied to Precast Concrete Structures The introduction of innovative structural systems for seismic response control is particularly effective for precast prestressed concrete structures. Precast structural elements, produced in the factory and trucked in the construction site, must be appropriately connected. The necessity to realize appropriate connections and to introduce a dissipation capacity not involving damage to structural elements make attractive the introduction of new systems, not based on the cast in place emulation, where connections are designed to develop a specific deformation pattern, independent from the large seismic action variability. The displacement capacity is basically related to the deformability in post-tensioned partially unbounded steel strands that, provided the elastic behavior, guarantee re-centering capacity, removing any residual deformation. The well-defined deformation pattern and the dissipation capacity concentration in external metallic energy dissipators give to the structure a reliable dissipation capacity, easily replaceable without relevant additional costs. Thanks to the introduced characteristics the conceived structural system improves performances of traditional precast concrete buildings without a sensible variation in the cost production.

Acknowledgements

Sicep Spa Be sponsored by a private company is a responsibility and an honor. Link the research objectives with the professional world needs, it is hard but it is a prelude to a new way to approach engineering problems. My first thank to the Sicep Spa, a company in the field of precast concrete structures, able to donate a PhD fellowship in a moment economically so difficult that have given to a student the possibility to grow up professionally and culturally. Special thanks to Ing. S. Porto and Ing. R. Partescano for the assistence and the collaboration all along the PhD program.

NEES - BNCS, Full-Scale Structural and Nonstructural Building System - Performance during Earthquakes and Post-Earthquake Fire. Be involved in this project, even only for a few months, has been a great possibility to grow up. Thanks to Professor T. Hutchinson, Professor J. Conte, Professor J. Restrepo, A. Gunthardt, and D. Radulescu. I knew that particpate at the structural inspection would have been a unique opportunity but I didn't know that would have been the way to make so important friends. Thanks to Hamed Ebrahimian, Rodrigo Astroza, Xiang Wang and to the other team members: Consuelo Aranda, Michelle Chen, Elias Espino, Elide Pantoli, and Yoshua Neuman.

NEES - Advanced precast concrete dual-shell steel columns. Particpate to this project has been fundamental to develop what is presented in this thesis. Thanks to Professor J. Restrepo, Noah Aldrich (UCSD Powell Structures Lab) and to the others researchers and graduate students involved in the Project: Gabriele Guerrini, Milena Massari, and Athanassios Vervelidis.

Cyclic axial Response tested on mild A 706 and Stainless Steel Bars including Inelastic Buckling effects. For the precious assistance through all my first experimental project. Thanks to Paul Greco.

SE 201B - Nonlinear Structural Analysis. A great assistance and opportunity to learn. For giving me the honor to participate, Thanks to Professor J. Conte.

SE 151A - Design of Structural Concrete, SE 223 - Advanced Seismic Design of Structures. A unique opportunity to deepen the design of Concrete Structures. Thanks to Professor P. Shing and Professor J. Restrepo.

University of California San Diego, Structural Engineering Department Make people feel like at home is not so simple and is not due. Thanks to Raquel Hall, Jacqueline Vo, Debra K. D. Bomar, and Lindsay Walton.. It sounds strange but I had a good time when I had problems with my PC. Thanks to Robert Beckley. Enter in a new life environment is not simple. Thanks to all the Italian friends at the UCSD Structural Engineering Department. Neither projects nor classes together. Non an Italian guy. I don't know where I can insert you! A friend can give what no one experimental project or lecture can do. So, special mention. Thanks to Juan Murcia Delso.

University of Catania, Department of Civil and Environmental Engineering. For the assistance during the PhD program and for some precious suggestions that I will never forget. Thanks to Professor Contrafatto. A few considerations, suggestions, and questions can assume a key role. Thanks to Professor A. Badala', Professor I. Calio', Professor M. Cuomo, and Professor P. Rossi. I spent an important part of my life at the Civil and Environmental Engineering Department at Catania with them and it was great. Thanks to all my Unict colleagues. For the particular assistance during my exam, but not only, special thanks to G. Di Venti and G. D'Agata.

S.A.P. Srl. A few meetings have been a precious professional, and human, support. Thanks to Ing. M. Granata.

Others. Of course I will miss someone, there are so many people that should stay in this page. I am sorry, but more important than be thanked is... to deserve to be thank. Special thank to you.

To the reader I want to apologize for my level of academic writing but I wanted to use the period of study necessary to write my PhD thesis to continue to grow up.

Advisors. A particular thought is due. I saw a Professor work very hard. I saw a way to educate students with results outstanding. *I saw a way to approach research problems genial that I am doing my best to never forget.* In Catania I have been close to a person with a particular sensibility. People are not educated with words but with attitudes of sacrifice and genius. Thanks to the period spent together I received a good *professional* education. I feel lucky. Thanks to Professor G. Oliveto. In San Diego I have found a Professor able to understand me with a few, probably wrong, words, that gave me the possibility to grow up obtaining from me the maximum result. To generously have donated to my research twenty years of experience allowing me to close in the best way a work started in Catania. To have given to me the possibility to audit three classes and to to have involved me in three experimental projects but in particular *to have shown interest in my personal growth.* I feel privileged. Thanks to Professor J. Restrepo. Professional and human qualities rare.

Family For the precious support, all along my long period of education in Catania.

Thanks to my sister and her family.

Abbiamo fatto del nostro meglio per darti delle possibilita'
che Noi non abbiamo mai avuto.

(We did our best to give you possibilities that We have never had.)

More than economic support. A thought transference that reflects the importance of knowledge to grow up both, professionally and personally.

Thanks to my parents.

Overview

Contents

List of Figures

List of Tables

Part I

Advanced Design Philosophies and Methodologies

Chapter 1

Analysis of Constant Ductility Inelastic Displacement Ratios

Contents

1.1 Earthquake Records Database

In this chapter, seventy Earthquakes, to characterize the seismic action are used. In particular, exclusively far-field earthquake records are considered on soil type B,C and D. Next table shows the characteristics of the considered records.

1.1.1 Hysteretic Systems Analyzed

In this study, hysteretic single degree of freedom systems with a large range of variation of the characterizing parameters are considered. Constant ductility response spectra and constant ductility inelastic displacement ratio are calculated for systems with a range of periods between 0.5 and 10 sec, a ductility range between 1 and 20 and a post-yield stiffness range between 1 and -0.05. Three hysteresis rules, Bilinear, Clough and Takeda, with $\alpha = 0.5$ and $\beta = 0.0$, are chosen to characterize the hysteretic behavior and two different viscous damp-

Table 1.1: Recorded earthquake ground motions considered (1/3)

N°	Earthquake	Station name	ID	Type	Mw	Year	Dir.	Dist.	Site	Scale	Source
1	CapeMendocino	FortunaBlvd	cm_fort.cp1	Far	7.1	1992	C0	20	C	1	NGA
2	CapeMendocino	FortunaBlvd	cm_fort.cp2	Far	7.1	1992	C90	20	C	1	NGA
3	CapeMendocino	RioDellOverpass-FF	cm_riod.cp1	Far	7.1	1992	C270	14	C	1	NGA
4	CapeMendocino	RioDellOverpass-FF	cm_riod.cp2	Far	7.1	1992	C360	14	C	1	NGA
5	Landers	DesertHotSprings	ln_dese.cp1	Far	7.3	1992	C0	22	C	1	NGA
6	Landers	DesertHotSprings	ln_dese.cp2	Far	7.3	1992	C90	22	C	1	NGA
7	Landers	YermoFireStation	ln_yerm.cp1	Far	7.3	1992	C270	24	D	1	NGA
8	Landers	YermoFireStation	ln_yerm.cp2	Far	7.3	1992	C360	24	D	1	NGA
9	LomaPrieta	Berkeley-LawrenceBerkleyLab	lp_blbl.cp1	Far	7.0	1989	C0	79	C	1	NGA
10	LomaPrieta	Berkeley-LawrenceBerkleyLab	lp_blbl.cp2	Far	7.0	1989	C90	79	C	1	NGA
11	LomaPrieta	Capitola	lp_capi.cp1	Far	7.0	1989	C0	15	D	1	NGA
12	LomaPrieta	Capitola	lp_capi.cp2	Far	7.0	1989	C90	15	D	1	NGA
13	LomaPrieta	GilroyArray3	lp_gil3.cp1	Far	7.0	1989	C0	12	D	1	NGA
14	LomaPrieta	GilroyArray3	lp_gil3.cp2	Far	7.0	1989	C90	12	D	1	NGA
15	LomaPrieta	GilroyArray4	lp_gil4.cp1	Far	7.0	1989	C0	14	D	1	NGA
16	LomaPrieta	GilroyArray4	lp_gil4.cp2	Far	7.0	1989	C90	14	D	1	NGA
17	LomaPrieta	GilroyArray7	lp_gil7.cp1	Far	7.0	1989	C0	23	D	1	NGA
18	LomaPrieta	GilroyArray7	lp_gil7.cp2	Far	7.0	1989	C90	23	D	1	NGA
19	LomaPrieta	HollisterDiffArray	lp_holl.cp1	Far	7.0	1989	C165	25	D	1	NGA
20	LomaPrieta	HollisterDiffArray	lp_holl.cp2	Far	7.0	1989	C255	25	D	1	NGA
21	LomaPrieta	Saratoga-WestValleyColl	lp_sara.cp1	Far	7.0	1989	C0	9	C	1	NGA
22	LomaPrieta	Saratoga-WestValleyColl	lp_sara.cp2	Far	7.0	1989	C270	9	C	1	NGA
23	LomaPrieta	SanFrancisco-DiamondHeights	lp_sfdh.cp1	Far	7.0	1989	C0	71	B	1	NGA

Table 1.2: Recorded earthquake ground motions considered (2/3)

N°	Earthquake	Station name	ID	Type	Mw	Year	Dir.	Dist.	Site	Scale	Source
24	LomaPrieta	SanFrancisco-DiamondHeights	lp_sfdh.cp2	Far	7.0	1989	C90	71	B	1	NGA
25	LomaPrieta	SanFrancisco-TelegraphHills	lp_sfth.cp1	Far	7.0	1989	C0	76	B	1	NGA
26	LomaPrieta	SanFrancisco-TelegraphHills	lp_sfth.cp2	Far	7.0	1989	C90	76	B	1	NGA
27	LomaPrieta	Woodside-FireStation	lp_wood.cp1	Far	7.0	1989	C0	34	C	1	NGA
28	LomaPrieta	Woodside-FireStation	lp_wood.cp2	Far	7.0	1989	C90	34	C	1	NGA
29	Morgan Hill	Gilroy-GavillanCollege	mh_ggc.cp1	Far	6.1	1984	C67	15	C	1	NGA
30	Morgan Hill	Gilroy-GavillanCollege	mh_ggc.cp2	Far	6.1	1984	C337	15	C	1	NGA
31	Morgan Hill	GilroyArray7	mh_gil7.cp1	Far	6.1	1984	C0	12	D	1	NGA
32	Morgan Hill	GilroyArray7	mh_gil7.cp2	Far	6.1	1984	C90	12	D	1	NGA
33	Northridge	BeverlyHills-14145MulhollandBlvd	nr_bhmb.cp1	Far	6.7	1994	C9	17	C	1	NGA
34	Northridge	BeverlyHills-14145MulhollandBlvd	nr_bhmb.cp2	Far	6.7	1994	C279	17	C	1	NGA
35	Northridge	CanogaPark-TopangaCanyon	nr_cptc.cp1	Far	6.7	1994	C106	15	D	1	NGA
36	Northridge	CanogaPark-TopangaCanyon	nr_cptc.cp2	Far	6.7	1994	C196	15	D	1	NGA
37	Northridge	Glendale-LasPalmas	nr_glp.cp1	Far	6.7	1994	C177	22	D	1	NGA
38	Northridge	Glendale-LasPalmas	nr_glp.cp2	Far	6.7	1994	C267	22	D	1	NGA
39	Northridge	LosAngeles-CityTerrace	nr_lact.cp1	Far	6.7	1994	C90	37	B	1	NGA
40	Northridge	LosAngeles-CityTerrace	nr_lact.cp2	Far	6.7	1994	C180	37	B	1	NGA
41	Northridge	LosAngeles-HollywoodStorage-FF	nr_lahs.cp1	Far	6.7	1994	C90	24	D	1	NGA
42	Northridge	LosAngeles-HollywoodStorage-FF	nr_lahs.cp2	Far	6.7	1994	C360	24	D	1	NGA
43	Northridge	LosAngeles-NorthFaringRoad	nr_lanf.cp1	Far	6.7	1994	C0	21	D	1	NGA
44	Northridge	LosAngeles-NorthFaringRoad	nr_lanf.cp2	Far	6.7	1994	C90	21	D	1	NGA
45	Northridge	LakeHughesArray9	nr_lha9.cp1	Far	6.7	1994	C0	25	B	1	NGA
46	Northridge	LakeHughesArray9	nr_lha9.cp2	Far	6.7	1994	C90	25	B	1	NGA

Table 1.3: Recorded earthquake ground motions considered (3/3)

N°	Earthquake	Station name	ID	Type	Mw	Year	Dir.	Dist.	Site	Scale	Source
47	Northridge	Littlerock-BrainardCanyon	nr_litt.cp1	Far	6.7	1994	C90	47	C	1	NGA
48	Northridge	Littlerock-BrainardCanyon	nr_litt.cp2	Far	6.7	1994	C180	47	C	1	NGA
49	Northridge	NorthHollywood-ColdwaterCanyon	nr_nhcc.cp1	Far	6.7	1994	C180	13	C	1	NGA
50	Northridge	NorthHollywood-ColdwaterCanyon	nr_nhcc.cp2	Far	6.7	1994	C270	13	C	1	NGA
51	Northridge	Sunland-MtGleasonAve	nr_smga.cp1	Far	6.7	1994	C170	13	C	1	NGA
52	Northridge	Sunland-MtGleasonAve	nr_smga.cp2	Far	6.7	1994	C260	13	C	1	NGA
53	Northridge	SanMarino-SWAcademy	nr_smsw.cp1	Far	6.7	1994	C90	35	C	1	NGA
54	Northridge	SanMarino-SWAcademy	nr_smsw.cp2	Far	6.7	1994	C360	35	C	1	NGA
55	SanFernando	Castic-OldRidgeRoute	sf_corr.cp1	Far	6.6	1971	C021	23	C	1	NGA
56	SanFernando	Castic-OldRidgeRoute	sf_corr.cp2	Far	6.6	1971	C291	23	C	1	NGA
57	SanFernando	LakeHughesArray12	sf_lha12.cp1	Far	6.6	1971	C021	19	C	1	NGA
58	SanFernando	LakeHughesArray12	sf_lha12.cp2	Far	6.6	1971	C291	19	C	1	NGA
59	SanFernando	LakeHughesArray9	sf_lha9.cp1	Far	6.6	1971	C021	23	B	1	NGA
60	SanFernando	LakeHughesArray9	sf_lha9.cp2	Far	6.6	1971	C291	23	B	1	NGA
61	SuperstitionHills	BrawleyAirport	sh_braw.cp1	Far	6.7	1987	C225	17	D	1	NGA
62	SuperstitionHills	BrawleyAirport	sh_braw.cp2	Far	6.7	1987	C315	17	D	1	NGA
63	SuperstitionHills	ElCentro-ImpCoCent	sh_elce.cp1	Far	6.7	1987	C0	18	D	1	NGA
64	SuperstitionHills	ElCentro-ImpCoCent	sh_elce.cp2	Far	6.7	1987	C90	18	D	1	NGA
65	SuperstitionHills	PlasterCity	sh_plas.cp1	Far	6.7	1987	C45	22	D	1	NGA
66	SuperstitionHills	PlasterCity	sh_plas.cp2	Far	6.7	1987	C135	22	D	1	NGA
67	Whittier	MtWilsonCIT	wh_mtwil.cp1	Far	6.1	1987	C0	23	B	1	NGA
68	Whittier	MtWilsonCIT	wh_mtwil.cp2	Far	6.1	1987	C90	23	B	1	NGA
69	Whittier	UnionOilYard	wh_unio.cp1	Far	6.1	1987	C0	26	C	1	NGA
70	Whittier	UnionOilYard	wh_unio.cp2	Far	6.1	1987	C90	26	C	1	NGA

ing ratio, 5% and 2%, to examine the effect of the viscous damping, were also investigated.

In the ranges previously specified, one hundred ninety one period of vibration (with a time step equal to 0.05), five different ductility levels (1, 2.5, 5, 10, 20) and nine bilinear factors (1.000, 0.800, 0.400, 0.200, 0.100, 0.050, 0.000, -0.025, -0.050) are considered.

Totally, including the three hysteresis rules and the two viscous damping ratio ($191 \cdot 5 \cdot 9 \cdot 3 \cdot 2$) 51,570 different systems are considered. Finally, seventy earthquakes, and therefore 3,609,900, displacement demands are calculated.

1.1.2 Constant Ductility Response Spectra

In this work, constant ductility response spectra was calculated by Inspect. In this context will be examined the influence of bilinear factor, ductility level, hysteresis rules and viscous damping ratio on the constant ductility response spectra. More specifically, with reference to all the previous earthquake records, Constant Ductility Response Spectra, for five different ductility levels for nine bilinear factors, for three hysteresis rules and two viscous damping ratios are calculated. To summarize and to highlight the effect of the previous parameters on the constant ductility response spectra, the mean response spectra, along the earthquake population considered, are calculated and plotted.

1.2 Iso-ductility inelastic displacement ratio, C_μ

1.2.1 Introduction

The constant ductility inelastic displacement ratio is defined as the ratio between the inelastic displacement demand $\Delta_{inelastic}$ and the elastic displacement demand $\Delta_{elastic}$ on the *corresponding linear system* subjected to the same excitation:

$$C_\mu = \frac{\Delta_{inelastic}}{\Delta_{elastic}} \tag{1.1}$$

where, a corresponding linear system is an elastic system with the same mass and damping and with stiffness equal to the initial stiffness of the hysteretic system. Traditionally, the inelastic displacement ratios introduced are calculated with reference to a viscous damping ratio equal to 5%.

Due to the physical mean of the constant ductility inelastic displacement ratio, the C_μ value must be equal to the constant ductility value for period equal zero and must be tends to 1 for periods that tend to infinite, for each bilinear factor, for each ductility level, for each hysteresis rules and for each viscous damping ratio. Moreover, must be equal 1 for bilinear factor equal 1 (for all the ductility level and for all hysteresis rules), and for ductility level equal to 1 (for all the bilinear factors and all the hysteresis rules). Symbolically, these boundary conditions can be written:

- $$T = \infty \Longrightarrow C_\mu = 1 \qquad \forall r, \forall \mu, \forall h, \forall \xi \tag{1.2}$$
- $$T = 0 \Longrightarrow C_\mu = \mu \qquad \forall r, \forall \mu, \forall h, \forall \xi \tag{1.3}$$
- $$\mu = 1 \Longrightarrow C_\mu = 1 \qquad \forall r, \forall T, \forall h, \forall \xi \tag{1.4}$$
- $$r = 1 \Longrightarrow C_\mu = 1 \qquad \forall \mu, \forall T, \forall h, \forall \xi \tag{1.5}$$

where with r the bilinear factor, with μ the ductility, with h the hysteresis rule with ξ the viscous damping ratio and with T the period are indicated.

1.2.2 C_μ variation with period

Generally it can be seen that there are three different characteristic behaviors. An initial range of periods where the C_μ value, starting from μ decrease with the increase of the period from zero, an intermediate range of periods where the constant ductility inelastic displacement oscillates around a C_μ value almost constant with the period, and a third range of periods where the inelastic demand compared to the corresponding elastic demand decrease with the increase of the period to one. The two periods that determine these three periods range are function of the ductility level, of the bilinear factor, of the hysteresis rule and of the viscous damping ratio considered...(..possibly). To highlight the C_μ variation with the period, the median value along the earthquake population, for two particular ductility levels, for two bilinear factor and for all the hysteresis rules is considered.

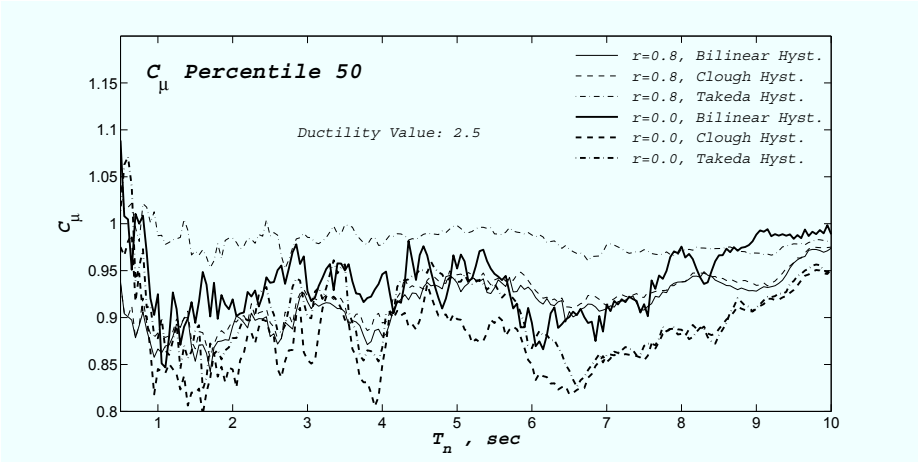

Figure 1.1: C_μ 50 Percentile: Effect of bilinear factor and hysteresis rules for ductility level equal to 2.5

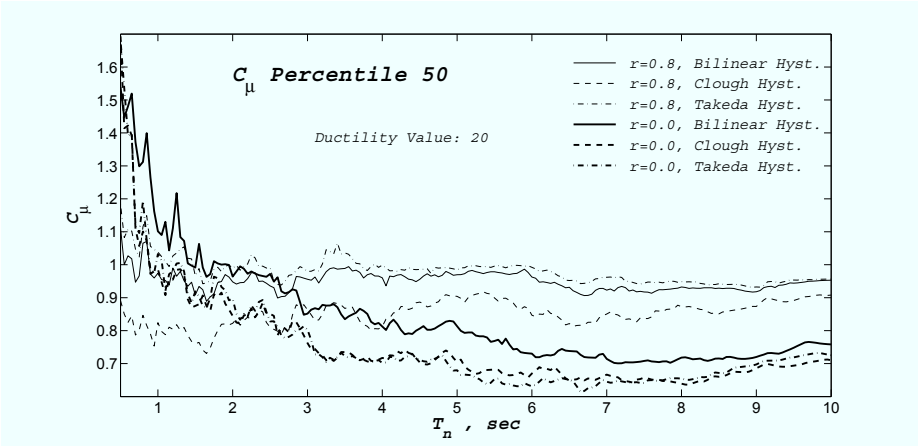

Figure 1.2: C_μ 50 Percentile: Effect of bilinear factor and hysteresis rules for ductility level equal to 20.0

Effect of the *Earthquakes*

To highlight the C_μ dispersion along the earthquake population the mean value and percentile 90% are plotted together for the three hysteresis rules, for bilinear factors equal to 0.0 and 0.8 and for ductility values equal to 2.5 and 20.

Effect of the *Ductility Levels*

Considering high bilinear factors, and in particular bilinear factor equal to 0.8, figure 1.3, it can be seen that, generally, a decrease in the bilinear factor causes an increase in the C_μ values. More detailed, the range of periods where the solution oscillates around a quite constant value doesn't show great change in amplitude with the variation of the ductility level. Considering low bilinear factor, and in particular bilinear factor equal to 0.0, figure 1.4, it can be seen

that the range of periods' amplitude, where the C_μ value oscillates around a constant value, is smaller, and in particular because the convergency to one start before for high ductility level.

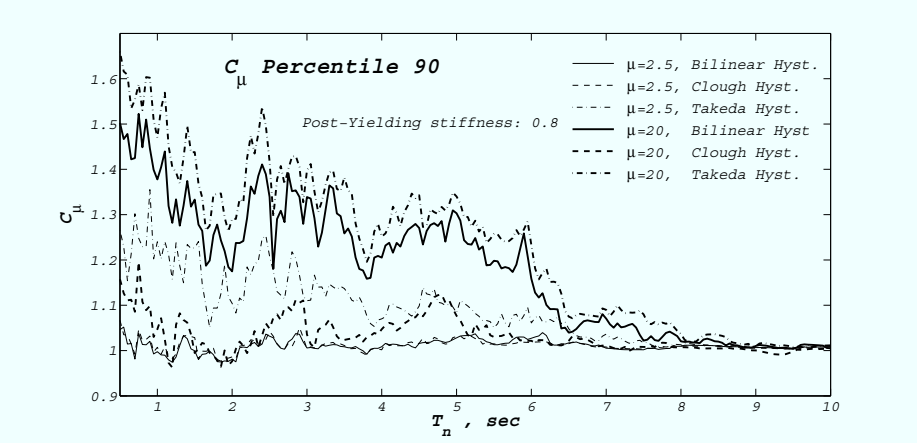

Figure 1.3: C_μ 90 Percentile: Effect of ductility levels and hysteresis rules for bilinear factor equal to 0.8

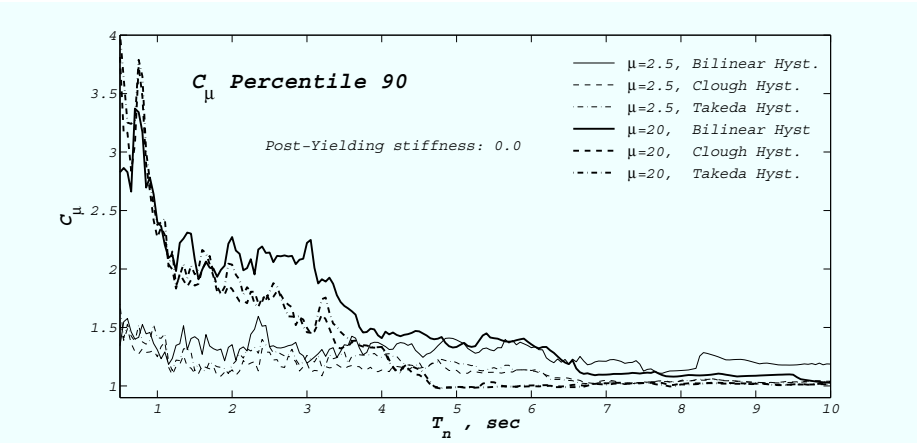

Figure 1.4: C_μ 90 Percentile: Effect of ductility levels and hysteresis rules for bilinear factor equal to 0.0

Effect of the *Bilinear Factors*

To summarize the results, 90 Percentile values along the earthquake population is plotted for the biggest and the lowest ductility level and for the biggest and the lowest bilinear factors considered excluding the trivial cases. The results are shown in the figures 1.5 and 1.6

Looking at the figure 1.5 it can be seen that for for low ductility values and for a periods range 1-5 seconds, in general, a decrease of the bilinear factor

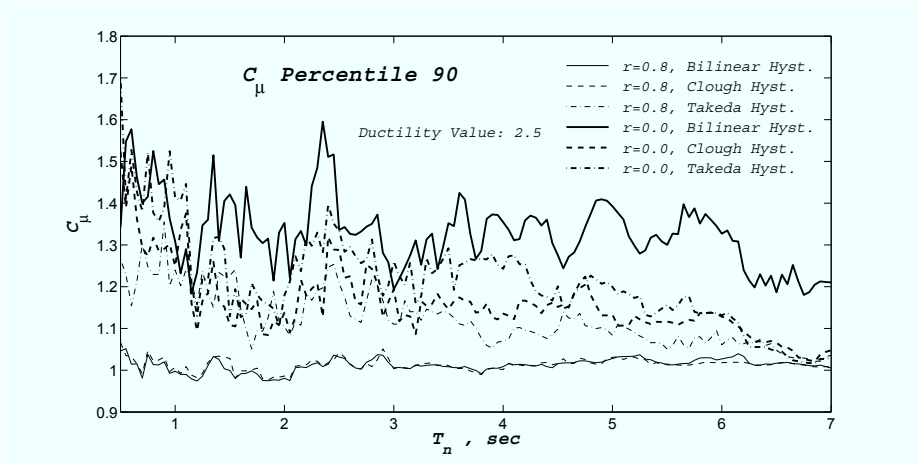

Figure 1.5: C_μ 90 Percentile: Effect of bilinear factor and hysteresis rules for ductility level equal to 2.5

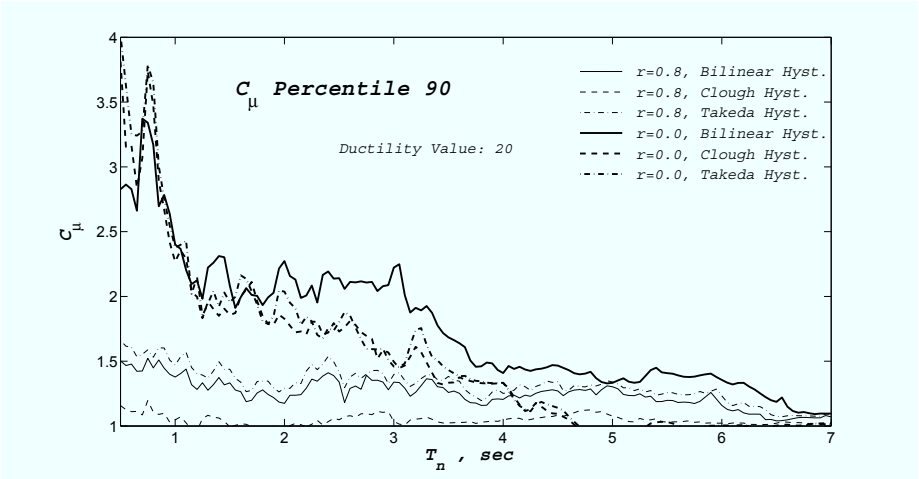

Figure 1.6: C_μ 90 Percentile: Effect of bilinear factor and hysteresis rules for ductility level equal to 20.0

leads to an increase of the inelastic demand compared the elastic demand of the corresponding system that oscillates around a value almost constant.

On average, for period smaller than 1 sec, the C_μ convergency to the ductility value, for period equal to zero, appears begin before for low bilinear factor and this leads to an increase of the inelastic demand.

For periods bigger than 5 sec., for low bilinear factors, clearly begin the C_μ convergency to one and this leads to a decrease of the inelastic demand compared to the elastic demand of the corresponding system with the increase of the period. Therefore, the increase of the inelastic demand with the decrease of the bilinear factor tends to reduce.

With reference to high ductility level, see figure 1.6, it can be seen that the range where the increment with the bilinear factor is quite constant is smaller

and both the range periods where there is the convergency to μ and the convergency to one begin before compare with the previous case.

Effect of the *Hysteresis Rules*

Looking at the figures 1.5 and 1.6, It can be seen that for low ductility levels and high bilinear factors C_μ for system with bilinear hysteresis and Clough hysteresis are very close. On the other hand, the C_μ values for system with Takeda hysteresis are substantially different, in the most part of the period range considered. In particular for these systems the inelastic demand is bigger than the inelastic demand for system with Bilinear and Clough Hysteresis. For low ductility but for bilinear factor close to zero the inelastic demand for system with Clough Hysteresis are quite close to the inelastic demand for system with Takeda Hysteresis. A different behavior is shown from systems with bilinear hysteresis and in particular a bigger inelastic demand. Moreover, for system with Bilinear hysteresis the C_μ convergency to one with the increase of the period is more slowly.

Looking

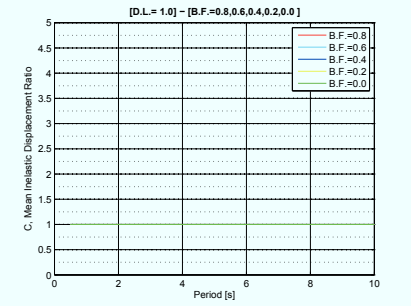

(a) *Ductility Level 1*

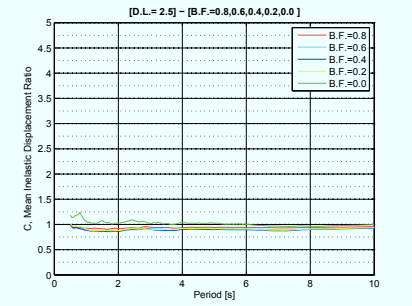

(b) *Ductility Level 2.5*

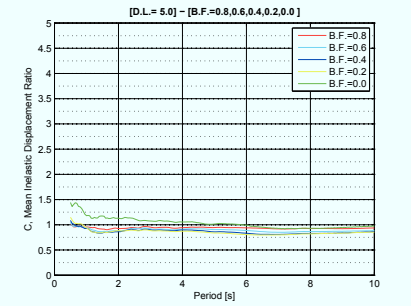

(c) *Ductility Level 5*

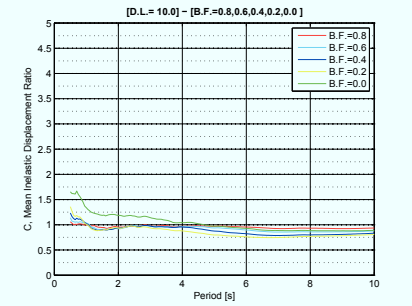

(d) *Ductility Level 10*

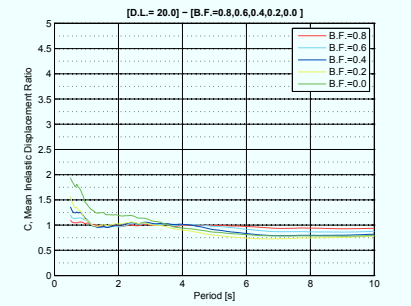

(e) *Ductility Level 20*

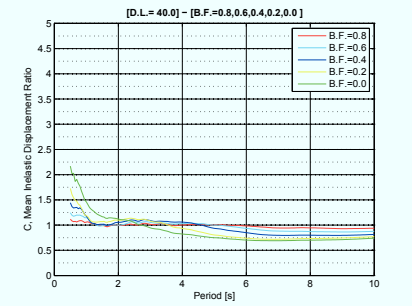

(f) *Ductility Level 40*

Figure 1.7: $C_{\mu,Mean.}$: Variation with Bilinear Factor - Different Ductility Values.

Percentiles

In this context will be considered the next particular percentiles: 10 30 50 70 90 In particular we are going to focus on the ninety percentiles.

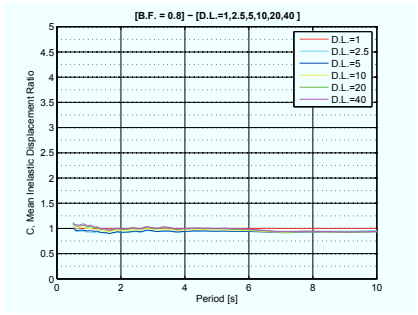

(a) Bilinear Factor 0.8

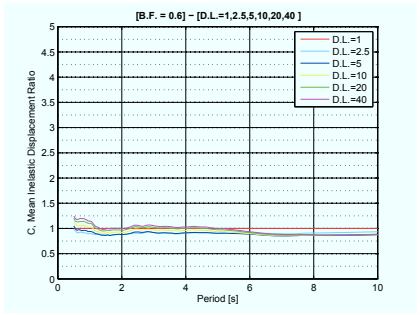

(b) Bilinear Factor 0.6

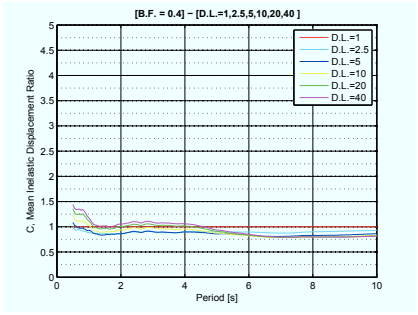

(c) Bilinear Factor 0.4

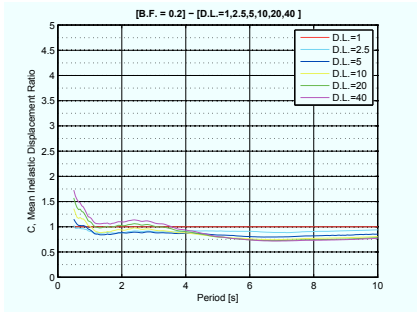

(d) Bilinear Factor 0.2

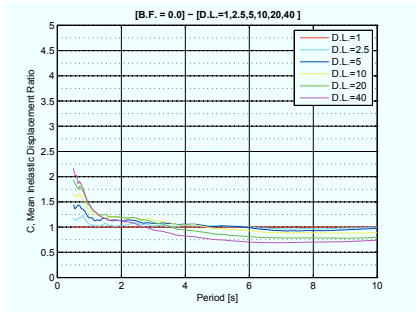

(e) Bilinear Factor 0.0

Figure 1.8: $C_{\mu,Mean.}$: Variation with Ductility Level - Different Bilinear Factor.

Percentiles: 10-30-50-70-90
Ductility value 2.5
Bilinear Factor 0.0-0.2-0.4-0.6-0.8

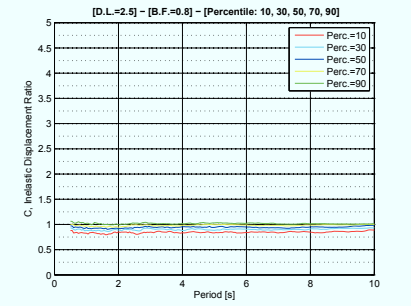

(a) *Bilinear Factor 0.8*

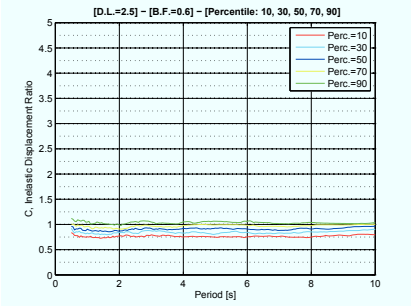

(b) *Bilinear Factor 0.6*

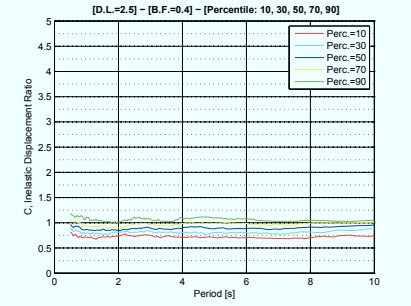

(c) *Bilinear Factor 0.4*

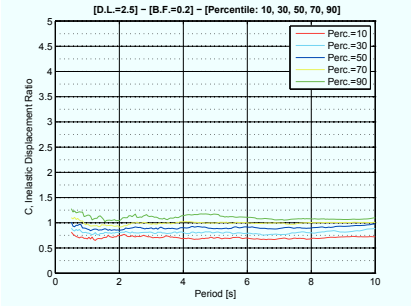

(d) *Bilinear Factor 0.2*

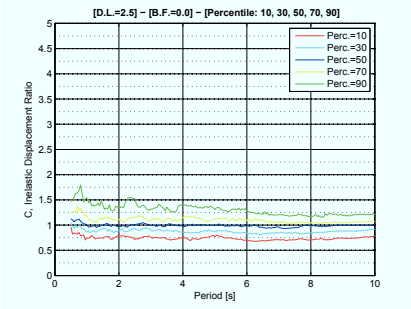

(e) *Bilinear Factor 0.0*

Figure 1.9: Percentiles: Ductility Value equal 2.5 - Different Bilinear Factor

Percentiles: 10-30-50-70-90
Ductility value 5
Bilinear Factor 0.0-0.2-0.4-0.6-0.8

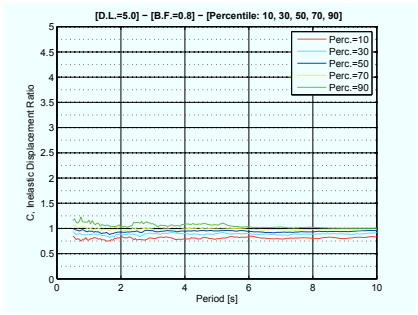

(a) *Bilinear Factor 0.8*

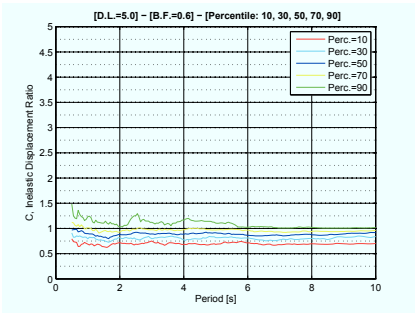

(b) *Bilinear Factor 0.6*

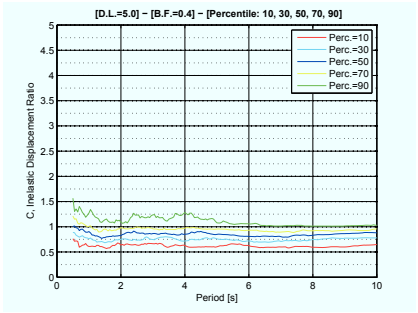

(c) *Bilinear Factor 0.4*

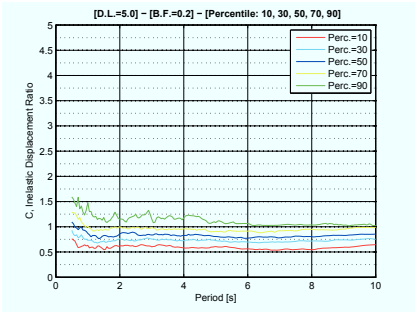

(d) *Bilinear Factor 0.2*

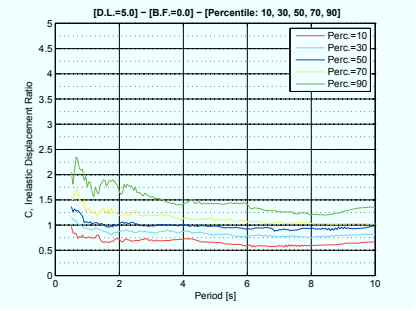

(e) *Bilinear Factor 0.0*

Figure 1.10: Percentiles: Ductility Value equal 5 - Different Bilinear Factor

Percentiles: 10-30-50-70-90
Ductility value 10
Bilinear Factor 0.0-0.2-0.4-0.6-0.8

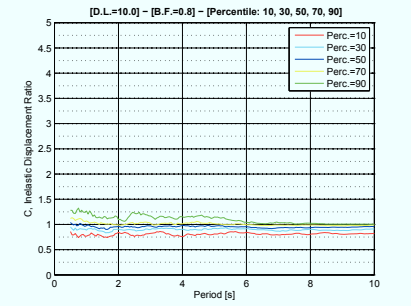

(a) *Bilinear Factor 0.8*

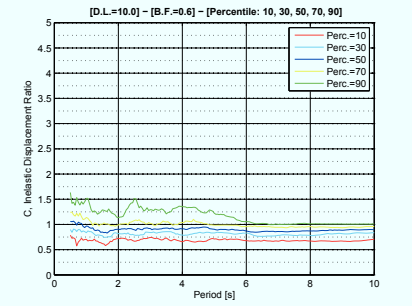

(b) *Bilinear Factor 0.6*

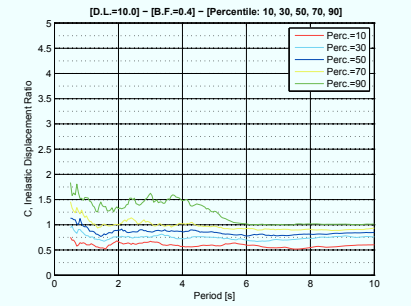

(c) *Bilinear Factor 0.4*

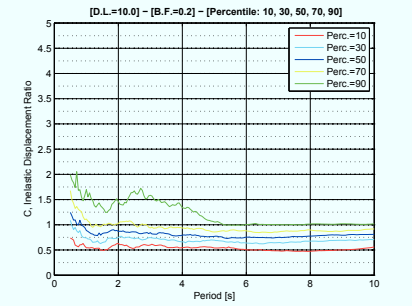

(d) *Bilinear Factor 0.2*

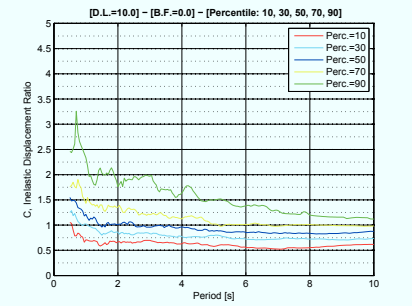

(e) *Bilinear Factor 0.0*

Figure 1.11: Percentiles: Ductility Value equal 10 - Different Bilinear Factor

Percentiles: 10-30-50-70-90
Ductility value 20
Bilinear Factor 0.0-0.2-0.4-0.6-0.8

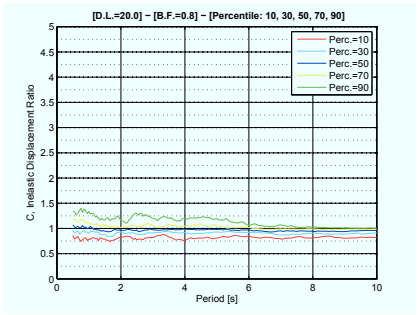

(a) *Bilinear Factor 0.8*

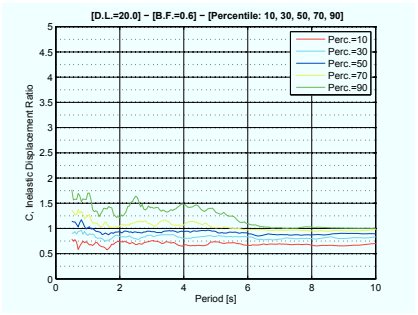

(b) *Bilinear Factor 0.6*

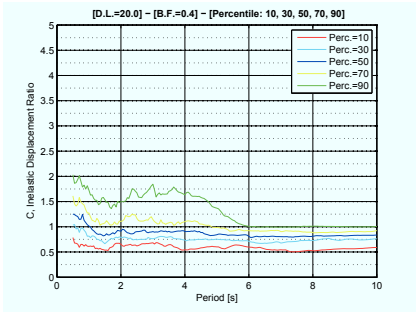

(c) *Bilinear Factor 0.4*

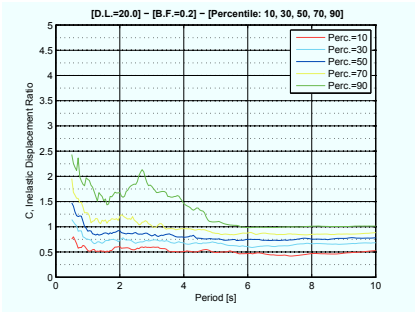

(d) *Bilinear Factor 0.2*

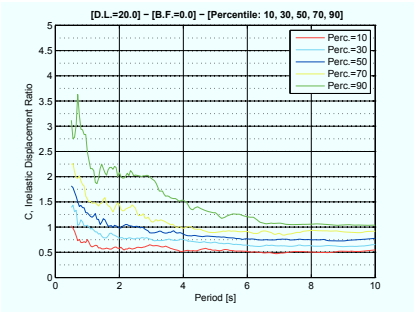

(e) *Bilinear Factor 0.0*

Figure 1.12: Percentiles: Ductility Value equal 20 - Different Bilinear Factor

Percentiles: 10-30-50-70-90
Ductility value 40
Bilinear Factor 0.0-0.2-0.4-0.6-0.8

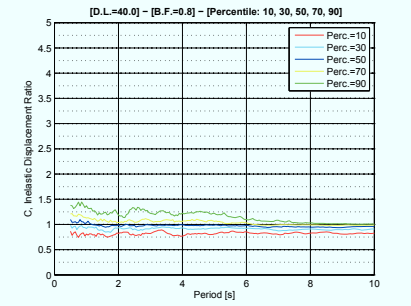

(a) *Bilinear Factor 0.8*

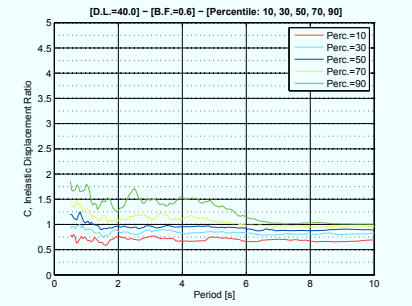

(b) *Bilinear Factor 0.6*

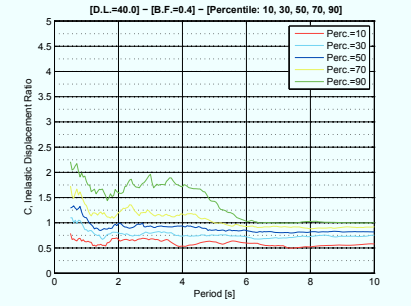

(c) *Bilinear Factor 0.4*

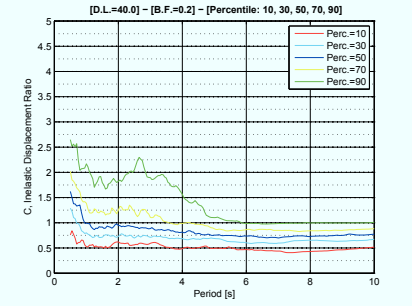

(d) *Bilinear Factor 0.2*

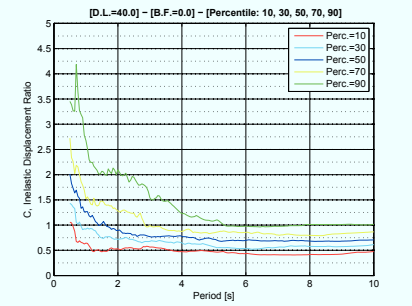

(e) *Bilinear Factor 0.0*

Figure 1.13: Percentiles: Ductility Value equal 40 - Different Bilinear Factor

Percentiles

Percentile 90%

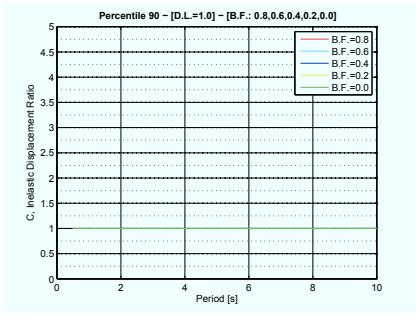

(a) *Ductility Level 1*

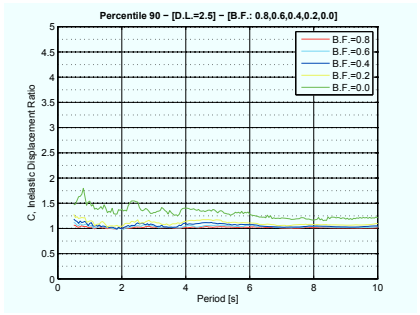

(b) *Ductility Level 2.5*

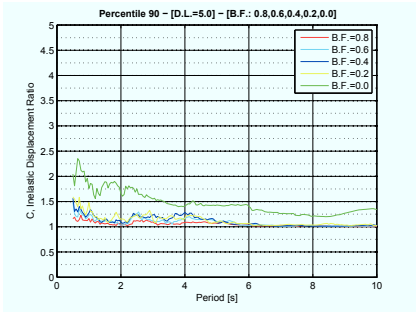

(c) *Ductility Level 5*

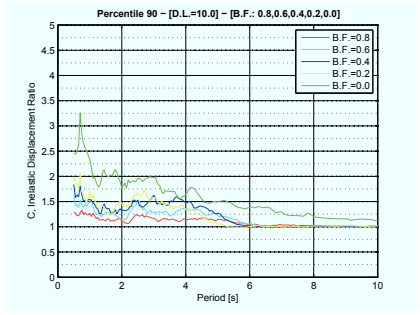

(d) *Ductility Level 10*

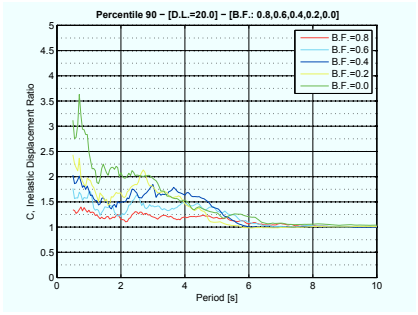

(e) *Ductility Level 20*

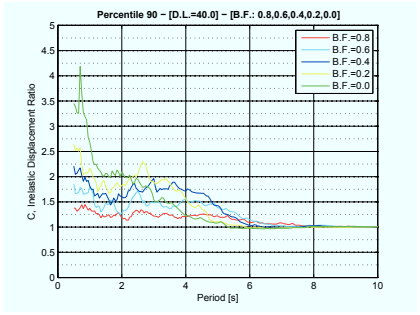

(f) *Ductility Level 40*

Figure 1.14: $C_{\mu,90Perc.}$: Variation with Bilinear Factors - Different Ductility Level

Percentile 90%

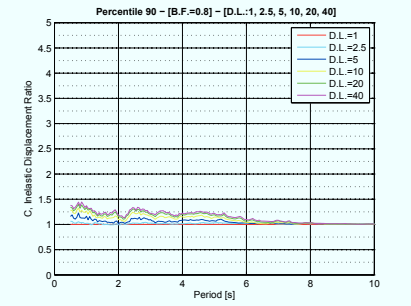

(a) *Bilinear Factor 0.8*

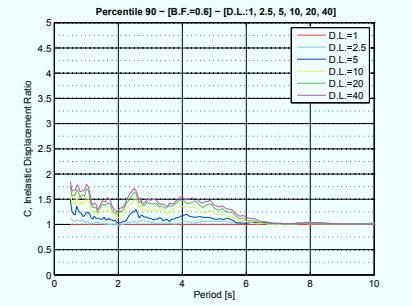

(b) *Bilinear Factor 0.6*

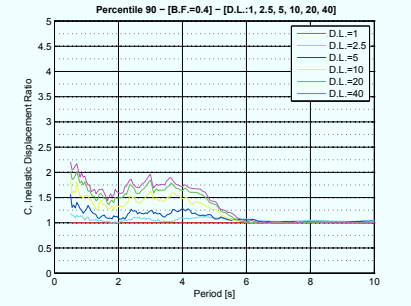

(c) *Bilinear Factor 0.4*

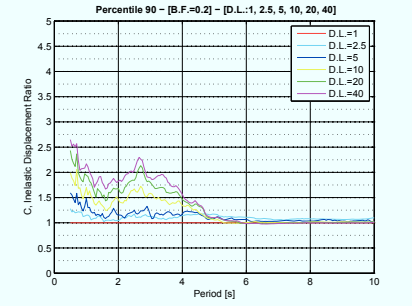

(d) *Bilinear Factor 0.2*

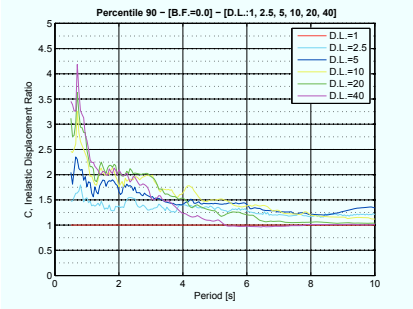

(e) *Bilinear Factor 0.0*

Figure 1.15: $C_{\mu,90Perc.}$: Variation with Ductility Values - Different Bilinear Factor

1.3 $C_{\mu,5/2}$, a new constant ductility inelastic displacement ratio

1.3.1 Introduction

The influence of the viscous damping on the response of hysteretic systems lead to the necessity of consider low viscous damping in the non-linear analysis of hysteretic systems. Based on this evidence and considering that in the Codes, to characterize the seismic action, 5% Damping spectra are presented, seems evident introduce the next inelastic displacement ratio:

$$C_{\mu,5/2} = \frac{\Delta_{inelastic,2\%}}{\Delta_{elastic,5\%}} \tag{1.6}$$

1.4 Analytical Estimate

1.4.1 $C_{\mu,5/2}$ Vs Period Analytical Estimate

fghhhhhh

Boundary Conditions

Considerations about the physical mean of the constant ductility Inelastic Displacement Ratio lead to the next boundary conditions:

1.
$$T = \infty \Longrightarrow C_\mu = 1 \qquad \forall r, \forall \mu \tag{1.7}$$

2.
$$T = 0 \Longrightarrow C_\mu = \mu \qquad \forall r \tag{1.8}$$

3.
$$\mu = 1 \Longrightarrow C_\mu = 1 \qquad \forall r, \forall T \tag{1.9}$$

4.
$$r = 1 \Longrightarrow C_\mu = 1 \qquad \forall T \tag{1.10}$$

Base Curves Construction

Looking at the graphics C_μ 90% Percentile, the most simple idea is to consider C_μ a negative exponential curve of the Period:

$$C_\mu = e^{-T} \tag{1.11}$$

For the first boundary condition we need to add 1 so the previous equation became:

$$C_\mu = 1 + e^{-T} \tag{1.12}$$

for the second and the third boundary condition we need to multiply the exponential term for $(1 - \mu)$ and to change the sign, so the previous equation became:

$$C_\mu = 1 - (1 - \mu)e^{-T} \tag{1.13}$$

To consider the effect of the bilinear factor in simple way and to consider the fourth boundary condition, we can modify the previous equation obtaining

$$C_\mu = 1 - (1 - \mu)e^{-\frac{T}{1-r}} \tag{1.14}$$

To generalize the determined equation, preserving the boundary conditions, we can consider the next equation

$$C_\mu = 1 - (1 - \mu)exp\left(-a\frac{T^b}{(1 - r^c)^d}\right) \tag{1.15}$$

Finally, to introduce the possibility of change with ductility value along the period we can consider

$$C_\mu = 1 - (1 - \mu)exp\left(-\frac{a}{\mu^b}\frac{T^c}{(1 - r^d)^e}\right) \tag{1.16}$$

where a,b,c,d and e are parameters that will be determinate with the regression analysis.

Curve Fitting: Error In this investigation non-linear regression analysis were done in order to minimize the C_μ Percentile 90% error given by

$$Error = \sum_{e=1}^{70}\sum_{t=1}^{195}\sum_{d=1}^{5}\sum_{r=1}^{7} abs\frac{(C_{\mu,Theor.} - C_{\mu,Stat.})}{70 * 195 * 5 * 7} \tag{1.17}$$

or

$$Error = \sum_{e=1}^{70}\sum_{t=1}^{195}\sum_{d=1}^{5}\sum_{r=1}^{7}\left[(1-r) + \frac{(\mu-1)}{19} + \frac{1}{2T}\right] abs\frac{(C_{\mu,Theor.} - C_{\mu,Stat.})}{70 * 195 * 5 * 7} \tag{1.18}$$

for each combination of the base curve parameters a,b,c,d,e.

Base Curve

Starting from the next equation:

$$C_\mu = a\left[bT^c - (\mu - 1)\right] exp(-dT) + 1 \tag{1.19}$$

to be the equation consistent with the boundary condition ($T = 0 \longrightarrow C_\mu = \mu$) the parameter a must be equal -1 so the equation became:

$$C_\mu = 1 - \left[aT^b - (\mu - 1)\right] exp(-cT) \tag{1.20}$$

or

$$C_\mu = 1 + \left[(\mu - 1) - aT^b\right] exp(-cT) \tag{1.21}$$

To consider the effect of the bilinear factor in simple way and to consider the fourth boundary condition, we can modify the previous equation obtaining

$$C_\mu = 1 + \left(\mu - 1) - aT^b\right] exp(-c\frac{T\mu}{(1-r)}) \tag{1.22}$$

To consider the boundary condition ($\mu = 1 \longrightarrow C_\mu = 1$) the previous was modified:

$$C_\mu = 1 + (\mu - 1)\left(1 - aT^b\right) exp(-c\frac{T\mu}{(1-r)}) \tag{1.23}$$

With the optimization process was obtained:

$$C_\mu = 1 + (\mu - 1)\left(1 + T^{\,(3.2+0.4\mu r)}\right) \exp\left(1.7\ \frac{\mu^{0.2}}{(r^{0.35}-1)^{0.3}}\ T^{0.7}\right) \tag{1.24}$$

Comparison Analytical Curve Statistical Data - Ductility value 2.5

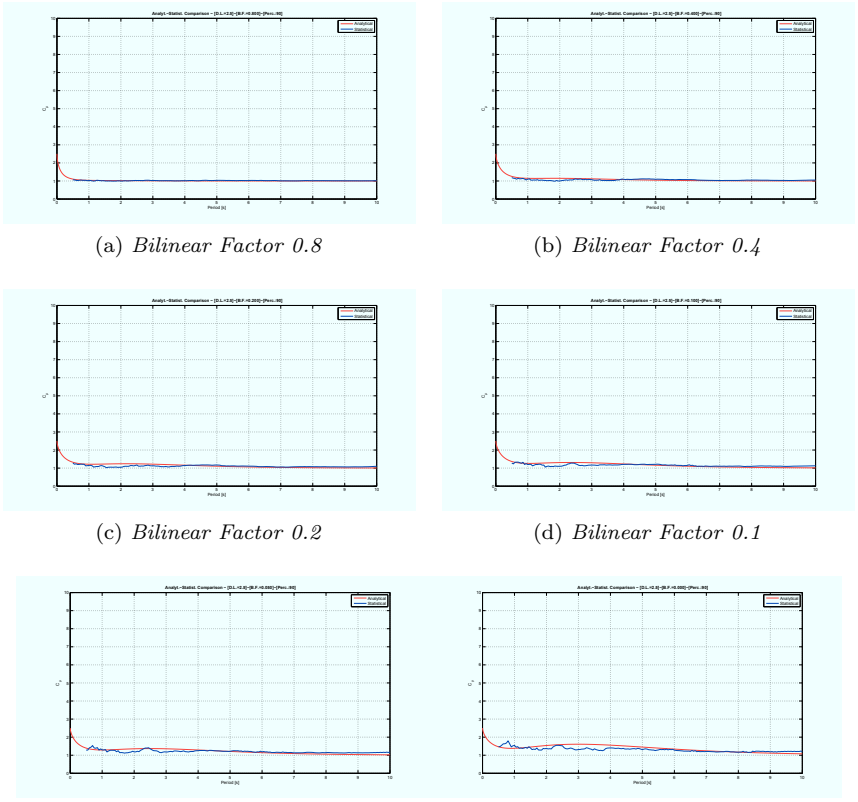

(a) *Bilinear Factor 0.8* (b) *Bilinear Factor 0.4*

(c) *Bilinear Factor 0.2* (d) *Bilinear Factor 0.1*

(e) *Bilinear Factor 0.05* (f) *Bilinear Factor 0.0*

Figure 1.16: Comparison: Ductility Value equal 2.5 - Different Bilinear Factor

Comparison Analytical Curve Statistical Data - Ductility value 5

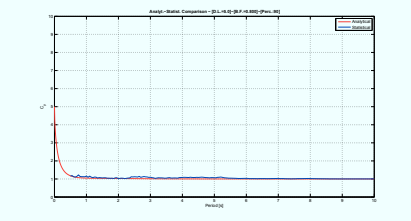

(a) *Bilinear Factor 0.8*

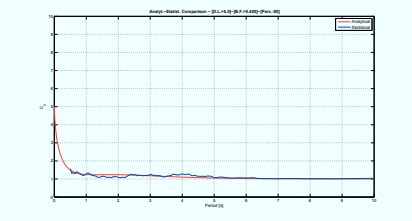

(b) *Bilinear Factor 0.4*

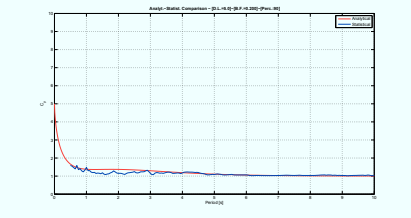

(c) *Bilinear Factor 0.2*

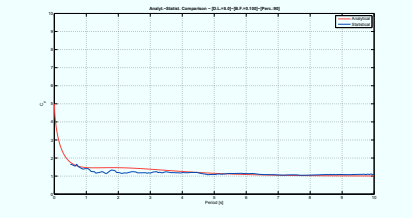

(d) *Bilinear Factor 0.1*

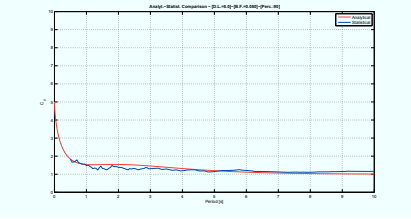

(e) *Bilinear Factor 0.05*

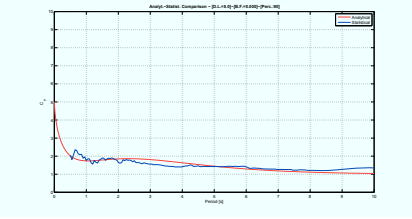

(f) *Bilinear Factor 0.0*

Figure 1.17: Comparison: Ductility Value equal 5 - Different Bilinear Factor

Comparison Analytical Curve Statistical Data - Ductility value 10

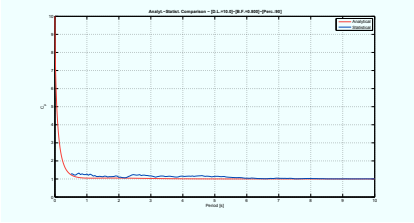

(a) *Bilinear Factor 0.8*

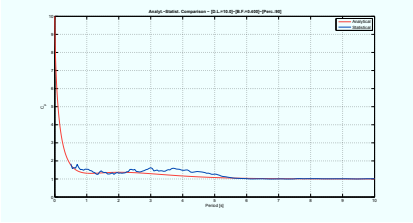

(b) *Bilinear Factor 0.4*

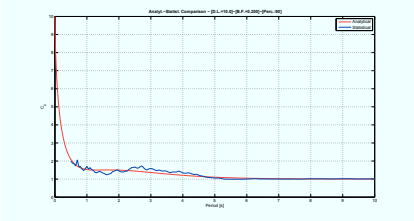

(c) *Bilinear Factor 0.2*

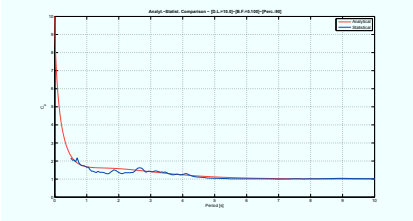

(d) *Bilinear Factor 0.1*

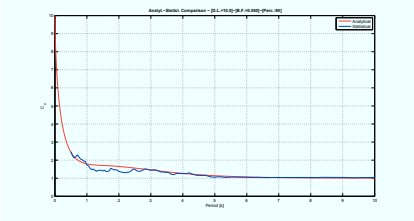

(e) *Bilinear Factor 0.05*

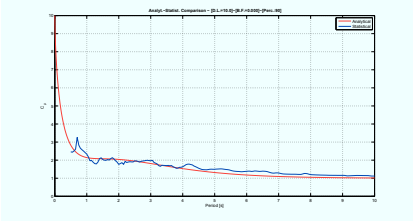

(f) *Bilinear Factor 0.0*

Figure 1.18: Comparison: Ductility Value equal 10 - Different Bilinear Factor

Comparison Analytical Curve Statistical Data - Ductility value 20

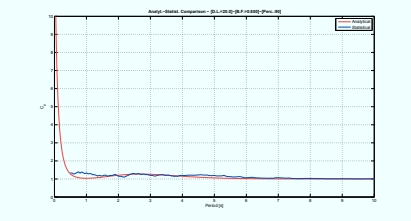

(a) *Bilinear Factor 0.8*

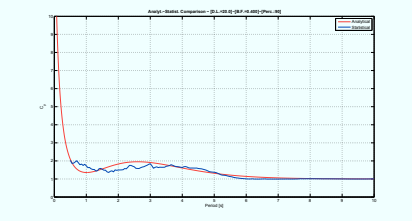

(b) *Bilinear Factor 0.4*

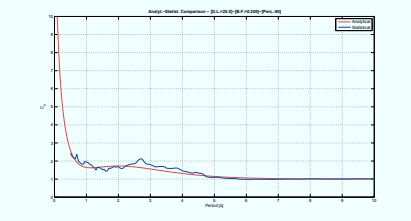

(c) *Bilinear Factor 0.2*

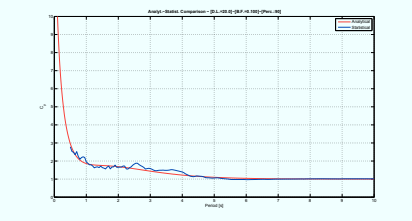

(d) *Bilinear Factor 0.1*

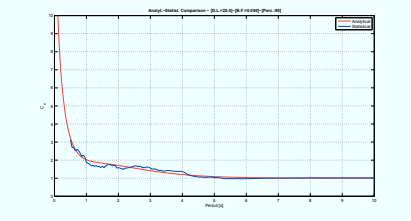

(e) *Bilinear Factor 0.05*

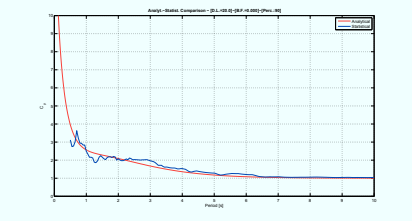

(f) *Bilinear Factor 0.0*

Figure 1.19: Comparison: Ductility Value equal 20 - Different Bilinear Factor

[1] [4]

Chapter 2

A Design Procedure for Structures equipped with Hysteretic Dampers

Contents

Preview

A DESIGN procedure for structural systems with hysteretic dampers is, in the following, presented. A key problem is the dependence of the system dynamic response from the considered earthquake. This dependence is largely influenced by a "compatibility" between the fundamental, excitation and structure, frequency content. In addition, a prediction of the frequency content of the design earthquake is, in general, not possible. A design procedure able to limit the amplitude response, whatever the excitation frequency content, is for that reason interesting. In the third chapter, based on the frequency response of bilinear single degree of freedom systems,a design procedures for system equipped with hysteretic dissipators, is presented.

2.1 Dynamic characteristics of hysteretic bilinear systems

An insight into the dynamic characteristics of structures equipped with hysteretic dampers can be gained by studying the steady-state response of an analogous non linear single-degree-of-freedom (SDOF) oscillator subjected to

harmonic excitation. This approach has been used extensively to characterize the behavior of nonlinear SDOF systems exhibiting various hysteretic models. Although seismic excitation has much broader frequency content than harmonic motion, it can be assumed that when a structure is excited by seismic loading, large portions of its response may be characterized by a quasi-resonant state at its effective fundamental period of vibration. The study carried out in this section is particularly useful in revealing the non dimensional parameters governing the response of a simple structure equipped with hysteretic dampers. By extension, these same parameters will be useful in developing a strategy for obtaining the load that activates the damper in order to minimize the seismic response of the structure, as discussed later in this chapter.

2.1.1 Frequency Response Analysis

The Steady-state response of a nonlinear single-degree-of-freedom system subjected to harmonic excitation

Steady-State Response Amplitude of SDOF System with Hysteretic Damper under Harmonic Base Excitation:
Closed-Form Frequency Response
T.K.CAUGHEY
Sinusoidal Excitation of a System with Bilinear Hysteresis,Journal of Applied Mechanics,27(4), 640 − 643, 1960

Essential Results

Posto

$$x_0 = \frac{F_{dy}}{k_d} \qquad x_{st} = \frac{x_{g0}\omega_g^2}{k_u} \qquad \sigma = \frac{\omega_g}{\omega_b}$$

$$u = 1 - \frac{k_u}{k_b} \qquad \vartheta^* = \cos^- 1\left[1 - \frac{2\left(\frac{x_0}{x_{st}}\right)}{\frac{A}{x_{st}}}\right] \qquad \bar{A} = \frac{A}{x_0}$$

segue

$$\sigma^2 = \begin{cases} 1 \pm \frac{x_{st}}{A} & \bar{A} \leq 1 \\ \frac{1}{\pi}\left[u\theta^* + (1-u)\pi - \frac{u}{2}\sin 2\vartheta^*\right] \pm \sqrt{\left(\frac{x_{st}}{A}\right)^2 - \left(\frac{u\sin^2\vartheta^*}{\pi}\right)^2} & \\ \bar{A} > 1 & \end{cases}$$

- The Activation load of the Hysteretic Damper for bounded response at resonance :

$$F_{dy} = \frac{\pi}{4} W \frac{a_{g0}}{g} \tag{2.1}$$

- The lateral load required to activate the Hysteretic Damper that minimizes the resonant amplitude

$$F_{dy} = \frac{\pi}{2} W \frac{a_{g0}}{g} \tag{2.2}$$

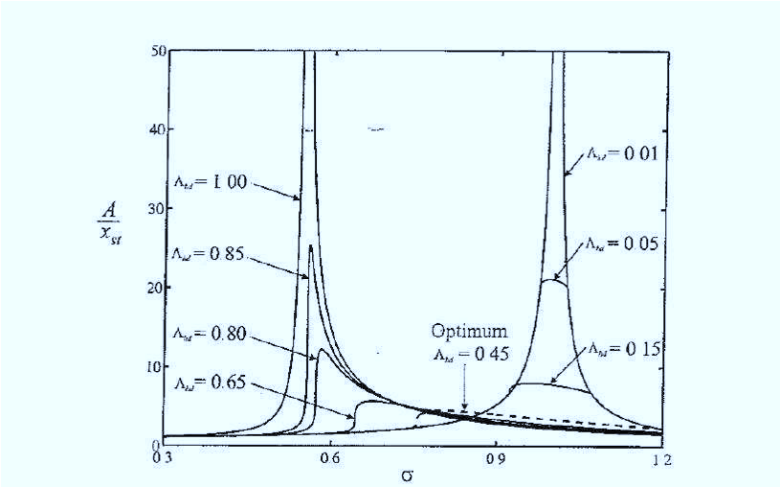

Figure 2.1: Steady-State Response Amplitude

- The Minimum resonant amplitude:

$$\frac{A^*}{x_{st}} = \frac{\pi k_b}{k_b - k_u} \tag{2.3}$$

- The frequency ratio σ_r^* at which this optimum resonance occurs:

$$F_{dy} = \frac{\pi}{2} W \frac{a_{g0}}{g} \tag{2.4}$$

starting from equation (2.3), and considering

$$x_{st} = \frac{x_{g0}\omega_g^2}{k_u} = \frac{a_{g0}}{k_u}\frac{W}{g}$$

because we have mass equal to W/g, and not unit mass, can be obtained

$$\boxed{k_d = \frac{1}{\frac{1}{\pi \frac{a_{g0}}{g}} \frac{A^*}{W} - \frac{1}{k_u}}} \tag{2.5}$$

2.1.2 Dampers stiffness influence on Resonant Amplitude

The amplitude variation of the resonant steady state response with the Stiffness ratio K_d/K_u, is next investigated. From Eq. (2.3) is obtained

$$A^* = \pi \frac{a_{g0}}{g} W \left(\frac{1}{K_d} + \frac{1}{K_u} \right) \tag{2.6}$$

or

$$\frac{A^*}{x_{st}} = \pi \left(1 + \frac{K_u}{K_d} \right) \tag{2.7}$$

2.2 Design Procedure for Bilinear Systems

2.2.1 Design Procedure for SDF Systems

Design of the dissipative System

The response *Optimization* of an hysteretic system, modeled as a generalized bilinear single degree of freedom system under earthquake excitations will be next considered. Ai fini della suddetta ottimizzazione l' input da considerare sarebbe una famiglia di terremoti di progetto da considerare in forma statistica. In particular, the design of the dissipative system is achieved minimizing the resonant steady state response under sinusoidal excitation. Therefore will be assumed an unknown exciting frequency, and the overall system will be designed in order to minimize the response related to the binding frequency content or, in other words, in a way to minimize the resonant response.

Starting point, in the design, will be considered the stiffness of the unbraced structure (K_u), stiffness related only to post tensioned strands which have to guarantee at least the structural stability under service loads,in absence of extreme excitation as wind and earthquake. Therefore the unbraced stiffness can be determined with the traditional design procedures.

In addition to the mentioned system a dissipative system will be added which will increased the system stiffness for frequent excitation, reducing absolute and relative displacements, and will provided dissipative capacity in presence of more extreme actions, as rare seismic actions.

Basically, the optimization procedure is achieved determining the optimal combination of the system stiffness related to the hysteretic dissipators (K_d) and to the global force which activates the dissipators (F_y). This combination, fixed the unbraced stiffness (K_u), will minimize the structural response.

The basic results are next summarized:

$$\tilde{f}_{dy} = \frac{F_{dy}}{W\frac{a_{g0}}{g}} \geq \frac{\pi}{4}$$

$$\tilde{f}^*_{dy} = \frac{\pi}{2}$$

$$\frac{A}{x_{g0}} = \frac{\pi}{\left(\frac{\omega_g^2}{\omega_b^2}\right)\left(1-\frac{\omega_u^2}{\omega_b^2}\right)}$$

$$\left(\frac{\omega_g}{\omega_b}\right)^2 = \frac{1}{2}\left(1+\frac{\omega_u}{\omega_b}\right)$$

$$\omega_g^2 = \frac{g}{2}\frac{k_b}{W}$$

$$A_t^* = \pi\frac{W}{k_d}\frac{a_{g0}}{g}$$

$$k_d = \pi\frac{W}{A_t}\frac{a_{g0}}{g}$$

$$k_b = k_u + k_d$$

$$\omega_g^2 = \frac{g}{2}\frac{k_b}{W}\left(1+\sqrt{\frac{k_u}{k_b}}\right)$$

[2], [3] [1] [5]

Chapter 3

Cyclic Axial Response tested on mild A 706 and Stainless Steel Bars including Inelastic Buckling Effects

Contents

3.1 Tensile and cyclic axial load tests of mild and stainless reinforcing bars including inelastic buckling effects

3.1.1 Introduction

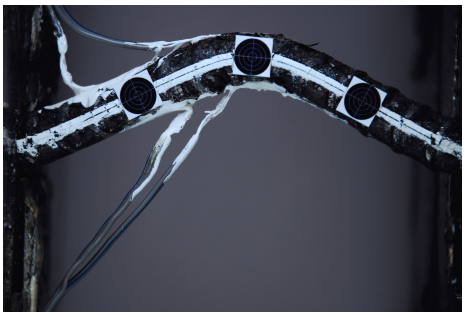

Figure 3.1: Inelastic Buckling, Overview

This section summarizes a number of tensile and cyclic axial load tests were conducted to obtain data for two types of reinforcing steel. Test samples were short, slender or moderately slender. The slenderness of the bars was used to obtain the effect of nonlinear geometry on the cyclic response of bars. Reinforcing bars are used as reinforcement in concrete structures. Some of these bars will experience large inelastic reversals during earthquakes. For this reason, the hysteretic response of the bars needs to be assessed. The bars tested had 0.5 inches in diameter. Grade 60 ASTM A706 Low-Alloy Steel and Grade 75 Stainless Steel Type 316LN bars were tested. ASTM A706 Low-Alloy Steel bars are widely used in construction of structures in seismic regions. Longitudinal reinforcing steel is provided in columns and beams where it can be used to dissipate energy by undergoing to large cyclic tensile and compressive strains. Transverse reinforcement is place around these bars to brace them and prevent premature bar buckling. When the tie spacing is large, bars can easily buckle and fracture prematurely, jeopardizing the stability of the structural member. Stainless Steel Type 316LN bars were also investigated because they have been proposed as reinforcement for emerging structural systems. These bars do not experience corrosion and have very high ductility, but their hysteretic response is largely unknown.

A tensile test also known as tension test was performed on ASTM A706 low alloy steel and 316 LN stainless steel bars. All the bars considered in this work have diameter equal to 0.5 inch. Fundamentally, the tensile tests provide ultimate strength (f_u), yield strength (f_y), ultimate strain (ε_u) and Young's Modulus of the materials. The cyclic test was performed on the bars by applying the axial compression and tension load sequentially. Once the bars reached to the yielding point, the bar behavior became non-linear and the result was a hysteretic energy dissipation which was transform from the internal friction that produce heat due to the cyclic test.

Table 3.1: ASTM A706 Low-Alloy Steel

Characteristics	Value
Minimum Yield Strength	60,000 psi
Maximum Yield Strength	78,000 psi
Minimum Tensile Strength	80,000 psi
Tensile Strength	1.25· Actual Yield Strength
Young's Modulus (E)	29200 ksi ($200 \cdot 10^6$ kN/m^2)

Table 3.2: Stainless Steel Type 316LN

Characteristics	Value
Yield Tensile Strength	73,090 psi
Ultimate Tensile Strength	112,590 psi
Elongation	25.63%
Corrosion	ASTM A 262 practice E

3.1.2 Typical mechanical properties of materials

ASTM A706 Low-Alloy Steel

ASTM A706 Low-Alloy Steel: Standard Specification for Low-Alloy Steel Deformed and Plain Bars for Concrete Reinforcement. This specification covers bars intended for special applications where weldability, bendability, or ductility is important.2 The A 706 specification required a larger elongation at failure and a more stringent bend test than A 615.2 A 706 limits the amounts of carbon, manganese, phosphorus, sulfur and silicon and limits the carbon percent.2 These bars are available in size 3 through 18 in Grade 60.2 The upper yield strengths of 80ksi (440Mpa) and the lower limit on the yield strength is 60 ksi (414 Mpa).

Stainless Steel 316LN

EnduraMet 316LN stainless is a nitrogen-strengthened version of Type 316L stainless. By means of solid solution strengthening, the nitrogen provides significantly higher yield and tensile strength as annealed than Type 316L without adversely affecting ductility, corrosion resistance or non0magnetic properties. In the hot rolled unannealed condition, yield strengths of 75ksi (518 MPa) or higher can be achieved for bar diameter up to 1.375 in (34.925 mm)

Mill cert for the stainless steel reinforcing bars:

Table 3.3: Strain History 1, d/b 3

Start or Reversal Point	Strain (%)
0	0.00
1	0.12
2	-0.12
3	0.14
4	-0.14
5	0.00
6	1.00
7	-0.60
8	2.00
9	-0.60
10	3.00
11	-0.60
12	unload - stop

3.1.3 Strain and Displacement History details

Note: average of two diametrically opposite strain gauges

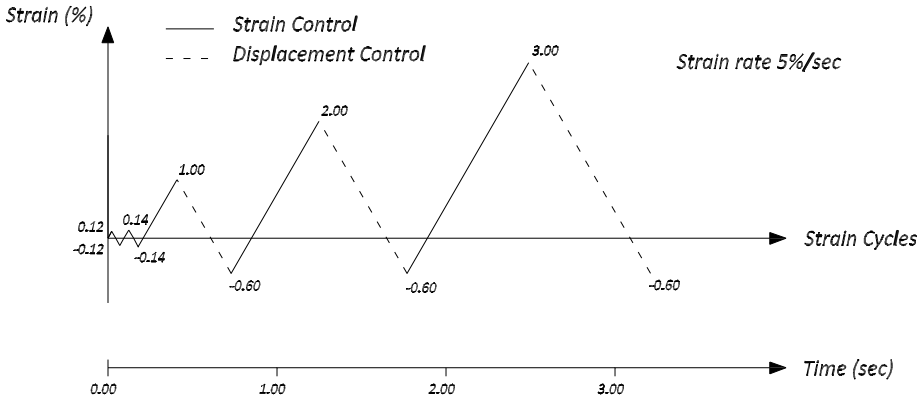

Figure 3.2: Strain History 1, d/b=3

Table 3.4: Strain History 1, d/b 6

Start or Reversal Point	Strain (%)	Displ. (mm)	Control
0	0.00		Strain control from this point on
1	0.12		
2	-0.12		
3	0.14		
4	-0.14		
5	0.00		
6	1.00		Displ. control from this point on
7		-0.457	Strain control from this point on
8	2.00		Displ. control from this point on
9		-0.457	Strain control from this point on
10	3.00		Displ. control from this point on
11	-0.457		Strain control from this point on
12	unload - stop		

Table 3.5: Strain History 1, d/b 9

Start or Reversal Point	Strain (%)	Displ. (mm)	Control
0	0.00		Strain control from this point on
1	0.12		
2	-0.12		
3	0.14		
4	-0.14		
5	0.00		
6	1.00		Displ. control from this point on
7		-0.686	Strain control from this point on
8	2.00		Displ. control from this point on
9		-0.686	Strain control from this point on
10	3.00		Displ. control from this point on
11		-0.686	Strain control from this point on
12	unload - stop		

Table 3.6: Strain History 2, d/b 3

Start or Reversal Point	Strain (%)
0	0.00
1	0.12
2	-0.12
3	0.14
4	-0.14
5	0.00
6	-0.60
7	-0.10
8	-0.30
9	-0.16
10	-0.30
11	-0.14
12	-0.28
13	-0.16
14	-0.36
15	0.24
16	0.04
17	0.80
18	-0.60
19	0.80
20	0.50
21	0.76
22	0.70
23	1.60
24	1.00
25	1.40
26	1.20
27	1.30
28	0.00
29	2.60
30	1.00
31	2.50
32	1.30
33	2.40
34	2.20
35	3.00
36	-1.00
37	1.00
38	0.00
39	3.40
40	unload - stop

Table 3.7: Strain History 2, d/b 6

Start or Reversal Point	Strain (%)	Displ. (mm)	Control
0	0.00		Strain control from this point on
1	0.12		
2	-0.12		
3	0.14		
4	-0.14		
5	0.00		Displ. control from this point on
6		-0.457	Strain control from this point on
7	-0.10		
8	-0.30		
9	-0.16		
10	-0.30		
11	-0.14		
12	-0.28		
13	-0.16		
14	-0.36		
15	0.24		
16	0.04		
17	0.80		Displ. control from this point on
18		-0.457	Strain control from this point on
19	0.80		
20	0.50		
21	0.76		
22	0.70		
23	1.60		
24	1.00		
25	1.40		
26	1.20		
27	1.30		Displ. control from this point on
28		0.000	Strain control from this point on
29	2.60		Displ. control from this point on
30		0.000	Strain control from this point on
31	2.50		Displ. control from this point on
32		0.000	Strain control from this point on
33	2.40		
34	2.20		
35	3.00		Displ. control from this point on
36	-1.00	-0.762	Strain control from this point on
37	1.00		
38	0.00	0.000	Displ. control from this point on
39	3.40		Strain control from this point on
40	unload - stop		

Table 3.8: Strain History 2, d/b 9

Start or Reversal Point	Strain (%)	Displ. (mm)	Control
0	0.00		Strain control from this point on
1	0.12		
2	-0.12		
3	0.14		
4	-0.14		
5	0.00		Displ. control from this point on
6		-0.686	Strain control from this point on
7	-0.10		
8	-0.30		
9	-0.16		
10	-0.30		
11	-0.14		
12	-0.28		
13	-0.16		
14	-0.36		
15	0.24		
16	0.04		
17	0.80		Displ. control from this point on
18		-0.686	Strain control from this point on
19	0.80		
20	0.50		
21	0.76		
22	0.70		
23	1.60		
24	1.00		
25	1.40		
26	1.20		
27	1.30		Displ. control from this point on
28		0.000	Strain control from this point on
29	2.60		Displ. control from this point on
30		0.000	Strain control from this point on
31	2.50		Displ. control from this point on
32		0.000	Strain control from this point on
33	2.40		
34	2.20		
35	3.00		Displ. control from this point on
36	-1.00	-1.143	Strain control from this point on
37	1.00		
38	0.00	0.000	Displ. control from this point on
39	3.40		Strain control from this point on
40	unload - stop		

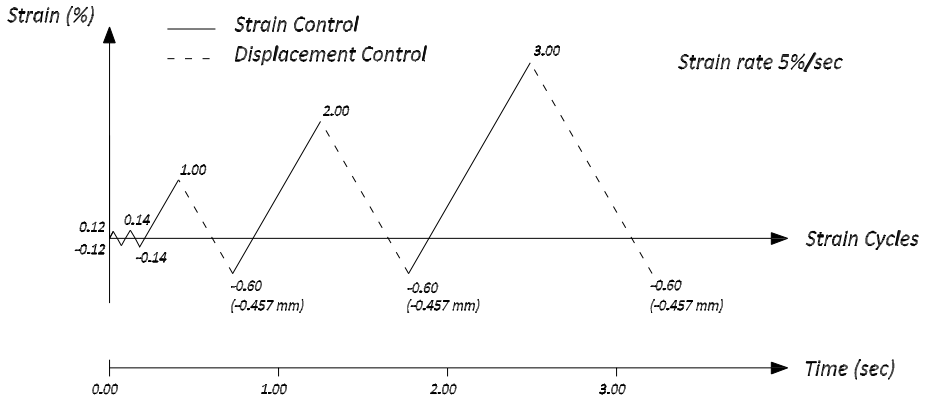

Figure 3.3: Strain History 1, d/b=6

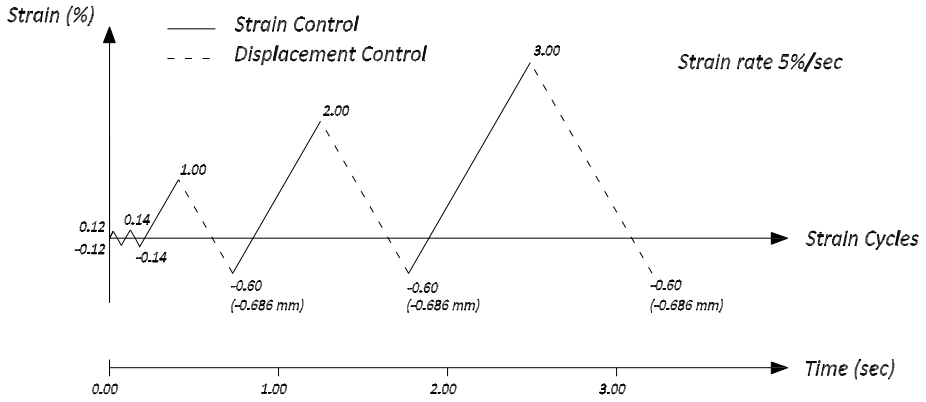

Figure 3.4: Strain History 1, d/b=9

3.1.4 Test Samples

In this 12 short steel bars were tested which consist of eight ASTM A706 low alloy steel bars and four 316 LN stainless steel bars. There were two 8.5 inches length, two 10 inches length, and three 11.5inches length of ASTM A706 low alloy steel bars and three 11.5inches length of 316 LN stainless steel bars are tested under various cyclic tests. The cyclic test was realized considering different time history with different test length of the materials which the detail data of the testing can be seen in (Table 1 and Table 2)

The test sample is constituted by 12 elements, eight of them are made by ASTM A706 Low Alloy Steel and four are made by Stainless Steel Type 316LN.

Three elements with length equal to 8.5 in, which are subjected to cyclic axial load test, and one with length equal to 17, which is subjected to tensile test, are included in the Stainless Steel test sample. Two elements with length

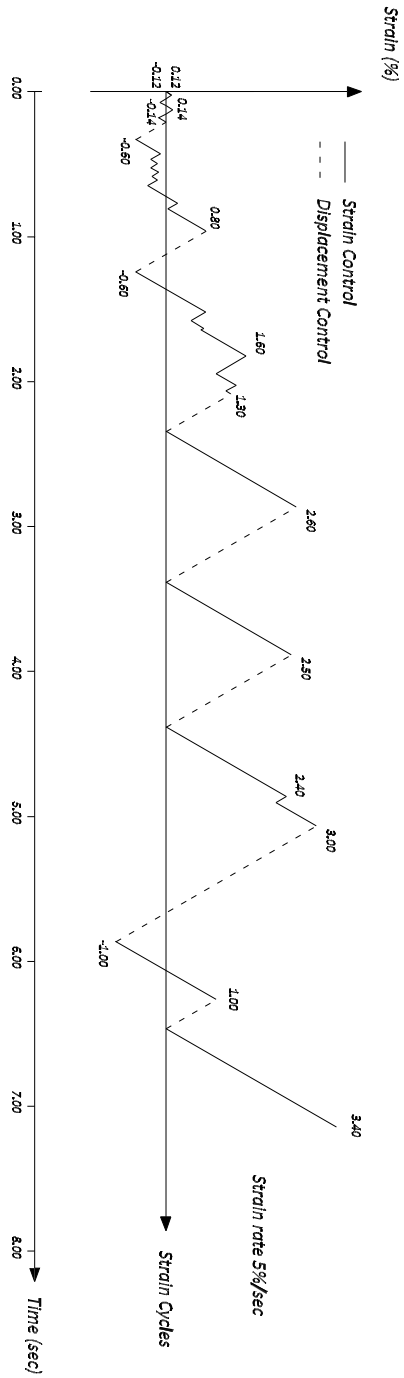

Figure 3.5: Strain History 2, d/b=3

equal to 8.5 in, two elements with length equal to 10.0 in, three elements with length equal to 11.5 in, which are subjected to cyclic axial load test, and one with length equal to 17, which is subjected to tensile test, are included in the

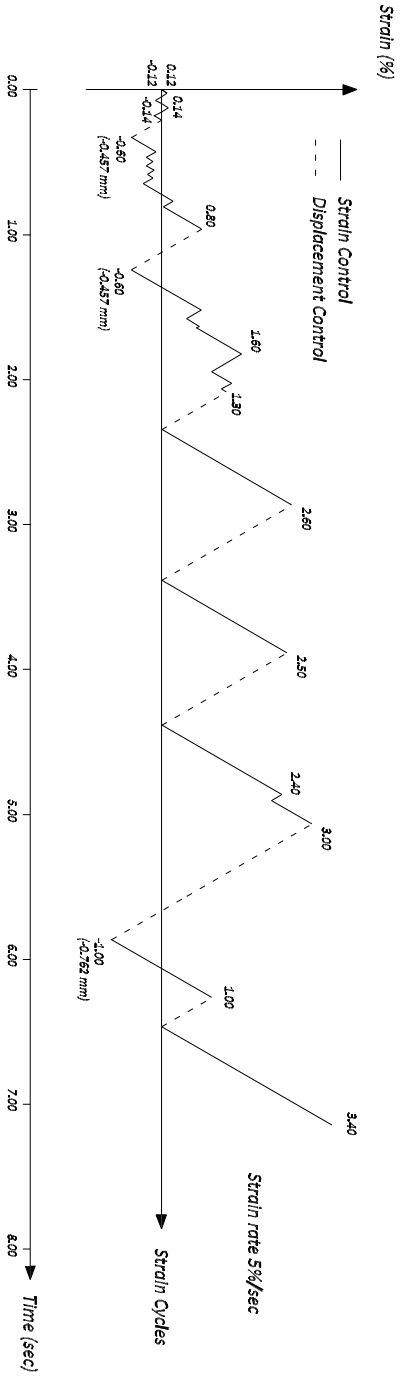

Figure 3.6: Strain History 2, d/b=6

Low Alloy Steel.

In particular, Test 3 (equal to Test 10) is considered, to setup the cyclic axial test procedure.

Table 3.9: Test Overview

Test	Bar Type	Test length (in)	Test History
1	A706	17.0	Standard tensile test
2	316LN	17.0	Standard tensile test
3	A706	11.5	Time History 3
4	A706	8.5	Time History 1
5	A706	8.5	Time History 4
6	316LN	8.5	Time History 1
7	316LN	8.5	Time History 4
8	316LN	8.5	Time History DSC Test
9	A706	10.0	Time History 2
10	A706	11.5	Time History 3
11	A706	10.0	Time History 5
12	A706	11.5	Time History 6

Table 3.10: Test Samples: Grip and Test length

Test Series	Grip End (in)	Test Length (in)	Total Length (in)
Series 1	3.5	1.5	8.5
Series 2	3.5	3.0	10.0
Series 3	3.5	4.5	11.5
Series 4	3.5	10.0	17.0

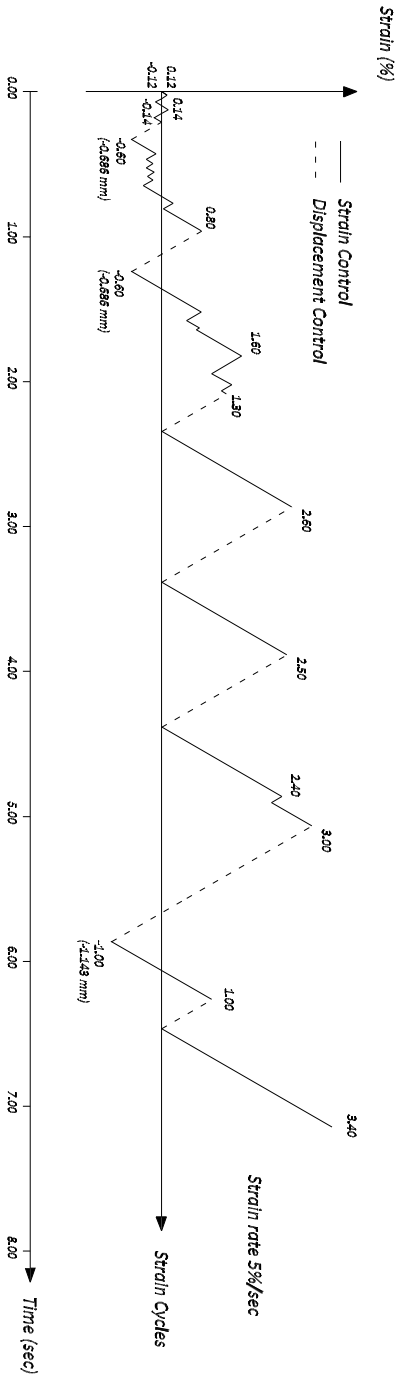

Figure 3.7: Strain History 2, d/b=9

3.2 Test Description

3.2.1 Tensile test Description

The following steps for the tensile test are considered:

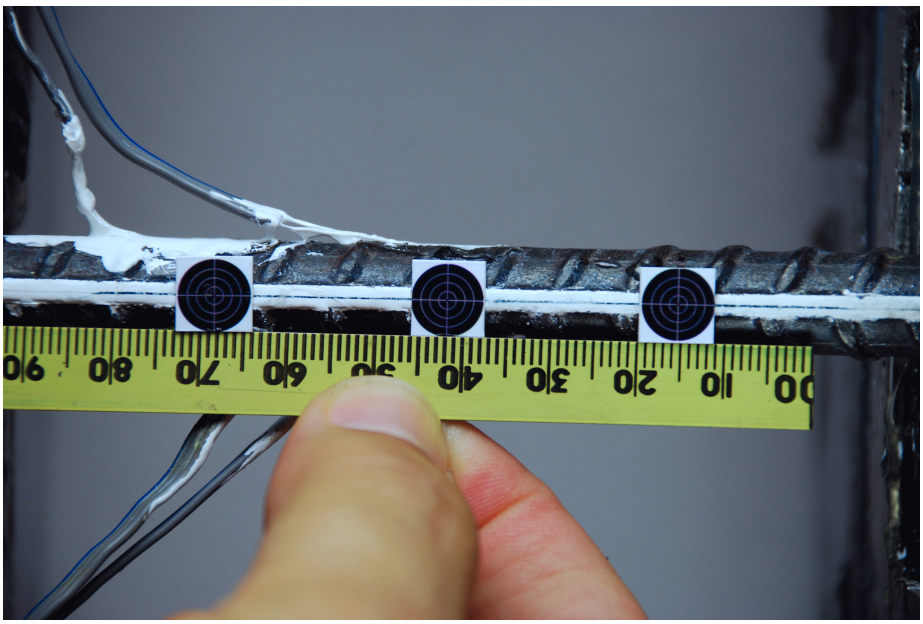

Figure 3.8: Test Sample, 9db

- Using a micrometer to 0.01 mm resolution, measure the diameter of bar between the longitudinal ribs at 3 different locations in the test length.
- Mark a line with a scriber where the measurement will take place.
- Measure longitudinal strains with an extensometer
- Remove the bar once the tensile load reaches 85 % of the peak load recorded
- Measure again the bar diameters

3.2.2 Test sample instrumentation: Strain gauges application procedure

The following steps for the cyclic test are considered:

- Clean all the steel bar with the metal brush
- Grind the rebar to remove the mill on the outside of the rebar
- Roughen up the surface to create a stronger bond by sanding the rebar
- Use a ball point pen and mark the exact location of the gauge
- Use the methyl ethyl ketone (MEK) with cotton ball to clean up the surface of the bar
- Tape two strain gauges with the metal side up to each steel bar and fasten the strain gauges wires

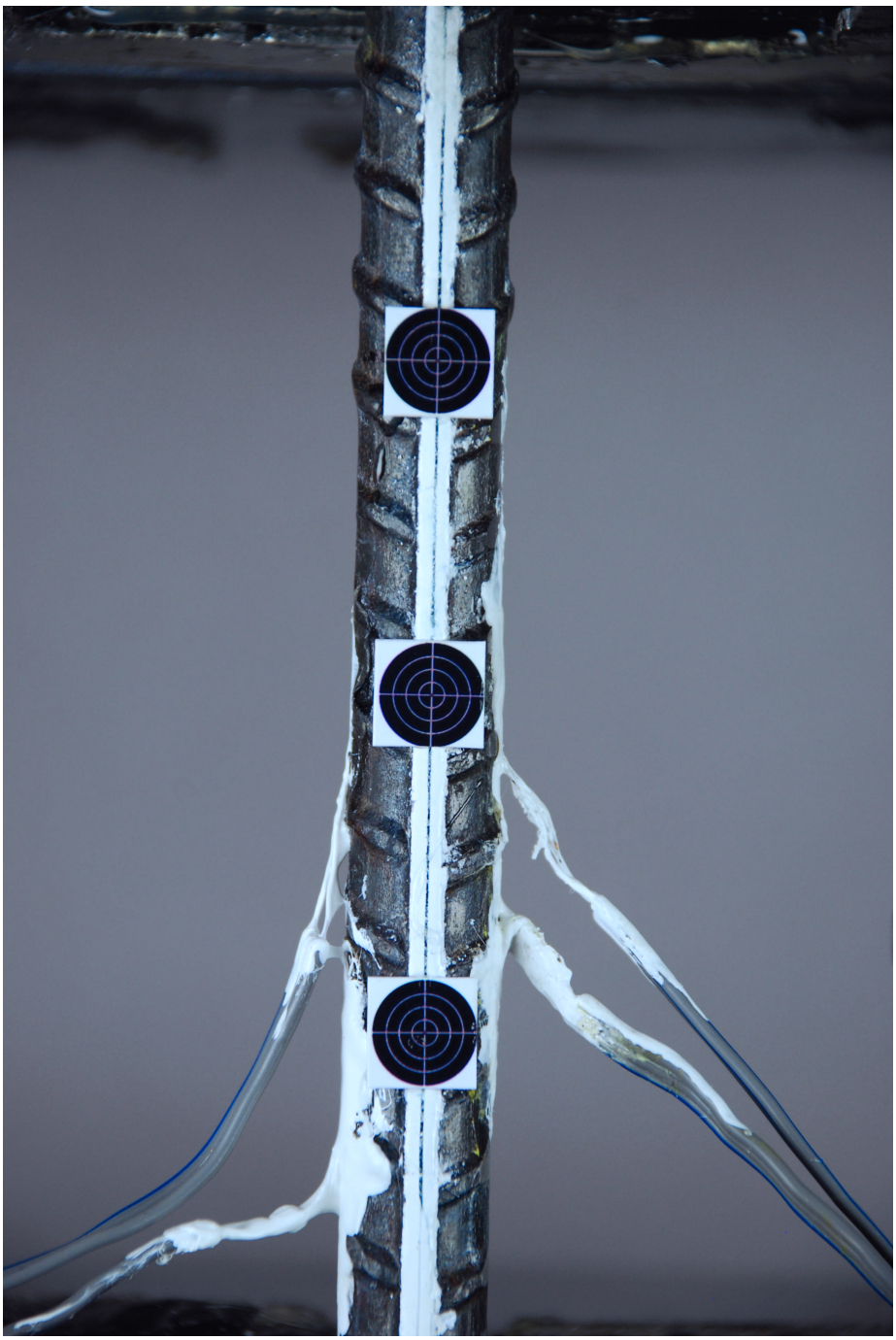

Figure 3.9: Test Sample, 9 db

- Apply cyanoacrylate to the strain gauge after lifting up the tape and hold down the gauge for 2-3 minutes
- Use the dental tool to lift up the metal wires so that there is no direct

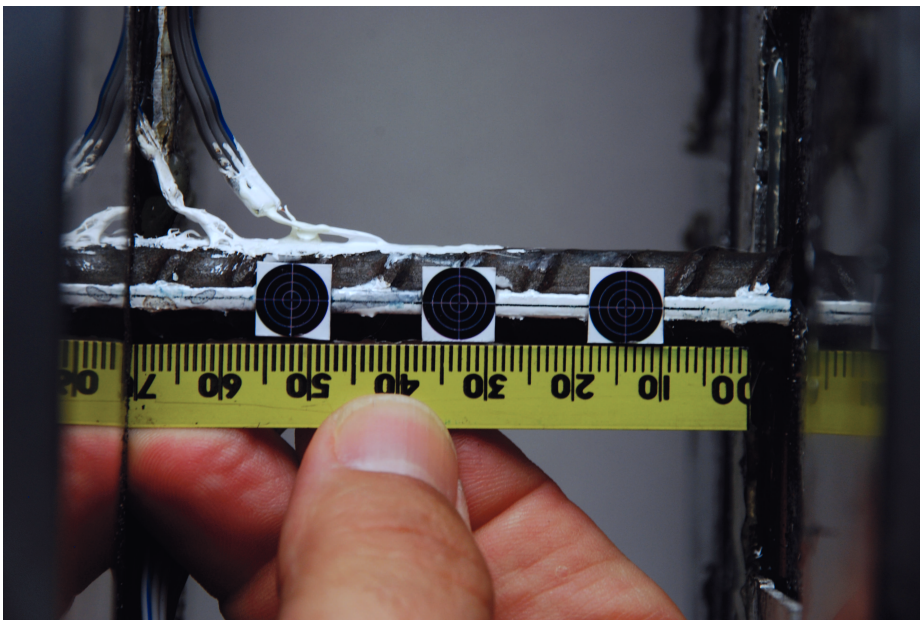

Figure 3.10: Test Sample, 6 db

Table 3.11: Test Samples Instrumentation

Test Series	S.G.	Where?	Linear pots	Clip G.	Ex. Buckling
Series 1	2	1/2 test length	None	No	No
Series 2	2	1/4 test length	Yes	No	V. limited
Series 3	2	1/4 test length	Yes	No	Yes
Series 4	None		None	Yes	No

contact between the gauge and the bar

- Apply 3 cost of M-coat for every 30 minutes on the gauges and wait over to have complete cure
- Test the voltage with digital multimeter (DMM) device across the strain gauge wires and across the steel bar and the wires for conductivity
- Apply the whiteout and draw a straight line on to the steel bar to assist in visual testing
- Clean the excess materials paint on the steel bar with the alcohol

The details of the strain history diagram is shown in figure 10 in appendix

3.2.3 Cyclic Test description

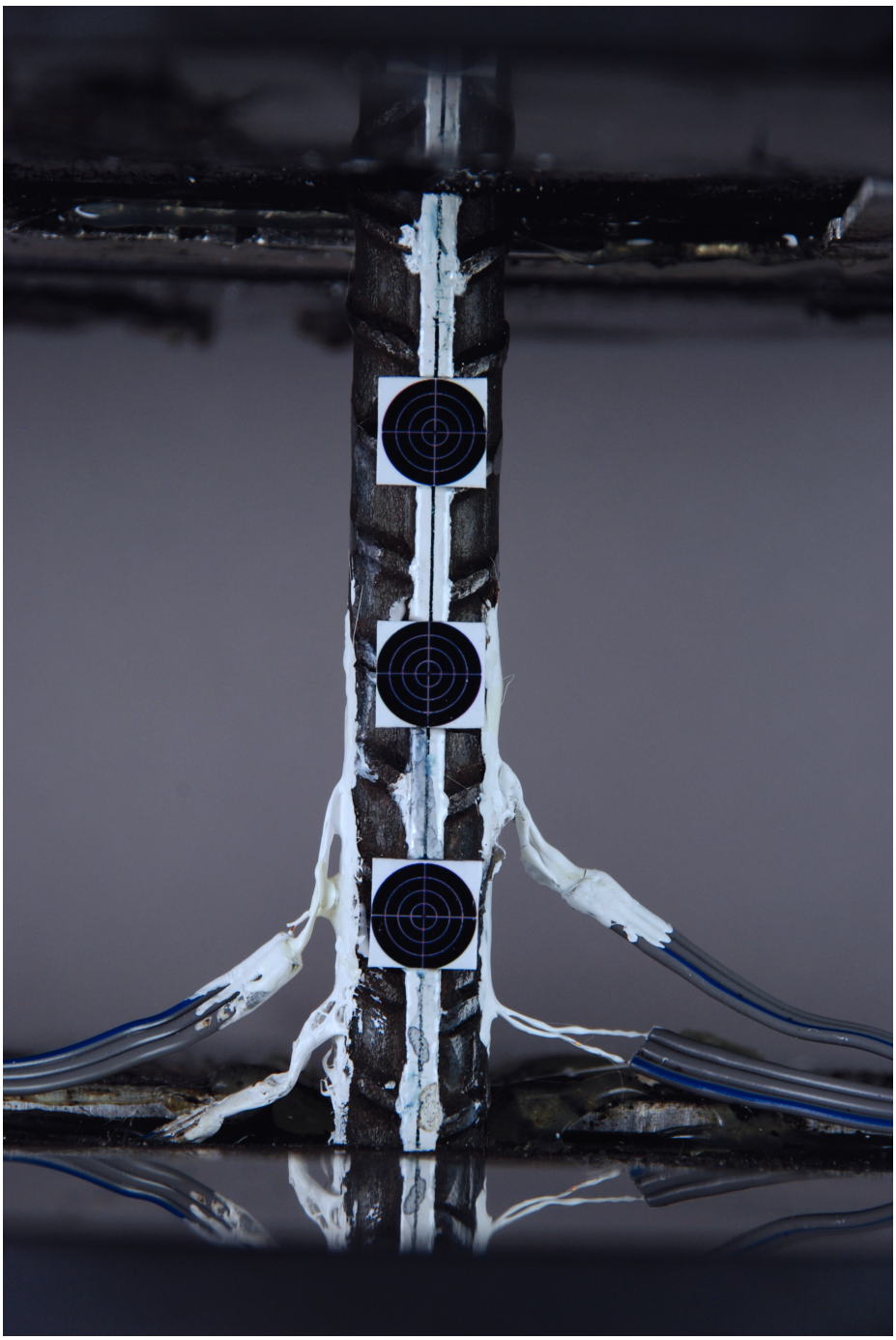

Figure 3.11: Test Sample, 6 db

3.3 Tensile Test Results

After the tensile test, the result of the axial displacement (inch), axial strain (in/in), axial force (lbf), time (sec), and axial stress (psi) was gathered. The

Figure 3.12: Micrometer

yielding point of the A706 steel bar occurred when strain is $\epsilon_y = 0.003$ and stress $f_y = 73.6$ ksi. The yielding point of the stainless steel bar occurred when strain is ?y=0.02 and stress fy=120 ksi. Plot the result of the strain (x-axis) vs. stress (y-axis) in excel and the plot of the A706 steel is shown in (figure 3) and the stainless steel in (figure 4).

Inserisci qui i risultati delle prove a trazione su A706 and Stainless Steel

Stainless - A706 Steel Comparison

Figure 3.13: A706 steel test sample, 9 db

3.4 Cyclic Axial Load tests Results

After the cyclic test, the result of the strain (in/in), pot1 (in), pot1 (in) and axial AVGPots (in) was gathered and plot the result of the strain (x-axial) and

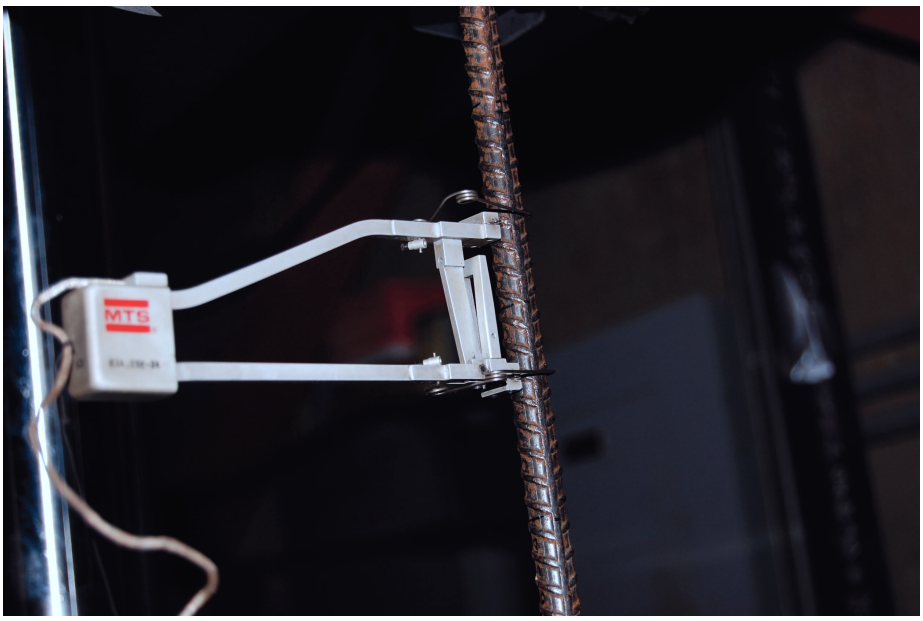

Figure 3.14: A706 steel test sample rupture

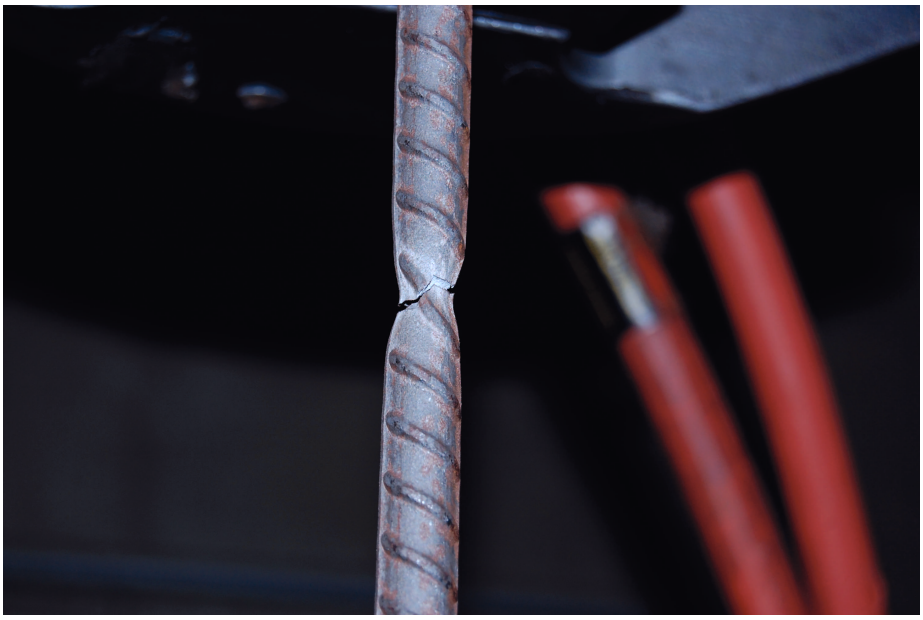

Figure 3.15: A706 steel test sample rupture

stress(y-axial) of the hysteretic response of A076 steel bar in figure (5) and for 316LN stainless steel bar in figure (6).These two figures compare the cyclic load behavior of ASTM A706 and 316 LN reinforce steel. A706 is well known to be excellence reinforcement for earthquake resistance structures. it dissipate good energy and it is stable. 316LN bar is unknown because hysteretic response was

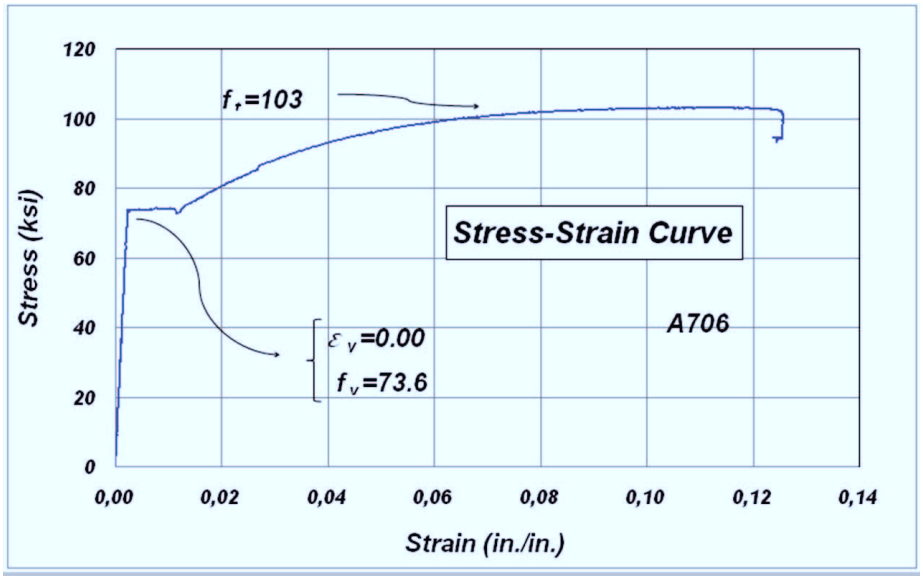

Figure 3.16: A706 steel

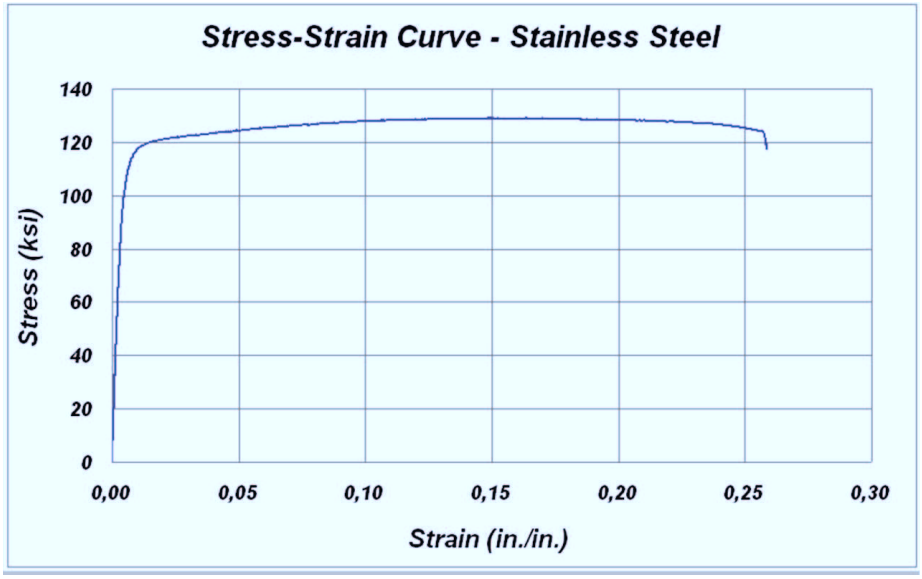

Figure 3.17: S steel

never been tested before. From these figures, one can see that both A706 steel bars and 316LN stainless steel bars experience very similar hysteretic response.

The cyclic test was performed on the rebar by applying the axial compression and tension load sequentially with the different test grip length and the details are shown in (figure 1 and figure 2). Once the rebar reached to the yielding point, the rebar behavior became non-linear and the result is a hysteretic energy dissipation which is equal to the area inside the loop. The instrumentation of

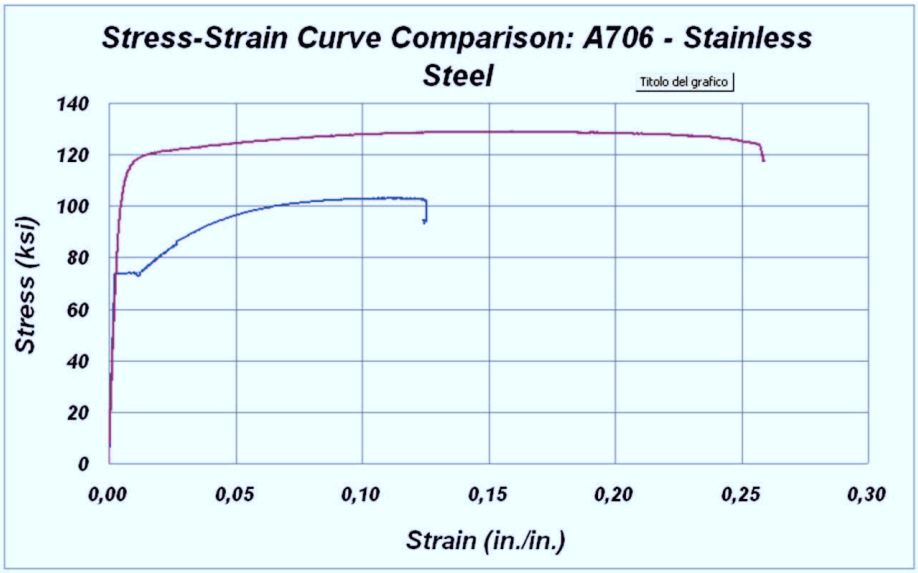

Figure 3.18: Tensile test comparison

the test samples for the different set series are also shown in table 3.

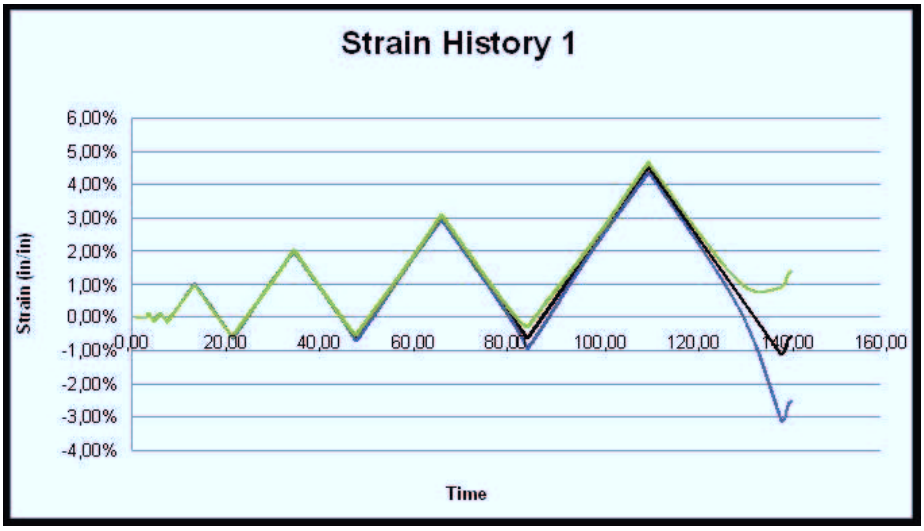

Figure 3.19: Strain History 1, 3db, Stainless

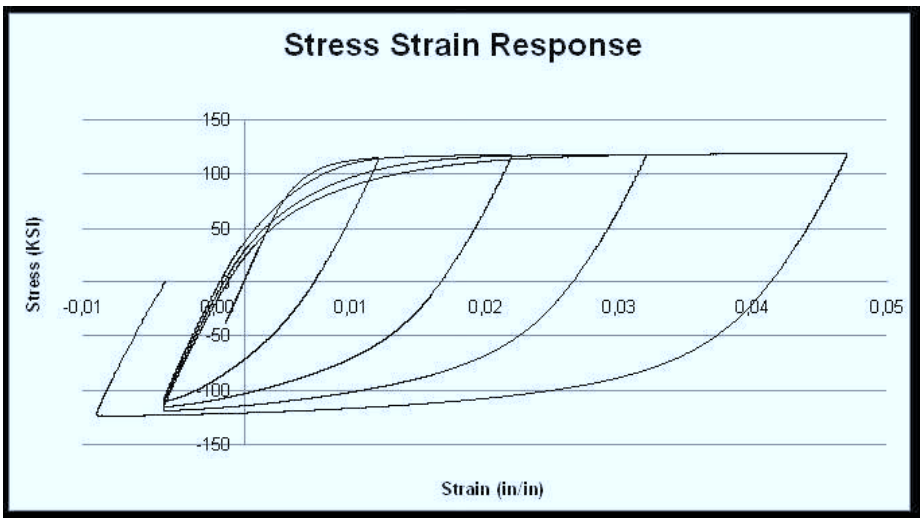

Figure 3.20: Stress-Strain response, 3db, Stainless, SH1

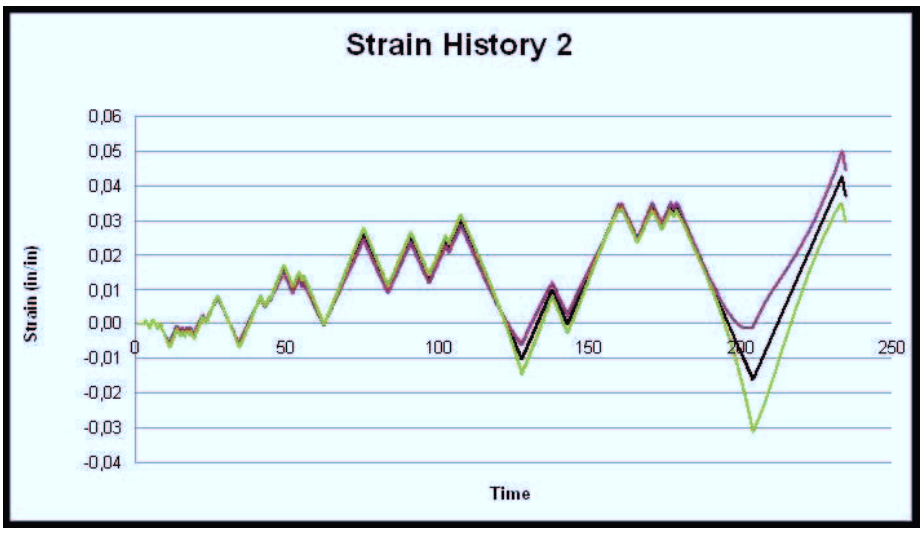

Figure 3.21: Strain History 2, 3db, Stainless

9 db A706 Steel short bars

3.4.1 Comments

The result from the tensile and cyclic testing was verified from the theoretical knowledge that learned from the structural engineering classes. In the tensile test plot, the curve of the strain vs. stress also shows the elastics and plastic deformation of the material. The yielding point of the A706 steel bar occurred when strain is $\varepsilon_y = 0.003$ and stress $f_y = 73.6ksi$. The yielding point of the stainless steel bar occurred when strain is $\varepsilon_y = 0.02$ and stress $f_y = 120ksi$. These two figures (figure 5 and figure 6) compare the cyclic load behavior of ASTM A706 and 316 LN reinforce steel tested before. From these figures, one

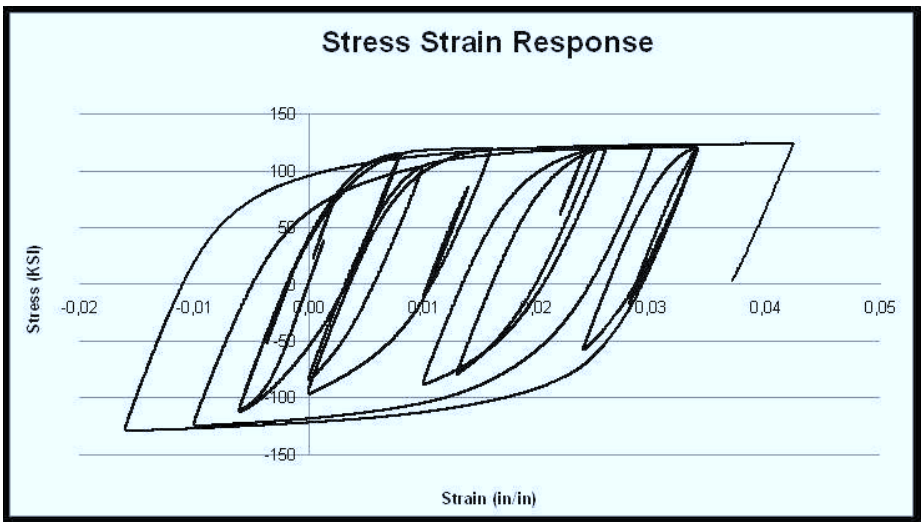

Figure 3.22: Stress-Strain response, 3db, Stainless, SH2

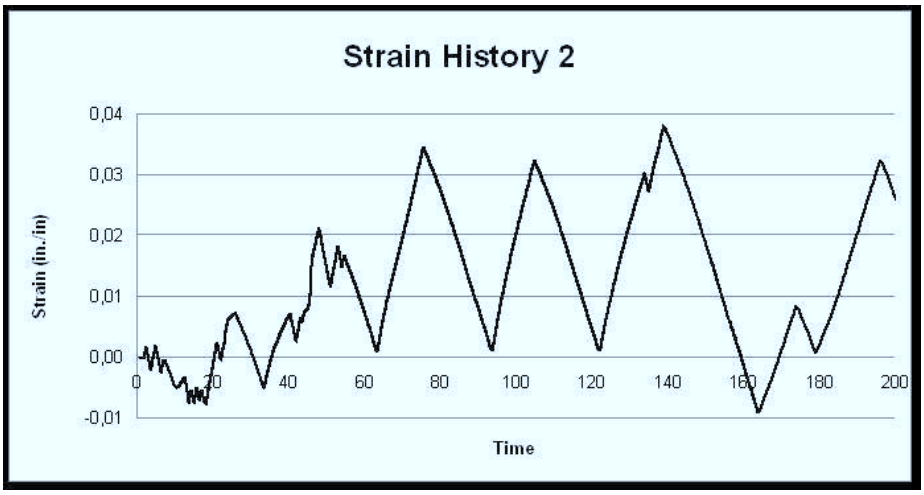

Figure 3.23: Strain History 2, 6db, A706

can see that both A706 steel bars and 316LN stainless steel bars experience very similar hysteretic response. For this reason, one can conclude that 316LN stainless steel reinforcement is acceptable to use in earthquake engineering design of reinforced concrete structures.

3.5 Conclusions

These tests explore the cyclic load behavior of reinforcement A706 steel bar which is well known and 316LN stainless steel bar which is unknown and the cyclic load behavior has not been tested before. Testing was carried out in the universal testing machine, the bars were instrumented and data was obtained

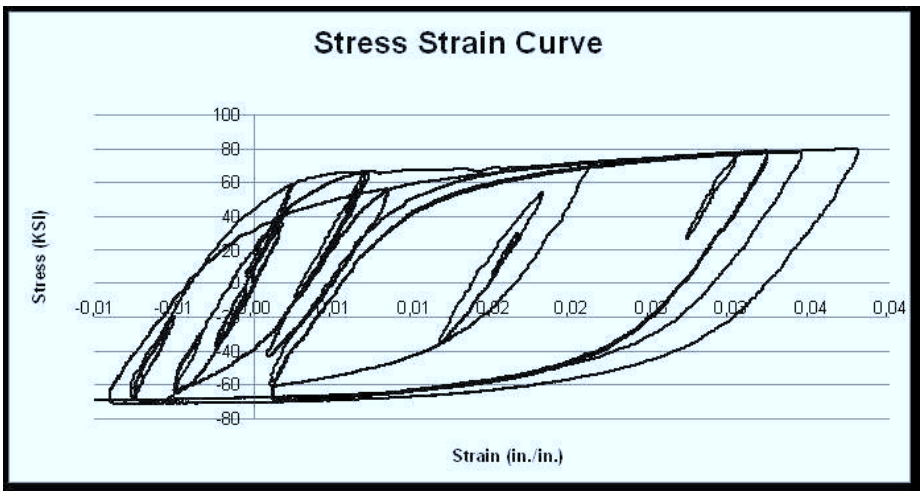

Figure 3.24: Stress-Strain response, 6db, A706, SH2

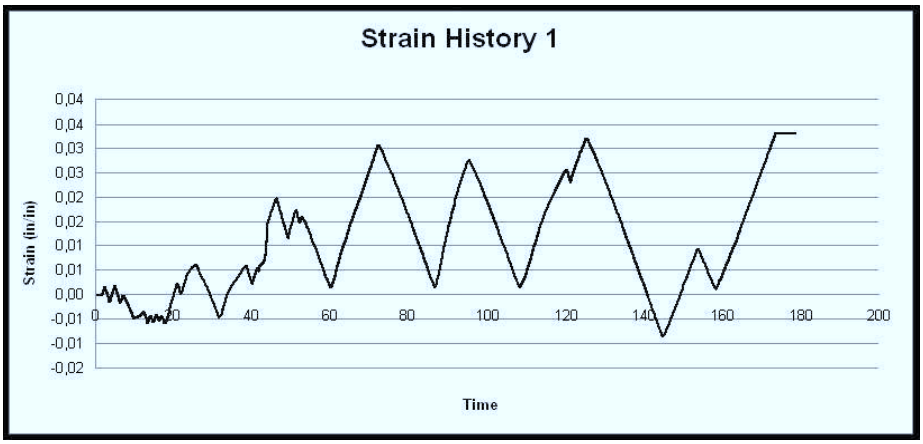

Figure 3.25: Strain History 1, 9db, A706

by monotonic as well as the cyclic load response. From the test data, one can conclude that 316LN stainless steel has very similar hysteretic response as A706steel bar. For this reason, 316LN stainless steel could be recommended for used in reinforcement earthquake resistance.

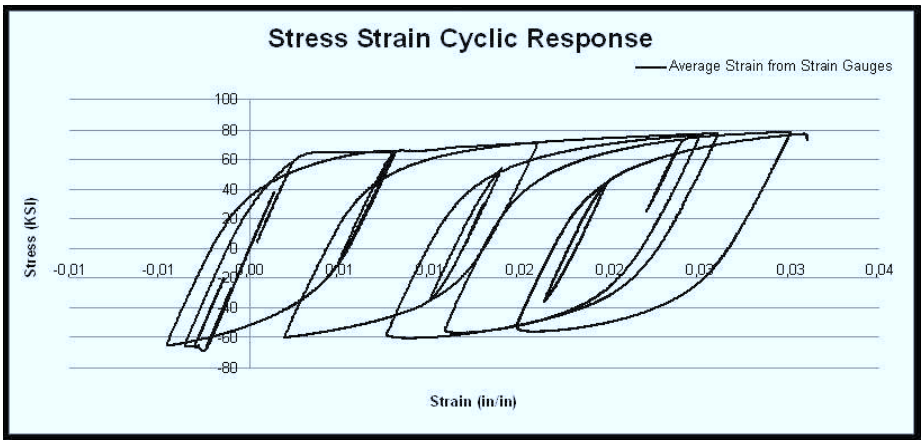

Figure 3.26: Strain History 1, 9db, A706

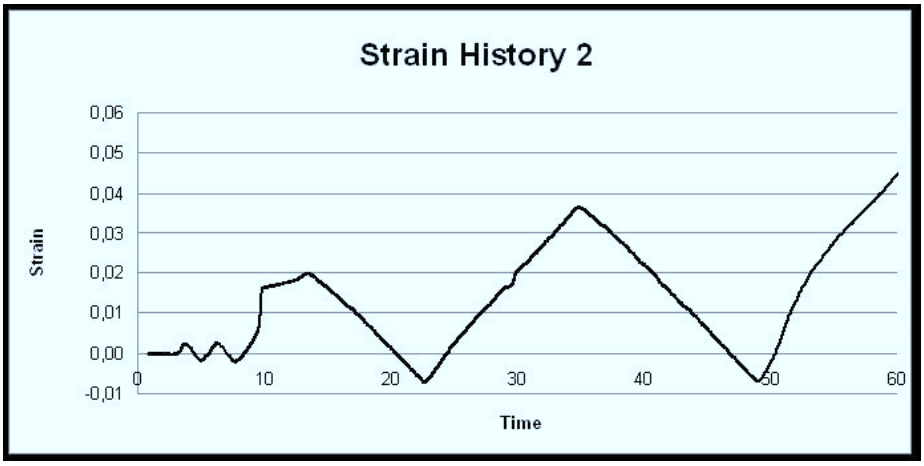

Figure 3.27: Stress-Strain response, 9db, A706, SH1

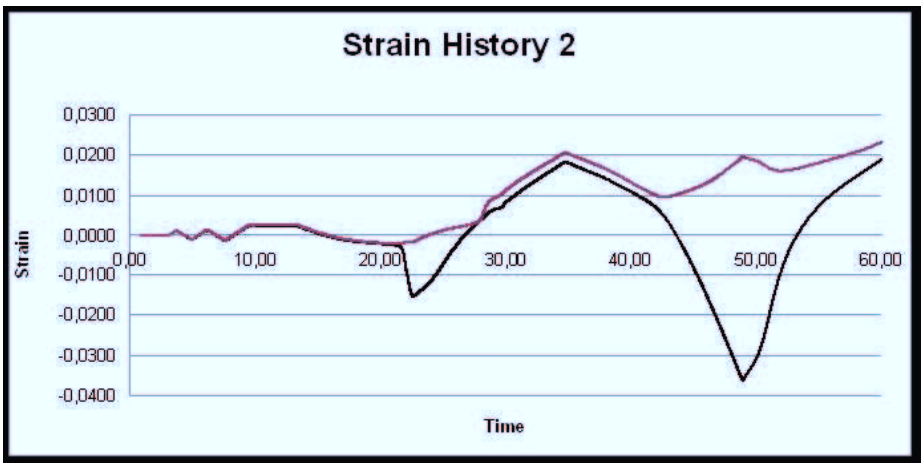

Figure 3.28: Strain History 2, 9db, A706

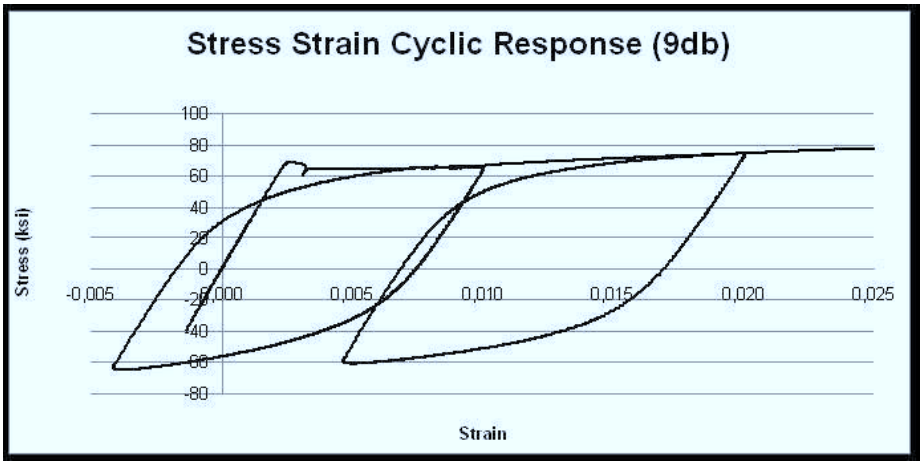

Figure 3.29: Stress-Strain response, 9db, A706, SH1

Part II

Development of Elementary Innovative Systems

PART II

Preview

THE second part of the thesis deals with the static and kinematic characterization of three elementary systems. All the introduced systems can be considered generalized single degree of freedom systems. The essential parameters that influence the static and dynamic response of these systems are identified, and the relations governing the response are evaluated.

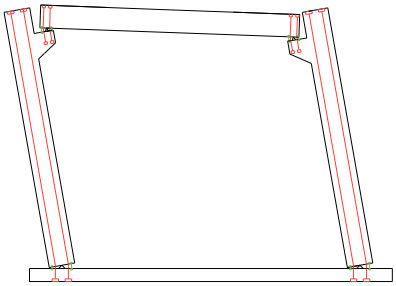

In more details, the first chapter moves from the static and kinematic characterization of a new connection at local level to the characterization at global level of a particular system, where the same connection is introduced. The connection is obtained introducing in hinged connections, beam-column and column-foundation, dissipators and post-tensioned strands. The obtained results are based on the assumptions of rigid structural members, elastic post-tensioned strands, and dissipators with elasto perfectly-plastic hysteresis rules.

In the second chapter under the same hypothesis already mentioned for structural elements, post-tensioned strands, and dissipators, the equation of motion of a portal frame subjected to earthquake excitation, in large and small displacement conditions, is determined. The natural vibration period, the buckling load, and the energy dissipated for cycle of quasi-static loading are explicated as a function of the constitutive parameters. The chapter ends with a study of the influence of elements deformability on the global response.

The third and last chapter of this part focused on an elementary system involving a double-rocking motion. Substantially the system can be assumed as a cantilever column. After the identification of parameters governing the static and kinematic response, the monotonic force-displacement relation is evaluated with the goal to determine the dependence of the hysteretic behavior from the constitutive parameters of the systems.

Chapter 4

An Innovative Precast Concrete Connection

Contents

Preview

In this opening chapter, after a brief geometry description, the kinematic and static relations for the connection under the hypothesis of rigid beam and column end were considered.

To obtain a first insight of the general problem, consistent with the performance index minimization related to the global dynamic response of the particular system considered, the connection implementation inside a simple portal frame was considered and studied. The tension field due to the load application sequence was primarily investigated and the Equation of motion of the system treated as a generalized SDF hysteretic system was then determined. Finally, the frequency response of a bilinear hysteretic system under sinusoidal excitation was considered to obtain a design criteria for the mechanical characteristics of unbonded post tensioning cables and dissipators with the goal of minimize the maximum resonant response.

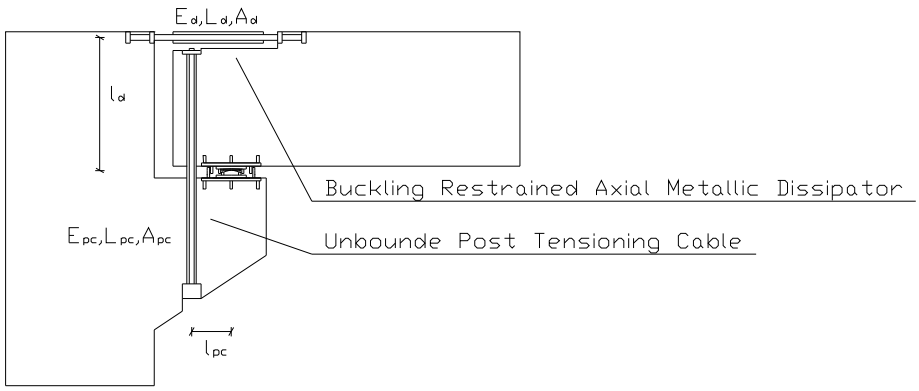

Figure 4.1: Connection overview

4.1 Preliminary Connection Analysis

4.1.1 Introduction

Basically, the conceived connection consists of a beam pivoted to a column by a structural hinge where a buckling restrained hysteretic dissipator and an elastic unbounded post-tensioned cable, as illustrated in fig...., was added. The dissipator and the unbounded post tensioned cable was inserted to provide respectively external energy dissipation and re-centering capacity. Note that the re-centering behavior is related to the activated hysteretic dissipators substitution.

4.1.2 Description

The parameters listed below were chosen to kinematically and statically characterize the considered connection. In particular the rotation ϑ around the structural hinge is the degree of freedom considered

- L_{pc}, Unbonded post tensioned cable length
- E_{pc}, Post tensioning cable elastic modulus
- A_{pc}, Cross sectional area
- l_{pc}, Distance between hinge and post tensioning cable, perpendicularly to the post tensioned cable direction
- L_{pc}, dissipator length
- E_{pc}, dissipator elastic modulus
- A_{pc}, dissipator cross sectional area
- l_{pc}, distance between hinge and dissipator, perpendicularly to the dissipator direction

4.1.3 Kinematic

As previously mentioned, the connection kinematic could be identified with a beam column rigid relative rotation around the structural hinge. Assuming large displacement and denoting with u and v, respectively, the displacement in the x direction and y direction, could be written:

$$\begin{aligned} u &= x(\cos\vartheta - 1) - y\sin\vartheta \\ v &= x\sin\vartheta + y(\cos\vartheta - 1) \end{aligned} \tag{4.1}$$

Considering small displacement ($\cos\vartheta = 1$ and $\sin\vartheta = \vartheta$) the beam kinematic will be reduced to the next simple conditions

$$\begin{aligned} u &= -y\vartheta \\ v &= x\vartheta \end{aligned} \tag{4.2}$$

4.1.4 Static problem position

Boundary Conditions

To can analyze and modeling in a simple way, during the total duration analysis the next conditions will be considered verified:

$$M + M_0 > 0 \qquad \forall\vartheta \tag{4.3}$$

or the equivalent

$$\vartheta + \vartheta_0 > 0 \qquad \forall M \tag{4.4}$$

where M_0 or (ϑ_0) denote the initial moment (the initial rotation) due to permanent (only if them contributes to post tension the cables) and to the post tension in the cables, and M (ϑ) is the generic moment developed after that the post tension cable was concluded as, for example, the moment due to the seismic action.

Verified the previous condition, the static problem could be treated identifying the Unbounded post tensioned cable with an bilateral elastic axial spring in the direction of the cable. Obviously, the buckling restrained hysteretic metallic dissipator will be modeled with a bilinear hysteretic axial spring. Moreover, in this context, the dissipator will be identified with an elastic axial spring.

4.2 An initial application: An innovative portal frame

4.2.1 Description

To obtain a first insight of the problem, that to put in evidence how the new connection modify the global behavior. We begin our study considering the Precast connection implemented inside the simple portal frame that was plotted in figure.

Unbounded cable are considered to be elastic and for the hysteretic dissipator a bilinear hysteresis rules is chosen with secondary stiffness equal to zero.

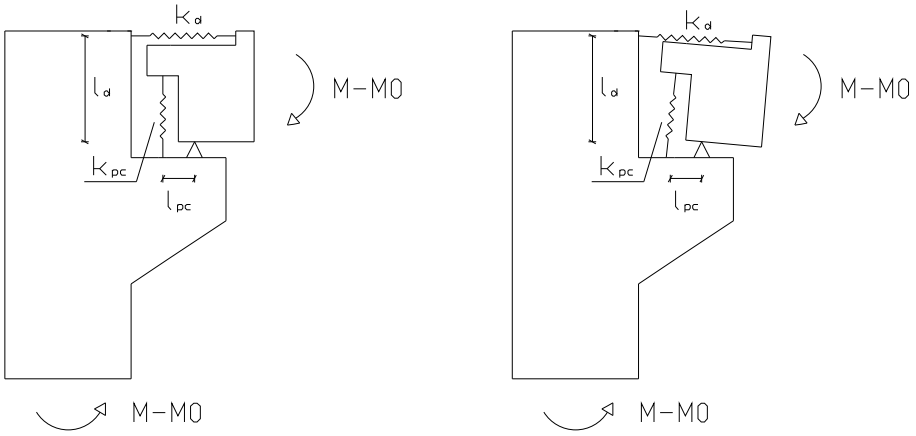

Figure 4.2: Connection modeling

Tension field due to a load application sequence

The sequence considered is presented :

1. Gravity and permanent Load
2. Cable Post tension (until the T_0 post tension force)
3. Metallic Hysteretic Dissipators introduction
4. Live Load

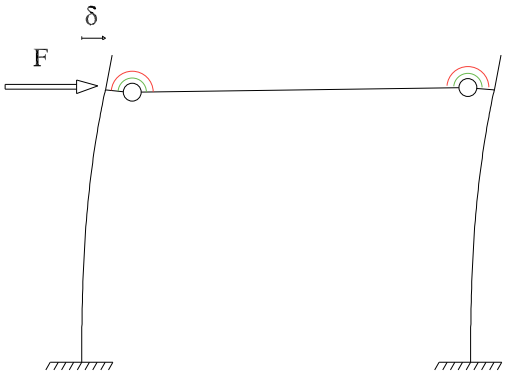

4.2.2 Transversal stiffness

Resolving with the principle of virtual work the portal frame with the two rotational spring could be obtained:

$$F = \frac{6E_cI_c}{H^3}\frac{1}{1-\frac{3}{4}\frac{1}{1+\frac{E_cI_c}{k_bH}+\frac{1}{6}\frac{L}{H}\frac{E_cI_c}{E_bI_b}}}\delta$$

Introducing the next non dimensional parameters

$$\alpha_b = \frac{k_bL}{E_bI_b} \qquad \lambda = \frac{L}{H} \qquad r_f = \frac{E_cI_c}{E_bI_b}$$

the force displacement relation could be written:

$$F = \frac{6E_cI_c}{H^3}\frac{1}{1-\frac{3}{4}\frac{1}{1+r_f\frac{\lambda}{\alpha_b}+\frac{1}{6}\lambda r_f}}\delta$$

It's simple to verify that for $\alpha_b = 0$ (absence of rotational spring) the previous relation became:

$$F = \frac{6E_cI_c}{H^3}\delta$$

On the other hand for $\alpha_b = 0$ and rigid beam $\Longrightarrow r_f = 0$ (since $E_bI_b = \infty$)

$$F = \frac{24E_cI_c}{H^3}\delta$$

4.2.3 Rotational stiffness effect on the translational lateral stiffness

Introducing the next coefficient

$$C^s = \frac{1}{1-\frac{3}{4}\frac{1}{1+r_f\frac{\lambda}{\alpha_b}+\frac{1}{6}\lambda r_f}}$$

The previous equation could be written in the form:

$$F = C^s\frac{6E_cI_c}{H^3}\delta$$

where $1 < C^s < 4$ is function of α_b, column-spring relative stiffness, λ, beam-column geometry ratio and of r_f, beam column stiffness ratio. It's interesting to evaluate the C* variation with r_f for fixed λ poiche' questo parametro determinare l' efficacia delle rigidezze rotazionali sulla rigidezza traslazionale

Chapter 5

An Elementary System for Seismic Response Control

Contents

Preview

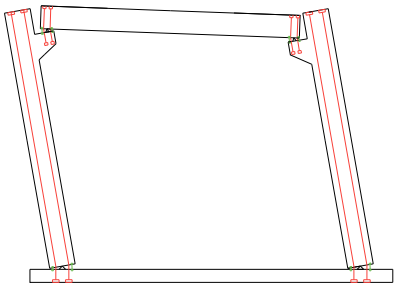

Figure 5.1: Rocking Frame

We begin our study formulating the equation of motion, for the precast prestressed rocking frame of Figure 6.7 subjected to an earthquake excitation and to an external horizontal applied force.

As shown in Figure 6.7 the system is a portal frame with rigid members (beam and columns) and elastic-plastic connections. These are composed of unbounded post-tensioned cables and hysteretic dampers. The unbounded post-tensioned cables ensure self centering capacity while the hysteretic dampers provide energy dissipation properties.

The equation of motion is formulated by application of the *Virtual Power Equation*.

Then the equation of motion is used to determine the natural vibration frequency and the buckling load of the system, idealized as a linear elastic system, as a function of geometric and mechanical parameters.

The document closes with the evaluation of the moment rotation relation and the energy dissipated by hysteretic damping in a cycle of quasi-static loading.

In the previous chapter part it will be assumed rigid structural elements, all the deformability is concentrated in the dampers and in the post tensioned strand.

5.1 Introduction

The first major self-centering systems were developed under the U.S.PRESSS (PREcast Seismic Structural Systems) program carried out for a decade in the 1990s and coordinated at the University of California, San Diego(Priestley1991, Nakaki et al. 1999, Priestley et al. 1999). The primary objective of the program was to developed innovative seismic resistant solutions for precast concrete buildings to replace the emulation of cast-in-place concrete that was used at the time. These innovative solutions used unbounded post-tensioned elements.

The inelastic demands on the systems are accommodated by allowing structural elements to separate relative to each other trough a rocking motion. This can be achieved with a number of structural configurations such as beams rocking on columns, segmental columns rocking on each other and on their foundations, and walls rocking on their foundations. This is achieved trough the opening and closing of an existing gap (rocking motion), while structural elements are basically designed to remain elastic. Rocking systems, with the help of the unbounded post-tensioned elements, tend to re-center to their original undeformed position at every cycle and therefore display a self-centering response.

Based on this concept, new structural systems that are capable of undergoing inelastic displacements similar to their traditional counterparts, while limiting

the damage to the structural system and assuring full re-centering capability without residual displacements, were developed. The feasibility and efficiency of unbounded post-tensioned solutions were investigated numerically by Priestley and Tao (1993) and experimentally validated through quasi-static loading of interior beam-column joint subassemblies (MacRae and Priestley 1994). These first systems relied only on unbounded post-tensioned to provide moment capacity and self-centering properties and therefore did not dissipate substantial amounts of energy at each loading cycle.

An hybrid system was then suggested where self-centering and energy dissipating properties were combined trough the use of unbounded post-tensioned tendons/bars and longitudinal non prestressed (mild) steel or additional external dissipation device designed to yield and to provide supplemental damping to the rocking systems.

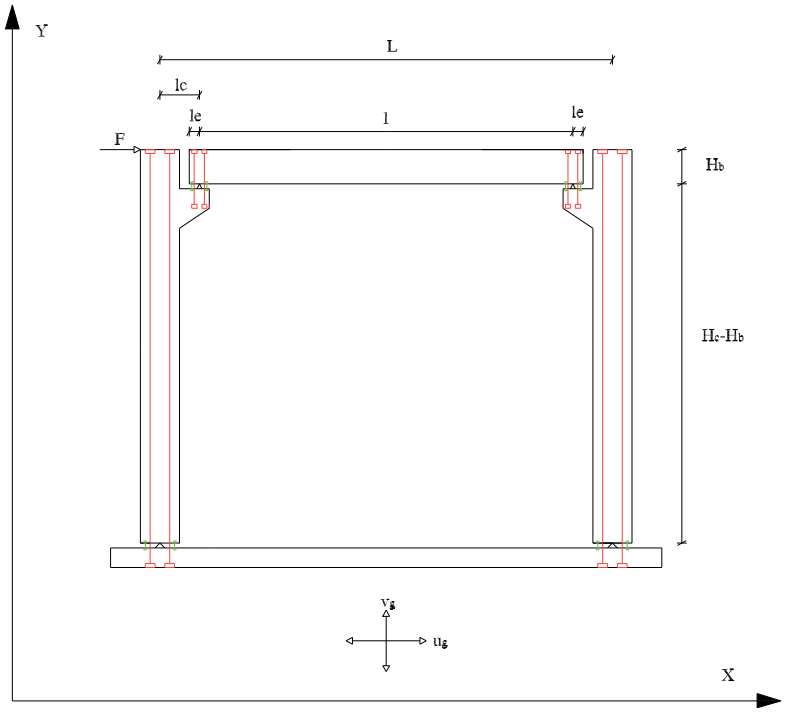

Figure 5.2: Frame Geometry

5.2 Description and Modeling Assumptions

5.2.1 Description

As illustrated in Fig. 5.2 the system consists of a rigid frame with columns pinned at the base and beam pinned at the columns. The mass of the two columns and beam, is distributed uniformly whereas the unbounded post tensioned elements and the dampers are massless.

In this *hybrid* system self-centering properties were provided trough the use of unbounded post-tensioned tendons/bars and the energy dissipating were provided trough the use of non prestressed (mild) steel devices designed to yield and to provide supplemental damping to the rocking systems. The grouting reinforcing bars are positioned into vertical ducts at the edges of the columns, so that they yield cyclically in tension and compression during an earthquake.

Provided that the post tensioned elements remain elastic, the structure can be represented by a nonlinear single degree of freedom system with self-centering and energy dissipating properties.

The geometry of the system is described trough the next positions:

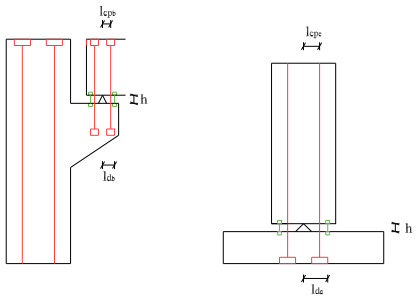

Figure 5.3: Frame details

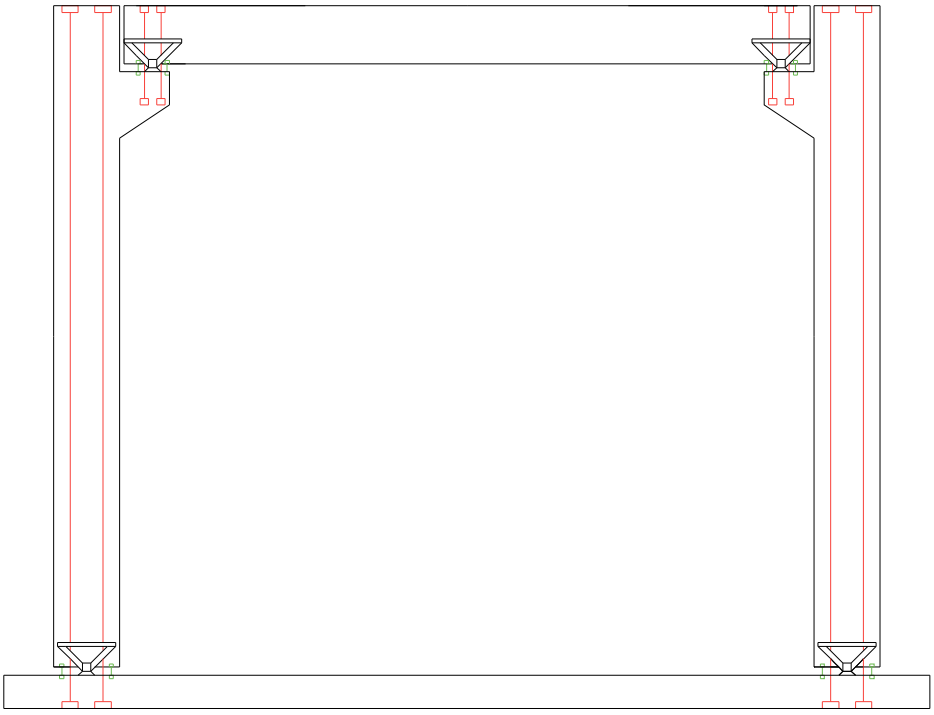

Figure 5.4: Hinge details

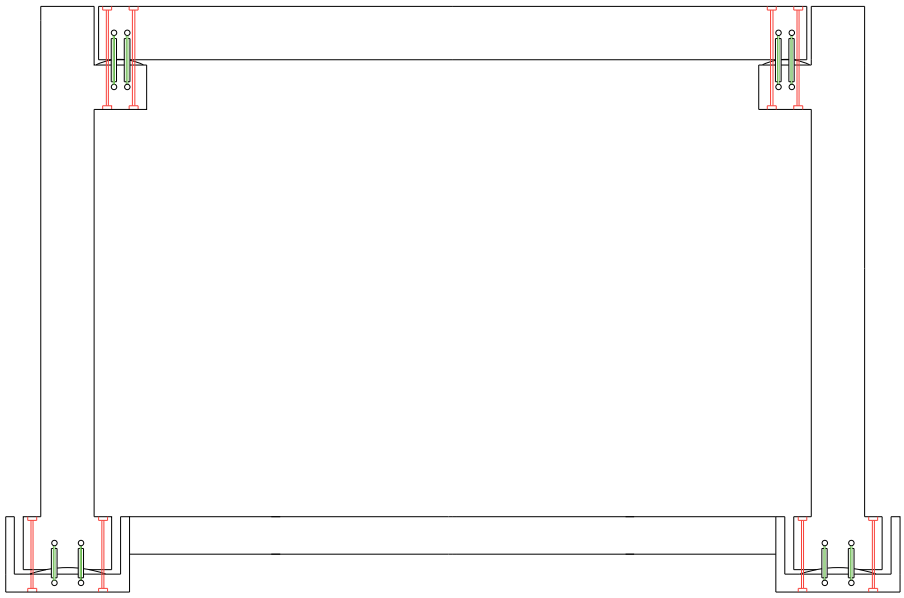

H_c	Column height,
H_b	Beam height,
$H_c - H_b$	Beam hinge height,
B_c	Column half width,
l	Distance between beam hinges
l_c	Distance between column and beam hinge
L	Distance between column hinges at the base
l_e	Distance between
l_{cp_c}	Distance between column hinges and Post-Tensioning element
l_{cp_d}	Distance between column hinges and column dissipators
l_{cp_b}	Distance between beam hinges and beam dissipators
m_{c1}	Left column mass
m_{c2}	Right column mass
m_b	Beam mass
L_{cp_c}	Length of Post-Tensioned element
L_{cp_c}	Length of dissipators

5.2.2 Modeling Assumptions

The system can be idealized as a generalized single degree of freedom system. However, for computational simplicity, it is idealized as three degree of freedom system, writing two equation among them that bring back the system to an

single degree of freedom system. The degrees of freedom system choose are:

ϑ	counterclockwise rotation about the left column hinge
ψ	counterclockwise rotation about the left beam hinge
φ	counterclockwise rotation about the right column hinge

A first insight into the the dynamic response of the rocking frame with supplemental hysteretic dampers can be achieved by idealizing

- beam and columns as rigid bodies
- post tensioned tendon as linear elastic elements
- hysteretic dampers as bilinear elastic-perfectly plastic elements

5.3 Equation of motion: Earthquake Excitation

5.3.1 Introduction

In this section the equation of motion for the system subjected to an earthquake excitation and to an external horizontal applied force is derived. This equation of motion can be formulated using Newton's Second Law of Motion or D'Alambert's principle etc ... Here we choose to use the Principle of Virtual Power. The equation of virtual power should include the power related to:

- Horizontal Force;
- Mass Forces;
- Inertia Forces;
- Unbounded post-tensioned tendons;
- Hysteretic dampers.

Symbolically, the equation of virtual power can be written:

$$\boxed{F\hat{\dot{u}}_F + \iiint_{Structure} \varrho(\mathbf{b}-\mathbf{a})\ \hat{\mathbf{v}}_s\, dV + T_{cp}\hat{\dot{L}}_{cp} + T_d\hat{\dot{L}}_d = 0} \tag{5.1}$$

where

$$\iiint_{Structure} = \iiint_{Column1} + \iiint_{Beam} + \iiint_{Column2} \tag{5.2}$$

5.3.2 Displacement, Velocity and Acceleration Field

The displacement field for the right column, left column and beam respectively, is:

Column 1

$$\begin{aligned} u &= u_g + x(\cos\vartheta - 1) - y\sin\vartheta \\ v &= v_g + x\sin\vartheta + y(\cos\vartheta - 1) \end{aligned} \tag{5.3}$$

Column 2

$$\begin{aligned} u &= u_g + x(\cos\varphi - 1) - y\sin\varphi \\ v &= v_g + x\sin\varphi + y(\cos\varphi - 1) \end{aligned} \tag{5.4}$$

Beam

$$\begin{aligned} u &= u_g + l_c(\cos\vartheta - 1) - (H_c - H_b)\sin\vartheta + x(\cos\psi - 1) - y\sin\psi \\ v &= v_g + l_c\sin\vartheta + (H_c - H_b)(\cos\vartheta - 1) + x\sin\psi + y(\cos\psi - 1) \end{aligned} \tag{5.5}$$

The velocity field is evaluated differentiating the displacement field:

Column 1

$$\begin{aligned} \dot{u} &= \dot{u}_g - (x\sin\vartheta + y\cos\vartheta)\dot{\vartheta} \\ \dot{v} &= \dot{v}_g + (x\cos\vartheta - y\sin\vartheta)\dot{\vartheta} \end{aligned} \tag{5.6}$$

Column 2

$$\begin{aligned} \dot{u} &= \dot{u}_g - (x\sin\varphi + y\cos\varphi)\dot{\varphi} \\ \dot{v} &= \dot{v}_g + (x\cos\varphi - y\sin\varphi)\dot{\varphi} \end{aligned} \tag{5.7}$$

Beam

$$\begin{aligned} \dot{u} &= \dot{u}_g - (l_c\sin\vartheta + (H_c - H_b)\cos\vartheta)\dot{\vartheta} - (x\sin\psi + y\cos\psi)\dot{\psi} \\ \dot{v} &= \dot{v}_g + (l_c\cos\vartheta - (H_c - H_b)\sin\vartheta)\dot{\vartheta} + (x\cos\psi - y\sin\psi)\dot{\psi} \end{aligned} \tag{5.8}$$

Finally, the acceleration field is evaluated differentiating twice the displacement field:

Column 1

$$\begin{aligned} \ddot{u} &= \ddot{u}_g - (x\sin\vartheta + y\cos\vartheta)\ddot{\vartheta} - (x\cos\vartheta - y\sin\vartheta)\dot{\vartheta}^2 \\ \ddot{v} &= \ddot{v}_g + (x\cos\vartheta - y\sin\vartheta)\ddot{\vartheta} - (x\sin\vartheta + y\cos\vartheta)\dot{\vartheta}^2 \end{aligned} \tag{5.9}$$

Column 2

$$\begin{aligned} \ddot{u} &= \ddot{u}_g - (x\sin\varphi + y\cos\varphi)\ddot{\varphi} - (x\cos\varphi - y\sin\varphi)\dot{\varphi}^2 \\ \ddot{v} &= \ddot{v}_g + (x\cos\varphi - y\sin\varphi)\ddot{\varphi} - (x\sin\varphi + y\cos\varphi)\dot{\varphi}^2 \end{aligned} \tag{5.10}$$

Beam

$$\begin{aligned} \ddot{u} = \ddot{u}_g &- (l_c\sin\vartheta + (H_c - H_b)\cos\vartheta)\ddot{\vartheta} - (l_c\cos\vartheta - (H_c - H_b)\sin\vartheta)\dot{\vartheta}^2 \\ &- (x\sin\psi + y\cos\psi)\ddot{\psi} - (x\cos\psi - y\sin\psi)\dot{\psi}^2 \end{aligned} \tag{5.11}$$

$$\begin{aligned} \ddot{v} = \ddot{v}_g &+ (l_c\cos\vartheta - (H_c - H_b)\sin\vartheta)\ddot{\vartheta} - (l_c\sin\vartheta + (H_c - H_b)\cos\vartheta)\dot{\vartheta}^2 \\ &+ (x\cos\psi - y\sin\psi)\ddot{\psi} - (x\sin\psi + y\cos\psi)\dot{\psi}^2 \end{aligned} \tag{5.12}$$

5.3.3 Conditions among angles

The coordinate of the point B can be evaluated as a function of ϑ and ψ:

$$\begin{aligned} x_B &= x_A + l\cos\psi \\ y_B &= y_A + l\sin\psi \end{aligned} \tag{5.13}$$

where

$$\begin{aligned} x_A &= d\cos(\alpha + \vartheta) \\ y_A &= d\sin(\alpha + \vartheta) \end{aligned} \tag{5.14}$$

expand sine and cosine we obtain:

$$\begin{aligned} x_A &= d[\cos\alpha\cos\vartheta - \sin\alpha\sin\vartheta] = l_c\cos\vartheta - (H_c - H_b)\sin\vartheta \\ y_A &= d[\sin\alpha\cos\vartheta + \cos\alpha\sin\vartheta] = l_c\sin\vartheta + (H_c - H_b)\cos\vartheta \end{aligned} \tag{5.15}$$

and then

$$\begin{aligned} x_B &= x_A + l_c\cos\psi = l_c\cos\vartheta - (H_c - H_b)\sin\vartheta + l\cos\psi \\ y_B &= y_A + l_c\sin\psi = l_c\sin\vartheta + (H_c - H_b)\cos\vartheta + l\sin\psi \end{aligned} \tag{5.16}$$

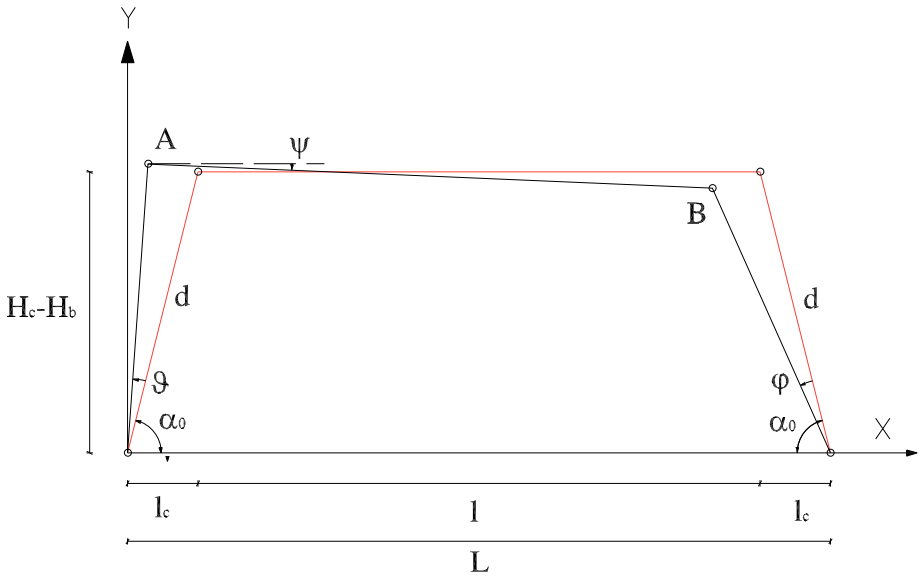

Figure 5.5: Conditions among Angles

The coordinate of the point B can also be evaluated as a function of φ:

$$\begin{aligned} \tilde{x}_B &= l + l_c - d\cos(\alpha - \varphi) \\ \tilde{y}_B &= H_c - H_b - d\sin\alpha + d\sin(\alpha - \varphi) \end{aligned} \tag{5.17}$$

or

$$\begin{aligned} \tilde{x}_B &= L - d[\cos\alpha\cos\varphi - \sin\alpha\sin\varphi] = L - l_c\cos\varphi - (H_c - H_b)\sin\varphi \\ \tilde{y}_B &= d\sin(\alpha - \varphi) = d[\sin\alpha\cos\vartheta + \cos\alpha\sin\vartheta] = (H_c - H_b)\cos\varphi - l_c\sin\varphi \end{aligned} \tag{5.18}$$

Assuming small displacement and observing that

$$x_B = \tilde{x}_B \qquad y_B = \tilde{y}_B$$

we obtain:

$$\begin{aligned} l_c - (H_c - H_b)\vartheta + l &= L - l_c - (H_c - H_b)\varphi \\ l_c\vartheta + (H_c - H_b) + l\psi &= (H_c - H_b) - l_c\varphi \end{aligned} \tag{5.19}$$

considering that $l + l_c = L - l_c$ results

$$\boxed{\vartheta = \varphi} \tag{5.20}$$

and

$$\boxed{\psi = -\frac{2l_c}{l}\varphi} \tag{5.21}$$

Assuming large displacement, from $x_B = \tilde{x}_B$ and $y_B = \tilde{y}_B$ we obtained:

$$\begin{aligned} l_c \cos\vartheta - (H_c - H_b)\sin\vartheta + l\cos\psi &= L - l_c\cos\varphi - (H_c - H_b)\sin\varphi \\ l_c \sin\vartheta + (H_c - H_b)\cos\vartheta + l\sin\psi &= (H_c - H_b)\cos\varphi - l_c\sin\varphi \end{aligned} \tag{5.22}$$

differentiating the two equation $x_B = \tilde{x}_B$ and $y_B = \tilde{y}_B$ we obtained:

$$\dot{x}_B = \dot{\tilde{x}}_B \qquad \dot{y}_B = \dot{\tilde{y}}_B$$

Substituting

$$\begin{aligned} -\left(l_c\sin\vartheta + (H_c - H_b)\cos\vartheta\right)\dot{\vartheta} - l\sin\psi\dot{\psi} &= \left(l_c\sin\varphi - (H_c - H_b)\cos\varphi\right)\dot{\varphi} \\ \left(l_c\cos\vartheta - (H_c - H_b)\sin\vartheta\right)\dot{\vartheta} + l\cos\psi\dot{\psi} &= -\left((H_c - H_b)\sin\varphi + l_c\cos\varphi\right)\dot{\varphi} \end{aligned} \tag{5.23}$$

Solving the two equations, for $\dot{\varphi}$ and $\dot{\psi}$ respectively leads to

$$\begin{aligned} \dot{\varphi} &= \left[\frac{(H_b - H_c)\cos(\psi - \vartheta) + l_c\sin(\psi - \vartheta)}{(H_b - H_c)\cos(\varphi - \psi) + l_c\sin(\varphi - \psi)}\right]\dot{\vartheta} \\ \dot{\psi} &= -\frac{2l_c}{l}\left[\frac{2(H_b - H_c)l_c\cos(\varphi - \vartheta) - [(H_b - H_c)^2 - l_c^2]\sin(\varphi - \vartheta)}{2l_c[(H_b - H_c)\cos(\varphi - \psi) + l_c\sin(\varphi - \psi)]}\right]\dot{\vartheta} \end{aligned} \tag{5.24}$$

Assuming small displacement the equations become:

$$\boxed{\dot{\varphi} = \dot{\vartheta}} \qquad \boxed{\dot{\psi} = -\frac{2l_c}{l}\dot{\vartheta}} \tag{5.25}$$

5.3.4 Equation of Virtual Power

Virtual Power related to Horizontal Force

The power related to the horizontal force is:

$$F\hat{\dot{u}}_F = -F\left(B_c\sin\hat{\vartheta} - H_c\cos\hat{\vartheta}\right)\hat{\dot{\vartheta}} \tag{5.26}$$

Virtual Power related to Weight Component

The power related to the Weight is:

$$\begin{aligned}
&\iiint_V \varrho\,(b)\ \hat{\mathbf{v}}_s = \iiint_V \varrho\, b\,[\dot{\hat{u}}_s + \dot{\hat{v}}_s]\,dxdydz = \\
&\iiint_{column1} \varrho\, b\,[\dot{\hat{u}} + \dot{\hat{v}}]\,dxdydz + \iiint_{column2} \varrho\, b\,[\dot{\hat{u}} + \dot{\hat{v}}]\,dxdydz + \\
&\iiint_{beam} \varrho\, b\,[\dot{\hat{u}} + \dot{\hat{v}}]\,dxdydz = W_{c1}\left[-\frac{H_c}{2}\sin\hat{\vartheta}\right]\dot{\hat{\vartheta}} + W_{c2}\left[-\frac{H_c}{2}\sin\hat{\varphi}\right]\dot{\hat{\varphi}} + \\
&+ W_b\left[\left(\frac{l}{2}\cos\hat{\psi} - \frac{H_b}{2}\sin\hat{\psi}\right)\right]\dot{\hat{\psi}} + W_b\left[\ \left(l_c\cos\hat{\vartheta} - (H_c - H_b)\sin\hat{\vartheta}\right)\right]\dot{\hat{\vartheta}}
\end{aligned} \tag{5.27}$$

where

for the column 1

$$\begin{aligned}
\dot{\hat{u}} &= -(x\sin\hat{\vartheta} + y\cos\hat{\vartheta})\dot{\hat{\vartheta}} \\
\dot{\hat{v}} &= +(x\cos\hat{\vartheta} - y\sin\hat{\vartheta})\dot{\hat{\vartheta}}
\end{aligned} \tag{5.28}$$

for the Column 2

$$\begin{aligned}
\dot{\hat{u}} &= -(x\sin\hat{\varphi} + y\cos\hat{\varphi})\dot{\hat{\varphi}} \\
\dot{\hat{v}} &= +(x\cos\hat{\varphi} - y\sin\hat{\varphi})\dot{\hat{\varphi}}
\end{aligned} \tag{5.29}$$

for the beam

$$\begin{aligned}
\dot{\hat{u}} &= -(l_c\sin\hat{\vartheta} + (H_c - H_b)\cos\hat{\vartheta})\dot{\hat{\vartheta}} - (x\sin\hat{\psi} + y\cos\hat{\psi})\dot{\hat{\psi}} \\
\dot{\hat{v}} &= +(l_c\cos\hat{\vartheta} - (H_c - H_b)\sin\hat{\vartheta})\dot{\hat{\vartheta}} + (x\cos\hat{\psi} - y\sin\hat{\psi})\dot{\hat{\psi}}
\end{aligned} \tag{5.30}$$

and W_{c1}, W_{c2}, W_b, are the weights of the left column, right column and beam, respectively.

Virtual Power related to Mass Component

The power related to the Mass Component is:

$$-\iiint_{Structure} \varrho\,\mathbf{a}\ \hat{\mathbf{v}}_s = -\iiint_{Structure} \varrho\,[\ddot{u} + \ddot{v}]\,[\dot{\hat{u}}_s + \dot{\hat{v}}_s]\,dxdydz = \tag{5.31}$$

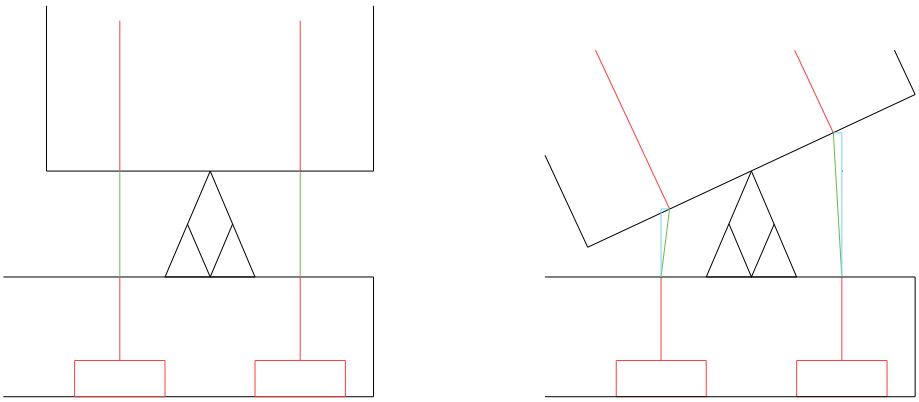

Figure 5.6: Unbounded Post-Tensioned Cables extension

Substituting is obtained:

$$
\begin{aligned}
&-\iiint_V \varrho\, \mathbf{a}\ \hat{\mathbf{v}}_s = \left[m_{c1}\ddot{u}_g \frac{H_c}{2}\cos\vartheta + m_{c1}\ddot{v}_g \frac{H_c}{2}\sin\vartheta - I_{c1}\ddot{\vartheta}\right]\hat{\vartheta} + \\
&+\left[m_{c2}\ddot{u}_g \frac{H_c}{2}\cos\varphi + m_{c2}\ddot{v}_g \frac{H_c}{2}\sin\varphi - I_{c2}\ddot{\varphi}\right]\hat{\varphi} + \\
&+\left[m_b\ddot{u}_g\left(\frac{H_b}{2}\cos\psi + \frac{l}{2}\sin\psi\right) + m_b\ddot{v}_g\left(\frac{H_b}{2}\sin\psi - \frac{l}{2}\cos\psi\right) - I_{b_{b1}}\ddot{\psi}\right]\hat{\psi} + \\
&+\left[m_b\ddot{u}_g\left((H_c - H_b)\cos\vartheta + l_c\sin\vartheta\right) + \right. \\
&\left. + m_b\ddot{v}_g\left((H_c - H_b)\sin\vartheta - l_c\cos\vartheta\right) - m_b\left(l_c^2 + (H_c - H_b)^2\right)\ddot{\vartheta}\right]\hat{\vartheta} + \\
&- m_b\Gamma\ddot{\vartheta}\hat{\psi} - m_b\Gamma\ddot{\psi}\hat{\vartheta} + \Delta_{\dot{\psi}^2}\dot{\psi}^2\hat{\vartheta} + \Delta_{\dot{\vartheta}^2}\dot{\vartheta}^2\hat{\psi} +
\end{aligned}
\tag{5.32}
$$

Virtual Power related to Unbounded Post Tensioned Elements

The power related to the Unbounded Post Tensioned Elements is:

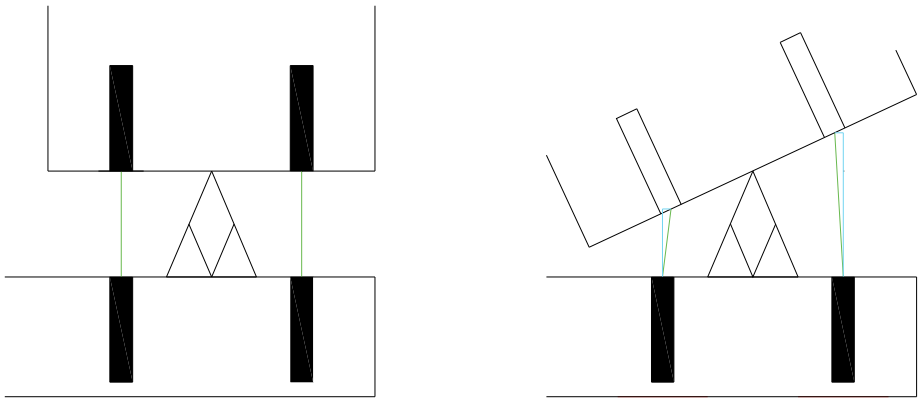

Figure 5.7: Dampers extension

$$
\begin{aligned}
T_{cp}\widehat{\dot{L}}_{cp} =& T_{cp_{lc1}}\widehat{\dot{L}}_{cp_{lc1}} + T_{cp_{rc1}}\widehat{\dot{L}}_{cp_{rc1}} + T_{cp_{lc2}}\widehat{\dot{L}}_{cp_{lc2}} + T_{cp_{rc2}}\widehat{\dot{L}}_{cp_{rc2}} + \\
&+ T_{cp_{lb1}}\widehat{\dot{L}}_{cp_{lb1}} + T_{cp_{rb1}}\widehat{\dot{L}}_{cp_{rb1}} + T_{cp_{lb2}}\widehat{\dot{L}}_{cp_{lb2}} + T_{cp_{rb2}}\widehat{\dot{L}}_{cp_{rb2}} = \\
=& + \left[-T_0\Delta_{cp_{c1}}l_{cp_{c1}} - 2\frac{(EA)_{cp_{c1}}}{L_{cp_{c1}}}\Lambda_{cp_{c1}}l^2_{cp_{c1}}\sin\vartheta\right]\hat{\dot{\vartheta}} + \\
&+ \left[-T_0\Delta_{cp_{c2}}l_{cp_{c2}} - 2\frac{(EA)_{cp_{c2}}}{L_{cp_{c2}}}\Lambda_{cp_{c2}}l^2_{cp_{c2}}\sin\varphi\right]\hat{\dot{\varphi}} + \\
&+ \left[-T_0\Delta_{cp_{b1}}l_{cp_{b1}} - 2\frac{(EA)_{cp_{b1}}}{L_{cp_{b1}}}\Lambda_{cp_{b1}}l^2_{cp_{b1}}\sin\tilde{\psi}_\vartheta\right]\hat{\dot{\tilde{\psi}}}_\vartheta + \\
&+ \left[-T_0\Delta_{cp_{b2}}l_{cp_{b2}} - 2\frac{(EA)_{cp_{b2}}}{L_{cp_{b2}}}\Lambda_{cp_{b2}}l^2_{cp_{b2}}\sin\tilde{\psi}_\varphi\right]\hat{\dot{\tilde{\psi}}}_\varphi
\end{aligned}
\tag{5.33}
$$

Virtual Power related to Hysteretic Dampers

The power related to the Hysteretic Dampers is:

$$
\begin{aligned}
T_d\widehat{\dot{L}}_d =& T_{d_{lc1}}\widehat{\dot{L}}_{d_{lc1}} + T_{d_{rc1}}\widehat{\dot{L}}_{d_{rc1}} + T_{d_{lc2}}\widehat{\dot{L}}_{d_{lc2}} + T_{d_{rc2}}\widehat{\dot{L}}_{d_{rc2}} + \\
&T_{d_{lb1}}\widehat{\dot{L}}_{d_{lb1}} + T_{d_{rb1}}\widehat{\dot{L}}_{d_{rb1}} + T_{d_{lb2}}\widehat{\dot{L}}_{d_{lb2}} + T_{d_{rb2}}\widehat{\dot{L}}_{d_{rb2}} = \\
=& + \left[-2\frac{(EA)_{d_{c1}}}{L_{d_{c1}}}\Lambda_{d_{c1}}l^2_{d_{c1}}\sin\vartheta\right]\hat{\dot{\vartheta}} + \left[-2\frac{(EA)_{d_{c2}}}{L_{d_{c2}}}\Lambda_{d_{c2}}l^2_{d_{c2}}\sin\varphi\right]\hat{\dot{\varphi}} + \\
&+ \left[-2\frac{(EA)_{d_{b1}}}{L_{d_{b1}}}\Lambda_{d_{b1}}l^2_{d_{b1}}\sin\tilde{\psi}_\vartheta\right]\hat{\dot{\tilde{\psi}}}_\vartheta + \left[-2\frac{(EA)_{d_{b2}}}{L_{d_{b2}}}\Lambda_{d_{b2}}l^2_{d_{b2}}\sin\tilde{\psi}_\varphi\right]\hat{\dot{\tilde{\psi}}}_\varphi
\end{aligned}
\tag{5.34}
$$

Equation of Virtual Power

Putting all previous contributions together leads to the equation of virtual power

$$
\begin{aligned}
&\Big[\, F(H_c\cos\vartheta - B_c\sin\vartheta)\Big]\,\hat{\vartheta} + \\
&+\left[-W_{c1}\frac{H_c}{2}\sin\vartheta\right]\hat{\vartheta} + \left[-W_{c2}\frac{H_c}{2}\sin\varphi\right]\hat{\varphi} + \\
&+\left[+W_b\left(\frac{l}{2}\cos\psi - \frac{H_b}{2}\sin\psi\right)\right]\hat{\psi} + \Big[\; + W_b\Big(\, l_c\cos\vartheta - (H_c - H_b)\sin\vartheta\Big)\Big]\,\hat{\vartheta} + \\
&+\left[m_{c1}\ddot{u}_g\frac{H_c}{2}\cos\vartheta + m_{c1}\ddot{v}_g\frac{H_c}{2}\sin\vartheta - I_{c1}\ddot{\vartheta}\right]\hat{\vartheta} + \\
&+\left[m_{c2}\ddot{u}_g\frac{H_c}{2}\cos\varphi + m_{c2}\ddot{v}_g\frac{H_c}{2}\sin\varphi - I_{c2}\ddot{\varphi}\right]\hat{\varphi} + \\
&+\Big[\, m_b\ddot{u}_g\left(\frac{H_b}{2}\cos\psi + \frac{l}{2}\sin\psi\right) + m_b\ddot{v}_g\left(\,\frac{H_b}{2}\sin\psi - \frac{l}{2}\cos\psi\right) - I_{b_{b1}}\ddot{\psi}\Big]\,\hat{\psi} + \\
&+\Big[\, m_b\ddot{u}_g\Big(\;(H_c - H_b)\cos\vartheta + l_c\sin\vartheta\Big) + \\
&+\; m_b\ddot{v}_g\Big(\;(H_c - H_b)\sin\vartheta - l_c\cos\vartheta\Big) - m_b\Big(\, l_c^2 + (H_c - H_b)^2\Big)\,\ddot{\vartheta}\Big]\,\hat{\vartheta} + \\
&- m_b\Gamma\ddot{\vartheta}\hat{\psi} - m_b\Gamma\ddot{\psi}\hat{\vartheta} + \Delta_{\dot{\psi}^2}\dot{\psi}^2\hat{\vartheta} + \Delta_{\dot{\vartheta}^2}\dot{\vartheta}^2\hat{\psi} + \\
&+\left[-T_0\Delta_{cp_{c1}}l_{cp_{c1}} - 2\frac{(EA)_{cp_{c1}}}{L_{cp_{c1}}}\Lambda_{cp_{c1}}l_{cp_{c1}}^2\sin\vartheta\right]\hat{\vartheta} + \\
&+\left[-T_0\Delta_{cp_{c2}}l_{cp_{c2}} - 2\frac{(EA)_{cp_{c2}}}{L_{cp_{c2}}}\Lambda_{cp_{c2}}l_{cp_{c2}}^2\sin\varphi\right]\hat{\varphi} + \\
&+\left[-T_0\Delta_{cp_{b1}}l_{cp_{b1}} - 2\frac{(EA)_{cp_{b1}}}{L_{cp_{b1}}}\Lambda_{cp_{b1}}l_{cp_{b1}}^2\sin\tilde{\psi}_\vartheta\right]\hat{\tilde{\psi}}_\vartheta + \\
&+\left[-T_0\Delta_{cp_{b2}}l_{cp_{b2}} - 2\frac{(EA)_{cp_{b2}}}{L_{cp_{b2}}}\Lambda_{cp_{b2}}l_{cp_{b2}}^2\sin\tilde{\psi}_\varphi\right]\hat{\tilde{\psi}}_\varphi + \\
&+\left[-2\frac{(EA)_{d_{c1}}}{L_{d_{c1}}}\Lambda_{d_{c1}}l_{d_{c1}}^2\sin\vartheta\right]\hat{\vartheta} + \left[-2\frac{(EA)_{d_{c2}}}{L_{d_{c2}}}\Lambda_{d_{c2}}l_{d_{c2}}^2\sin\varphi\right]\hat{\varphi} + \\
&+\left[-2\frac{(EA)_{d_{b1}}}{L_{d_{b1}}}\Lambda_{d_{b1}}l_{d_{b1}}^2\sin\tilde{\psi}_\vartheta\right]\hat{\tilde{\psi}}_\vartheta + \left[-2\frac{(EA)_{d_{b2}}}{L_{d_{b2}}}\Lambda_{d_{b2}}l_{d_{b2}}^2\sin\tilde{\psi}_\varphi\right]\hat{\tilde{\psi}}_\varphi = 0
\end{aligned}
\tag{5.35}
$$

expressing relations among the angles is obtained

$$
\begin{aligned}
&\Big\{ F(H_c\cos\vartheta - B_c\sin\vartheta) + \\
&- W_{c1}\frac{H_c}{2}\sin\vartheta - W_{c2}\frac{H_c}{2}\Phi\sin\varphi + \\
&+ W_b\left[\Big(l_c\cos\vartheta - (H_c - H_b)\sin\vartheta\Big) + \left(\frac{l}{2}\cos\psi - \frac{H_b}{2}\sin\psi\right)\left(-\frac{2l_c}{l}\Psi\right)\right] + \\
&+ m_{c1}\ddot{u}_g\frac{H_c}{2}\cos\vartheta + m_{c1}\ddot{v}_g\frac{H_c}{2}\sin\vartheta - I_{c1}\ddot{\vartheta} + \\
&+ \left[m_{c2}\ddot{u}_g\frac{H_c}{2}\cos\varphi + m_{c2}\ddot{v}_g\frac{H_c}{2}\sin\varphi - I_{c2}\ddot{\varphi}\right]\Phi + \\
&+ \left[m_b\ddot{u}_g\left(\frac{H_b}{2}\cos\psi + \frac{l}{2}\sin\psi\right) + m_b\ddot{v}_g\left(\frac{H_b}{2}\sin\psi - \frac{l}{2}\cos\psi\right) - I_{b_{b1}}\ddot{\psi}\right]\left(-\frac{2l_c}{l}\Psi\right) + \\
&+ m_b\ddot{u}_g\Big[\ (H_c - H_b)\cos\vartheta + l_c\sin\vartheta\Big] + \\
&+ m_b\ddot{v}_g\Big[\ (H_c - H_b)\sin\vartheta - l_c\cos\vartheta\Big] - m_b\Big[\ l_c^2 + (H_c - H_b)^2\Big]\ddot{\vartheta} + \\
&- m_b\Gamma\ddot{\vartheta}\left(-\frac{2l_c}{l}\Psi\right) - m_b\Gamma\ddot{\psi} + \Delta_{\dot{\psi}^2}\dot{\psi}^2 + \Delta_{\dot{\vartheta}^2}\dot{\vartheta}^2\left(-\frac{2l_c}{l}\Psi\right) + \\
&- T_0\Delta_{cp_{c1}}l_{cp_{c1}} - 2\frac{(EA)_{cp_{c1}}}{L_{cp_{c1}}}\Lambda_{cp_{c1}}l_{cp_{c1}}^2\sin\vartheta + \\
&- T_0\Delta_{cp_{c2}}l_{cp_{c2}} - 2\frac{(EA)_{cp_{c2}}}{L_{cp_{c2}}}\Lambda_{cp_{c2}}\Phi l_{cp_{c2}}^2\sin\varphi + \\
&+ \left[-T_0\Delta_{cp_{b1}}l_{cp_{b1}} - 2\frac{(EA)_{cp_{b1}}}{L_{cp_{b1}}}\Lambda_{cp_{b1}}l_{cp_{b1}}^2\sin\tilde{\psi}_{\vartheta}\right]\left(-\frac{2l_c}{l}\Psi - 1\right) + \\
&+ \left[-T_0\Delta_{cp_{b2}}l_{cp_{b2}} - 2\frac{(EA)_{cp_{b2}}}{L_{cp_{b2}}}\Lambda_{cp_{b2}}l_{cp_{b2}}^2\sin\tilde{\psi}_{\varphi}\right]\left(-\frac{2l_c}{l}\Psi - 1\right) + \\
&- 2\frac{(EA)_{d_{c1}}}{L_{d_{c1}}}\Lambda_{d_{c1}}l_{d_{c1}}^2\sin\vartheta - 2\frac{(EA)_{d_{c2}}}{L_{d_{c2}}}\Lambda_{d_{c2}}\Phi l_{d_{c2}}^2\sin\varphi + \\
&+ \left[-2\frac{(EA)_{d_{b1}}}{L_{d_{b1}}}\Lambda_{d_{b1}}l_{d_{b1}}^2\sin\tilde{\psi}_{\vartheta} - 2\frac{(EA)_{d_{b2}}}{L_{d_{b2}}}\Lambda_{d_{b2}}l_{d_{b2}}^2\sin\tilde{\psi}_{\varphi}\right]\left(-\frac{2l_c}{l}\Psi - 1\right)\Big\}\hat{\ddot{\vartheta}} = 0
\end{aligned}
\tag{5.36}
$$

where

$$\tilde{\psi}_{\vartheta} = \psi - \vartheta \tag{5.37}$$

$$\tilde{\psi}_{\varphi} = \psi - \varphi \tag{5.38}$$

$$\Phi = \left[\frac{(H_b - H_c)\cos(\psi - \vartheta) + l_c \sin(\psi - \vartheta)}{(H_b - H_c)\cos(\varphi - \psi) + l_c \sin(\varphi - \psi)}\right]$$

$$\Psi = \frac{2(H_b - H_c) l_c \cos(\varphi - \vartheta) - [(H_b - H_c)^2 - l_c^2]\sin(\varphi - \vartheta)}{2l_c[(H_b - H_c)\cos(\varphi - \psi) + l_c \sin(\varphi - \psi)]}$$

$$\begin{aligned} I_{c_{c1}} = I_{c_{c2}} = I_{c_c} &= \frac{2}{3}\rho B_c H_c (B_c^2 + H_c^2) = \frac{1}{3} m_c (B_c^2 + H_c^2) \\ I_{b_{b1}} &= \frac{1}{12} m_b [H_b^2 + (l + 2l_e)^2] + m_b \left(\frac{H_b}{2}\right)^2 + m_b \left(\frac{l}{2}\right)^2 = \\ &= \frac{1}{3} m_b \left[H_b^2 + l^2 + l l_e + l_e^2\right] \\ I_{b_b} &= \frac{1}{12} m_b [H_b^2 + (l + 2l_e)^2] + m_b \left[(H_c - H_b)\frac{l}{2l_c} - \frac{H_b}{2}\right]^2 \end{aligned} \tag{5.39}$$

$$
\begin{aligned}
\Lambda_{cp_{c1}} =& \frac{1}{2}\left[\left(\frac{l_{cp_{c1}}^2(\cos\vartheta-1)^2}{(h-l_{cp_{c1}}\sin\vartheta)^2}+1\right)^{\frac{1}{2}}+\left(1-\left(\frac{l_{cp_{c1}}^2(\cos\vartheta-1)^2}{(h-l_{cp_{c1}}\sin\vartheta)^2}+1\right)^{\frac{1}{2}}\right)\frac{h}{l_{cp_{c1}}\sin\vartheta}\right] \\
& \left[\left(\frac{l_{cp_{c1}}^2(\cos\vartheta-1)^2}{(h-l_{cp_{c1}}\sin\vartheta)^2}+1\right)^{-\frac{1}{2}}\left(\frac{h-l_{cp_{c1}}\tan\vartheta}{\frac{h}{\cos\vartheta}-l_{cp_{c1}}\tan\vartheta}\right)\right]+ \\
& \frac{1}{2}\left[\left(\frac{l_{cp_{c1}}^2(\cos\vartheta-1)^2}{(h+l_{cp_{c1}}\sin\vartheta)^2}+1\right)^{\frac{1}{2}}+\left(\left(\frac{l_{cp_{c1}}^2(\cos\vartheta-1)^2}{(h+l_{cp_{c1}}\sin\vartheta)^2}+1\right)^{\frac{1}{2}}-1\right)\frac{h}{l_{cp_{c1}}\sin\vartheta}\right] \\
& \left[\left(\frac{l_{cp_{c1}}^2(\cos\vartheta-1)^2}{(h+l_{cp_{c1}}\sin\vartheta)^2}+1\right)^{-\frac{1}{2}}\left(\frac{h+l_{cp_{c1}}\tan\vartheta}{\frac{h}{\cos\vartheta}+l_{cp_{c1}}\tan\vartheta}\right)\right] \\
\Lambda_{cp_{c2}} =& \frac{1}{2}\left[\left(\frac{l_{cp_{c2}}^2(\cos\varphi-1)^2}{(h-l_{cp_{c2}}\sin\varphi)^2}+1\right)^{\frac{1}{2}}+\left(1-\left(\frac{l_{cp_{c2}}^2(\cos\varphi-1)^2}{(h-l_{cp_{c2}}\sin\varphi)^2}+1\right)^{\frac{1}{2}}\right)\frac{h}{l_{cp_{c2}}\sin\varphi}\right] \\
& \left[\left(\frac{l_{cp_{c2}}^2(\cos\varphi-1)^2}{(h-l_{cp_{c2}}\sin\varphi)^2}+1\right)^{-\frac{1}{2}}\left(\frac{h-l_{cp_{c2}}\tan\varphi}{\frac{h}{\cos\varphi}-l_{cp_{c2}}\tan\varphi}\right)\right]+ \\
& \frac{1}{2}\left[\left(\frac{l_{cp_{c2}}^2(\cos\varphi-1)^2}{(h+l_{cp_{c2}}\sin\varphi)^2}+1\right)^{\frac{1}{2}}+\left(\left(\frac{l_{cp_{c2}}^2(\cos\varphi-1)^2}{(h+l_{cp_{c2}}\sin\varphi)^2}+1\right)^{\frac{1}{2}}-1\right)\frac{h}{l_{cp_{c2}}\sin\varphi}\right] \\
& \left[\left(\frac{l_{cp_{c2}}^2(\cos\varphi-1)^2}{(h+l_{cp_{c2}}\sin\varphi)^2}+1\right)^{-\frac{1}{2}}\left(\frac{h+l_{cp_{c2}}\tan\varphi}{\frac{h}{\cos\varphi}+l_{cp_{c2}}\tan\varphi}\right)\right] \\
\Lambda_{cp_{b1}} =& \frac{1}{2}\left[\left(\frac{l_{cp_{b1}}^2(\cos\tilde{\psi}_\vartheta-1)^2}{(h-l_{cp_{b1}}\sin\tilde{\psi}_\vartheta)^2}+1\right)^{\frac{1}{2}}+\left(1-\left(\frac{l_{cp_{b1}}^2(\cos\tilde{\psi}_\vartheta-1)^2}{(h-l_{cp_{b1}}\sin\tilde{\psi}_\vartheta)^2}+1\right)^{\frac{1}{2}}\right)\frac{h}{l_{cp_{b1}}\sin\tilde{\psi}_\vartheta}\right] \\
& \left[\left(\frac{l_{cp_{b1}}^2(\cos\tilde{\psi}_\vartheta-1)^2}{(h-l_{cp_{b1}}\sin\tilde{\psi}_\vartheta)^2}+1\right)^{-\frac{1}{2}}\left(\frac{h-l_{cp_{b1}}\tan\tilde{\psi}_\vartheta}{\frac{h}{\cos\tilde{\psi}_\vartheta}-l_{cp_{b1}}\tan\tilde{\psi}_\vartheta}\right)\right]+ \\
& \frac{1}{2}\left[\left(\frac{l_{cp_{b1}}^2(\cos\psi-1)^2}{(h+l_{cp_{b1}}\sin\psi)^2}+1\right)^{\frac{1}{2}}+\left(\left(\frac{l_{cp_{b1}}^2(\cos\tilde{\psi}_\vartheta-1)^2}{(h+l_{cp_{b1}}\sin\tilde{\psi}_\vartheta)^2}+1\right)^{\frac{1}{2}}-1\right)\frac{h}{l_{cp_{b1}}\sin\tilde{\psi}_\vartheta}\right] \\
& \left[\left(\frac{l_{cp_{b1}}^2(\cos\tilde{\psi}_\vartheta-1)^2}{(h+l_{cp_{b1}}\sin\tilde{\psi}_\vartheta)^2}+1\right)^{-\frac{1}{2}}\left(\frac{h+l_{cp_{b1}}\tan\tilde{\psi}_\vartheta}{\frac{h}{\cos\tilde{\psi}_\vartheta}+l_{cp_{b1}}\tan\tilde{\psi}_\vartheta}\right)\right] \\
\Lambda_{cp_{b2}} =& \frac{1}{2}\left[\left(\frac{l_{cp_{b2}}^2(\cos\tilde{\psi}_\varphi-1)^2}{(h-l_{cp_{b2}}\sin\tilde{\psi}_\varphi)^2}+1\right)^{\frac{1}{2}}+\left(1-\left(\frac{l_{cp_{b2}}^2(\cos\tilde{\psi}_\varphi-1)^2}{(h-l_{cp_{b2}}\sin\tilde{\psi}_\varphi)^2}+1\right)^{\frac{1}{2}}\right)\frac{h}{l_{cp_{b2}}\sin\tilde{\psi}_\varphi}\right] \\
& \left[\left(\frac{l_{cp_{b2}}^2(\cos\tilde{\psi}_\varphi-1)^2}{(h-l_{cp_{b2}}\sin\tilde{\psi}_\varphi)^2}+1\right)^{-\frac{1}{2}}\left(\frac{h-l_{cp_{b2}}\tan\tilde{\psi}_\varphi}{\frac{h}{\cos\tilde{\psi}_\varphi}-l_{cp_{b2}}\tan\tilde{\psi}_\varphi}\right)\right]+ \\
& \frac{1}{2}\left[\left(\frac{l_{cp_{b2}}^2(\cos\tilde{\psi}_\varphi-1)^2}{(h+l_{cp_{b2}}\sin\tilde{\psi}_\varphi)^2}+1\right)^{\frac{1}{2}}+\left(\left(\frac{l_{cp_{b2}}^2(\cos\tilde{\psi}_\varphi-1)^2}{(h+l_{cp_{b2}}\sin\tilde{\psi}_\varphi)^2}+1\right)^{\frac{1}{2}}-1\right)\frac{h}{l_{cp_{b2}}\sin\tilde{\psi}_\varphi}\right] \\
& \left[\left(\frac{l_{cp_{b2}}^2(\cos\tilde{\psi}_\varphi-1)^2}{(h+l_{cp_{b2}}\sin\tilde{\psi}_\varphi)^2}+1\right)^{-\frac{1}{2}}\left(\frac{h+l_{cp_{b2}}\tan\tilde{\psi}_\varphi}{\frac{h}{\cos\tilde{\psi}_\varphi}+l_{cp_{b2}}\tan\tilde{\psi}_\varphi}\right)\right]
\end{aligned}
\tag{5.40}
$$

$$
\begin{aligned}
\Lambda_{d_{c1}} =& \frac{1}{2}\left[\left(\frac{l_{d_{c1}}^2(\cos\vartheta-1)^2}{(h-l_{d_{c1}}\sin\vartheta)^2}+1\right)^{\frac{1}{2}}+\left(1-\left(\frac{l_{d_{c1}}^2(\cos\vartheta-1)^2}{(h-l_{d_{c1}}\sin\vartheta)^2}+1\right)^{\frac{1}{2}}\right)\frac{h}{l_{d_{c1}}\sin\vartheta}\right]\\
&\left[\left(\frac{l_{d_{c1}}^2(\cos\vartheta-1)^2}{(h-l_{d_{c1}}\sin\vartheta)^2}+1\right)^{-\frac{1}{2}}\left(\frac{h-l_{d_{c1}}\tan\vartheta}{\frac{h}{\cos\vartheta}-l_{d_{c1}}\tan\vartheta}\right)\right]+\\
&\frac{1}{2}\left[\left(\frac{l_{d_{c1}}^2(\cos\vartheta-1)^2}{(h+l_{d_{c1}}\sin\vartheta)^2}+1\right)^{\frac{1}{2}}+\left(\left(\frac{l_{d_{c1}}^2(\cos\vartheta-1)^2}{(h+l_{d_{c1}}\sin\vartheta)^2}+1\right)^{\frac{1}{2}}-1\right)\frac{h}{l_{d_{c1}}\sin\vartheta}\right]\\
&\left[\left(\frac{l_{d_{c1}}^2(\cos\vartheta-1)^2}{(h+l_{d_{c1}}\sin\vartheta)^2}+1\right)^{-\frac{1}{2}}\left(\frac{h+l_{d_{c1}}\tan\vartheta}{\frac{h}{\cos\vartheta}+l_{d_{c1}}\tan\vartheta}\right)\right]\\
\Lambda_{d_{c2}} =& \frac{1}{2}\left[\left(\frac{l_{d_{c2}}^2(\cos\varphi-1)^2}{(h-l_{d_{c2}}\sin\varphi)^2}+1\right)^{\frac{1}{2}}+\left(1-\left(\frac{l_{d_{c2}}^2(\cos\varphi-1)^2}{(h-l_{d_{c2}}\sin\varphi)^2}+1\right)^{\frac{1}{2}}\right)\frac{h}{l_{d_{c2}}\sin\varphi}\right]\\
&\left[\left(\frac{l_{d_{c2}}^2(\cos\varphi-1)^2}{(h-l_{d_{c2}}\sin\varphi)^2}+1\right)^{-\frac{1}{2}}\left(\frac{h-l_{d_{c2}}\tan\varphi}{\frac{h}{\cos\varphi}-l_{d_{c2}}\tan\varphi}\right)\right]+\\
&\frac{1}{2}\left[\left(\frac{l_{d_{c2}}^2(\cos\varphi-1)^2}{(h+l_{d_{c2}}\sin\varphi)^2}+1\right)^{\frac{1}{2}}+\left(\left(\frac{l_{d_{c2}}^2(\cos\varphi-1)^2}{(h+l_{d_{c2}}\sin\varphi)^2}+1\right)^{\frac{1}{2}}-1\right)\frac{h}{l_{d_{c2}}\sin\varphi}\right]\\
&\left[\left(\frac{l_{d_{c2}}^2(\cos\varphi-1)^2}{(h+l_{d_{c2}}\sin\varphi)^2}+1\right)^{-\frac{1}{2}}\left(\frac{h+l_{d_{c2}}\tan\varphi}{\frac{h}{\cos\varphi}+l_{d_{c2}}\tan\varphi}\right)\right]\\
\Lambda_{d_{b1}} =& \frac{1}{2}\left[\left(\frac{l_{d_{b1}}^2(\cos\tilde{\psi}_\vartheta-1)^2}{(h-l_{d_{b1}}\sin\tilde{\psi}_\vartheta)^2}+1\right)^{\frac{1}{2}}+\left(1-\left(\frac{l_{d_{b1}}^2(\cos\tilde{\psi}_\vartheta-1)^2}{(h-l_{d_{b1}}\sin\tilde{\psi}_\vartheta)^2}+1\right)^{\frac{1}{2}}\right)\frac{h}{l_{d_{b1}}\sin\tilde{\psi}_\vartheta}\right]\\
&\left[\left(\frac{l_{d_{b1}}^2(\cos\tilde{\psi}_\vartheta-1)^2}{(h-l_{d_{b1}}\sin\tilde{\psi}_\vartheta)^2}+1\right)^{-\frac{1}{2}}\left(\frac{h-l_{d_{b1}}\tan\tilde{\psi}_\vartheta}{\frac{h}{\cos\tilde{\psi}_\vartheta}-l_{d_{b1}}\tan\tilde{\psi}_\vartheta}\right)\right]+\\
&\frac{1}{2}\left[\left(\frac{l_{cp_{b1}}^2(\cos\tilde{\psi}_\vartheta-1)^2}{(h+l_{cp_{b1}}\sin\tilde{\psi}_\vartheta)^2}+1\right)^{\frac{1}{2}}+\left(\left(\frac{l_{d_{b1}}^2(\cos\tilde{\psi}_\vartheta-1)^2}{(h+l_{d_{b1}}\sin\tilde{\psi}_\vartheta)^2}+1\right)^{\frac{1}{2}}-1\right)\frac{h}{l_{d_{b1}}\sin\tilde{\psi}_\vartheta}\right]\\
&\left[\left(\frac{l_{d_{b1}}^2(\cos\tilde{\psi}_\vartheta-1)^2}{(h+l_{d_{b1}}\sin\tilde{\psi}_\vartheta)^2}+1\right)^{-\frac{1}{2}}\left(\frac{h+l_{d_{b1}}\tan\tilde{\psi}_\vartheta}{\frac{h}{\cos\tilde{\psi}_\vartheta}+l_{d_{b1}}\tan\tilde{\psi}_\vartheta}\right)\right]\\
\Lambda_{d_{b2}} =& \frac{1}{2}\left[\left(\frac{l_{d_{b2}}^2(\cos\tilde{\psi}_\varphi-1)^2}{(h-l_{d_{b2}}\sin\tilde{\psi}_\varphi)^2}+1\right)^{\frac{1}{2}}+\left(1-\left(\frac{l_{d_{b2}}^2(\cos\tilde{\psi}_\varphi-1)^2}{(h-l_{d_{b2}}\sin\tilde{\psi}_\varphi)^2}+1\right)^{\frac{1}{2}}\right)\frac{h}{l_{d_{b2}}\sin\tilde{\psi}_\varphi}\right]\\
&\left[\left(\frac{l_{d_{b2}}^2(\cos\tilde{\psi}_\varphi-1)^2}{(h-l_{d_{b2}}\sin\tilde{\psi}_\varphi)^2}+1\right)^{-\frac{1}{2}}\left(\frac{h-l_{d_{b2}}\tan\tilde{\psi}_\varphi}{\frac{h}{\cos\tilde{\psi}_\varphi}-l_{d_{b2}}\tan\tilde{\psi}_\varphi}\right)\right]+\\
&\frac{1}{2}\left[\left(\frac{l_{d_{b2}}^2(\cos\tilde{\psi}_\varphi-1)^2}{(h+l_{d_{b2}}\sin\tilde{\psi}_\varphi)^2}+1\right)^{\frac{1}{2}}+\left(\left(\frac{l_{d_{b2}}^2(\cos\tilde{\psi}_\varphi-1)^2}{(h+l_{d_{b2}}\sin\tilde{\psi}_\varphi)^2}+1\right)^{\frac{1}{2}}-1\right)\frac{h}{l_{d_{b2}}\sin\tilde{\psi}_\varphi}\right]\\
&\left[\left(\frac{l_{d_{b2}}^2(\cos\tilde{\psi}_\varphi-1)^2}{(h+l_{cp_{b2}}\sin\tilde{\psi}_\varphi)^2}+1\right)^{-\frac{1}{2}}\left(\frac{h+l_{d_{b2}}\tan\tilde{\psi}_\varphi}{\frac{h}{\cos\tilde{\psi}_\varphi}+l_{d_{b2}}\tan\tilde{\psi}_\varphi}\right)\right]
\end{aligned}
\tag{5.41}
$$

$$
\begin{aligned}
\Delta_{cp_{c1}} &= \left(\frac{l_{cp_{c1}}^2(\cos\vartheta-1)^2}{(h+l_{cp_{c1}}\sin\vartheta)^2}+1\right)^{-\frac{1}{2}}\left(\frac{h+l_{cp_{c1}}\tan\vartheta}{\frac{h}{\cos\vartheta}+l_{cp_{c1}}\tan\vartheta}\right)+\\
&-\left(\frac{l_{cp_{c1}}^2(\cos\vartheta-1)^2}{(h-l_{cp_{c1}}\sin\vartheta)^2}+1\right)^{-\frac{1}{2}}\left(\frac{h-l_{cp_{c1}}\tan\vartheta}{\frac{h}{\cos\vartheta}-l_{cp_{c1}}\tan\vartheta}\right)\\
\Delta_{cp_{c2}} &= \left(\frac{l_{cp_{c2}}^2(\cos\varphi-1)^2}{(h+l_{cp_{c2}}\sin\varphi)^2}+1\right)^{-\frac{1}{2}}\left(\frac{h+l_{cp_{c2}}\tan\varphi}{\frac{h}{\cos\varphi}+l_{cp_{c1}}\tan\varphi}\right)+\\
&-\left(\frac{l_{cp_{c2}}^2(\cos\varphi-1)^2}{(h-l_{cp_{c2}}\sin\varphi)^2}+1\right)^{-\frac{1}{2}}\left(\frac{h-l_{cp_{c2}}\tan\varphi}{\frac{h}{\cos\varphi}-l_{cp_{c2}}\tan\varphi}\right)\\
\Delta_{cp_{b1}} &= \left(\frac{l_{cp_{b1}}^2(\cos\psi-1)^2}{(h+l_{cp_{b1}}\sin\psi)^2}+1\right)^{-\frac{1}{2}}\left(\frac{h+l_{cp_{b1}}\tan\psi}{\frac{h}{\cos\psi}+l_{cp_{b1}}\tan\psi}\right)+\\
&-\left(\frac{l_{cp_{b1}}^2(\cos\psi-1)^2}{(h-l_{cp_{b1}}\sin\psi)^2}+1\right)^{-\frac{1}{2}}\left(\frac{h-l_{cp_{b1}}\tan\psi}{\frac{h}{\cos\psi}-l_{cp_{b1}}\tan\psi}\right)\\
\Delta_{cp_{b2}} &= \left(\frac{l_{cp_{b2}}^2(\cos\widetilde{\psi}-1)^2}{(h+l_{cp_{b2}}\sin\widetilde{\psi})^2}+1\right)^{-\frac{1}{2}}\left(\frac{h+l_{cp_{b2}}\tan\widetilde{\psi}}{\frac{h}{\cos\widetilde{\psi}}+l_{cp_{b1}}\tan\widetilde{\psi}}\right)+\\
&-\left(\frac{l_{cp_{b2}}^2(\cos\widetilde{\psi}-1)^2}{(h-l_{cp_{b2}}\sin\widetilde{\psi})^2}+1\right)^{-\frac{1}{2}}\left(\frac{h-l_{cp_{b2}}\tan\widetilde{\psi}}{\frac{h}{\cos\widetilde{\psi}}-l_{cp_{b2}}\tan\widetilde{\psi}}\right)
\end{aligned}
\tag{5.42}
$$

$$
\begin{aligned}
\Gamma &= -m_b\left[((H_c-H_b)\cos\vartheta+l_c\sin\vartheta)\left(\frac{l}{2}\sin\psi+\frac{H_b}{2}\cos\psi\right)\right]+\\
&-m_b\left[(l_c\cos\vartheta-(H_c-H_b)\sin\vartheta)\left(\frac{l}{2}\cos\psi-\frac{H_b}{2}\sin\psi\right)\right]\\
\Delta_{\dot{\vartheta}^2} &= -m_b\left[(l_c\cos\vartheta-(H_c-H_b)\sin\vartheta)\left(\frac{l}{2}\sin\psi+\frac{H_b}{2}\cos\psi\right)\right]+\\
&-m_b\left[((H_c-H_b)\cos\vartheta+l_c\sin\vartheta)\left(\frac{l}{2}\cos\psi-\frac{H_b}{2}\sin\psi\right)\right]\\
\Delta_{\dot{\psi}^2} &= -m_b\left[((H_c-H_b)\cos\vartheta+l_c\sin\vartheta)\left(\frac{l}{2}\cos\psi+\frac{H_b}{2}\sin\psi\right)\right]+\\
&-m_b\left[((H_c-H_b)\sin\vartheta-l_c\cos\vartheta)\left(\frac{l}{2}\sin\psi+\frac{H_b}{2}\cos\psi\right)\right]
\end{aligned}
\tag{5.43}
$$

5.3.5 Equation of motion

Assuming large displacements the equation of motion is

$$
\begin{aligned}
&F(B_c \sin\vartheta - H_c \cos\vartheta) + \\
&- W_{c1}\frac{H_c}{2}\sin\vartheta - W_{c2}\frac{H_c}{2}\Phi\sin\varphi + \\
&+ W_b\left[\Big(l_c\cos\vartheta - (H_c - H_b)\sin\vartheta\Big) + \left(\frac{l}{2}\cos\psi - \frac{H_b}{2}\sin\psi\right)\left(-\frac{2l_c}{l}\Psi\right)\right] + \\
&+ m_{c1}\ddot{u}_g\frac{H_c}{2}\cos\vartheta + m_{c1}\ddot{v}_g\frac{H_c}{2}\sin\vartheta - I_{c1}\ddot{\vartheta} + \\
&+ \left[m_{c2}\ddot{u}_g\frac{H_c}{2}\cos\varphi + m_{c2}\ddot{v}_g\frac{H_c}{2}\sin\varphi - I_{c2}\ddot{\varphi}\right]\Phi + \\
&+ \left[m_b\ddot{u}_g\left(\frac{H_b}{2}\cos\psi + \frac{l}{2}\sin\psi\right) + m_b\ddot{v}_g\left(\frac{H_b}{2}\sin\psi - \frac{l}{2}\cos\psi\right) - I_{b_{b1}}\ddot{\psi}\right]\left(-\frac{2l_c}{l}\Psi\right) + \\
&+ m_b\ddot{u}_g\Big[\ (H_c - H_b)\cos\vartheta + l_c\sin\vartheta\Big] + \\
&+ m_b\ddot{v}_g\Big[\ (H_c - H_b)\sin\vartheta - l_c\cos\vartheta\Big] - m_b\Big[\ l_c^2 + (H_c - H_b)^2\Big]\ddot{\vartheta} + \\
&- m_b\Gamma\ddot{\vartheta}\left(-\frac{2l_c}{l}\Psi\right) - m_b\Gamma\ddot{\psi} + \Delta_{\dot{\psi}^2}\dot{\psi}^2 + \Delta_{\dot{\vartheta}^2}\dot{\vartheta}^2\left(-\frac{2l_c}{l}\Psi\right) + \\
&- T_0\Delta_{cp_{c1}}l_{cp_{c1}} - 2\frac{(EA)_{cp_{c1}}}{L_{cp_{c1}}}\Lambda_{cp_{c1}}l_{cp_{c1}}^2\sin\vartheta + \\
&- T_0\Delta_{cp_{c2}}l_{cp_{c2}} - 2\frac{(EA)_{cp_{c2}}}{L_{cp_{c2}}}\Lambda_{cp_{c2}}\Phi l_{cp_{c2}}^2\sin\varphi + \\
&+ \left[-T_0\Delta_{cp_{b1}}l_{cp_{b1}} - 2\frac{(EA)_{cp_{b1}}}{L_{cp_{b1}}}\Lambda_{cp_{b1}}l_{cp_{b1}}^2\sin\tilde{\psi}_\vartheta\right]\left(-\frac{2l_c}{l}\Psi - 1\right) + \\
&+ \left[-T_0\Delta_{cp_{b2}}l_{cp_{b2}} - 2\frac{(EA)_{cp_{b2}}}{L_{cp_{b2}}}\Lambda_{cp_{b2}}l_{cp_{b2}}^2\sin\tilde{\psi}_\varphi\right]\left(-\frac{2l_c}{l}\Psi - 1\right) + \\
&- 2\frac{(EA)_{d_{c1}}}{L_{d_{c1}}}\Lambda_{d_{c1}}l_{d_{c1}}^2\sin\vartheta - 2\frac{(EA)_{d_{c2}}}{L_{d_{c2}}}\Lambda_{d_{c2}}\Phi l_{d_{c2}}^2\sin\varphi + \\
&+ \left[-2\frac{(EA)_{d_{b1}}}{L_{d_{b1}}}\Lambda_{d_{b1}}l_{d_{b1}}^2\sin\tilde{\psi}_\vartheta - 2\frac{(EA)_{d_{b2}}}{L_{d_{b2}}}\Lambda_{d_{b2}}l_{d_{b2}}^2\sin\tilde{\psi}_\varphi\right]\left(-\frac{2l_c}{l}\Psi - 1\right) = 0
\end{aligned}
\tag{5.44}
$$

with the next conditions among angles

$$\begin{aligned} &l_c\cos\vartheta-(H_c-H_b)\sin\vartheta+l\cos\psi=L-l_c\cos\varphi-(H_c-H_b)\sin\varphi\\ &l_c\sin\vartheta+(H_c-H_b)\cos\vartheta+l\sin\psi=(H_c-H_b)\cos\varphi-l_c\sin\varphi \end{aligned} \tag{5.45}$$

Assuming small displacements and considering the relations among angles

$$\begin{aligned} &\sin\vartheta=\vartheta, && \cos\vartheta=1,\\ &\sin\varphi=\varphi=\vartheta, && \cos\varphi=1,\\ &\sin\psi=\psi=-\frac{2l_c}{l}\vartheta, && \cos\psi=1,\\ &\sin\tilde{\psi}_\vartheta=\tilde{\psi}_\vartheta=\psi-\vartheta=-\frac{2l_c}{l}\vartheta-\vartheta, && \cos\tilde{\psi}_\vartheta=1,\\ &\sin\tilde{\psi}_\varphi=\tilde{\psi}_\varphi=\psi-\varphi=-\frac{2l_c}{l}\vartheta-\vartheta, && \cos\tilde{\psi}_\varphi=1. \end{aligned}$$

substituting

$$\Delta_{cp_{c1}}=\Delta_{cp_{c2}}=\Delta_{cp_{b1}}=\Delta_{cp_{b2}}=0,$$

$$\Psi=\Phi=1$$

$$\Lambda_{cp_{c1}}=\Lambda_{cp_{c2}}=\Lambda_{cp_{b1}}=\Lambda_{cp_{b2}}=\Lambda_{d_{c1}}=\Lambda_{d_{c2}}=\Lambda_{d_{b1}}=\Lambda_{d_{b2}}=1.$$

The equation of motion for the idealized structure, assumed to be linearly elastic, subjected to an external force and to earthquake excitation becomes

$$\begin{aligned} &F(B_c\vartheta-H_c)+\\ &-W_cH_c\vartheta+W_b\left[(H_c-H_b)\frac{l}{2l_c}-\frac{H_b}{2}-\frac{H_b}{2}\left(-\frac{2l_c}{l}-1\right)\right]\left(-\frac{2l_c}{l}\right)\vartheta+\\ &+m_c\ddot{u}_gH_c+m_b\ddot{u}_g\left[-(H_c-H_b)\frac{l}{2l_c}+\frac{H_b}{2}+\frac{l}{2}\left(-\frac{2l_c}{l}-1\right)\vartheta\right]\left(-\frac{2l_c}{l}\right)+\\ &+m_c\ddot{v}_gH_c\vartheta+m_b\ddot{v}_g\left[-(H_c-H_b)\frac{l}{2l_c}+\frac{H_b}{2}+\frac{H_b}{2}\left(-\frac{2l_c}{l}-1\right)\right]\left(-\frac{2l_c}{l}\right)\vartheta+\\ &-I_{c1}\ddot{\vartheta}-I_{c2}\ddot{\vartheta}-\left(\frac{2l_c}{l}\right)^2I_{c_b}\ddot{\vartheta}+\\ &-4\frac{(EA)_{cp_c}}{L_{cp_c}}l_{cp_c}^2\vartheta-4\frac{(EA)_{cp_b}}{L_{cp_b}}\frac{L^2}{l^2}l_{cp_b}^2\vartheta-4\frac{(EA)_{d_c}}{L_{d_c}}l_{d_c}^2\vartheta-4\frac{(EA)_{d_b}}{L_{d_b}}\frac{L^2}{l^2}l_{d_b}^2\vartheta=0 \end{aligned} \tag{5.46}$$

introducing $\tilde{H} = (H_c - H_b)\frac{l}{2l_c} - \frac{H_b}{2}$, distance between the beam center of mass and the beam absolute center of rotation , can be written

$$
\begin{aligned}
&F(B_c\vartheta - H_c) - W_c H_c\vartheta + W_b\left[\tilde{H} - \frac{H_b}{2}\left(-\frac{2l_c}{l} - 1\right)\right]\left(-\frac{2l_c}{l}\right)\vartheta + \\
&+ m_c\ddot{u}_g H_c + m_b\ddot{u}_g\left[-\tilde{H} + \frac{l}{2}\left(-\frac{2l_c}{l} - 1\right)\vartheta\right]\left(-\frac{2l_c}{l}\right) + \\
&+ m_c\ddot{v}_g H_c\vartheta + m_b\ddot{v}_g\left[-\tilde{H} + \frac{H_b}{2}\left(-\frac{2l_c}{l} - 1\right)\right]\left(-\frac{2l_c}{l}\right)\vartheta + \\
&- I_{c1}\ddot{\vartheta} - I_{c2}\ddot{\vartheta} - \left(\frac{2l_c}{l}\right)^2 I_{c_b}\ddot{\vartheta} + \\
&- 4\frac{(EA)_{cp_c}}{L_{cp_c}} l_{cp_c}^2\vartheta - 4\frac{(EA)_{cp_b}}{L_{cp_b}}\frac{L^2}{l^2} l_{cp_b}^2\vartheta - 4\frac{(EA)_{d_c}}{L_{d_c}} l_{d_c}^2\vartheta - 4\frac{(EA)_{d_b}}{L_{d_b}}\frac{L^2}{l^2} l_{d_b}^2\vartheta = 0
\end{aligned}
\tag{5.47}
$$

or

$$
\begin{aligned}
&F(B_c\vartheta - H_c) - W_c H_c\vartheta - W_b\left[\tilde{H} - \frac{H_b}{2}\left(-\frac{2l_c}{l} - 1\right)\right]\left(\frac{2l_c}{l}\right)\vartheta + \\
&+ m_c\ddot{u}_g H_c + m_b\ddot{u}_g\left[\tilde{H} - \frac{l}{2}\left(-\frac{2l_c}{l} - 1\right)\vartheta\right]\left(\frac{2l_c}{l}\right) + \\
&+ m_c\ddot{v}_g H_c\vartheta + m_b\ddot{v}_g\left[\tilde{H} - \frac{H_b}{2}\left(-\frac{2l_c}{l} - 1\right)\right]\left(\frac{2l_c}{l}\right)\vartheta - 2I_c\ddot{\vartheta} - \left(\frac{2l_c}{l}\right)^2 I_{c_b}\ddot{\vartheta} + \\
&- 4\frac{(EA)_{cp_c}}{L_{cp_c}} l_{cp_c}^2\vartheta - 4\frac{(EA)_{cp_b}}{L_{cp_b}}\frac{L^2}{l^2} l_{cp_b}^2\vartheta - 4\frac{(EA)_{d_c}}{L_{d_c}} l_{d_c}^2\vartheta - 4\frac{(EA)_{d_b}}{L_{d_b}}\frac{L^2}{l^2} l_{d_b}^2\vartheta = 0
\end{aligned}
\tag{5.48}
$$

5.4 Natural Vibration Frequency and Period

In this section we determine the natural vibration frequency and period of the system. Assuming small displacements, without earthquake excitation and external force, the equation governing the motion is

$$\left[-2I_c - \left(\frac{2l_c}{l}\right)^2 I_{c_b}\right]\ddot{\vartheta} - W_c H_c \vartheta - W_b\left[\tilde{H} - \frac{H_b}{2}\left(-\frac{2l_c}{l} - 1\right)\right]\left(\frac{2l_c}{l}\right)\vartheta +$$

$$- 4\frac{(EA)_{cp_c}}{L_{cp_c}} l^2_{cp_c}\vartheta - 4\frac{(EA)_{cp_b}}{L_{cp_b}}\frac{L^2}{l^2} l^2_{cp_b}\vartheta - 4\frac{(EA)_{d_c}}{L_{d_c}} l^2_{d_c}\vartheta - 4\frac{(EA)_{d_b}}{L_{d_b}}\frac{L^2}{l^2} l^2_{d_b}\vartheta = 0 \tag{5.49}$$

the previous equation, after the positions

$K_{cp} = 4\frac{(EA)_{cp_c}}{L_{cp_c}} l^2_{cp_c} + 4\frac{(EA)_{cp_b}}{L_{cp_b}}\frac{L^2}{l^2} l^2_{cp_b}$, $\quad K_d = 4\frac{(EA)_{d_c}}{L_{d_c}} l^2_{d_c} + 4\frac{(EA)_{d_b}}{L_{d_b}}\frac{L^2}{l^2} l^2_{d_b}$,
$K_{cp,d} = K_{cp} + K_d$, $\quad K_w = -W_c H_c \vartheta - W_b\left[\tilde{H} - \frac{H_b}{2}\left(-\frac{2l_c}{l} - 1\right)\right]\left(\frac{2l_c}{l}\right)\vartheta$,
$I_0 = 2I_c + \left(\frac{2l_c}{l}\right)^2 I_{c_b}$.

can be written as:

$$\boxed{I_0\ddot{\vartheta} + (K_{cp,d} - K_w)\vartheta = 0}$$

thus the natural vibration frequency of the system is:

$$\boxed{\omega = \sqrt{\frac{K_{cp,d} - K_w}{I_0}}} \tag{5.50}$$

and the natural vibration period is

$$\boxed{T = \frac{2\pi}{\omega} = 2\pi\sqrt{\frac{I_0}{K_{cp,d} - K_w}}} \tag{5.51}$$

5.5 Buckling Load

The equation of motion presented in the preceding sections of this chapter provides a basis to determine the buckling load of a structure.

Here to determine critical load, the equation of virtual power for the system is written with two vertical external force applied on the top of each column.

Considering large displacement, the equation of motion is

$$
\begin{aligned}
&-\frac{P}{2}H_c\sin\vartheta-\frac{P}{2}H_c\Phi\sin\varphi+F(B_c\sin\vartheta-H_c\cos\vartheta)+\\
&-W_{c1}\frac{H_c}{2}\sin\vartheta-W_{c2}\frac{H_c}{2}\Phi\sin\varphi+\\
&+W_b\left[\Big(\,l_c\cos\vartheta-(H_c-H_b)\sin\vartheta\Big)+\left(\frac{l}{2}\cos\psi-\frac{H_b}{2}\sin\psi\right)\left(-\frac{2l_c}{l}\Psi\right)\right]+\\
&-I_{c1}\ddot{\vartheta}-I_{c2}\ddot{\varphi}\Phi-I_{b_{b1}}\ddot{\psi}\left(-\frac{2l_c}{l}\Psi\right)-m_b\left[\,l_c^2+(H_c-H_b)^2\right]\ddot{\vartheta}+\\
&-m_b\Gamma\ddot{\vartheta}\left(-\frac{2l_c}{l}\Psi\right)-m_b\Gamma\ddot{\psi}+\Delta_{\dot{\psi}^2}\dot{\psi}^2+\Delta_{\dot{\vartheta}^2}\dot{\vartheta}^2\left(-\frac{2l_c}{l}\Psi\right)+\\
&-T_0\Delta_{cp_{c1}}l_{cp_{c1}}-2\frac{(EA)_{cp_{c1}}}{L_{cp_{c1}}}\Lambda_{cp_{c1}}l_{cp_{c1}}^2\sin\vartheta+\\
&-T_0\Delta_{cp_{c2}}l_{cp_{c2}}-2\frac{(EA)_{cp_{c2}}}{L_{cp_{c2}}}\Lambda_{cp_{c2}}\Phi l_{cp_{c2}}^2\sin\varphi+\\
&+\left[-T_0\Delta_{cp_{b1}}l_{cp_{b1}}-2\frac{(EA)_{cp_{b1}}}{L_{cp_{b1}}}\Lambda_{cp_{b1}}l_{cp_{b1}}^2\sin\tilde{\psi}_\vartheta\right]\left(-\frac{2l_c}{l}\Psi-1\right)+\\
&+\left[-T_0\Delta_{cp_{b2}}l_{cp_{b2}}-2\frac{(EA)_{cp_{b2}}}{L_{cp_{b2}}}\Lambda_{cp_{b2}}l_{cp_{b2}}^2\sin\tilde{\psi}_\varphi\right]\left(-\frac{2l_c}{l}\Psi-1\right)+\\
&-2\frac{(EA)_{d_{c1}}}{L_{d_{c1}}}\Lambda_{d_{c1}}l_{d_{c1}}^2\sin\vartheta-2\frac{(EA)_{d_{c2}}}{L_{d_{c2}}}\Lambda_{d_{c2}}\Phi l_{d_{c2}}^2\sin\varphi+\\
&+\left[-2\frac{(EA)_{d_{b1}}}{L_{d_{b1}}}\Lambda_{d_{b1}}l_{d_{b1}}^2\sin\tilde{\psi}_\vartheta-2\frac{(EA)_{d_{b2}}}{L_{d_{b2}}}\Lambda_{d_{b2}}l_{d_{b2}}^2\sin\tilde{\psi}_\varphi\right]\left(-\frac{2l_c}{l}\Psi-1\right)=0
\end{aligned}
\tag{5.52}
$$

Because of the difficulty in obtaining the critical load using the equation of motion assuming large displacement, the buckling load is evaluated assuming small displacements. The previous equation of motion, without horizontal

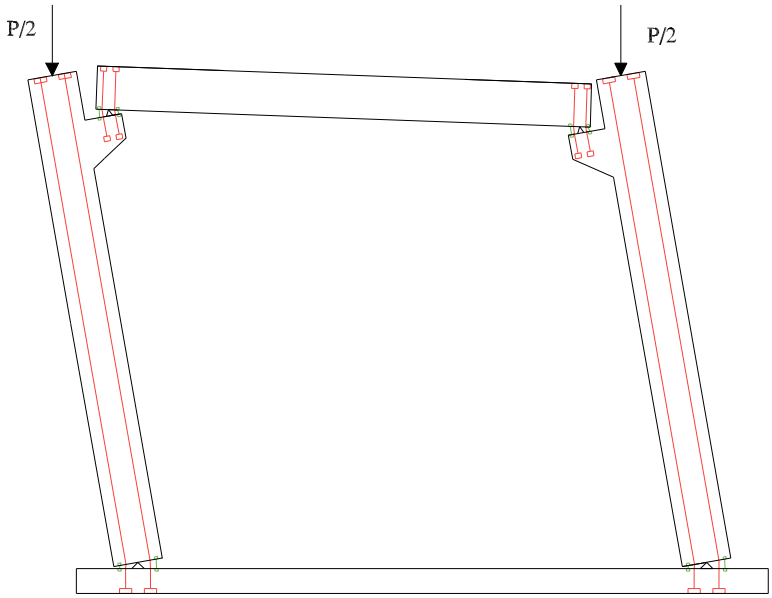

Figure 5.8: Buckling Load

external force, becomes:

$$-PH_c\vartheta - W_cH_c\vartheta - W_b\left[\tilde{H} - \frac{H_b}{2}\left(-\frac{2l_c}{l} - 1\right)\right]\left(\frac{2l_c}{l}\right)\vartheta + \\ -4\frac{(EA)_{cp_c}}{L_{cp_c}}l^2_{cp_c}\vartheta - 4\frac{(EA)_{cp_b}}{L_{cp_b}}\frac{L^2}{l^2}l^2_{cp_b}\vartheta - 4\frac{(EA)_{d_c}}{L_{d_c}}l^2_{d_c}\vartheta - 4\frac{(EA)_{d_b}}{L_{d_b}}\frac{L^2}{l^2}l^2_{d_b}\vartheta = 0 \tag{5.53}$$

As shown in figure **??** in the displaced position of the frame, the vertical external force introduces a moment and decreases the stiffness of the system. Introducing the previous positions we can be write

$$PH_c\vartheta + (K_{cp,d} - K_w)\vartheta = 0 \tag{5.54}$$

or

$$[PH_c + (K_{cp,d} - K_w)]\vartheta = 0 \tag{5.55}$$

and therefore, the stiffness of the system become zero if the external vertical force, critical force, is

$$\boxed{P_{crit} = -\frac{(K_{cp,d} - K_w)}{H_c}} \tag{5.56}$$

5.6 Conditions for post-tensioned strands

5.6.1 Conditions to avoid compression in post tensioned strands

Defined T_{0_c} the initial tension in post-tensioned elements, the tension for the same elements is:

$$T_c = -T_{0_c} + \frac{(EA)_{cp_c}}{L_{cp_c}} l_{cp_c} \vartheta \tag{5.57}$$

Imposing $T_c = 0$ can be write:

$$\vartheta_{scar} = T_{0_c} \frac{L_{cp_c}}{(EA)_{cp_c} l_{cp_c}} = \frac{T_{0_c}}{k_{cp_c} l_{cp_c}} \tag{5.58}$$

Define T_{0_b} the initial tension of post tensioned strands for the beams, is obtained:

$$T_b = -T_{0_b} + \frac{(EA)_{cp_b}}{L_{cp_b}} l_{cp_b} \left(\frac{2l_c}{l} + 1 \right) \vartheta = -T_{0_b} + \frac{(EA)_{cp_b}}{L_{cp_b}} l_{cp_b} \frac{L}{l} \vartheta \tag{5.59}$$

and then

$$\vartheta_{scar} = T_{0_b} \frac{L_{cp_b}}{(EA)_{cp_b} l_{cp_b}} \frac{l}{L} = \frac{T_{0_b}}{k_{cp_b} l_{cp_b}} \frac{l}{L} \tag{5.60}$$

5.6.2 Conditions to avoid the yielding of post tensioned strands

Defined $\sigma_y = F_y / A_{cp_c}$ the yielding strength of post tensioned strands to avoid the yielding must be verified:

$$T_c = T_{0_c} + \frac{(EA)_{cp_c}}{L_{cp_c}} l_{cp_c} \vartheta \leq F_{y_c} = \sigma_y A_{cp_c} \tag{5.61}$$

From the previous defining $\sigma_{0_c} = T_{0_c} / A_{cp_c}$ follow

$$\sigma_y \geq \sigma_{0_c} + \frac{E_{cp_c}}{L_{cp_c}} l_{cp_c} \vartheta \tag{5.62}$$

$$\vartheta_{yielding} = (\sigma_y - \sigma_{0_c}) \frac{L_{cp_c}}{E_{cp_c} l_{cp_c}} \tag{5.63}$$

Egual considerations for the beam drive to the next

$$T_b = T_{0_b} + \frac{(EA)_{cp_b}}{L_{cp_b}} l_{cp_b} \left(\frac{2l_c}{l} + 1 \right) \vartheta \leq F_{y_b} = \sigma_y A_{cp_b} \tag{5.64}$$

$$\sigma_y \geq \sigma_{0_b} + \frac{E_{cp_b}}{L_{cp_b}} l_{cp_b} \frac{L}{l} \vartheta \tag{5.65}$$

$$\vartheta_{yielding} = (\sigma_y - \sigma_{0_b}) \frac{L_{cp_b}}{E_{cp_b} l_{cp_b}} \frac{l}{L} \tag{5.66}$$

5.7 Quasi-Static External Force-Rotation Relation

The static force rotation relation is next developed. In particular the force is assumed horizontal and applied at the top of the left column and the considered rotation is the left column rotation around the hinge positioned at the same column base.

Starting from the equation of motion (5.44) and not considering earthquake excitation and inertial forces is obtained:

$$F(B_c\vartheta - H_c) - W_c H_c \vartheta - W_b \left[\tilde{H} - \frac{H_b}{2}\left(-\frac{2l_c}{l} - 1\right)\right]\left(\frac{2l_c}{l}\right)\vartheta + \\ - 4\frac{(EA)_{cp_c}}{L_{cp_c}} l_{cp_c}^2 \vartheta - 4\frac{(EA)_{cp_b}}{L_{cp_b}} \frac{L^2}{l^2} l_{cp_b}^2 \vartheta - 4\frac{(EA)_{d_c}}{L_{d_c}} l_{d_c}^2 \vartheta - 4\frac{(EA)_{d_b}}{L_{d_b}} \frac{L^2}{l^2} l_{d_b}^2 \vartheta = 0 \tag{5.67}$$

the previous equation, assuming $M_F(\vartheta) = F(B_c\vartheta - H_c)$, positive if counter-clockwise could be written

$$M_F - W_c H_c \vartheta - W_b \left[\tilde{H} - \frac{H_b}{2}\left(-\frac{2l_c}{l} - 1\right)\right]\left(\frac{2l_c}{l}\right)\vartheta + \\ - 4\frac{(EA)_{cp_c}}{L_{cp_c}} l_{cp_c}^2 \vartheta - 4\frac{(EA)_{cp_b}}{L_{cp_b}} \frac{L^2}{l^2} l_{cp_b}^2 \vartheta - 4\frac{(EA)_{d_c}}{L_{d_c}} l_{d_c}^2 \vartheta - 4\frac{(EA)_{d_b}}{L_{d_b}} \frac{L^2}{l^2} l_{d_b}^2 \vartheta = 0 \tag{5.68}$$

or, in a more compact way,

$$M_F = (k_{cp} + k_d - k_w)\vartheta \tag{5.69}$$

In Fig. 5.9 and Fig. 5.10 the hysteresis loop for the post tensioned elements, for the dissipators and for the global system is shown step by step. In the same figures it's possible to appreciate the tension variation in each element of the system and globally. The

5.8 Residual Rotation

It's evident that as soon as we are in presence of dissipators activation, a residual deformation will appeared. On the other hand assuming elastic behavior for post tensioned strands, with the activated dissipators substitution, the tension variation presents in these elements in the deformed configuration respect to the un-deformed configuration will recentering the structure in an automatic way. Therefore the re-centering is enforced with the only activated dissipators substitution. However, it'll be important to have control and to limit the residual deformation and for this reasons the relation between residual rotation, directly related to the residual deformation, and the mechanical parameters characterizing the system will be determined. Looking at Fig. 5.9 and Fig. 5.10 it can be seen that the residual rotation can be expressed

$$\begin{aligned} \vartheta_{res} =& \vartheta_u - 2\vartheta_y - \frac{F_u - 2Fy}{k_2} = \\ =& \vartheta_u - 2\vartheta_y - \frac{1}{k_2}[k_1\vartheta_y + k_2(\vartheta_u - \vartheta_y)] + 2\frac{k_1}{k_2}\vartheta_y \end{aligned} \tag{5.70}$$

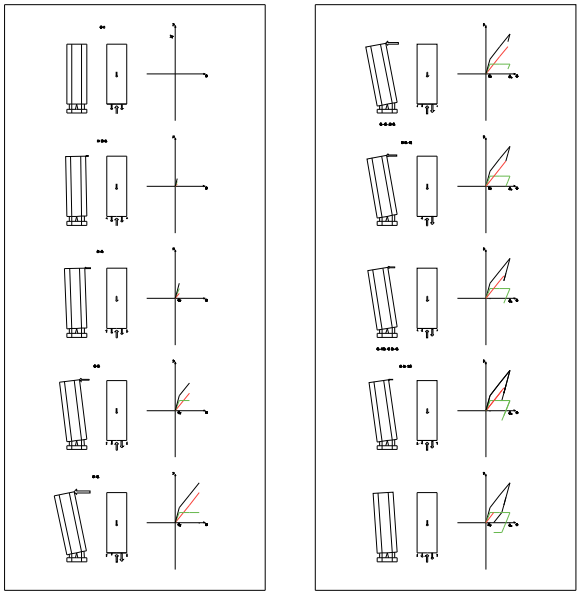

Figure 5.9: Hysteresis Loops (a)

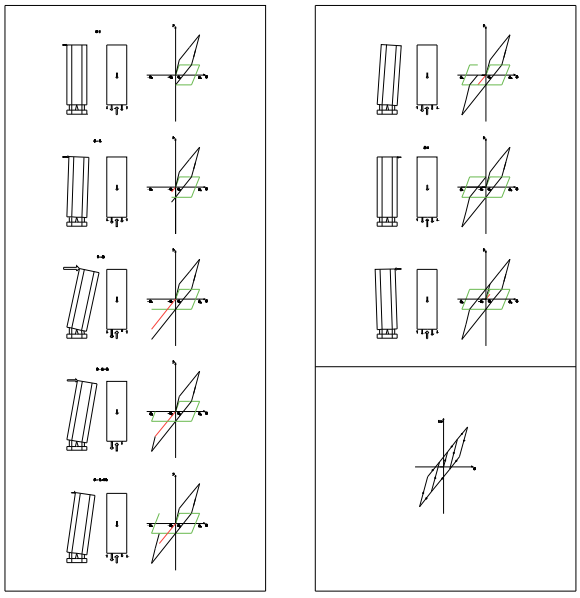

Figure 5.10: Hysteresis Loops (b)

or

$$\vartheta_{res} = \left[\frac{k_1}{k_2} - 1\right] \vartheta_y \tag{5.71}$$

considering k_1 and k_2 follow

$$\vartheta_{res} = \left[\frac{k_{cp,w} + k_d}{k_{cp,w}} - 1\right] \vartheta_y \tag{5.72}$$

or

$$\boxed{\vartheta_{res} = \left[\frac{k_d}{k_{cp,w}}\right] \vartheta_y} \tag{5.73}$$

$$\boxed{\vartheta_{res} = \left[\frac{k_d}{k_{cp,w}}\right] \vartheta^*} \tag{5.74}$$

where $\vartheta^* < \vartheta_y$

5.9 Dissipated Energy in a cycle of quasi-static loading

The energy dissipated for cycle of quasi-static loading can be evaluated, considering the area that is shown in figure. Obviously, the input energy imparted to the considered system is dissipated by both viscous and hysteretic damping. In this context, viscous damping is neglected and will be assumed that the global energy dissipation is related exclusively to the energy dissipated through the hysteretic dampers. In the next the energy dissipated is obtained determining the area inside the dampers hysteresis loop. It,s simple to verify that at the same result could be arrived considering the area inside the hysteresis loop of the global system. The area is

$$E_D = 4k_d\vartheta_y(\vartheta_u - \vartheta_y) \tag{5.75}$$

considering that k_d is obtained

$$E_D = 4(4\frac{(EA)_{d_c}}{L_{d_c}}l_{d_c}^2 + 4\frac{(EA)_{d_b}}{L_{d_b}}\frac{L^2}{l^2}l_{d_b}^2)\vartheta_y(\vartheta_u - \vartheta_y) \tag{5.76}$$

5.10 Condition for the simultaneous dissipators activation

$$k_{d_c}l_{d_c}\vartheta_y = k_{d_b}l_{d_b}\left(\frac{2l_c}{l} + 1\right)\vartheta_y \tag{5.77}$$

therefore

$$\frac{k_{d_c}}{k_{d_b}}\frac{l_{d_c}}{l_{d_b}} = \frac{2l_c}{l} + 1 \tag{5.78}$$

or

$$\frac{k_{d_c}}{k_{d_b}}\frac{l_{d_c}}{l_{d_b}} = \frac{L}{l} \tag{5.79}$$

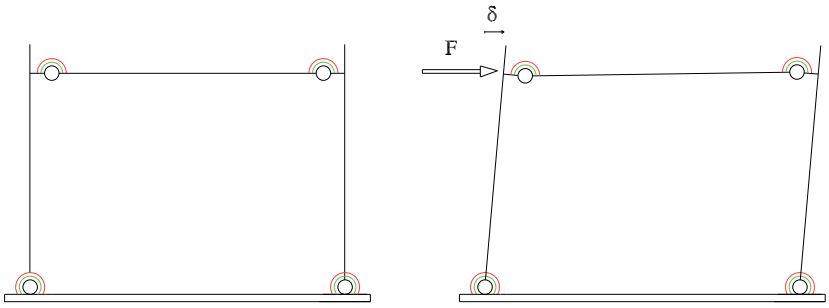

Figure 5.11: Portal frame with rigid beam and columns

5.11 Lateral Stiffness: Rigid and Flexural Beam Columns

We next consider the global translational stiffness assuming rigid structural elements initially and considering the elements deformability later.

5.11.1 Rigid structural elements

The horizontal translational force displacement relation of the system with rigid beam and columns is

$$F = \frac{2(k_b + k_c)}{H^2}\delta \tag{5.80}$$

Introduced the next positions

$$\alpha_c = \frac{k_c H}{E_c I_c} \qquad \alpha_b = \frac{k_b L}{E_b I_b} \qquad \lambda = \frac{L}{H} \qquad r_f = \frac{E_c I_c}{E_b I_b} \tag{5.81}$$

Eq. (5.80) can be written

$$F = \frac{6E_c I_c}{H^3}\left[\frac{1}{3}\left(\alpha_c + \frac{\alpha_b}{\lambda r_f}\right)\right]\delta \tag{5.82}$$

or, in synthetic form:

$$F = K_R \delta \tag{5.83}$$

where

$$K_R = \frac{6E_c I_c}{H^3}\left[\frac{1}{3}\left(\alpha_c + \frac{\alpha_b}{\lambda r_f}\right)\right] \tag{5.84}$$

Obviously, in presence of rigid structural elements,

$$\alpha_c = \infty \quad (Fixed\,Columns) \quad \Longrightarrow \quad K_{Rig} = \infty \quad \forall\,\alpha_b, p \tag{5.85}$$

$$\alpha_b = \infty \quad (Rigid\,B-C\,Conn.) \quad \Longrightarrow \quad K_{Rig} = \infty \quad \forall\,\alpha_c, p \tag{5.86}$$

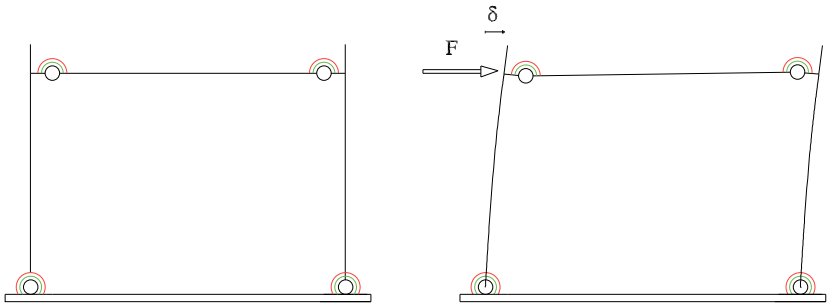

Figure 5.12: Portal frame with flexural beam and columns

5.11.2 Flexural structural elements

To obtain the global force displacement relation, in presence of elements deformability, it'll be necessary to resolve the not statically determinate system. The result, introduced the adimensional parameters, will be

$$F = \frac{6E_cI_c}{H^3}\frac{1}{1+\frac{3}{\alpha_c}-\frac{3\left(\frac{1}{2}+\frac{1}{\alpha_c}\right)^2}{\frac{1}{\alpha_c}+1+r_f\frac{\lambda}{\alpha_b}+\frac{1}{6}\lambda r_f}}\delta \tag{5.87}$$

or

$$F = K_S\,\delta \tag{5.88}$$

where

$$K_S = \frac{6E_cI_c}{H^3}\frac{1}{1+\frac{3}{\alpha_c}-\frac{3\left(\frac{1}{2}+\frac{1}{\alpha_c}\right)^2}{\frac{1}{\alpha_c}+1+r_f\frac{\lambda}{\alpha_b}+\frac{1}{6}\lambda r_f}} \tag{5.89}$$

Fixed Columns and rigid beam columns connections:

$$\alpha_c = \infty \qquad \alpha_b = \infty \qquad r_f = 0 \qquad (E_bI_b = \infty)$$

$$K_R = (4)\,\frac{6E_cI_c}{H^3} \qquad \forall\,\lambda \tag{5.90}$$

In Fig. (5.11) and Fig. (5.12) is shown the initial and deformed configuration in the hypothesis of rigid and flexural beam and columns.

5.11.3 Comparison with a Traditional Precast Concrete System

Traditional precast concrete structures in Italy can be modeled considering columns fixed at the base and pinned beam column connections. The hori-

zontal force displacement relation for those systems can be easily derived from Eq. (5.89) imposing $\alpha_c = \infty$ $\alpha_b = 0$. Substituting is obtained

$$F = \frac{6E_cI_c}{H^3} \tag{5.91}$$

5.11.4 Elements flexural deformability influence on translational stiffness

The influence of the element deformability respect to transversal stiffness for systems with flexural beam and columns is now analyzed. To do this, in the next, the ratio between the transversal stiffness with flexural and rigid elements, respectively, will be investigated with the variation of the introduced adimensional parameters. Considering Eq. (5.84) and Eq. (5.89), the mentioned stiffness ratio can be easily calculated:

$$\Lambda = K_S/K_R = \frac{1}{\frac{1}{3}\left(\alpha_c + \frac{\alpha_b}{p}\right)\left(1 + \frac{3}{\alpha_c} - \frac{3\left(\frac{1}{2}+\frac{1}{\alpha_c}\right)^2}{\frac{1}{\alpha_c}+1+p\left(\frac{1}{\alpha_b}+\frac{1}{6}\right)}\right)} \tag{5.92}$$

where the parameter $p = \lambda\ r_f$ is introduced. Therefore, symbolically, we had obtained:

$$\Lambda = K_S/K_R = f(\alpha_c, \alpha_b, p) \tag{5.93}$$

$$K_S = \Lambda\, K_R \tag{5.94}$$

Obviously, the defined stiffness ratio will always be less than one, and the goal will be the ratio maximization. For example, $\Lambda = 1$ means that the stiffness of the system with deformable structural elements is equal to the stiffness of the system with rigid elements, therefore, all the deformability of the system is related only to the spring deformability (only to post tensioned strands and dampers deformation) or that we don't have deformability in the structural elements. Bigger will be the defined stiffness ratio minor will be the influence of the element deformability on the structural deformability.

Defining Δ_S, Δ_R and Δ_E as

$$\Delta_S = \frac{1}{K_s} \qquad \Delta_R = \frac{1}{K_R} \qquad \Delta_E = \frac{1}{K_E} \tag{5.95}$$

then, the deformability due to the structural elements can be obtained as

$$\Delta_E = \frac{1}{K_E} = \frac{1}{K_s} - \frac{1}{K_R} = \Delta_S - \Delta_R \tag{5.96}$$

Considering Eq. (5.84) and Eq. (5.89), the mentioned deformability ratio can be easily calculated:

$$\Delta_E = \frac{1}{K_E} = \frac{H^3}{6E_cI_c}\left[1 + \frac{3}{\alpha_c} - \frac{3\left(\frac{1}{2}+\frac{1}{\alpha_c}\right)^2}{\frac{1}{\alpha_c}+1+r_f\frac{\lambda}{\alpha_b}+\frac{1}{6}\lambda r_f} - \frac{3}{\alpha_c+\frac{\alpha_b}{p}}\right] \tag{5.97}$$

To evaluate the structural elements deformability influence on the global deformability, the next deformability ratio will be introduced and analyzed

$$\frac{\Delta_E}{\Delta_R} = \frac{(\Delta_S - \Delta_R)}{\Delta_S} = 1 - \frac{K_S}{K_R} = 1 - \Lambda \tag{5.98}$$

will be next diagrammed for fixed $p = \lambda r_f$ values for five rotational stiffness around the columns base α_c with α_b. Obviously, the goal will be the stiffness ratio minimization.

5.12 Design Considerations

Preview

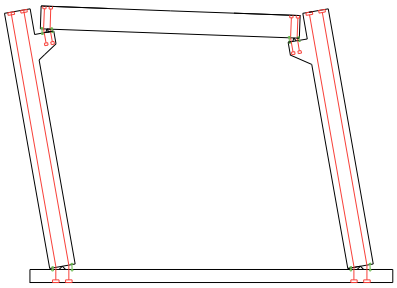

Figure 5.13: Rocking Frame

The Design of a simple portal frame will be next considered. The structural system is shown in Fig. 6.7

5.12.1 Description

In the Design will be assumed that the structural element geometry and section will be known. The post-tensioned strand length, area and arm related to the column base connection and to the beam column connection will be considered unknown.

The materials mechanical properties which We use for post tensioned strand and dissipators will be considered known:

$$E_{pt} \qquad f_{y,pt} \qquad E_d \qquad f_{y,d}$$

Unknown parameters will be considered:

$$\begin{array}{cccccc} l_{pt,c} & L_{pt,c} & A_{pt,c} & l_{pt,b} & L_{pt,b} & A_{pt,b} \\ l_{d,c} & L_{d,c} & A_{d,c} & l_{d,b} & L_{d,b} & A_{d,b} \end{array}$$

The system is considered symmetric respect to the vertical axis.

5.12.2 Compatibility Conditions

In the next will be considered a few conditions that will reduced the number of independent parameters.

Condition 1: Elastic Post-Tensioned Strands

Considering, for $\vartheta = \vartheta_u$, the tension in the post tensioned elements non bigger than $f_{y,pt}$ is obtained

$$T_0 + \Delta T_u = f_{y,pt} A_{pt} \geq \frac{E_{pt} A_{pt}}{L_{pt}} l_{pt} \vartheta_u \tag{5.99}$$

from equation

$$\frac{L_{pt}}{l_{pt}} \geq \frac{E_{pt}}{f_{y,pt}} \vartheta_u \tag{5.100}$$

The previous equation must be verified for the post tensioned elements positioned around the hinge at the columns base and around the beam column connections. Obviously, for an optimal design will be considered:

$$\frac{L_{pt,c}}{l_{pt,c}} = \frac{E_{pt}}{f_{y,pt}} \vartheta_u \qquad \frac{L_{pt,b}}{l_{pt,b}} = \frac{E_{pt}}{f_{y,pt}} \vartheta_u$$

It's simple to verify that, the previous relations guarantee simultaneous post tensioned elements yielding.

Condition 2: Dissipators Activation for $\vartheta = \vartheta_y$

Considering, for $\vartheta = \vartheta_y$, the tension in the dissipators equal to $f_{y,d}$,

$$f_{y,d} A_d = \frac{E_d A_d}{L_d} l_d \vartheta_y \tag{5.101}$$

from this..

$$\frac{L_d}{l_d} = \frac{E_d}{f_{y,d}} \vartheta_y \tag{5.102}$$

The previous equation must be verified for the dissipators positioned around the hinge at the columns base and around the beam column connections:

$$\frac{L_{d,c}}{l_{d,c}} = \frac{E_d}{f_{y,d}} \vartheta_y \qquad \frac{L_{d,b}}{l_{d,b}} = \frac{E_d}{f_{y,d}} \vartheta_y$$

It's simple to verify that, the previous guarantee the simultaneous dissipators activation and the Bi-linearity of the system

Chapter 6

An Elementary *Hybrid* System

Contents

Preview

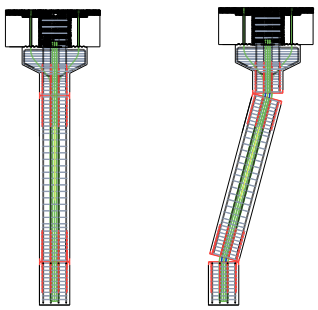

Figure 6.1: Rocking Column

We begin our study formulating the monotonic force displacement relation, for the rocking column of Figure 6.7 subjected to an external horizontal applied force.

As shown in Fig. 6.7 the considered system is rigid members (beam and columns) and elastic-plastic connections. These are composed of unbounded post-tensioned cables and hysteretic dampers. The unbounded post-tensioned cables ensure self centering capacity while the hysteretic dampers provide energy dissipation properties.

The relation between force and displacement is determined for equilibrium

6.1 Introduction

The first major self-centering systems were developed under the U.S.PRESSS (PREcast Seismic Structural Systems) program carried out for a decade in the 1990s and coordinated at the University of California, San Diego(Priestley1991, Nakaki et al. 1999, Priestley et al. 1999). The primary objective of the program was to developed innovative seismic resistant solutions for precast concrete buildings to replace the emulation of cast-in-place concrete that was used at the time. These innovative solutions used unbounded post-tensioned elements.

The inelastic demands on the systems are accommodated by allowing structural elements to separate relative to each other trough a rocking motion. This can be achieved with a number of structural configurations such as beams rocking on columns, segmental columns rocking on each other and on their foundations, and walls rocking on their foundations. This is achieved trough the opening and closing of an existing gap (rocking motion), while structural elements are basically designed to remain elastic. Rocking systems, with the help of the unbounded post-tensioned elements, tend to re-center to their original undeformed position at every cycle and therefore display a self-centering response. Based on this concept, new structural systems that are capable of undergoing inelastic displacements similar to their traditional counterparts, while limiting the damage to the structural system and assuring full re-centering capability without residual displacements, were developed. The feasibility and efficiency of unbounded post-tensioned solutions were investigated numerically by Priestley and Tao (1993) and experimentally validated through quasi-static loading of interior beam-column joint subassemblies (MacRae and Priestley 1994). These first systems relied only on unbounded post-tensioned to provide moment capacity and self-centering properties and therefore did not dissipate substantial amounts of energy at each loading cycle.

An hybrid system was then suggested where self-centering and energy dissipating properties were combined trough the use of unbounded post-tensioned tendons/bars and longitudinal non prestressed (mild) steel or additional external dissipation device designed to yield and to provide supplemental damping to the rocking systems.

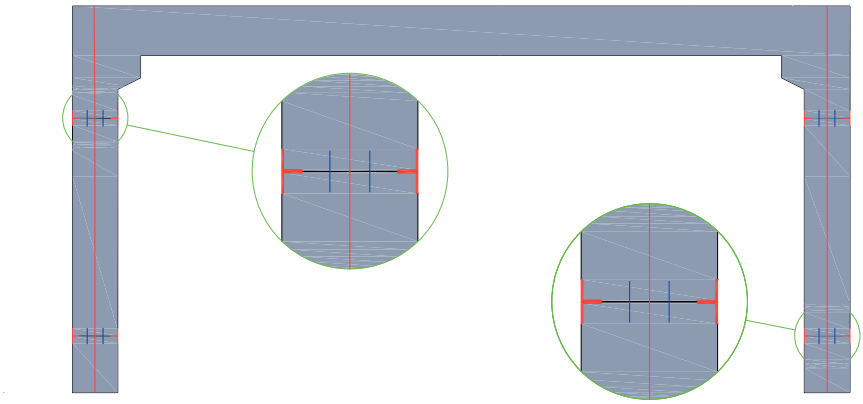

Figure 6.2: Qualitative Hybrid frame, Initial Configuration

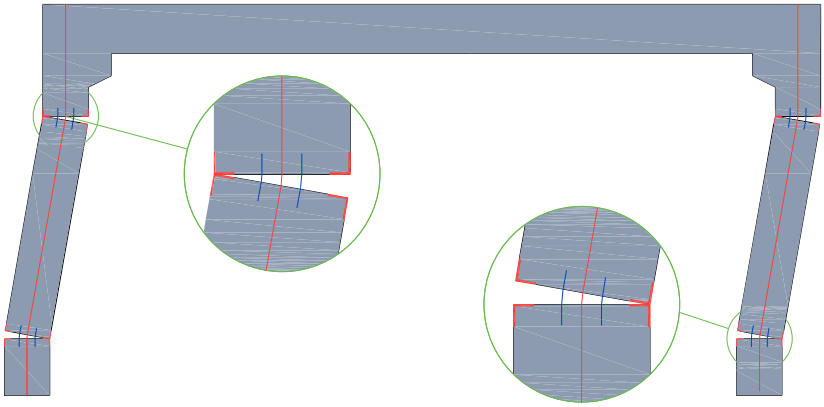

Figure 6.3: Qualitative Hybrid frame, Deformed Configuration

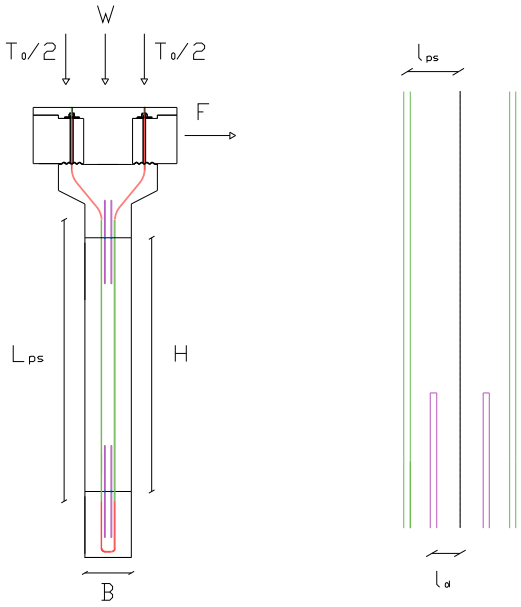

Figure 6.4: Geometrical description

6.2 Limit states and behavior region: Analytical characterization

With reference to the rocking column displayed in Fig. , the monotonic force displacement relation is next determined. The considered model includes rigid column, elastic post tensioned strands and elasto-perfectly plastic dissipators elements. Boundary conditions guarantee the similarity with the behavior characterizing a generic system modeled globally.

6.2.1 Limit I: Decompression

Decompression is the deformation state where the strain at the outer most fibre approaches zero and rotation of the base is initiated. The neutral axis depth (c) is located at the edge of the section (c =Lw).

The force value associated is

$$F_{Rock} = \frac{1}{H}(W + T_0)B \tag{6.1}$$

For force value less the system is not subjected to any displacements. In non dimensional form, the previous equation can be written

$$\Delta = 0 \qquad \forall f \leq f_{Rock} \tag{6.2}$$

where $f_{Rock} = F_{Rock}/(W + T_0)$.

Under the hypothesis of rigid column, the stiffness, in this first phase is infinity

$$k_1 = \infty \tag{6.3}$$

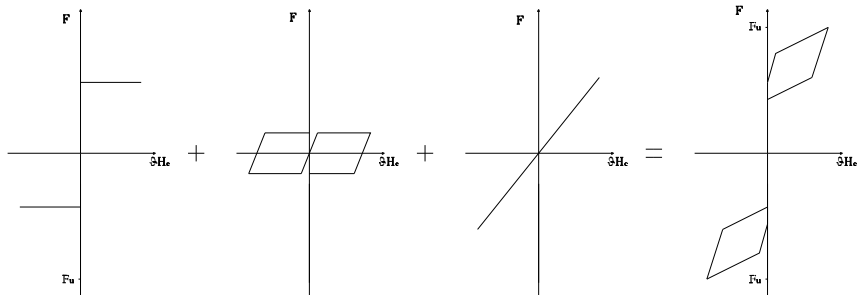

Figure 6.5: Weight, Dissipators and Strands: Mechanical hypothesis

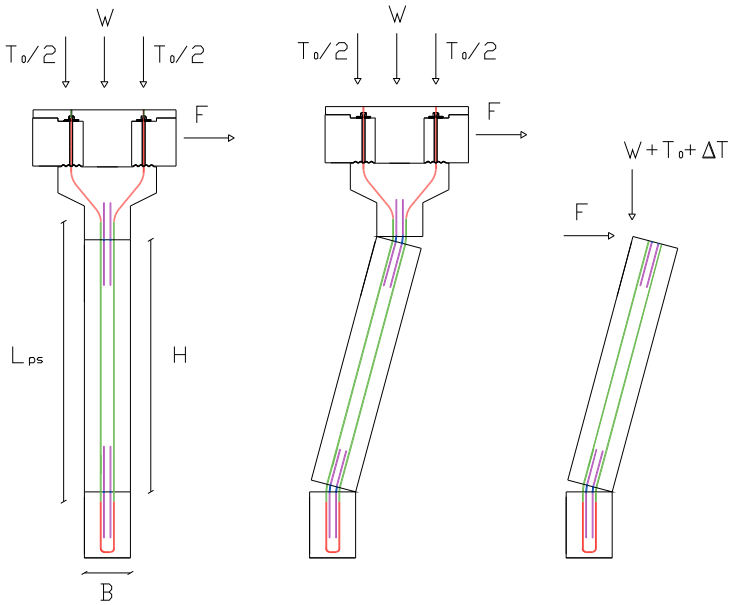

Figure 6.6: Kinematic, Overview

6.2.2 Phase I-II: Rocking activation

To determine the stiffness over the previous point, the equilibrium equation around the point (0) is evaluated.
Considering a first order kinematics, can be obtained:

$$\begin{aligned}
&F(H+B\vartheta)-(W+T_0)\,(B-H\vartheta)+\\
&\quad-\left(\frac{E_{ps}A_{ps}}{L_{ps}}\right)_{left}\left[\left(\frac{B}{2}+l_{ps}\right)+\left(\frac{B}{2}-l_{ps}\right)\right]\vartheta\,(B-H_1\vartheta)+\\
&\quad-\left(\frac{E_{ps}A_{ps}}{L_{ps}}\right)_{right}\left[\left(\frac{B}{2}+l_{ps}\right)+\left(\frac{B}{2}-l_{ps}\right)\right]\vartheta\,(B-H_1\vartheta)+\\
&\quad-\left(\frac{E_dA_d}{L_d}\right)_{left,bottom}\left(\frac{B}{2}+l_d\right)\vartheta\left(\frac{B}{2}+l_d\right)+\\
&\quad-\left(\frac{E_dA_d}{L_d}\right)_{right,bottom}\left(\frac{B}{2}-l_d\right)\vartheta\left(\frac{B}{2}-l_d\right)+\\
&\quad-\left(\frac{E_dA_d}{L_d}\right)_{left,top}\left(\frac{B}{2}-l_d\right)\vartheta\left(\frac{B}{2}-l_d\right)+\\
&\quad-\left(\frac{E_dA_d}{L_d}\right)_{right,top}\left(\frac{B}{2}+l_d\right)\vartheta\left(\frac{B}{2}+l_d\right)=0
\end{aligned}\tag{6.4}$$

Assuming

$$B\vartheta \ll H \qquad\qquad H\vartheta \ll B$$

is obtained

$$\begin{aligned}
&FH-(W+T_0)B-B^2\left[\left(\frac{E_{ps}A_{ps}}{L_{ps}}\right)_{left}+\left(\frac{A_{ps}}{L_{ps}}\right)_{right}\right]\vartheta+\\
&\quad-\left(\frac{E_dA_d}{L_d}\right)_{left,bottom}\left(\frac{B}{2}+l_d\right)^2\vartheta+\\
&\quad-\left(\frac{E_dA_d}{L_d}\right)_{right,bottom}\left(\frac{B}{2}-l_d\right)^2\vartheta+\\
&\quad-\left(\frac{E_dA_d}{L_d}\right)_{left,top}\left(\frac{B}{2}-l_d\right)^2\vartheta+\\
&\quad-\left(\frac{E_dA_d}{L_d}\right)_{right,top}\left(\frac{B}{2}+l_d\right)^2\vartheta=0
\end{aligned}\tag{6.5}$$

Under the hypothesis of equal geometry and mechanical properties for the dis-

sipators at the right and at the left side of the column axes is derived

$$\begin{aligned} FH-(W+T_0)B-B^2\left[\left(\frac{E_{ps}A_{ps}}{L_{ps}}\right)_{left}+\left(\frac{A_{ps}}{L_{ps}}\right)_{right}\right]\vartheta+ \\ -\left(\frac{E_dA_d}{L_d}\right)_{bottom}\left[\left(\frac{B}{2}+l_d\right)^2+\left(\frac{B}{2}-l_d\right)^2\right]\vartheta+ \\ -\left(\frac{E_dA_d}{L_d}\right)_{top}\left[\left(\frac{B}{2}-l_d\right)^2+\left(\frac{B}{2}+l_d\right)^2\right]\vartheta=0 \end{aligned} \tag{6.6}$$

finally, if same dissipators are used between the gap at the bottom and at the top and if the hypothesis of same geometry and mechanical properties is done for post tensioned strands at the left and at the right of the column axes too, the next equation is determined

$$\begin{aligned} FH-(W+T_0)B-2E_{ps}B^2\left(\frac{A_{ps}}{L_{ps}}\right)\vartheta+ \\ -2\left(\frac{E_dA_d}{L_d}\right)\left[\left(\frac{B}{2}+l_d\right)^2+\left(\frac{B}{2}-l_d\right)^2\right]\vartheta=0 \end{aligned} \tag{6.7}$$

Adimensional form

Introducing the next non dimensional parameters

$$f=\frac{F}{W+T_0} \qquad \lambda=\frac{H}{B} \qquad R_{ps}=\frac{E_{ps}A_{ps}}{W+T_0} \qquad R_d=\frac{E_dA_d}{W+T_0} \tag{6.8}$$

$$\nu_{ps}=\frac{H}{L_{ps}} \qquad \nu_d=\frac{H}{L_d} \qquad \xi_d=\frac{l_d}{\frac{B}{2}} \tag{6.9}$$

the previous equation, dividing for $W+T_0$ and H both side, in non dimensional form, can be written :

$$f=\lambda+2\lambda^2\left\{4\nu_{ps}R_{ps}+\nu_dR_d\left[(1+\xi_d)^2+(1-\xi_d)^2\right]\right\}\vartheta \tag{6.10}$$

For the inter story drift (Δ), can be written

$$\Delta=\frac{\delta}{H}=\frac{H\vartheta}{H}=\vartheta \tag{6.11}$$

then, the previous equation can be formulated in the next form

$$f=\lambda+2\lambda^2\left\{4\nu_{ps}R_{ps}+\nu_dR_d\left[(1+\xi_d)^2+(1-\xi_d)^2\right]\right\}\Delta \tag{6.12}$$

or

$$f=\lambda+2\lambda^2\left\{4K^*_{ps}+K^*_d\left[(1+\xi_d)^2+(1-\xi_d)^2\right]\right\}\Delta \tag{6.13}$$

where the next two non dimensional parameters are, conveniently, introduced

$$K^*_{ps}=\nu_{ps}R_{ps} \qquad K^*_d=\nu_dR_d \tag{6.14}$$

Finally, the system stiffness in this second phase is:

$$k_2 = 2\lambda^2 \left\{ 4K_{ps}^* + K_d^* \left[(1+\xi_d)^2 + (1-\xi_d)^2 \right] \right\} \tag{6.15}$$

It's evident how the stiffness increases with the column slenderness, with the dissipators axial stiffness and with the increase of the distance from the column axes.

Limit 2: Yielding of the first two Dissipators

Yielding of the mild steel reinforcement can occur either before or after the geometric non-linearity point depending on the section dimensions and location of the steel reinforcement. Stiffness further reduces with strength continuing to increase due to the elongation of the prestressed reinforcement due to the continued opening of the gap at the base of the wall.

The determined stiffness changes as soon as the first two dissipators yield (contemporaneously for the particular kinematic), in particular the one at the bottom and the one at the top more distant from the point of rocking. Trivially, the system stiffness loses the contribution of the activated dissipators:

$$k_3 = 2\lambda^2 \left[4K_{ps}^* + K_d^* \left(1-\xi_d\right)^2 \right] \tag{6.16}$$

Limit 3: Yielding of the first two Dissipators

As soon as even the remained dissipators yield, the stiffness system changes again and loses even the contribution of them:

$$k_4 = 8\lambda^2 K_{ps}^* \tag{6.17}$$

It's clear, how the slenderness and the post-tensioned strand axial stiffness affects the value of this stiffness

Summary

Finally, the obtained stiffness value in parametric and non dimensional form are listed:

$$k_1 = \infty \qquad k_2 = 2\lambda^2 \left\{ 4K_{ps}^* + K_d^* \left[(1+\xi_d)^2 + (1-\xi_d)^2 \right] \right\} \tag{6.18}$$

$$k_3 = 2\lambda^2 \left[4K_{ps}^* + K_d^* \left(1-\xi_d\right)^2 \right] \qquad k_4 = 8\lambda^2 K_{ps}^* \tag{6.19}$$

6.3 Rotation related to the dissipators yielding

Dissipators more distant from the rocking point

Dissipators more distant from the rocking point will yield for a rotation value equal to:

$$\vartheta_{d,y,1} = \varepsilon_y L_d \frac{1}{\left(\frac{B}{2} + l_d\right)}$$

It's evident that, the yielding rotation increase when :

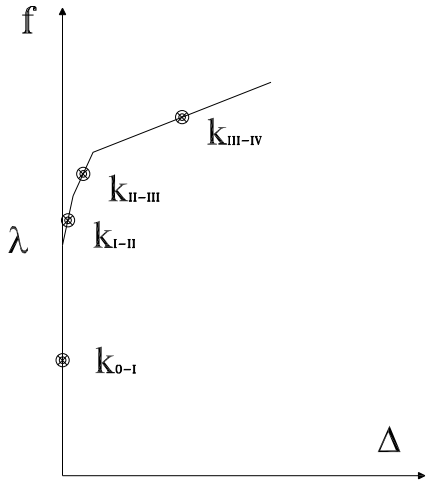

Figure 6.7: Stiffness

- increase the steel yielding strain
- increase the dissipator length
- decrease the arm
- decrease the column width

Dissipators closer from the rocking point

Dissipators closer to the rocking point will yield for a rotation value equal to:

$$\vartheta_{d,y,2} = \varepsilon_y L_d \frac{1}{\left(\frac{B}{2} - l_d\right)}$$

It's evident that, the yielding rotation increase when :

- increase the steel yielding strain
- increase the dissipator length
- increase the arm
- decrease the column width

6.4 Ultimate rotations

6.4.1 Ultimate rotation related to the elastic strands behavior

A first limit for the ultimate rotation capacity, in this context, can be assumed with the ultimate rotation coincident with the elastic limit of the post-tensioned

strands.

$$T_{left}-T_0 = \left(\frac{E_{ps}A_{ps}}{L_{ps}}\right)\left[\left(\frac{B}{2}+l_{ps}\right)+\left(\frac{B}{2}-l_{ps}\right)\right]\vartheta = \frac{E_{ps}A_{ps}}{L_{ps}}B\vartheta = T_{right}-T_0 \tag{6.20}$$

Imposing elastic behavior for post-tensioned strands is obtained:

$$T_{left}+T_0 = A_{ps}f_{y,ps} = T_{right}+T_0 \tag{6.21}$$

$$A_{ps}f_{y,ps} = \left(\frac{E_{ps}A_{ps}}{L_{ps}}\right)B\vartheta_u + T_0 \tag{6.22}$$

then

$$\vartheta_u = \left(f_{y,ps}-\frac{T_0}{A_{ps}}\right)\frac{L_{ps}}{E_{ps}B} \tag{6.23}$$

or

$$\vartheta_u = (\varepsilon_{y,ps}-\varepsilon_{0,ps})\frac{L_{ps}}{B} \tag{6.24}$$

Clearly, the ultimate rotation increase with the post tensioned strands length, and decrease with the initial tension in the strands and with the column width.

If the ultimate rotation is defined then the strands length can be determined in accordance with the next:

$$L_{ps} = \frac{B}{\varepsilon_{y,ps}-\varepsilon_{0,ps}}\vartheta_u \tag{6.25}$$

6.4.2 Ultimate rotation related to the dissipators rupture

Dissipators closer from the rocking point

The closer Dissipators will break for a rotation value equal to:

$$\vartheta_{d,u,1} = \varepsilon_u L_d \frac{1}{\left(\frac{B}{2}+l_d\right)}$$

It's evident that, the ultimate rotation increase when :

- increase the steel ultimate strain
- increase the strand length
- decrease the initial force in pre/post-tensioned strands.
- decrease the column width

Dissipators more distant from the rocking point

The more distant dissipators will break for a rotation value equal to:

$$\vartheta_{d,u,2} = \varepsilon_u L_d \frac{1}{\left(\frac{B}{2}-l_d\right)}$$

It's evident that, the ultimate rotation increase when :

- increase the steel ultimate strain
- increase the strand length
- decrease the initial force in pre/post-tensioned strands.
- decrease the column width

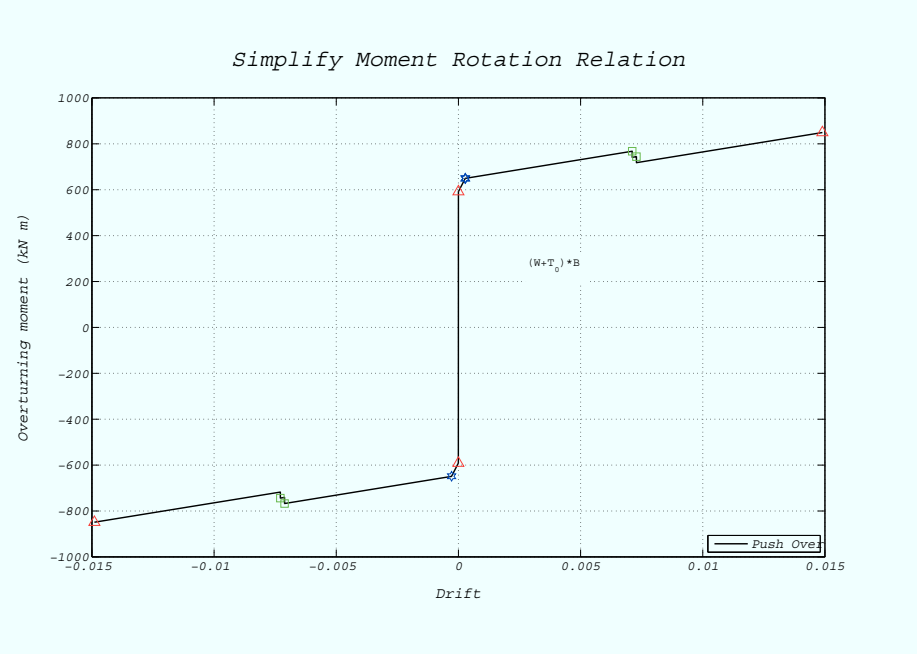

Figure 6.8: Simplify analytical moment-rotation relation

6.5 Monotonic moment rotation relation

$$M_0 = \frac{W + T_0}{B} \tag{6.26}$$

$$\begin{aligned} M_1 =& (W + T_0)(B - H\vartheta_{d,y,1}) + 2B^2 E_{ps} \frac{A_{ps}}{L_{ps}} \vartheta_{d,y,1} + \\ & 2\frac{E_d A_d}{L_d}\left(\frac{B}{2} - l_d\right)\vartheta_{d,y,1} + 2\frac{E_d A_d}{L_d}\left(\frac{B}{2} + l_d\right)\vartheta_{d,y,1} \end{aligned} \tag{6.27}$$

considering that... the previous equation can be written

$$\begin{aligned} M_1 =& (W + T_0)(B - H\vartheta_{d,y,1}) + 2B^2 E_{ps} \frac{A_{ps}}{L_{ps}} \vartheta_{d,y,1} + \\ & 2\frac{E_d A_d}{L_d}\left(\frac{B}{2} - l_d\right)\vartheta_{d,y,1} + 2A_d f_{yd}\left(\frac{B}{2} + l_d\right) \end{aligned} \tag{6.28}$$

where

$$\vartheta_{d,y,1} = \varepsilon_y L_d \frac{1}{\left(\frac{B}{2} + l_d\right)} \tag{6.29}$$

When, even the other dissipators are activated the moment

$$M_2 = (W + T_0)(B - H\vartheta_{d,y,2}) + 2B^2 \frac{E_{ps} A_{ps}}{L_{ps}} \vartheta_{d,y,2} + 2BA_d f_{yd} \tag{6.30}$$

where

$$\vartheta_{d,y,2} = \varepsilon_y L_d \frac{1}{\left(\frac{B}{2} - l_d\right)} \tag{6.31}$$

$$M_3 = (W + T_0)(B - H\vartheta_{ps,y}) + 2B^2 \frac{E_{ps}A_{ps}}{L_{ps}}\vartheta_{ps,y} + 2BA_d f_{yd} \tag{6.32}$$

where

$$\vartheta_{ps,y} = (\varepsilon_{y,ps} - \varepsilon_{0,ps})\frac{L_{ps}}{B} \tag{6.33}$$

6.6 Secant period at ultimate condition

In the next, the secant period is evaluated with reference to the fundamental system parameters.

$$T = 2\pi\sqrt{\frac{W}{gK_{Sec}}} \tag{6.34}$$

$$K_{Sec} = \frac{F_u}{\Delta_u} = \frac{M_u}{H}\frac{1}{H\vartheta_u} = \frac{M_u}{H^2}\frac{1}{\vartheta_u} \tag{6.35}$$

Considering the ultimate condition equal to the post tensioned strands yielding and the dissipator at the yielding but not at the rupture the ultimate moment is equal to

$$M_u = (W + T_0)(B - H\vartheta_u) + 2B^2 \frac{E_{ps}A_{ps}}{L_{ps}}\vartheta_u + 2BA_d f_{yd} \tag{6.36}$$

$$\frac{T^2}{4\pi^2} = \frac{1}{\lambda\left[\frac{1}{H\vartheta_u}\left(1 + \frac{T_0}{W}\right) + 2\lambda\frac{K_{ps}}{W}\right]}$$

Part III

Performances of Traditional and Innovative Precast Concrete Industrial/Commercial Structures

PART III

Preview

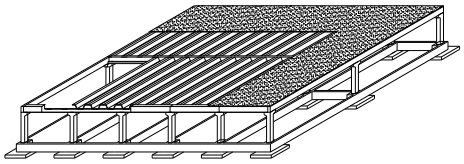

This final part develops the design of a precast concrete one-story building, in traditional and innovative ways. Structural performances and costs of innovative and traditional solutions are analyzed.

In the first chapter, the design of a traditional precast concrete one story building, with reference to the actual Italian code, NTC 2008. The particular simple structural scheme, suggested the idea to develop a simple program to optimize the traditional design of a one story building. In the same chapter, this program is introduced and described and it is reported in Appendix B.

In Chapter 8 the same building designed in traditional way, is designed in innovative way with an *Hybrid* solution.

In Chapter 9 Performances of traditional and innovative systems are determined and compared.

Chapter 7

Seismic Design of Traditional Precast Concrete Structures according to 2008 NTC Code

Contents

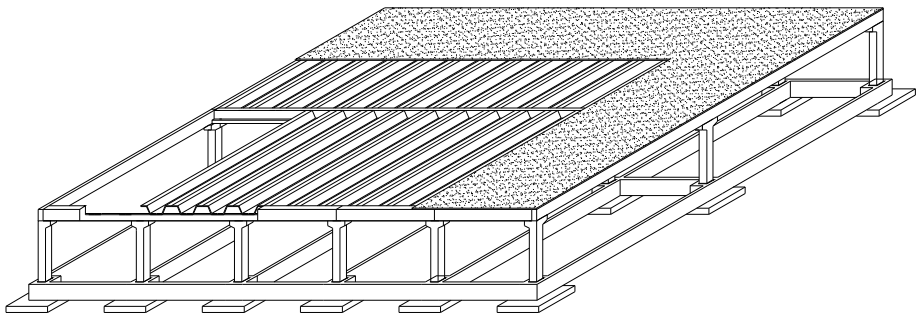

Figure 7.1: Precast concrete one story industrial building

Preview

PERFORMANCES evaluation of innovative systems, in this thesis, is obtained through a comparison with traditional precast concrete structures performances. For that reason, the seismic design and the performance evaluation of a traditional precast concrete one story industrial building is in the following considered.

The design complies to the actual Italian Code: *Norme tecniche per le costruzioni - D.M. 14/01/2008.*

Both the design cases of, low dissipative capacity (LDC) and high dissipative capacity (HDC) were considered.

The building is supposed located in Catania in a moderate seismic zone, on soil type B and on a flat surface of type T1 according the 2008 NTC Italian code. Considering the design dominated by seismic actions, only the seismic design was developed, and has not been conducted analysis for wind or other actions.

7.1 Structural system description

The one story building structure considered is a common typology in Italy, particularly for buildings use to economic or industrial activities.

As shown in Fig.7.2, a rectangular building shape in plan was considered. The one story building has two axes of symmetry. The plan is 32.0 meters in north-south and 40.0 meters in east-west direction. The Columns heights are 4.95 meters. All the columns are supposed fix at he base and all the beams are supposed pinned at the columns. On the whole, the building structure consists of five, two bays, transversal frames, with bay length equal to 16 meters and of three, five bays, longitudinal frames, with bay length equal to 8 meters.

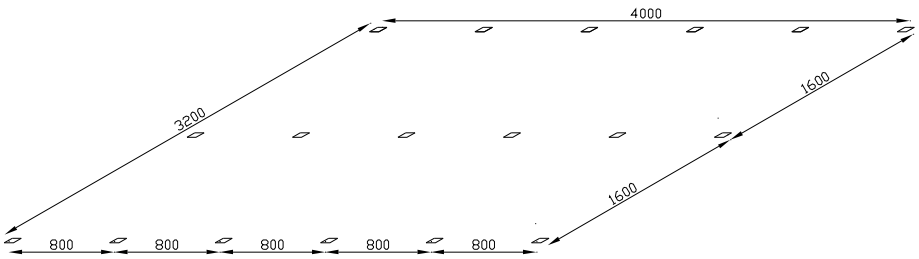

Figure 7.2: Plan dimensions

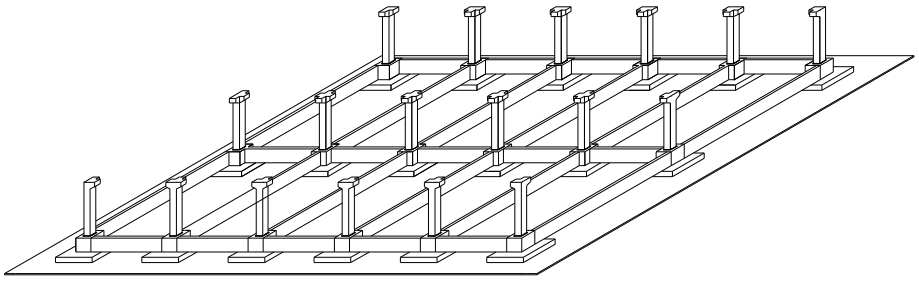

Figure 7.3: foundation

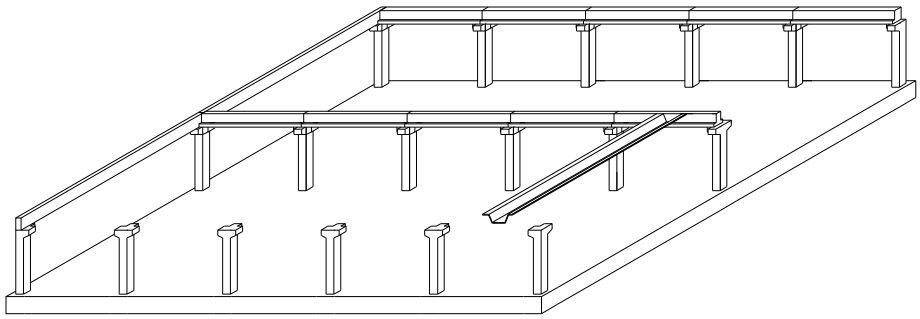

Figure 7.4: Roof elements overview

Foundation system

The foundation system is realized by Combined footing (Spread footing with link beams). A global view of the foundation system is presented in Fig.7.3.

Columns

All columns are supposed to have the same square section.

Roof

Three different beam sections are considered. The external longitudinal beams are supposed to have a rectangular section (*Trave R*) whereas a L section is considered for the external transversal beams(*Trave TL*). The internal beams are supposed to have a inverted T shape (*Trave TR*). A general view is presented in Fig. 7.4

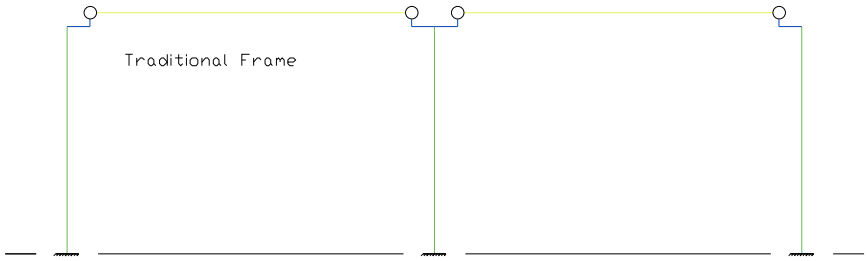

Figure 7.5: Structural Scheme, Initial Configuration

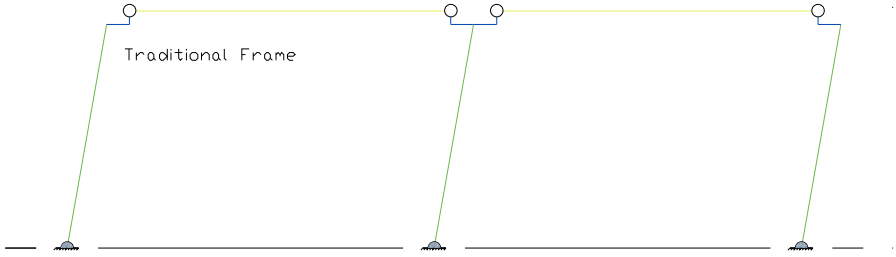

Figure 7.6: Structural Scheme, Ultimate Condition

7.1.1 Mechanical properties of materials

In the following, the mechanical properties used in the design are presented. The *Characteristic* values are the 95% probability to be grater than the generic measured values and the *cylindrical* adjective means that the considered characteristic has been measured on cylindrical elements

Concrete **C40/50**

Characteristic compressive strength tested on cylinder element	$f_{ck} = 40$	N/mm^2
Characteristic compressive strength tested on cubic elements	$Rck = 50$	N/mm^2
Strength reduction factor	$\gamma_c = 1.5$	
Reduction factor for long term effects	$\alpha_{cc} = 0.85$	
Design compressive strength	$f_{cd} = 22,66$	N/mm^2
Mean compressive strength	$f_{cm} = 48,00$	N/mm^2
Elastic modulus	$E_c = 35200$	N/mm^2

Steel for reinforcing bars **B450C**

Characteristic yielding strength	$f_{yk} = 450$	N/mm^2
Characteristic tensile strength	$f_{tk} = 540$	N/mm^2
Strength reduction factor	$\gamma_s = 1.15$	
Design yielding strength	$f_{yd} = 22.66$	N/mm^2
Elastic modulus	$E_s = 200000$	N/mm^2

7.2 Dead and Live Loads

7.2.1 Dead Loads

The dead load on a structural element is the weight of the member itself, plus the weights of all materials permanently incorporated into the structure and supported by the member in question. The weight of the structural elements is based on the unit weight listed below:

- 3,15 kN/mq, for a transversal length of 2,5 ml, for *Tegolo Vigor 70*
- 12,00 kN/ml, for *trave TR*
- 14,31 kN/ml, for *trave TL*

Tab. 7.1 gives a summary of unit weights and quantity of structural and non structural elements considered to evaluate Dead and Live Loads.

Dead load distribution between frames

Starting to the previous analysis on the elements weight, it's possible to calculate the dead loads distribution between frames. External walls are assumed supported by the foundation system, therefore them don't give any contribution at the loads distribution on frames.

External transversal frames

External transversal beam	$9 * 32.6 = 293.40$	kN
External longitudinal beams	$9 * 32.6 = 293.40$	kN
Tegoli	$2 * (16 + 0.30 - 0.55 - 0.2)*$	
	$*3.90 * 3.15 = 382.06$	kN
Caldana and finiture	$8.0 * 32.6 * (2 + 2,5) = 1173.60$	kN
Columns	$3 * 0.6 * 0.6 * 4.95 * 25 = 133.65$	kN
	Total at roof level **1597.85**	**kN**
	Total at foundation level **1731.50**	**kN**

Internal transversal frames

External transversal beam	$2 * 8.00 * 14.31 = 228.96$	kN
External longitudinal beams	$8 * 12.00 = 96.00$	kN
Tegoli	$2 * (16 + 0.30 - 0.55 - 0.22)*$	
	$*8.00 * 3.15 = 783,72$	kN
Caldana and finiture	$8.0 * 32.6 * (2 + 2.5) = 1173,60$	kN
Columns	$3 * 0.6 * 0.6 * 4.95 * 25 = 133,65$	kN
	Total at roof level **2282.28**	**kN**
	Total at foundation level **2415.93**	**kN**

External longitudinal frames

External transversal beams	$2 * 8.3 * 9 = 149.40$	kN
External longitudinal beam	$39.8 * 14.31 = 569.54$	kN
Tegoli	$(8 + 0,30 - 0,55 - 0,2)*$	
	$*(40,6 - 0,8) * 3,15 = 946.54$	kN
Caldana and finiture	$8.3 * 40.6 * (2 + 2.5) = 1516.41$	kN
Columns	$6 * 0.6 * 0.6 * 4.95 = 267.30$	kN
	Total at roof level **3181.89**	**kN**
	Total at foundation level **3449.19**	**kN**

Internal longitudinal frames

External transversal beams	$2 * 16 * 9 = 288.00$	kN
External longitudinal beam	$39.8 * 12.00 = 477.60$	kN
Tegoli	$16 * (40.6 - 0.8) * 3.15 = 2005.92$	kN
Caldana and finiture	$16 * 40.6 * (2 + 2.5) = 2923.20$	kN
Columns	$6 * 0.6 * 0.6 * 4.95 * 25 = 267.30$	kN
	Total at roof level **5694.72**	**kN**
	Total at foundation level **5962.02**	**kN**

To verify the calculation up until now done, the total transversal weight and the total longitudinal weight are calculated and reported.

Total transversal Weight		
at roof level	$2 * 1464.20 + 4 * 2282.28 = 12057$	kN
Total longitudinal Weight		
at roof level	$2 * 3181.89 + 5694.72 = 12058$	kN

Total transversal Weight		
at foundation level	$2 * 1464.20 + 4 * 2282.28 + 6 * 133.65 = 12858$	kN
Total longitudinal Weight		
at foundation level	$2 * 3181.89 + 5694.72 + 3 * 267.30 = 12859$	kN

7.2.2 Live Loads

It's supposed to use the designed structure like a parking structure, so in addition, a (roof) live load equal to 2.5 kN/mq, as reported in 2008 Italian code Tab. 3.1.II, is considered.

This table for parking structures gives the live load value reported in Equ. 8.1.

$$q_k = 2.5 \quad kN/m^2 \tag{7.1}$$

The total weight of the building (dead and live) which is considered in all analysis is about 15132 kN giving a total mass of about 1482 tons. Must be clear that the previous is only the total mass that is not coincident with the seismic mass. Tab. 7.1 presents a summary of dead and live loads.

Table 7.1: Dead and Live Loads

	Unit Weight	SI Units	Quantity	SI Units	Total	SI Units
Tegoli	3.15	kN/mq	1237.78	m^2	3899.07	kN
External transversal beams	9.00	kN/ml	65.20	m	586.80	kN
External longitudinal beams	14.31	kN/ml	79.60	m	1139.08	kN
Central longitudinal beam	12.00	kN/ml	39.80	m	477.60	kN
Other permanent elements	2.00	kN/mq	1323.56	m^2	2647.12	kN
Live loads (Parking structures)	2.50	kN/mq	1323.56	m^2	3308.90	kN
			Roof level		12058.50	kN
Columns	9.00	kN/ml	89.10	m	801.90	kN
			Ground level		12860.40	kN
External Walls	3.50	kN/mq	878.40	m^2	3074.40	kN
			Total Dead + Live Loads		15132.9	kN

7.3 Design Seismic Action, 2008 NTC Code

7.3.1 Mass

According to the 2008 NTC Code, the effects induced by the seismic action are evaluated with reference to masses calculated through Equ. 8.2,

$$G_1 + G_2 + \sum_j \Psi_{2,j} Q_{k,j} \tag{7.2}$$

where the $\Psi_{2,j}$ coefficients are codified and reported in Tab. 2.5.I, 2008 NTC Code. According to the Italian Code, for H category roof is $\Psi_{2,j} = \Psi_{1,j} = \Psi_{0,j} = 0$ then, in the current design, the induced seismic effects are evaluated according to Equ. 8.3.

$$G_1 + G_2 \tag{7.3}$$

7.3.2 Force Reduction Factors, and structural typologies, according to 2008 NTC Code

Generality

The force reduction factor is, in this context, introduced and its determination is presented according to the current Italian Code. To do this, a few sections of the code are cited.

> Il valore del fattore di struttura q da utilizzare per ciascuna direzione della azione sismica, dipende dalla tipologia strutturale, dal suo grado di iperstaticità e dai criteri di progettazione adottati e prende in conto le non linearità di materiale. Esso può essere calcolato tramite la seguente espressione:
>
> $$q = q_0 \cdot K_R \tag{7.4}$$
>
> dove:
>
> q_0 è il valore massimo del fattore di struttura che dipende dal livello di duttilità attesa, dalla tipologia strutturale e dal rapporto α_u/α_1 tra il valore dell'azione sismica p er il quale si verifica la formazione di un numero di cerniere plastich e tali da rendere la struttura labile e quello per il quale il primo elemento strutturale raggiunge la plasticizzazione a flessione;
>
> K_R è un fattore riduttivo che dipende dalle car atteristiche di regolarità in altezza della costruzione, con valore pari ad 1 per costruzioni regolari in altezza e pari a 0,8 per costruzioni non regolari in altezza.
>
> Per le costruzioni regolari in pianta, qualora non si proceda ad un'analisi non lineare finalizzata alla valutazione del rapporto α_u/α_1, per esso possono essere adottati i valori indicati nei paragrafi successivi per le diverse tipologie costruttive.
>
> Per le costruzioni non regolari in pianta, si possono adottare valori di α_u/α_1 pari alla media tra 1,0 ed i valori di volta in volta forniti per le diverse tipologie costruttive.

Concrete Structures

The considered Code presents specific suggestions for concrete structures that, in the following, are cited.

Le strutture sismo-resistenti in cemento armato previste dalle presenti norme possono essere classificate nelle seguenti tipologie:

- *strutture a telaio*, nelle quali la resistenza alle azioni sia verticali che orizzontali è affidata principalmente a telai spaziali, aventi resistenza a taglio alla base 65
- *strutture a pareti*, nelle quali la resistenza alle azioni sia verticali che orizzontali è affidata principalmente a pareti, singole o accoppiate, aventi resistenza a taglio alla base 65% della resistenza a taglio totale [1];
- *strutture miste telaio-pareti*, nelle quali la resistenza alle azioni verticali è affidata prevalentemente ai telai, la resistenza alle azioni orizzontali è affidata in parte ai telai ed in parte alle pareti, singole o accoppiate; se più del 50% dell'azione orizzontale è assorbita dai telai si parla di strutture miste equivalenti a telai, altrimenti si parla di strutture miste equivalenti a pareti;
- strutture deformabili torsionalmente, composte da telai e/o pareti, la cui rigidezza torsionale non soddisfa ad ogni piano la condizione $r/l_s > 0,8$, nella quale:
  r^2 = rapporto tra rigidezza torsionale e flessionale di piano
  $l^2 = (L_2 + B_2)/12$ (L e B dimensioni in pianta del piano)
- *strutture a pendolo inverso*, nelle quali almeno il 50% della massa è nel terzo superiore dell'altezza della costru zione o nelle quali la dissipazione d'energia avviene alla base di un singolo elemento strutturale [2].

Le strutture delle costruzioni in calcestruzzo possono essere classificate come appartenenti ad una tipologia in una direzione orizzontale ed ad un'altra tipologia nella direzione orizzontale ortogon ale alla precedente.

Una struttura a pareti è da considerarsi come struttura a pareti estese debolmente armate se, nella direzione orizzontale d'interesse, essa ha un periodo fondamentale, calcolato nell'ipotesi di assenza di rotazioni alla base, non superiore a T_C, e comprende almeno due pareti con una dimensione orizzontale non inferiore al minimo tra 4,0 m ed i 2/3 della loro altezza, che nella situazione sismica portano insieme almeno il 20% del carico gravitazionale.

Se una struttura non è classificata come struttura a pareti estese debolmente armate, tutte le sue pareti devono essere p rogettate come duttili.

Fattori di struttura Il fattore di struttura da utilizzare per ciascuna direzione della azione sismica orizzontale è calcolato come riportato nel § 7.3. 1. I massimi valori di q_0 relativi alle diverse tipologie ed alle due classi di duttilità considerate (CD"A" e CD"B") sono contenuti nella tabella 8.2.

[1] Una parete è un elemento strutturale d i supporto per altri elementi che ha una sezione trasversale caratterizzata da un rapporto tra dimensione massima e minima in pianta superiore a 4. Si definisce parete di forma composta l'insieme di pareti semplici collegate in modo da formare sezioni a L, T, U, I ecc. Una parete accoppiata consiste di due o più pareti singole collegate tra loro da travi duttili ("travi di accoppiamento") distribuite in modo regolare lungo l'altezza. Ai fini della determinazione del fattore di struttura q una parete si definisce accoppiata quando è verificata la condizione che il mo mento totale alla base prodotto dalle azioni orizzontali è equilibrato, per almeno il 20coppia prodotta dagli sforzi verticali indotti nelle pareti dell' azione sismica.

[2] Non appartengono a questa categoria i telai ad un piano con i pilastri collegati in sommità lungo entrambe le direzioni principali dell'edificio e per i quali la forza assiale non eccede il 30sezione di calcestruzzo

Table 7.2: Valori di q_0

Structural Typology, q_0	CD B	CD A
Strutture a telaio, a pareti accoppiate, miste	$3,0\alpha_u/\alpha_1$	$4,5\alpha_u/\alpha_1$
Strutture a pareti non accoppiate	3,0	$4,0\alpha_u/\alpha_1$
Strutture deformabili torsionalmente	2,0	3,0
Strutture a pendolo inverso	1,5	2,0

Le strutture a pareti estese debolmente armate devono essere progettare in CD "B". Strutture aventi i telai resistenti all'azione sismica composti, anche in una sola delle direzioni principali, con travi a spessore devono essere progettate in CD"B" a meno che tali travi non si possano considerare elementi strutturali "secondari". Per strutture regolari in pianta, possono essere adottati i seguenti valori di α_u/α_1:

a) Strutture a telaio o miste equivalenti a telai

- *strutture a telaio di un piano* $\alpha_u/\alpha_1 = 1,1$
- *strutture a telaio con piu piani ed una sola campata* $\alpha_u/\alpha_1 = 1,2$
- *strutture a telaio con piu piani e piu campate* $\alpha_u/\alpha_1 = 1,3$

b) Strutture a pareti o miste equivalenti a pareti

- *strutture con solo due pareti non accoppiate per direzione orizzontale* $\alpha_u/\alpha_1 = 1,0$
- *altre strutture a pareti non accoppiate* $\alpha_u/\alpha_1 = 1,1$
- *strutture a pareti accoppiate o miste equivalenti a pareti* $\alpha_u/\alpha_1 = 1,2$

Precast Structures

In addition to presented specifications, the 2008 Italian Code presents specific considerations about force reduction factors related to precast structures. In the following, for this particular typology of structures, the mentioned recommendation, are cited.

La prefabbricazione di parti di una struttura progettata per rispondere alle prescrizioni relative agli edifici in cemento armato richiede la dimostrazione che il collegamento in opera delle parti è tale da conferir e il previsto livello di monoliticità in termini di resistenza, rigidezza e duttilità.

Le prescrizioni di cui al presente § 7.4.5 sono aggiuntive rispetto a quelle contenute nei capitoli preced enti, per quanto applicabili e non esplicitamente modificate.

Tipologie strutturali e fattori di struttura

Le presenti norme prendono in considerazione le seguenti tipologie di sistemi strutturali, già definite nel § 7.4.3.1: - strutture a telaio; - strutture a pareti; - strutture miste telaio-pareti. In aggiunta si considerano anche le seguenti categorie: - strutture a pannelli; - strutture monolitiche a cella; - strutture a pilastri isostatici (strutture monopiano, con elementi di copertura sostenuti da appoggi fissi gravanti su pilastri isostatici). I valori massimi di q_0 per queste ultime categorie sono contenuti nella tabella 8.3.

Table 7.3: Valori di q_0

Structural Typology, q_0	CD B	CD A
Struttura a pannelli	3,0	$4,0\alpha_u/\alpha_1$
Strutture monolitiche a cella	2,0	3,0
Strutture a pilastri isostatici	2,5	3,5

Table 7.4: Allow Force Reduction factors

Structural Typology	Low Dissipative Cap. Design	High Dissipative Cap. Design
Strutture a pendolo inverso	1.5	2.0
Strutture a telaio, a pareti accoppiate, miste con *regolarità* in pianta di un piano	3.3	4.95
Strutture prefabbricate a pilastri isostatici	2.5	3.5
Other values, for other justified typology	...	...

Altre tipologie possono essere utilizzate giustificando i fattori di struttura adottati e impiegando regole di dettaglio tali da garantire i r equisiti generali di sicurezza di cui alle presenti norme.

Nelle strutture prefabbricate il meccanismo di dissipazione energetica è associato prevalentemente alle rotazioni plastiche nelle zone critiche. In aggiunta, la dissipazione può avvenire attraverso meccanismi plastici a taglio nelle connessioni, purché le forze di richiamo non diminuiscano significativamente al susseguirsi dei cicli dell'azione sismica e si evitino fenomeni d'instabilità. Nella scelta del fattore di struttura complessivo q possono essere considerate le capacità di dissipazione per meccanismi a taglio, specialmente nei sistemi a pareti prefabbricate, tenendo conto dei valori di duttilità locali a scorrimento μ_s

Allowable force reduction factors for one story industrial precast buildings

For one story industrial precast buildings, presented considerations give the possibility to choose between different values of force reduction factors. In Tab. 8.4, for high and low ductility classes and for different possible structural typologies, allowable force reduction factors are reported. It's evident how assuming the considered structure either, member of one or of the other structural typology, there is a big variability in the force reduction factor value.

7.3.3 2008 NTC Code Design Spectra

Nominal life*, *Category of importance*, and *Base period

To deal with the seismic action determination, the actual Italian Code introduces the definition of *Nominal life* (*vita nominale*), V_N, of a structure. Within of the number of years equal to the *nominal life*, the structure must be fully operative.

Based on the future use of the structure, the Italian Code introduces the definition of *category of importance*, (*Classe d'uso*), C_U. It represents a measure of importance of a structure and consequently a measure of the required performance level. According to the descriptions presented in the Code, it seems appropriate to identify the designed building with the category of importance II. For this importance category is $C_U = 1,0$.

Finally, the *base period* (*periodo di riferimento*), V_R , equal to the product between the previous two parameters, is introduced. In the developed design, the base period is equal to 50 years, ($V_R = V_N \cdot C_U = 50 \cdot 1 = 50$).

Base requirements for the limit state procedure

Basically,in the 2008 NTC Code, four limit states are introduced:

- Operative limit state, SLO (Stato limite di operatività);
- Immediate occupancy limit state, SLD (Stato limite di Danno);
- Life safety limit state, SLV (Stato limite di salvaguardia della vita);
- Collapse prevention limit state, SLC (Stato limite di prevenszione del collasso);

The first two limit states belong to the serviceability limit state and the others at the ultimate limit state.

If specific suggestions are missing, the design, according to the limit states procedure, can be considered verified:

- At the serviceability limit states, validating the design at the damage limit state (SLD)
- At the ultimate limit states, validating the design at the life safety limit state (SLV)

Seismic Action Characterization

The evaluation of the design seismic action is based on a *base seismic risk*, (*pericolosita' sismica di base*), related to the construction site. It represents the base element to characterize the design seismic action.

The definition of the base seismic risk is based on the peak ground acceleration, a_g, in free field condition on a flat surface (category of soil A, according to the 2008 NTC Code), and on the ordinate, in the design spectrum, corresponding to the fundamental period T, $Se(T)$, for the specified probability of non-exceedance P_{V_R}, as defined in the same Code, in the base period V_R. The design spectrum, for a fixed probability of non-exceedance P_{V_R} is based on the next three parameters:

Table 7.5: Site Seismic Hazard Characterization

Limit state	T_r $[years]$	a_g $[g]$	F_0 $[-]$	$T_c{}^*$ $[s]$
Operational	30	0.053	2.550	0.244
Immediate Occupancy	50	0.066	2.529	0.270
Life Safety	475	0.212	2.356	0.390
Collapse Prevention	975	0.299	2.373	0.460

- a_g, peak ground acceleration
- F_0, in the acceleration response spectrum, the maximum value of the amplification factor
- T_C^*, in the acceleration response spectrum, period corresponding to the start of the part with constant velocity

The assumed construction site is the Sicep.Spa main office. For the considered site, according to the 2008 NTC Italian Code, the a_g, F_0, and T_C^* values are reported in Tab. 7.5 for each limit state.

Elastic Design Spectrum

The 2008 NTC Italian Code defines the Design Spectrum by Equ. 7.5.

$$\begin{aligned}
0 \le T < T_B \qquad & S_e(T) = a_g \cdot S \cdot \eta \cdot F_0 \cdot \left[\frac{T}{T_B} + \frac{1}{\eta \cdot F_0} \left(1 - \frac{T}{T_B} \right) \right] \\
T_B \le T < T_C \qquad & S_e(T) = a_g \cdot S \cdot \eta \cdot F_0 \\
T_C \le T < T_D \qquad & S_e(T) = a_g \cdot S \cdot \eta \cdot F_0 \left(\frac{T_C}{T} \right) \\
T_D \le T \qquad & S_e(T) = a_g \cdot S \cdot \eta \cdot F_0 \left(\frac{T_C T_D}{T^2} \right)
\end{aligned} \tag{7.5}$$

Parameter values for the design spectrum characterization are presented in Tab. 7.6.

Inelastic Design Spectra for high and low dissipative capacity

According to the 2008 NTC Code the inelastic spectra is obtained scaling the elastic design spectrum by the force reduction factor already introduced.

Table 7.6: Parameter values for spectrum characterization

Description	Symbol	Value	Comments
Peak ground acceleration	a_g	0.21	[g]
Damping	η	0.05	Critical damping
Amplification factor	F_0	2.36	
	${T_C}^*$	0.39	
	C_C	1.33	
	S_S	1.20	
	S_T	1.00	
	S	1.20	$S_S \cdot C_C$
	T_B	0.17	$T_C/3$
	T_C	0.52	$C_C \cdot {T_C}^*$
	T_D	1.67	$4 \cdot \frac{a_g}{g} + 1.6$

7.4 Strength Demand Assessment by Equivalent Lateral Force Analysis

7.4.1 Natural Period

At this point, the hypothesis of rigid roof is introduced to can assume all the columns shaking in unison, with the the same period of vibration. From this hypothesis also descend that, for each horizontal direction, there is only one natural period.

Related to the horizontal translational component, the period of vibration can be obtained considering the stiffness of two external cantilever columns and the stiffness of a central column fixed at the top, with boundary conditions of rigid floor. To calculate that period, it 's necessary to determine in advance the stiffness of the column sections. To do this the next parameters and values are considered:

Modulus of Elasticity of Concrete	$E_c = E_{cm} = 35200$	N/mm^2
Columns Height	$H = 4.95$	m
Square section side	$l = 60$	cm
Moment of inertia (Gross section)	$I_{cls} = 1080000$	cm^4

To evaluate the vibration period, half of a section stiffness, with reference only to the concrete, is considered $(0.5 \cdot EI)$. The stiffness of the general column is:

$$k_i = 3\left(\frac{E_{cm}}{2} I_{cls}\right)/H^3 = 4701.56 \quad kN/m \tag{7.6}$$

then the total stiffness of the equivalent cantilever column is:

$$K = 18 \cdot k_i = 84628.10 \quad kN/m \tag{7.7}$$

Half of the mass of the column is concentrated at the top and half at the base. Consequently, only half a mass of the total number of columns must be assigned to the global model. With reference to the external walls, that are

Table 7.7: Seismic Mass

	$P_{External\ walls}/2$ $[kg]$	$P_{Columns}/2$ $[kg]$	$P_{At\ the\ top}$ $[kg]$	Seismic Mass $[kg]$
Transv./Long. Direction	44770	81743	1229205	1355719

Table 7.8: Fundamental Seismic Parameters

	Stiffness, K_{Global} $[kN/m]$	Seismic Mass, M $[kg]$	Period, T $[Sec]$
Transv./Long. Direction	84628.10	1355719	0.795

assumed hinged both at the base and at the top, the same hypothesis valid for the mass of the columns are introduced.Tab. 7.7 presents mass values considered for the seismic action evaluation.

Finally, the calculated period value is, next, reported:

$$T = 2\pi\sqrt{\frac{M}{K}} = 0.795 \quad sec \tag{7.8}$$

Tab. 7.8 resumes, for each principal direction, stiffness, mass, and natural period.

7.4.2 Base Shear

Design spectral acceleration

The design spectral acceleration values, equals for both directions, corresponding to the determined natural period is, next, reported:

$$\begin{aligned} &In\ Low\ Ductility\ Class\ (CDB)\ is\ obtained && S_d(T_1, x, y) = 0.118 \\ &In\ High\ Ductility\ Class\ (CDA)\ is\ obtained && S_d(T_1, x, y) = 0.079 \end{aligned}$$

Tab. 7.9 presents the base shear for both, high and low ductility class.

Table 7.9: Base Shear

Directions X,Y	Low Dissipative Capacity Design		High Dissipative Capacity Design	
Mass	1355719.00	kg	1355719.00	kg
Weight	13299.60	kN	13299.60	kN
Pseudo Acceleration	0.118	g	0.079	g
Base Shear	1569.35	kN	1050.67	kN

7.4.3 Loads combination, 2008 NTC Code

Dead and live load combination, 2008 NTC Code

At the ultimate limit state, the dead and live loads must be combined according to the next equation:

$$\gamma_{G1} \cdot G1 + \gamma_{G2} \cdot G2 + \gamma_P \cdot P + \gamma_{Q1} \cdot Q_{k1} + \gamma_{Q2} \cdot \Psi_{02} \cdot Q_{k2} + \gamma_{Q3} \cdot \Psi_{03} \cdot Q_{k3} + \ldots \tag{7.9}$$

In the current design, this combination is not examined assuming the design dominated by the seismic combination.

Earthquake load combination, 2008 NTC Code

For both, ordinary and industrial building, the design, at the ultimate limit state and at the serviceability limit state, with reference to the 2008 NTC Code, must be realized according to the next seismic combination:

$$G_1 + G_2 + P + E + \sum_j \Psi_{2,j} Q_{k,j} \tag{7.10}$$

where, as already introduced, the seismic action effects are evaluated considering masses according to the next load combination:

$$G_1 + G_2 + \sum_j \Psi_{2,j} Q_{k,j} \tag{7.11}$$

and, the $\Psi_{2,j}$ coefficients values are codified and reported in Tab. 2.5.I 2008 NTC Code.

7.4.4 Strength demand for seismic combination, prior to capacity design

Axial demand

Axial loads on columns, at the top and at the base, due to the gravitational loads are reported in 7.10. These values are obtained distributing the roof gravity loads as a function of influence areas.

Shear demand

Tab. 7.11 presents the shear demand, for low and high ductility class that is entirely due to the seismic action. The hypothesis of rigid floor and columns realized with the same cross sectional area make the shear demand equal for all the columns.

Bending moment demand

The bending moment demand for both cases, seismic action along the x direction, and y direction, coincide and is equal to:

Table 7.10: Strength Demand Axial Force

Column	Column Weight $N_{Col,W}$ $[kN]$	At the top N_{Top} $[kN]$	At the base N $[kN]$
Column 1	44.55	318.189	362.74
Column 2	44.55	636.38	680.93
Column 3	44.55	636.38	680.93
Column 4	44.55	636.38	680.93
Column 5	44.55	636.38	680.93
Column 6	44.55	318.189	362.74
Column 7	44.55	569.47	614.02
Column 8	44.55	1138.94	1183.49
Column 9	44.55	1138.94	1183.49
Column 10	44.55	1138.94	1183.49
Column 11	44.55	1138.94	1183.49
Column 12	44.55	569.47	614.02
Column 13	44.55	318.189	362.74
Column 14	44.55	636.38	680.93
Column 15	44.55	636.38	680.93
Column 16	44.55	636.38	680.93
Column 17	44.55	636.38	680.93
Column 18	44.55	318.189	362.74

Table 7.11: Strength Demand Shear Force

Column	Earthquake direction X,Y Low Dissipation $V_{x,y}$ $[kN]$	Earthquake direction X,Y High dissipation $V_{x,y}$ $[kN]$
Column 1	87.19	58.37
Column 2	87.19	58.37
Column 3	87.19	58.37
Column 4	87.19	58.37
Column 5	87.19	58.37
Column 6	87.19	58.37
Column 7	87.19	58.37
Column 8	87.19	58.37
Column 9	87.19	58.37
Column 10	87.19	58.37
Column 11	87.19	58.37
Column 12	87.19	58.37
Column 13	87.19	58.37
Column 14	87.19	58.37
Column 15	87.19	58.37
Column 16	87.19	58.37
Column 17	87.19	58.37
Column 18	87.19	58.37

$$M_{x-x} = M_{y-y} = 87.19 \cdot 4.95 = 431.59 \quad kN \cdot m \quad for\, low\, ductility\, class \tag{7.12}$$

and

$$M_{x-x} = M_{y-y} = 58.37 \cdot 4.95 = 288,93 \quad kN \cdot m \quad for\, high\, ductility\, class \tag{7.13}$$

Additional moments due to the eccentricity of the beam support are not considered.

Strength Demand considering earthquake load spatial variability, Low and High Dissipative Capacity Design

When the response is evaluated via linear static or dynamic analysis procedures, effects due to the simultaneous action of different ground motions components, according to the 2008 NTC Code, can be evaluated by Equ. 7.14:

$$1.00 \cdot E_x + 0.30 \cdot E_y + 0.30 \cdot E_z \tag{7.14}$$

where the coefficient must be combined to evaluated the most disadvantageous condition. In the developed design, the vertical component of the seismic action is not considered, then the previous is simplified in the next:

$$1.00 \cdot E_x + 0.30 \cdot E_y \tag{7.15}$$

Tab. 7.12 and Tab. 7.13 present the resulting strength demand for the low ductility class, respectively, for Combination 1 and Combination 2 . Tab. 7.14 and Tab. 7.15 present the same resulting strength demand for the high ductility class.

Demand summary for seismic combination prior capacity design

Effects that must be verified are reported, respectively, for high and low ductility class in Tab. 7.16 and in Tab. 7.17

Considering columns with the same transversal section, combinations that, must be analyzed, are reduced and reported in Tab. 7.18 and in Tab. 7.19

Table 7.12: Strength Demand for Low Ductility Class, Comb.1

Low Dissipation Combination $E_x + 0.3E_y + D$	V_x $[kN]$	V_y $[kN]$	N $[kN]$	M_{x-x} $[kNm]$	M_{y-y} $[kNm]$
Column 1	87.19	26.16	362.74	129.48	431.59
Column 2	87.19	26.16	680.93	129.48	431.59
Column 3	87.19	26.16	680.93	129.48	431.59
Column 4	87.19	26.16	680.93	129.48	431.59
Column 5	87.19	26.16	680.93	129.48	431.59
Column 6	87.19	26.16	362.74	129.48	431.59
Column 7	87.19	26.16	614.02	129.48	431.59
Column 8	87.19	26.16	1183.4	129.48	431.59
Column 9	87.19	26.16	1183.4	129.48	431.59
Column 10	87.19	26.16	1183.4	129.48	431.59
Column 11	87.19	26.16	1183.4	129.48	431.59
Column 12	87.19	26.16	614.02	129.48	431.59
Column 13	87.19	26.16	362.74	129.48	431.59
Column 14	87.19	26.16	680.93	129.48	431.59
Column 15	87.19	26.16	680.93	129.48	431.59
Column 16	87.19	26.16	680.93	129.48	431.59
Column 17	87.19	26.16	680.93	129.48	431.59
Column 18	87.19	26.16	362.74	129.48	431.59

Table 7.13: Strength Demand for Low Ductility Class, Comb.2

Low Dissipation Combination $0.3E_x + E_y + D$	V_x $[kN]$	V_y $[kN]$	N $[kN]$	M_{x-x} $[kNm]$	M_{y-y} $[kNm]$
Column 1	26.16	87.19	362.74	431.59	129.48
Column 2	26.16	87.19	680.93	431.59	129.48
Column 3	26.16	87.19	680.93	431.59	129.48
Column 4	26.16	87.19	680.93	431.59	129.48
Column 5	26.16	87.19	680.93	431.59	129.48
Column 6	26.16	87.19	362.74	431.59	129.48
Column 7	26.16	87.19	614.02	431.59	129.48
Column 8	26.16	87.19	1183.4	431.59	129.48
Column 9	26.16	87.19	1183.4	431.59	129.48
Column 10	26.16	87.19	1183.4	431.59	129.48
Column 11	26.16	87.19	1183.4	431.59	129.48
Column 12	26.16	87.19	614.02	431.59	129.48
Column 13	26.16	87.19	362.74	431.59	129.48
Column 14	26.16	87.19	680.93	431.59	129.48
Column 15	26.16	87.19	680.93	431.59	129.48
Column 16	26.16	87.19	680.93	431.59	129.48
Column 17	26.16	87.19	680.93	431.59	129.48
Column 18	26.16	87.19	362.74	431.59	129.48

Table 7.14: Strength Demand for High Ductility Class, Comb.1

Low Dissipation Combination $E_x + 0.3E_y + D$	V_x $[kN]$	V_y $[kN]$	N $[kN]$	M_{x-x} $[kNm]$	M_{y-y} $[kNm]$
Column 1	58.37	17.51	362.74	86.68	288.93
Column 2	58.37	17.51	680.93	86.68	288.93
Column 3	58.37	17.51	680.93	86.68	288.93
Column 4	58.37	17.51	680.93	86.68	288.93
Column 5	58.37	17.51	680.93	86.68	288.93
Column 6	58.37	17.51	362.74	86.68	288.93
Column 7	58.37	17.51	614.02	86.68	288.93
Column 8	58.37	17.51	1183.4	86.68	288.93
Column 9	58.37	17.51	1183.4	86.68	288.93
Column 10	58.37	17.51	1183.4	86.68	288.93
Column 11	58.37	17.51	1183.4	86.68	288.93
Column 12	58.37	17.51	614.02	86.68	288.93
Column 13	58.37	17.51	362.74	86.68	288.93
Column 14	58.37	17.51	680.93	86.68	288.93
Column 15	58.37	17.51	680.93	86.68	288.93
Column 16	58.37	17.51	680.93	86.68	288.93
Column 17	58.37	17.51	680.93	86.68	288.93
Column 18	58.37	17.51	362.74	86.68	288.93

Table 7.15: Strength Demand for High Ductility Class, Comb.2

High Dissipation Combination $0.3E_x + E_y + D$	V_x $[kN]$	V_y $[kN]$	N $[kN]$	M_{x-x} $[kNm]$	M_{y-y} $[kNm]$
Column 1	17.51	58.37	362.74	288.93	86.68
Column 2	17.51	58.37	680.93	288.93	86.68
Column 3	17.51	58.37	680.93	288.93	86.68
Column 4	17.51	58.37	680.93	288.93	86.68
Column 5	17.51	58.37	680.93	288.93	86.68
Column 6	17.51	58.37	362.74	288.93	86.68
Column 7	17.51	58.37	614.02	288.93	86.68
Column 8	17.51	58.37	1183.4	288.93	86.68
Column 9	17.51	58.37	1183.4	288.93	86.68
Column 10	17.51	58.37	1183.4	288.93	86.68
Column 11	17.51	58.37	1183.4	288.93	86.68
Column 12	17.51	58.37	614.02	288.93	86.68
Column 13	17.51	58.37	362.74	288.93	86.68
Column 14	17.51	58.37	680.93	288.93	86.68
Column 15	17.51	58.37	680.93	288.93	86.68
Column 16	17.51	58.37	680.93	288.93	86.68
Column 17	17.51	58.37	680.93	288.93	86.68
Column 18	17.51	58.37	362.74	288.93	86.68

Table 7.16: Strength demand for Low Ductility Class

Low Dissipation	V_x $[kN]$	V_y $[kN]$	N $[kN]$	M_{x-x} $[kNm]$	M_{y-y} $[kNm]$
Column 10	87.19	26.16	1183.49	129.48	431.59
Column 18	87.19	26.16	362.74	129.48	431.59
Column 10	26.16	87.19	1183.49	431.59	129.48
Column 18	26.16	87.19	362.74	431.59	129.48

Table 7.17: Strength Demand for High Ductility Class

High Dissipation	V_x $[kN]$	V_y $[kN]$	N $[kN]$	M_{x-x} $[kNm]$	M_{y-y} $[kNm]$
Column 10	58.37	17.51	1183.49	86.68	288.93
Column 18	58.37	17.51	362.74	86.68	288.93
Column 10	17.51	58.37	1183.49	288.93	86.68
Column 18	17.51	58.37	362.74	288.93	86.68

Table 7.18: Strength Demand for Low Ductility Class

Low Dissipation Column	$V_{x,y}$ $[kN]$	N $[kN]$	$M_{x-x,y-y}$ $[kNm]$	$M_{y-y,x-x}$ $[kNm]$
	87.19	1183.49	129.48	431.59
	87.19	362.74	129.48	431.59

Table 7.19: Strength Demand for High Ductility Class

High Dissipation Column	$V_{x,y}$ $[kN]$	N $[kN]$	$M_{x-x,y-y}$ $[kNm]$	$M_{y-y,x-x}$ $[kNm]$
	58.37	1183.49	86.68	288.93
	58.37	362.74	86.68	288.93

7.4.5 Strength Demand according to Capacity Design, 2008 NTC Code

Design Strength Demand, Bending Moment

In this context, the strength demand is introduced and its determination is presented according to the current Italian Code. To do this, a few sections of the code are cited.

> Per ciascuna direzione e per ciascun verso di applicazione delle azioni sismiche, si devono proteggere i pilastri dalla plasticizzazione prematura adottando opportuni momenti flettenti di calcolo; tale condizione si consegue qualora, per ogni nodo trave-pilastro ed ogni direzione e verso dell' azione sismica, la resistenza complessiva dei pilastri sia maggiore della resistenza complessiva delle travi amplificata del coefficiente γ_{Rd}, in accordo con la formula:
>
> $$\sum M_{c,Rd} \geq \gamma_{Rd} \cdot \sum M_{b,Rd} \tag{7.16}$$
>
> dove $\gamma_{Rd} = 1.3$ per le strutture in CDA e $\gamma_{Rd} = 1.1$ per le strutture in CDB, $M_{c,Rd}$ è il momento resistente del generico pilastro convergente nel nodo, calcolato per i livelli di sollecitazione assiale presenti nelle combinazioni sismiche delle azioni, e $M_{b,Rd}$ è il momento resistente della generica trave convergente nel nodo.
>
> Nella 7.16 si assume il nodo in equilibrio ed i momenti, sia nei pilastri che nelle travi, tra loro concordi. Nel caso in cui i momenti nel pilastro al di sopra ed al di sotto del nodo siano tra loro discordi, uno dei momenti del pilastro si va a sommare a quelli delle travi. Di ciò si può rendersene conto banalmente considerando l' equilibro nodale del nodo.
>
> Per la sezione di base dei pilastri del piano terreno si adotta come momento di calcolo il maggiore tra il momento risultante dall' analisi ed il momento $M_{c,Rd}$ della sezione di sommità del pilastro.
>
> Il suddetto criterio di gerarchia delle resistenze non si applica ale sezioni di sommità dei pilastri dell' ultimo piano.
>
> In generale, per colonne appartenenti alla classe di duttilità alta, i valori di progetto dei momenti flettenti sollecitanti devono essere ottenuti in accordo al criterio della gerarchia delle resistenze, considerando considerando cioè l' equilibrio del nodo trave-colonna soggetto alla più sfavorevole combinazione dei momenti resistenti relativi a tutte le sezioni terminali delle travi che convergono nel nodo per entrambe le direzioni di applicazione dell' azione sismica.

Design Strength Demand, Shear

Al fine di escludere la formazione di meccanismi inelastici dovuti al taglio, le sollecitazioni di taglio da utilizzare per le verifiche ed il dimensionamento delle armature si ottengono dalla condizione di equilibrio del pilastro soggetto all' azione dei momenti resistenti nelle sezioni di estremità superiore $M^s_{C,Rd}$ ed inferiore $M^i_{C,Rd}$ secondo l' espressione:

$$V_{Ed} = \gamma_{Rd} \cdot \frac{M^s_{c,Rd} + M^i_{c,Rd}}{l_p} \tag{7.17}$$

Table 7.20: Strength Demand for Low Dissipative Capacity Design

Low Dissipation	V_x $[kN]$	V_y $[kN]$	N $[kN]$	M_{x-x} $[kNm]$	M_{y-y} $[kNm]$
Column 10	163.4	49.02	1183.49	129.48	431.59
Column 18	163.4	49.02	362.74	129.48	431.59
Column 10	49.02	163.4	1183.49	431.59	129.48
Column 18	49.02	163.4	362.74	431.59	129.48

Table 7.21: Strength Demand for High Dissipative Capacity Design

High Dissipation	V_x $[kN]$	V_y $[kN]$	N $[kN]$	M_{x-x} $[kNm]$	M_{y-y} $[kNm]$
Column 10	146.0	43.8	1183.49	86.68	288.93
Column 18	146.0	43.8	362.74	86.68	288.93
Column 10	43.8	146.0	1183.49	288.93	86.68
Column 18	43.8	146.0	362.74	288.93	86.68

Definitive Strength Demand (According to Capacity Design)

The effects combinations that must be verified are reported in the next tables, respectively for low and high ductility level.

Considering square columns with equal dimension:

Table 7.22: Strength Demand for Low Dissipative Capacity Design

Low Dissipation Column	$V_{x,y}$ $[kN]$	N $[kN]$	$M_{x-x,y-y}$ $[kNm]$	$M_{y-y,x-x}$ $[kNm]$
	163.4	1183.49	129.48	431.59
	163.4	362.74	129.48	431.59

Table 7.23: Strength Demand for High Dissipative Capacity Design

High Dissipation Column	$V_{x,y}$ $[kN]$	N $[kN]$	$M_{x-x,y-y}$ $[kNm]$	$M_{y-y,x-x}$ $[kNm]$
	146.0	1183.49	86.68	288.93
	146.0	362.74	86.68	288.93

7.5 Design Summary

To summarize we had obtained:

Low Dissipative Capacity Design

A $70 \cdot 70$ square section
Longitudinal reinforcement: 16 ϕ 20 mm

Transversal reinforcement:
63 stirrups ϕ 10 mm, s=8 cm in the total length $4.95m$

High Dissipative Capacity Design

A $60 \cdot 60$ square section
Longitudinal reinforcement: 16 ϕ 18 mm

Transversal reinforcement:
36 stirrups ϕ 10 mm, s=9 cm in a length equal to $4.95 - 1.65 = 3.30m$ 28 stirrups ϕ 10 mm, s=6 cm in a critical length equal to $1.65m$

A total of 64 stirrups is obtained for each column.

7.6 Costs

The cost analysis, for materials, concrete and steel, and labor for the traditional structure in Ductility Class B is next reported

- Concrete : 2730 Euro
- Steel for Reinforcement: 3805 Euro
- labor 6614 Euro

The same analysis for the traditional structure in Ductility Class B is:

- Concrete : 3165 Euro
- Steel for Reinforcement: 2006 Euro
- labor 4860 Euro

Must be considered that the labor cost determined is based on the concrete volume! Details about the cost analysis can be find in the Appendix related to the Optimal Traditional Design Procedure for precast one-story building.

7.7 Optimal Design Procedure complies with the NTC 2008 Code

In appendix is reported a program developed to economically optimize the design of a traditional precast one story building according to the 2008 NTC Italian Code. The procedure, define the construction site and consequently the seismic hazard of the site, allow to know which design, low or high ductility class, is more convenient and for each of them determines the best combination of concrete section and longitudinal and transversal reinforcement. The analysis is based of unit costs of materials and of labor costs function of the concrete volume need. Substantially this procedure follow the steps considered in the previous design and develop a design for each combination of concrete section and longitudinal and transversal reinforcement and the related analysis of the cost. The obtained design can verified the request of the considered code or no. Between the verified design one is less expensive and is the solution. This is developed for both high and low ductility class. Finally the more economic solution between the best solution in high and low ductility class represents the objective of the procedure.

Chapter 8

Seismic Design of a *Hybrid* Precast Concrete Structure according to 2008 NTC Code

Contents

Preview

The design of a Hybrid structure, with reference to the current Italian code NTC 2008 is, in the following, developed. In the capacity design is assumed the plastic hinge formation in the columns, at the base for external columns and at the base and at the top for internal columns. The innovative system introduced is modeled and designed:

- At the serviceability limit state, to avoid the rocking activation under dead and live load, as a frame with fixed beam columns connections and fixed columns at the base.
- At the Ultimate limit state, allowing the rocking motion activation, as a frame with pinned beam columns connection, for external columns and fixed beam column connections for internal columns.

In particular, the idea at the ultimate limit state, is to develop the design according to the Capacity Design, as engineer use to do in high or low ductility class, calculating the resisting moment but giving this moment with a rocking connection instead than a plastic hinge activation. Finally, the moment at the rocking activation must be less than the moment that We obtain at the serviceability limit state and the maximum moment allow at the rocking interface must be equal to the moment obtained at the ultimate limit state according to the capacity design.

Observe that, for the reasons previously mentioned, analysis of two different structural scheme must be conducted, at the serviceability limit state and at the ultimate limit state.

8.1 General description

The industrial building, designed in a traditional way with reference to the 2008 NTC Italian Code, is now designed considering the self-centering elementary innovative structural system already introduced.This innovative system is constituted of column with a double rocking, at the base and at the top, and post-tensioned strands. Hysteretic metallic axial dissipators are introduced to provide supplemental energy dissipation and to mitigate the acceleration response. In Fig. the transversal section view is represented. As shown in Fig.9.23, a rectangular building shape in plan was considered. The one story building have two axes of symmetry. The plan is 32.0 meters in north-south and 40.0 meters in east-west direction. The Columns heights are 4.95 meters. All the columns are supposed fix at the base and all the all the beam column connections are supposed fixed.

The post-tensioned strands anchor at the column base is realized, without particular strand anchors but considering a bounded strands length..

The same post-tensioned strands are not interrupted at the base but them go through the column from one beam to another. Looking at fig. is possible to appreciate where the strands are unbounded and where them are bounded.

The one story building structure considered is a common typology in Italy, particularly for buildings use to economic or industrial activities.

As shown in Fig.8.2, a rectangular building shape in plan was considered. The one story building has two axes of symmetry. The plan is 32.0 meters in

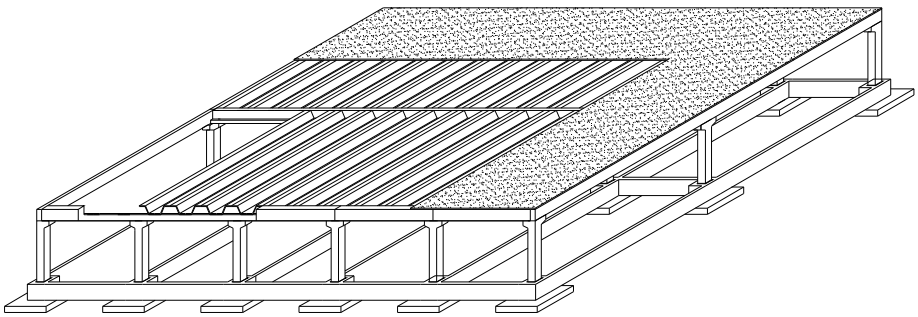

Figure 8.1: Precast concrete one story industrial building

north-south and 40.0 meters in east-west direction. The Columns heights are 4.95 meters. All the columns are supposed fix at he base and all the beams are supposed pinned at the columns. On the whole, the building structure consists of five, two bays, transversal frames, with bay length equal to 16 meters and of three, five bays, longitudinal frames, with bay length equal to 8 meters.

Foundation system

The foundation system is realized by Combined footing (Spread footing with link beams). A global view of the foundation system is presented in Fig.8.3.

Columns

All columns are supposed to have the same square section.

Roof

Three different beam sections are considered. The external longitudinal beams are supposed to have a rectangular section (*Trave R*) whereas a L section is considered for the external transversal beams(*Trave TL*). The internal beams are supposed to have a inverted T shape (*Trave TR*). A general view is presented in Fig. B.36

Consideration about losses due to friction related to the curvature ducts

The post-tensioned strands, close to the beam column connections, to be anchor to the beams, need to curve. Due to the friction between the tendons and the surrounding concrete ducts, loos of prestressing occurs in post-tensioned members. The magnitude of this loss is a function of the tendon form.

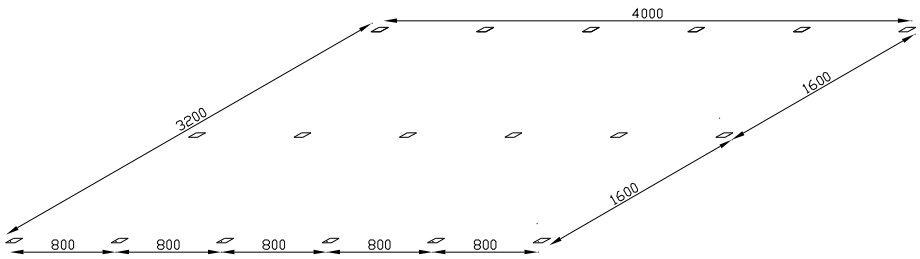

Figure 8.2: Plan dimensions

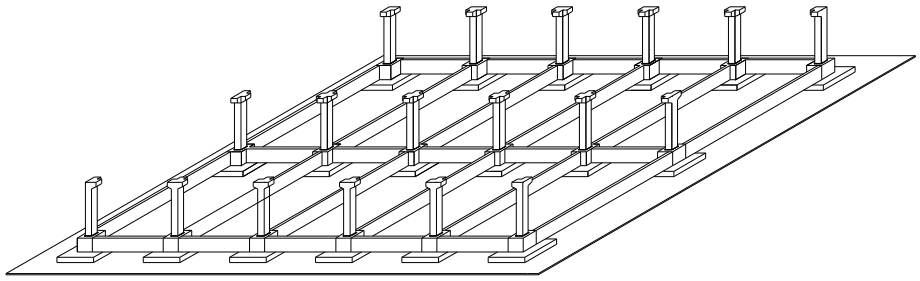

Figure 8.3: foundation

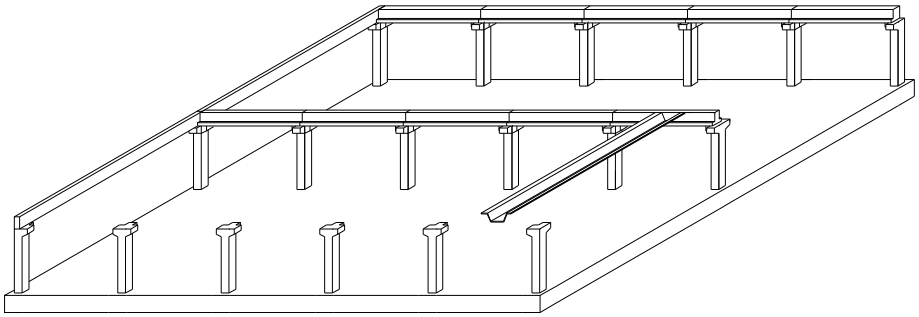

Figure 8.4: Roof elements overview

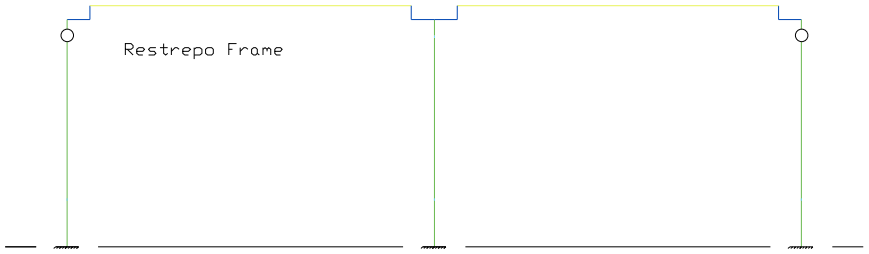

Figure 8.5: Structural Scheme, Initial Configuration

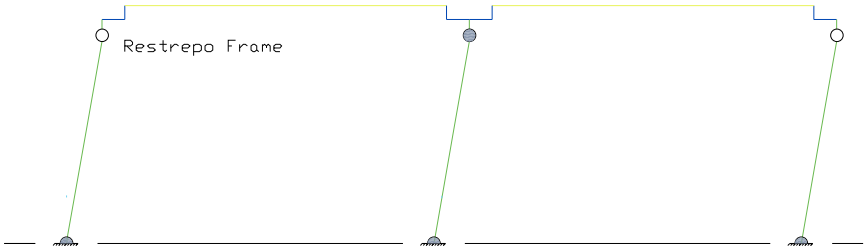

Figure 8.6: Structural Scheme, Ultimate Conditions

8.1.1 Mechanical properties of materials

In the following, the mechanical properties used in the design are presented. The *Characteristic* values are the 95% probability to be grater than the generic measured values and the *cylindrical* adjective means that the considered characteristic has been measured on cylindrical elements

Concrete **C40/50**

Characteristic compressive strength tested on cylinder element	$f_{ck} = 40$	N/mm^2
Characteristic compressive strength tested on cubic elements	$Rck = 50$	N/mm^2
Strength reduction factor	$\gamma_c = 1.5$	
Reduction factor for long term effects	$\alpha_{cc} = 0.85$	
Design compressive strength	$f_{cd} = 22,66$	N/mm^2
Mean compressive strength	$f_{cm} = 48,00$	N/mm^2
Elastic modulus	$E_c = 35200$	N/mm^2

Steel for reinforcing bars **B450C**

Characteristic yielding strength	$f_{yk} = 450$	N/mm^2
Characteristic tensile strength	$f_{tk} = 540$	N/mm^2
Strength reduction factor	$\gamma_s = 1.15$	
Design yielding strength	$f_{yd} = 22.66$	N/mm^2
Elastic modulus	$E_s = 200000$	N/mm^2

8.2 Dead and Live Loads

8.2.1 Dead Loads

The dead load on a structural element is the weight of the member itself, plus the weights of all materials permanently incorporated into the structure and supported by the member in question. The weight of the structural elements is based on the unit weight listed below:

- 3,15 kN/mq, for a transversal length of 2,5 ml, for *Tegolo Vigor 70*
- 12,00 kN/ml, for *trave TR*
- 14,31 kN/ml, for *trave TL*

Tab. 8.1 gives a summary of unit weights and quantity of structural and non structural elements considered to evaluate Dead and Live Loads.

Dead load distribution between frames

Starting to the previous analysis on the elements weight, it's possible to calculate the dead loads distribution between frames. External walls are assumed supported by the foundation system, therefore them don't give any contribution at the loads distribution on frames. **External transversal frames**

External transversal beam	$9 * 32.6 = 293.40$	kN
External longitudinal beams	$9 * 32.6 = 293.40$	kN
Tegoli	$2 * (16 + 0.30 - 0.55 - 0.2) *$	
	$*3.90 * 3.15 = 382.06$	kN
Caldana and finiture	$8.0 * 32.6 * (2 + 2,5) = 1173.60$	kN
Columns	$3 * 0.6 * 0.6 * 4.95 * 25 = 133.65$	kN
	Total at roof level **1597.85**	**kN**
	Total at foundation level **1731.50**	**kN**

Internal transversal frames

External transversal beam	$2 * 8.00 * 14.31 = 228.96$	kN
External longitudinal beams	$8 * 12.00 = 96.00$	kN
Tegoli	$2 * (16 + 0.30 - 0.55 - 0.22) *$	
	$*8.00 * 3.15 = 783,72$	kN
Caldana and finiture	$8.0 * 32.6 * (2 + 2.5) = 1173,60$	kN
Columns	$3 * 0.6 * 0.6 * 4.95 * 25 = 133,65$	kN
	Total at roof level **2282.28**	**kN**
	Total at foundation level **2415.93**	**kN**

External longitudinal frames

External transversal beams	$2 * 8.3 * 9 = 149.40$	kN
External longitudinal beam	$39.8 * 14.31 = 569.54$	kN
Tegoli	$(8 + 0,30 - 0,55 - 0,2)*$	
	$*(40,6 - 0,8) * 3,15 = 946.54$	kN
Caldana and finiture	$8.3 * 40.6 * (2 + 2.5) = 1516.41$	kN
Columns	$6 * 0.6 * 0.6 * 4.95 = 267.30$	kN
	Total at roof level 3181.89	**kN**
	Total at foundation level 3449.19	**kN**

Internal longitudinal frames

External transversal beams	$2 * 16 * 9 = 288.00$	kN
External longitudinal beam	$39.8 * 12.00 = 477.60$	kN
Tegoli	$16 * (40.6 - 0.8) * 3.15 = 2005.92$	kN
Caldana and finiture	$16 * 40.6 * (2 + 2.5) = 2923.20$	kN
Columns	$6 * 0.6 * 0.6 * 4.95 * 25 = 267.30$	kN
	Total at roof level 5694.72	**kN**
	Total at foundation level 5962.02	**kN**

To verify the calculation up until now done, the total transversal weight and the total longitudinal weight are calculated and reported.

Total transversal Weight		
at roof level	$2 * 1464.20 + 4 * 2282.28 = 12057$	kN
Total longitudinal Weight		
at roof level	$2 * 3181.89 + 5694.72 = 12058$	kN

Total transversal Weight		
at foundation level	$2 * 1464.20 + 4 * 2282.28 + 6 * 133.65 = 12858$	kN
Total longitudinal Weight		
at foundation level	$2 * 3181.89 + 5694.72 + 3 * 267.30 = 12859$	kN

8.2.2 Live Loads

It's supposed to use the designed structure like a parking structure, so in addition, a (roof) live load equal to 2.5 kN/mq, as reported in 2008 Italian code Tab. 3.1.II, is considered.

This table for parking structures gives the live load value reported in Equ. 8.1.

$$q_k = 2.5 \quad kN/m^2 \tag{8.1}$$

The total weight of the building (dead and live) which is considered in all the analysis is about 15132 kN giving a total mass of about 1482 tons. Must be clear that the previous is only the total mass that is not coincident with the seismic mass. Tab. 8.1 presents a summary of dead and live loads.

Table 8.1: Dead and Live Loads

	Unit Weight	SI Units	Quantity	SI Units	Total	SI Units
Tegoli	3.15	kN/mq	1237.78	m^2	3899.07	kN
External transversal beams	9.00	kN/ml	65.20	m	586.80	kN
External longitudinal beams	14.31	kN/ml	79.60	m	1139.08	kN
Central longitudinal beam	12.00	kN/ml	39.80	m	477.60	kN
Other permanent elements	2.00	kN/mq	1323.56	m^2	2647.12	kN
Live loads (Parking structures)	2.50	kN/mq	1323.56	m^2	3308.90	kN
			Roof level		12058.50	kN
Columns	9.00	kN/ml	89.10	m	801.90	kN
			Ground level		12860.40	kN
External Walls	3.50	kN/mq	878.40	m^2	3074.40	kN
			Total Dead + Live Loads		15132.9	kN

8.3 Design Seismic Action, 2008 NTC Code

8.3.1 Mass

According to the 2008 NTC Code, the effects induced by the seismic action are evaluated with reference to masses calculated through Equ. 8.2,

$$G_1 + G_2 + \sum_j \Psi_{2,j} Q_{k,j} \tag{8.2}$$

where the $\Psi_{2,j}$ coefficients are codified and reported in Tab. 2.5.I, 2008 NTC Code. According to the Italian Code, for H category roof is $\Psi_{2,j} = \Psi_{1,j} = \Psi_{0,j} = 0$ then, in the current design, the induced seismic effects are evaluated according to Equ. 8.3.

$$G_1 + G_2 \tag{8.3}$$

8.3.2 Force Reduction Factors, and structural typologies, according to 2008 NTC Code

Generality

The force reduction factor is, in this context, introduced and its determination is presented according to the current Italian Code. To do this, a few sections of the code are cited.

> Il valore del fattore di struttura q da utilizzare per ciascuna direzione della azione sismica, dipende dalla tipologia strutturale, dal suo grado di iperstaticità e dai criteri di progettazione adottati e prende in conto le non linearità di materiale. Esso può essere calcolato tramite la seguente espressione:
>
> $$q = q_0 \cdot K_R \tag{8.4}$$
>
> dove:
>
> q_0 è il valore massimo del fattore di struttura che dipende dal livello di duttilità attesa, dalla tipologia strutturale e dal rapporto α_u/α_1 tra il valore dell'azione sismica p er il quale si verifica la formazione di un numero di cerniere plastich e tali da rendere la struttura labile e quello per il quale il primo elemento strutturale raggiunge la plasticizzazione a flessione;
>
> K_R è un fattore riduttivo che dipende dalle car atteristiche di regolarità in altezza della costruzione, con valore pari ad 1 per costruzioni regolari in altezza e pari a 0,8 per costruzioni non regolari in altezza.
>
> Per le costruzioni regolari in pianta, qualora non si proceda ad un'analisi non lineare finalizzata alla valutazione del rapporto α_u/α_1, per esso possono essere adottati i valori indicati nei paragrafi successivi per le diverse tipologie costruttive.
>
> Per le costruzioni non regolari in pianta, si possono adottare valori di α_u/α_1 pari alla media tra 1,0 ed i valori di volta in volta forniti per le diverse tipologie costruttive.

Concrete Structures

The considered Code presents specific suggestions for concrete structures that, in the following, are cited.

Le strutture sismo-resistenti in cemento armato previste dalle presenti norme possono essere classificate nelle seguenti tipologie:

- *strutture a telaio*, nelle quali la resistenza alle azioni sia verticali che orizzontali è affidata principalmente a telai spaziali, aventi resistenza a taglio alla base 65
- *strutture a pareti*, nelle quali la resistenza alle azioni sia verticali che orizzontali è affidata principalmente a pareti, singole o accoppiate, aventi resistenza a taglio alla base 65% della resistenza a taglio totale [1];
- *strutture miste telaio-pareti*, nelle quali la resistenza alle azioni verticali è affidata prevalentemente ai telai, la resistenza alle azioni orizzontali è affidata in parte ai telai ed in parte alle pareti, singole o accoppiate; se più del 50% dell'azione orizzontale è assorbita dai telai si parla di strutture miste equivalenti a telai, altrimenti si parla di strutture miste equivalenti a pareti;
- strutture deformabili torsionalmente, composte da telai e/o pareti, la cui rigidezza torsionale non soddisfa ad ogni piano la condizione $r/l_s > 0,8$, nella quale:
  r^2 = rapporto tra rigidezza torsionale e flessionale di piano
  $l^2 = (L_2 + B_2)/12$ (L e B dimensioni in pianta del piano)
- *strutture a pendolo inverso*, nelle quali almeno il 50% della massa è nel terzo superiore dell'altezza della costru zione o nelle quali la dissipazione d'energia avviene alla base di un singolo elemento strutturale [2].

Le strutture delle costruzioni in calcestruzzo possono essere classificate come appartenenti ad una tipologia in una direzione orizzontale ed ad un'altra tipologia nella direzione orizzontale ortogon ale alla precedente.

Una struttura a pareti è da considerarsi come struttura a pareti estese debolmente armate se, nella direzione orizzontale d'interesse, essa ha un periodo fondamentale, calcolato nell'ipotesi di assenza di rotazioni alla base, non superiore a T_C, e comprende almeno due pareti con una dimensione orizzontale non inferiore al minimo tra 4,0 m ed i 2/3 della loro altezza, che nella situazione sismica portano insieme almeno il 20% del carico gravitazionale.

Se una struttura non è classificata come struttura a pareti estese debolmente armate, tutte le sue pareti devono essere p rogettate come duttili.

Fattori di struttura Il fattore di struttura da utilizzare per ciascuna direzione della azione sismica orizzontale è calcolato come riportato nel § 7.3. 1. I massimi valori di q_0 relativi alle diverse tipologie ed alle due classi di duttilità considerate (CD"A" e CD"B") sono contenuti nella tabella 8.2.

[1] Una parete è un elemento strutturale d i supporto per altri elementi che ha una sezione trasversale caratterizzata da un rapporto tra dimensione massima e minima in pianta superiore a 4. Si definisce parete di forma composta l'insieme di pareti semplici collegate in modo da formare sezioni a L, T, U, I ecc. Una parete accoppiata consiste di due o più pareti singole collegate tra loro da travi duttili ("travi di accoppiamento") distribuite in modo regolare lungo l'altezza. Ai fini della determinazione del fattore di struttura q una parete si definisce accoppiata quando è verificata la condizione che il mo mento totale alla base prodotto dalle azioni orizzontali è equilibrato, per almeno il 20coppia prodotta dagli sforzi verticali indotti nelle pareti dell' azione sismica.

[2] Non appartengono a questa categoria i telai ad un piano con i pilastri collegati in sommità lungo entrambe le direzioni principali dell'edificio e per i quali la forza assiale non eccede il 30sezione di calcestruzzo

Table 8.2: Valori di q_0

Structural Typology, q_0	CD B	CD A
Strutture a telaio, a pareti accoppiate, miste	$3,0\alpha_u/\alpha_1$	$4,5\alpha_u/\alpha_1$
Strutture a pareti non accoppiate	3,0	$4,0\alpha_u/\alpha_1$
Strutture deformabili torsionalmente	2,0	3,0
Strutture a pendolo inverso	1,5	2,0

Le strutture a pareti estese debolmente armate devono essere progettare in CD "B". Strutture aventi i telai resistenti all'azione sismica composti, anche in una sola delle direzioni principali, con travi a spessore devono essere progettate in CD"B" a meno che tali travi non si possano considerare elementi strutturali "secondari". Per strutture regolari in pianta, possono essere adottati i seguenti valori di α_u/α_1:

a) Strutture a telaio o miste equivalenti a telai

- *strutture a telaio di un piano* $\alpha_u/\alpha_1 = 1,1$
- *strutture a telaio con piu piani ed una sola campata* $\alpha_u/\alpha_1 = 1,2$
- *strutture a telaio con piu piani e piu campate* $\alpha_u/\alpha_1 = 1,3$

b) Strutture a pareti o miste equivalenti a pareti

- *strutture con solo due pareti non accoppiate per direzione orizzontale* $\alpha_u/\alpha_1 = 1,0$
- *altre strutture a pareti non accoppiate* $\alpha_u/\alpha_1 = 1,1$
- *strutture a pareti accoppiate o miste equivalenti a pareti* $\alpha_u/\alpha_1 = 1,2$

Precast Structures

In addition to the presented specifications, the 2008 Italian Code presents specific considerations about force reduction factors related to precast structures. In the following, for this particular typology of structures, the mentioned recommendation, are cited.

La prefabbricazione di parti di una struttura progettata per rispondere alle prescrizioni relative agli edifici in cemento armato richiede la dimostrazione che il collegamento in opera delle parti è tale da conferir e il previsto livello di monoliticità in termini di resistenza, rigidezza e duttilità.

Le prescrizioni di cui al presente § 7.4.5 sono aggiuntive rispetto a quelle contenute nei capitoli preced enti, per quanto applicabili e non esplicitamente modificate.

Tipologie strutturali e fattori di struttura

Le presenti norme prendono in considerazione le seguenti tipologie di sistemi strutturali, già definite nel § 7.4.3.1: - strutture a telaio; - strutture a pareti; - strutture miste telaio-pareti. In aggiunta si considerano anche le seguenti categorie: - strutture a pannelli; - strutture monolitiche a cella; - strutture a pilastri isostatici (strutture monopiano, con elementi di copertura sostenuti da appoggi fissi gravanti su pilastri isostatici). I valori massimi di q_0 per queste ultime categorie sono contenuti nella tabella 8.3.

Table 8.3: Valori di q_0

Structural Typology, q_0	CD B	CD A
Struttura a pannelli	3,0	$4,0\alpha_u/\alpha_1$
Strutture monolitiche a cella	2,0	3,0
Strutture a pilastri isostatici	2,5	3,5

Table 8.4: Allow Force Reduction factors

Structural Typology	Low Dissipative Cap. Design	High Dissipative Cap. Design
Strutture a pendolo inverso	1.5	2.0
Strutture a telaio, a pareti accoppiate, miste con *regolarità* in pianta di un piano	3.3	4.95
Strutture prefabbricate a pilastri isostatici	2.5	3.5
Other values, for other justified typology	...	...

Altre tipologie possono essere utilizzate giustificando i fattori di struttura adottati e impiegando regole di dettaglio tali da garantire i r equisiti generali di sicurezza di cui alle presenti norme.

Nelle strutture prefabbricate il meccanismo di dissipazione energetica è associato prevalentemente alle rotazioni plastiche nelle zone critiche. In aggiunta, la dissipazione può avvenire attraverso meccanismi plastici a taglio nelle connessioni, purché le forze di richiamo non diminuiscano significativamente al susseguirsi dei cicli dell'azione sismica e si evitino fenomeni d'instabilità. Nella scelta del fattore di struttura complessivo q possono essere considerate le capacità di dissipazione per meccanismi a taglio, specialmente nei sistemi a pareti prefabbricate, tenendo conto dei valori di duttilità locali a scorrimento μ_s

Allowable force reduction factors for one story industrial precast buildings

For one story industrial precast buildings, presented considerations give the possibility to choose between different values of force reduction factors. In Tab. 8.4, for high and low ductility classes and for different possible structural typologies, allowable force reduction factors are reported. It's evident how assuming the considered structure either, member of one or of the other structural typology, there is a big variability in the force reduction factor value.

8.3.3 2008 NTC Code Design Spectra

Nominal life*, *Importance category*, and *Base period

To deal with the seismic action determination, the actual Italian Code introduces the definition of *Nominal life* (*vita nominale*), V_N, of a structure. Within of the number of years equal to the *nominal life*, the structure must be fully operative.

Based on the future use of the structure, the Italian Code introduces the definition of *category of importance*, (*Classe d'uso*), C_U. It represents a measure of importance of a structure and consequently a measure of the required performance level. According to the descriptions presented in the Code, it seems appropriate to identify the designed building with the category of importance II. For this importance category is $C_U = 1,0$.

Finally, the *base period* (*periodo di riferimento*), V_R , equal to the product between the previous two parameters, is introduced. In the developed design, the base period is equal to 50 years, ($V_R = V_N \cdot C_U = 50 \cdot 1 = 50$).

Base requirements for the limit state procedure

Basically,in the 2008 NTC Code, four limit states are introduced:

- Operative limit state, SLO (Stato limite di operatività);
- Immediate occupancy limit state, SLD (Stato limite di Danno);
- Life safety limit state, SLV (Stato limite di salvaguardia della vita);
- Collapse prevention limit state, SLC (Stato limite di prevenszione del collasso);

The first two limit states belong to the serviceability limit state and the others at the ultimate limit state.

If specific suggestions are missing, the design, according to the limit states procedure, can be considered verified:

- At the serviceability limit states, validating the design at the damage limit state (SLD)
- At the ultimate limit states, validating the design at the life safety limit state (SLV)

Seismic Action Characterization

The evaluation of the design seismic action is based on a *base seismic risk*, (*pericolosita' sismica di base*), related to the construction site. It represents the base element to characterize the design seismic action.

The definition of the base seismic risk is based on the peak ground acceleration, a_g, in free field condition on a flat surface (category of soil A, according to the 2008 NTC Code), and on the ordinate, in the design spectrum, corresponding to the fundamental period T, $Se(T)$, for the specified probability of non-exceedance P_{V_R}, as defined in the same Code, in the base period V_R. The design spectrum, for a fixed probability of non-exceedance P_{V_R} is based on the next three parameters:

Table 8.5: Site Seismic Hazard Characterization

Limit state	T_r $[years]$	a_g $[g]$	F_0 $[-]$	$T_c{}^*$ $[s]$
Operational	30	0.053	2.550	0.244
Immediate Occupancy	50	0.066	2.529	0.270
Life Safety	475	0.212	2.356	0.390
Collapse Prevention	975	0.299	2.373	0.460

- a_g, peak ground acceleration
- F_0, in the acceleration response spectrum, the maximum value of the amplification factor
- T_C^*, in the acceleration response spectrum, period corresponding to the start of the part with constant velocity

The assumed construction site is the Sicep.Spa main office. For the considered site, according to the 2008 NTC Italian Code, the a_g, F_0, and T_C^* values are reported in Tab. 9.1 for each limit state.

Elastic Design Spectrum

The 2008 NTC Italian Code defines the Design Spectrum by Equ. 8.5.

$$\begin{aligned}
0 \le T < T_B \qquad & S_e(T) = a_g \cdot S \cdot \eta \cdot F_0 \cdot \left[\frac{T}{T_B} + \frac{1}{\eta \cdot F_0} \left(1 - \frac{T}{T_B} \right) \right] \\
T_B \le T < T_C \qquad & S_e(T) = a_g \cdot S \cdot \eta \cdot F_0 \\
T_C \le T < T_D \qquad & S_e(T) = a_g \cdot S \cdot \eta \cdot F_0 \left(\frac{T_C}{T} \right) \\
T_D \le T \qquad & S_e(T) = a_g \cdot S \cdot \eta \cdot F_0 \left(\frac{T_C T_D}{T^2} \right)
\end{aligned} \tag{8.5}$$

Parameter values for the design spectrum characterization are presented in Tab. 8.6.

Inelastic Design Spectra for high and low dissipative capacity

According to the 2008 NTC Code the inelastic spectra is obtained scaling the elastic design spectrum by the force reduction factor already introduced.

Table 8.6: Parameter values for spectrum characterization

Description	Symbol	Value	Comments
Peak ground acceleration	a_g	0.21	[g]
Damping	η	0.05	Critical damping
Amplification factor	F_0	2.36	*
	${T_C}^*$	0.39	*
	C_C	1.33	
	S_S	1.20	
	S_T	1.00	
	S	1.20	$S_S \cdot C_C$
	T_B	0.17	$T_C/3$
	T_C	0.52	$C_C \cdot {T_C}^*$
	T_D	1.67	$4 \cdot \frac{a_g}{g} + 1.6$

8.4 Strength Demand Assessment by Equivalent Lateral Force Analysis

8.4.1 Natural Period

At this point, the hypothesis of rigid roof is introduced to can assume all the columns shaking in unison, with the the same period of vibration. From this hypothesis also descend that, for each horizontal direction, there is only one natural period.

Related to the horizontal translational component, the period of vibration can be obtained considering the stiffness of two external cantilever columns and the stiffness of a central column fixed at the top, with boundary conditions of rigid floor. To calculate that period, it 's necessary to determine in advance the stiffness of the column sections. To do this the next parameters and values are considered:

Modulus of Elasticity of Concrete	$E_c = E_{cm} = 35200$	N/mm^2
Columns Height	$H = 4.95$	m
Square section side	$l = 50$	cm
Moment of inertia (Gross section)	$I_{cls} = 520833$	cm^4

To evaluate the vibration period, half of a section stiffness, with reference only to the concrete, is considered $(0.5 \cdot EI)$. For the external columns stiffness:

$$k_{i,ex} = 3\left(\frac{E_{cm}}{2} I_{cls}\right)/H^3 = 2267 \quad kN/m \tag{8.6}$$

For the internal column stiffness:

$$k_{i,in} = 12\left(\frac{E_{cm}}{2} I_{cls}\right)/H^3 = 9069 \quad kN/m \tag{8.7}$$

The frame horizontal stiffness is:

$$K = 6 \cdot (2 \cdot k_{i,ex} + k_{i,in}) = 81623 \quad kN/m \tag{8.8}$$

Table 8.7: Seismic Mass

	$P_{External\ walls}/2$ $[kg]$	$P_{Columns}/2$ $[kg]$	$P_{At\ the\ top}$ $[kg]$	Seismic Mass $[kg]$
Transv./Long. Direction	44770	81743	1229205	1355719

Table 8.8: Fundamental Seismic Parameters

	Stiffness, K_{Global} $[kN/m]$	Seismic Mass, M $[kg]$	Period, T $[Sec]$
Transv./Long. Direction	81623	1355719	0.81

Half of the mass of the column is concentrated at the top and half at the base. Consequently, only half a mass of the total number of columns must be assigned to the global model. With reference to the external walls, that are assumed hinged both at the base and at the top, the same hypothesis valid for the mass of the columns are introduced.Tab. 8.7 presents mass values considered for the seismic action evaluation.

Finally, the calculated period value is, next, reported:

$$T = 2\pi\sqrt{\frac{M}{K}} = 0.81 \quad sec \tag{8.9}$$

Tab. 8.8 resumes, for each principal direction, stiffness, mass, and natural period.

8.4.2 Base Shear

Design spectral acceleration

The design spectral acceleration values, equals for both directions, corresponding to the determined natural period is, next, reported:

In Low Ductility Class (CDB) *is obtained*	$S_d(T_1, x, y) = 0.116$
In High Ductility Class (CDA) *is obtained*	$S_d(T_1, x, y) = 0.077$

Tab. 8.9 presents the base shear for both, high and low ductility class.

Table 8.9: Base Shear

Directions X,Y	Low Dissipative Capacity Design		High Dissipative Capacity Design	
Mass	1355719.00	kg	1355719.00	kg
Weight	13299.60	kN	13299.60	kN
Pseudo Acceleration	0.116	g	0.077	g
Base Shear	1542.75	kN	1024.07	kN
Base Shear (internal frame)	257.12	kN	171	kN

8.4.3 Loads combination, 2008 NTC Code

Dead and live load combination, 2008 NTC Code

At the ultimate limit state, the dead and live loads must be combined according to the next equation:

$$\gamma_{G1} \cdot G1 + \gamma_{G2} \cdot G2 + \gamma_P \cdot P + \gamma_{Q1} \cdot Q_{k1} + \gamma_{Q2} \cdot \Psi_{02} \cdot Q_{k2} + \gamma_{Q3} \cdot \Psi_{03} \cdot Q_{k3} + \dots \tag{8.10}$$

Earthquake load combination, 2008 NTC Code

For both, ordinary and industrial building, the design, at the ultimate limit state and at the serviceability limit state, with reference to the 2008 NTC Code, must be realized according to the next seismic combination:

$$G_1 + G_2 + P + E + \sum_j \Psi_{2,j} Q_{k,j} \tag{8.11}$$

where, as already introduced, the seismic action effects are evaluated considering masses according to the next load combination:

$$G_1 + G_2 + \sum_j \Psi_{2,j} Q_{k,j} \tag{8.12}$$

and, the $\Psi_{2,j}$ coefficients values are codified and reported in Tab. 2.5.I 2008 NTC Code.

8.4.4 Strength demand, prior to capacity design

In the following, the design will be developed exclusively with reference to the High Ductility Class. The structural scheme of the considered frame subjected to the loads combination introduced in the previous sections, is resolved by a finite element analysis software, (SAP2000), and the results for Axial load, Shear load, and Bending moment are presented.

Strength demand for dead and live loads combination

For the dead and live load combination reported in the 2008 NTC Code, Tab. 8.10, Tab. 8.11, and Tab. 8.12, presents, respectively, the axial load, shear load, and bending moment, strength demand, for the two external columns and for the internal column both, at the base and at the top.

Table 8.10: Strength Demand Axial Force

Column	Column Weight $N_{Col,W}$ $[kN]$	At the top N_{Top} $[kN]$	At the base N $[kN]$
Ex. Column, left	30	676	706
In. Column	30	2250	2280
Ex. Column, right	30	676	706

Table 8.11: Strength Demand Shear Force

Column	Earthquake direction X,Y At the top $V_{x,y}$ $[kN]$	Earthquake direction X,Y At the base $V_{x,y}$ $[kN]$
Ex. Column, left	0	0
In. Column	0	0
Ex. Column, right	0	0

Table 8.12: Strength Demand Bending Moment

Column	Earthquake direction X,Y At the top M_x $[kNm]$	Earthquake direction X,Y At the base M_x $[kNm]$
Ex. Column, left	0	0
In. Column	0	0
Ex. Column, right	0	0

Table 8.13: Strength Demand Axial Force, no amplification factors

Column	Column Weight $N_{Col,W}$ $[kN]$	At the top N_{Top} $[kN]$	At the base N $[kN]$
Ex. Column, left	30	-520	-550
In. Column	30	-1360	-1390
Ex. Column, right	30	-520	-550

Table 8.14: Strength Demand Shear Force, no amplification factors

Column	Earthquake direction X,Y At the top $V_{x,y}$ $[kN]$	Earthquake direction X,Y At the base $V_{x,y}$ $[kN]$
Ex. Column, left	+223	-223
In. Column	0	0
Ex. Column, right	-223	+223

Strength Demand for Dead and Live Loads Combination, without any amplification, for fixed beam-column connections To avoid the Rocking activation under dead and live loads, the structural scheme with fixed beam-column connections, even for the external columns, will be now considered.

For the dead and live load combination without any amplification factor, Tab. 8.13, Tab. 8.14, and Tab. 8.15 present, respectively, the axial load, shear load, and bending moment strength demand, for the two external columns and for the internal column both, at the base and at the top.

Strength demand for seismic combination

For the seismic combination reported in the 2008 NTC Code, Tab. 8.16, Tab. 8.17, and Tab. 8.18 present, respectively, the axial load, shear load, and bending moment strength demand, for the two external columns and for the internal column both, at the base and at the top.

Table 8.15: Strength Demand Bending Moment, no amplification factors

Column	Earthquake direction X,Y At the top M_x $[kNm]$	Earthquake direction X,Y At the base M_x $[kNm]$
Ex. Column, left	745	360
In. Column	0	0
Ex. Column, right	745	360

Table 8.16: Strength Demand Axial Force

Column	Column Weight $N_{Col,W}$ $[kN]$	At the top N_{Top} $[kN]$	At the base N $[kN]$
Ex. Column, left	-30	-463	-493
In. Column	-30	-1562	-1592
Ex. Column, right	-30	-477	-507

Table 8.17: Strength Demand Shear Force

Column	Earthquake direction X,Y At the top $V_{x,y}$ $[kN]$	Earthquake direction X,Y At the base $V_{x,y}$ $[kN]$
Ex. Column, left	35	-35
In. Column	100	-100
Ex. Column, right	-35	35

Table 8.18: Strength Demand Bending Moment

Column	Earthquake direction X,Y At the top M_x $[kNm]$	Earthquake direction X,Y At the base M_x $[kNm]$
Ex. Column, left	0	175
In. Column	215	280
Ex. Column, right	0	175

8.4.5 Strength Demand according to Capacity Design, 2008 NTC Code

Design strength demand, Bending Moment

In the Capacity Design of the one-story industrial building considered, is assumed to develop plastic hinges at the base and at the top of the columns, avoiding the develop of plasticity in beams. So, for columns, the evaluated seismic demand is the final demand to be consider and moments in the beam must be amplify, through the γ_{Rd} coefficient, according to the next equation:

$$\sum M_{b,Rd} \geq \gamma_{Rd} \cdot \sum M_{c,Rd} \tag{8.13}$$

where $\gamma_{Rd} = 1.3$ for High Ductility Class (DCA) and $\gamma_{Rd} = 1.1$ for Low Ductility Class (DCB), and $M_{c,Rd}$ and $M_{b,Rd}$ are the resisting moment, at the top of the column and, at the beam-column connection.

Substantially, a section with a resisting moment greater than the moment demand obtained from the analysis in absence of capacity design, for the particular axial force must to be considered.

The resisting moment of the beams must be greater than the resisting moment of the columns according to the safety coefficient, γ_{Rd}, valid for the considered ductility class.

Design Strength Demand, Shear

To avoid plastic mechanisms related to shear, the shear demand must be determined even according to Equ. 8.14

$$V_{Ed} = \gamma_{Rd} \cdot \frac{M^s_{c,Rd} + M^i_{c,Rd}}{l_p} \tag{8.14}$$

For high ductility class and for an axial force equal to N=-1604 kN, a square section with side equal to 50 cm and with 4, 18 mm diameter, bars at the corner and 8, 16 mm diameter, bars at the center gives a resisting moment $M_{Rd} = 412$ kNm. For the particular structural scheme, the moment at the top of external columns must zero $M^s_{C,Rd} = 0$. On the other side, introducing the mentioned resisting moment, as resisting moment at the top and at the base for internal column and at the base for external column is obtained:

$$V_{Ed,ex} = \gamma_{Rd} \cdot \frac{M^i_{c,Rd}}{l_p} = 1.3 \cdot \frac{412}{4.95} = 108 \quad kN \tag{8.15}$$

for external columns and

$$V_{Ed,in} = \gamma_{Rd} \cdot \frac{M^s_{c,Rd} + M^i_{c,Rd}}{l_p} = 1.3 \cdot \frac{412 + 412}{4.95} = 216 \quad kN \tag{8.16}$$

for the internal column. Both, for external and internal columns, the obtained shear demand is grater than the one obtained prior to capacity design. Therefore this is the shear demand that must be considered.

Table 8.19: Strength Demand for High Ductility Class

Low Dissipation	V_x $[kN]$	V_y $[kN]$	N $[kN]$	M_{x-x} $[kNm]$	M_{y-y} $[kNm]$
External Column	108	32	-505	52	175
Internal Column	216	65	-1604	84	280

Table 8.20: Strength Demand for High Ductility Class

High Dissipation Column	$V_{x,y}$ $[kN]$	N $[kN]$	$M_{x-x,y-y}$ $[kNm]$	$M_{y-y,x-x}$ $[kNm]$
External Column	108	-505	52	175
Internal Column	216	-1604	84	280

8.4.6 Effects combination to consider the earthquake spatial variability

When the response is evaluated via linear static or dynamic analysis procedures, effects due to the simultaneous action of different ground motions components, according to the 2008 NTC Code, can be evaluated:

$$1.00 \cdot E_x + 0.30 \cdot E_y + 0.30 \cdot E_z \tag{8.17}$$

where the coefficient must be combined to evaluated the most disadvantageous condition. In the developed design, the vertical component of the seismic action is not considered, then the previous is simplified in the next:

$$1.00 \cdot E_x + 0.30 \cdot E_y \tag{8.18}$$

Tab. 8.19 presents the resulting strength demand. Considering columns with the same transversal section, combinations that, must be analyzed, are reported in Tab. 8.20

Analysis for deformability (Excessive deflections) at the serviceability limit state:Summary

In the next table, stiffness and shear values that must be considered are reported together with the obtained demand and capacity in terms of displacement.

Both sections are verified.

Table 8.21: Base Shear

Directions X,Y	Low Dissipative Capacity Design	High Dissipative Capacity Design	
Column Stiffness	17420.44	9403.12	kN/m
Column Shear	138.17	101.22	kN
Design Displacement (δ)	7.93	10.76	mm
Displ. Objective (δ_{lim})	24.75	24.75	mm
Section	Appropriate	Appropriate	

8.5 Design summary

For ductility class A, summarizing, for each column, is obtained:
A $50 \cdot 50$ square section

Longitudinal reinforcement: 4 ϕ 18 mm + 8 ϕ 16 mm

Transversal reinforcement:
50 stirrups ϕ 10 mm, s=100 mm

8.6 Costs

The cost analysis, for materials, concrete and steel, and labor for the innovative structure (in Ductility Class A) is next reported:

- Concrete : 1392 Euro
- Steel for Reinforcement: 2173 Euro
- labor 3375 Euro

where the labor cost is based on the concrete volume!

8.6.1 Traditional Vs Innovative: Cost comparison

The costs comparison between the traditional solutions, in ductility class B and A, and the innovative solution is now presented.

- Traditional Design, CDB: 13 148 Euro
- Traditional Design, CDA: 10 031 Euro
- Innovative Design, CDA: 6 940 Euro

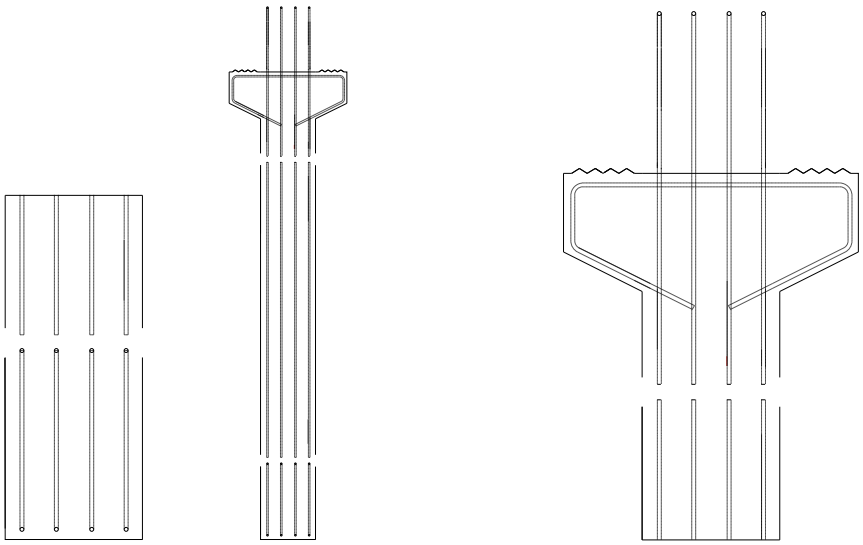

Figure 8.7: Internal Column Longitudinal Reinforcements

8.7 Structural Details

In the following figures are shown structural details related to central columns. Particular about longitudinal and transversal reinforcing bars, steel angular and related anchorage at the rocking interface, dissipators and post-tensioned strands.

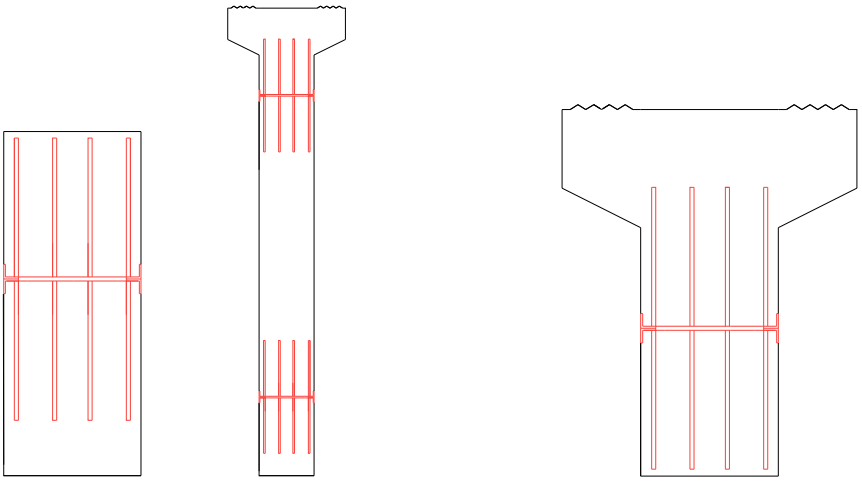

Figure 8.8: Steel Angular and anchorage at the rocking interface

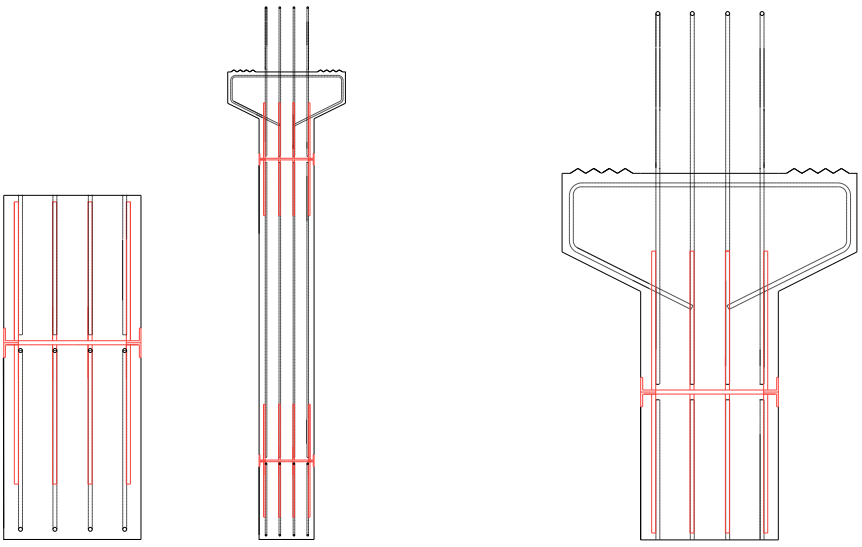

Figure 8.9: Progressive construction

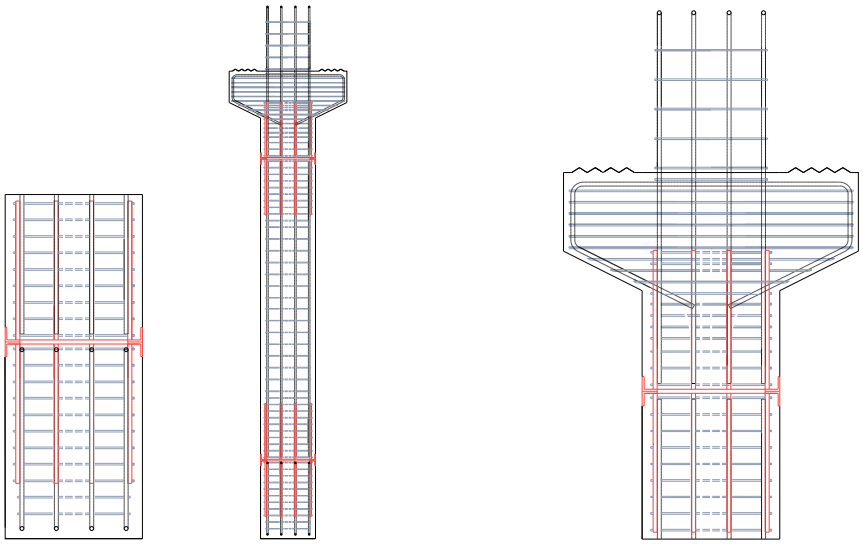

Figure 8.10: Internal Column transversal reinforcements

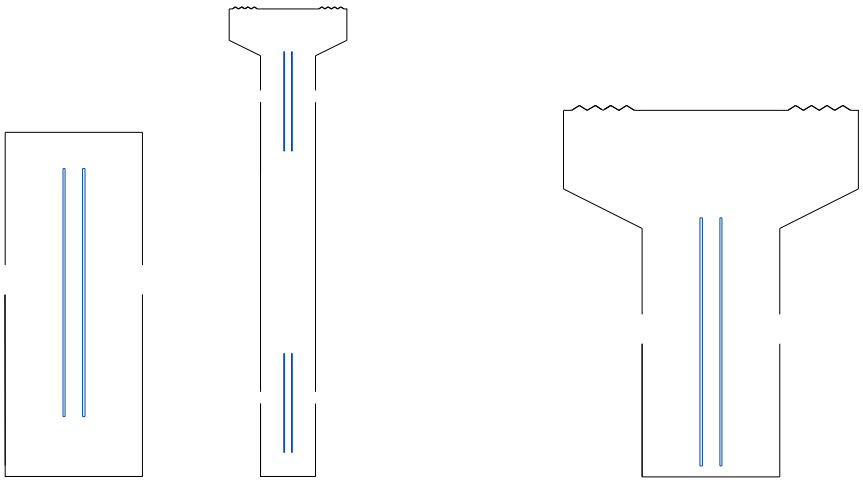

Figure 8.11: Dissipators

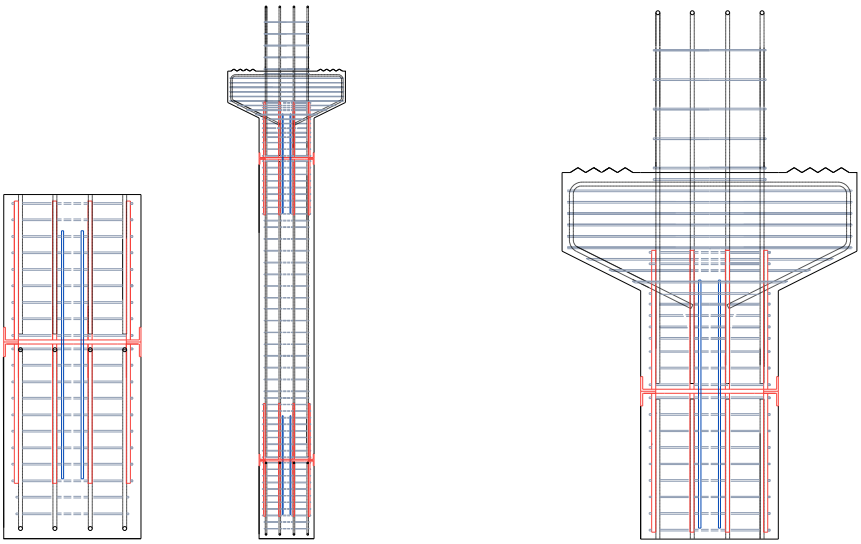

Figure 8.12: Progressive construction

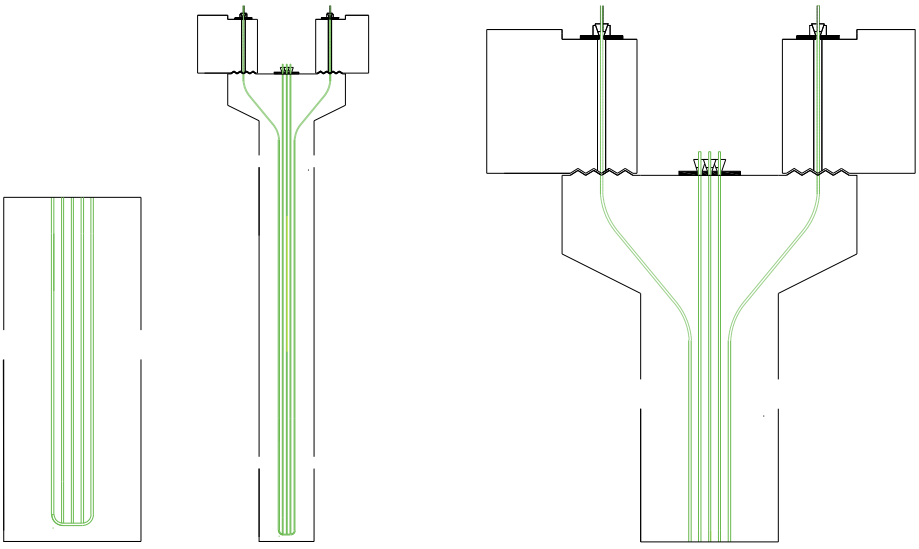

Figure 8.13: Post-Tensioned Strands

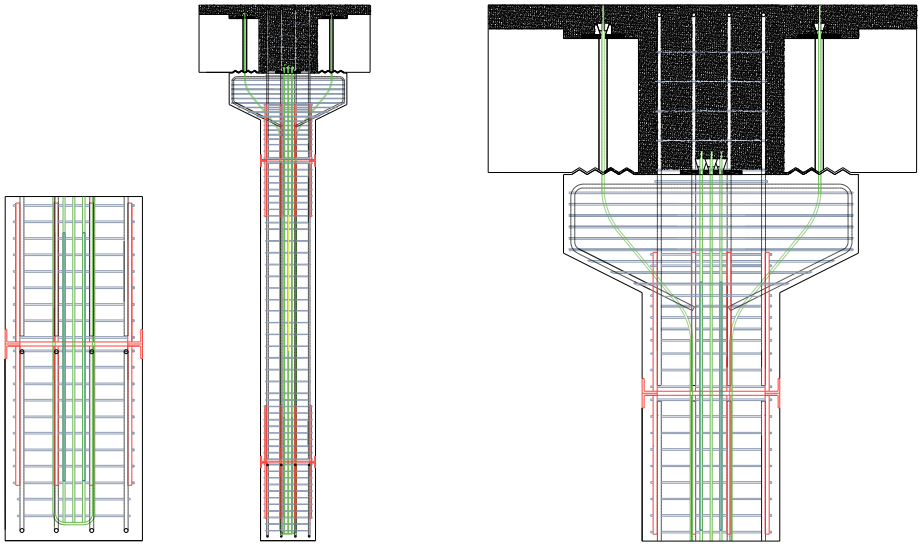

Figure 8.14: Progressive construction

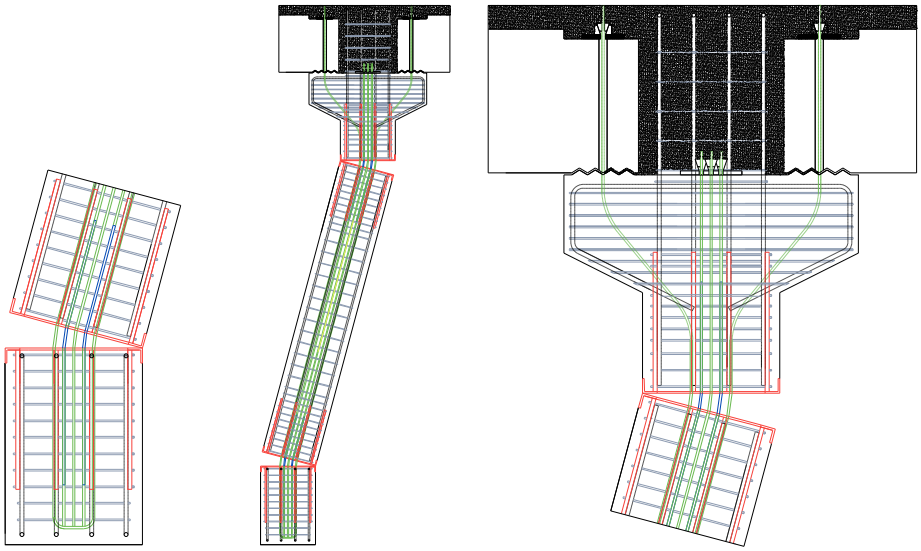

Figure 8.15: Deformed Configuration

Chapter 9

Performances of a *Hybrid* Precast Concrete Industrial Building

Contents

9.1 Introduction

The performance assessment of the Hybrid structure designed in the previous chapter is now presented. Generally, the procedure presents the performances objectives definition for structural and non structural component. More in detail, the performance objectives definition involves a performance level characterization for each earthquake level. The model considered to perform non linear dynamic analysis is after described. The characterization of the design ground motion is considered and the performance assessment by cyclic static analysis is developed.

Finally a Performance Comparison is introduced to highlight the performance of innovative structures.

Table 9.1: Hazard Level as in Vision 2000

Event	Recurrence Interval $[years]$	Probability of exceedence [%] in $[years]$
Frequent	30	50 % in 30 years
Occasional	50	50 % in 50 years
Rare	475	10 % in 50 years
Very rare	975	10 % in 100 years

Table 9.2: Hazard Levels and Performance Levels: Basic, Essential\Hazardous and Safety Critical Objectives

H.L.\ P.L.	Operational	I. Occupancy	Life Safety	Collapse Prev.
Frequent	Basic	Unacceptable	Unacceptable	Unacceptable
Occasional	Ess.\Haz.	Basic	Unacceptable	Unacceptable
Rare	Safety Crit.	Ess.\Haz.	Basic	Unacceptable
Very Rare		Safety Crit.	Ess.\Haz.	Basic

9.2 Performance Objectives and Engineering Damage Indices

In the next the performance objectives will be divided into performance objectives related to structural elements and into performance objectives related to non structural components and contents. Fundamentally, the idea is to increase the *base* performance level, to obtain an *higher* performance level to obtain immediate occupancy even under a moderate/severe earthquake. The industrial building designed is supposed non accommodate particular elements that need a specific limitation on the acceleration. For that reason is not considered any particular restriction on the floor acceleration values. It's considered to guarantee absence of structural damage at structural elements even under a moderate/severe earthquake and this could be identified with the immediate occupancy performance level for a rare hazard level. Therefore for rare hazard level, is not necessary to guarantee the operational performance limit. With reference to the effects noticed after the Emilia earthquake, this limits allow to resolve the main problem observed and inherently the quick recover of the interrupted economic activities. If, the functionality of particular elements is recommended, this must be considered at this moment of the project and the engineering performance indices able to guarantee the operation of elements performance must be here introduced.

9.2.1 Performance Objectives and Hazard Levels

Table [**?**] represent the Hazard level as considered in Vision 2000. In the next table are represent admissible performance for basic structures, for Important Structures and finally for Critical and Safety Structures.

The designed structure will be considered with reference to the next

Table 9.3: Hazard Levels and Performance Levels: Considered Objectives

H.L.\ P.L.	Operational	I. Occupancy	Life Safety	Collapse Prev.
Occasional	Admissible	Unacceptable	Unacceptable	Unacceptable
Rare	Admissible	Admissible	Unacceptable	Unacceptable
Very Rare	Admissible	Admissible	Admissible	Admissible

Table 9.4: Performance and Engineering damage indices Levels for concrete structural elements

Strain\P.L.	Operational	I. Occupancy	Life Safety	Collapse Prev.
Concrete	C1	CII	CIII	CIV
Rebars	S1	SI	SIII	Unacceptable
Dissipators		Admissible	Admissible	Admissible

9.2.2 Performance Objectives and Engineering Damage indices: Structural Elements

The Performance objectives related to structural elements is to avoid completely the damage to this elements. Damage and develop of plasticity must be avoid in all the structural elements with the exception of the energy dissipation devices. The better way to characterize damage, for structural concrete elements is to monitored the deformations. So the engineering damage indices used to characterize damage to concrete structural elements will be the strain in the concrete and the strain in the reinforcing bars and in the metallic axial dissipators.

Table 9.5: Hazard and Engineering Damage Indices Levels for concrete structural elements

Strain\Recurrence Interval	30	50	475	975
Concrete	C1	CII	CIII	CIV
Rebars	S1	SI	SIII	SIV
Dissipators	SIII		Admissible	Admissible

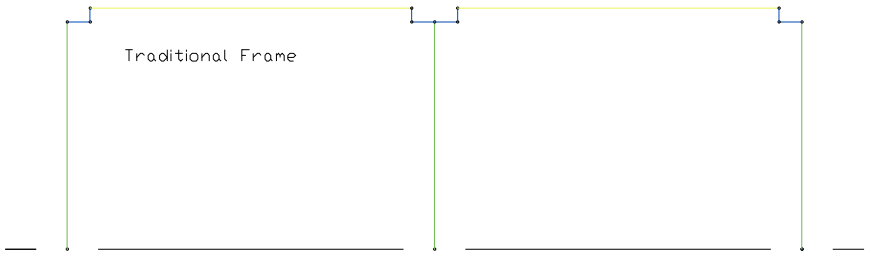

Figure 9.1: Traditional frame, model

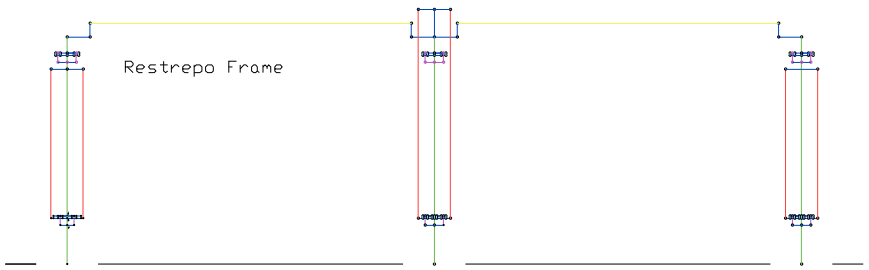

Figure 9.2: Hybrid frame, model

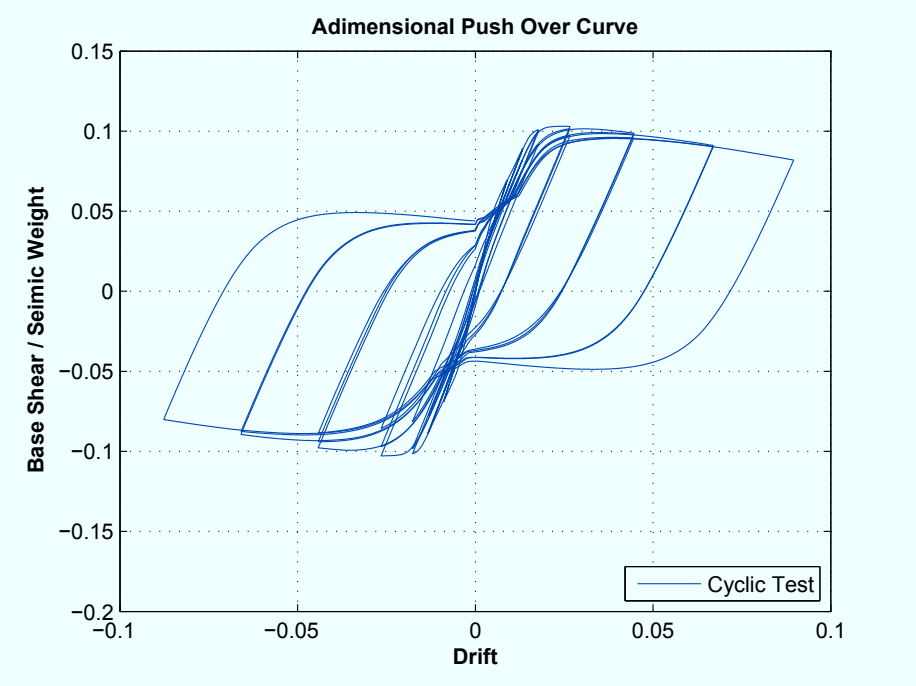

Figure 9.3: Traditional frame, model

9.3 Performance Evaluation

The Performance evaluation is done by cyclic static analysis. In particular is considered the global behavior and the strain tension relation in fibers with maximum demand. For the innovative system is considered the strain stress relation in both dissipators and post-tensioned strands. The comparison shown that in the innovative system the demand in strain is remarkable reduced. Both the traditional and the innovative systems have been modeled with OpenSees a FEM software.

Figure 9.4: Traditional frame, model

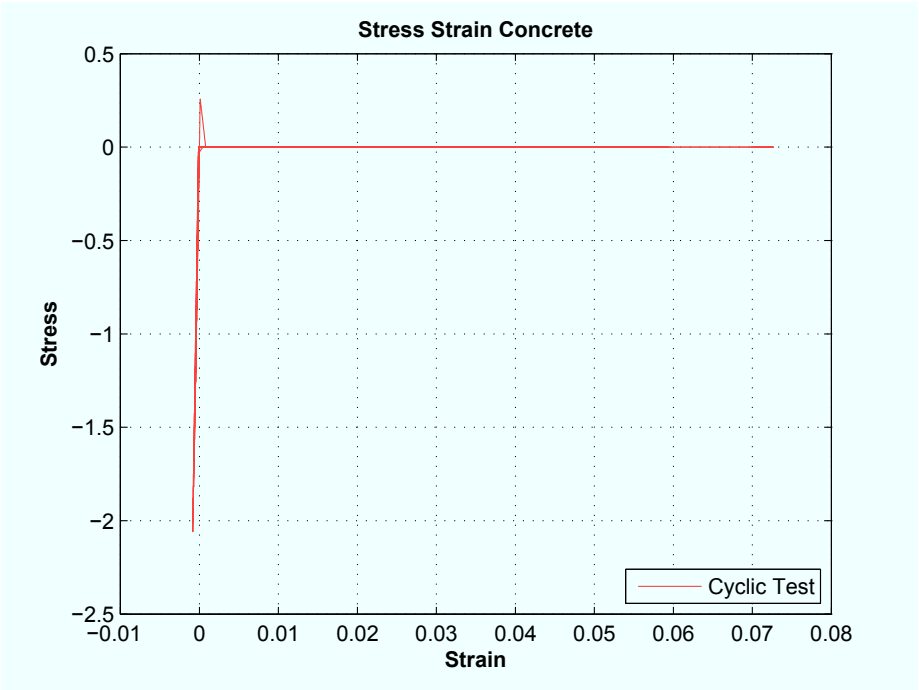

Figure 9.5: Traditional frame, model

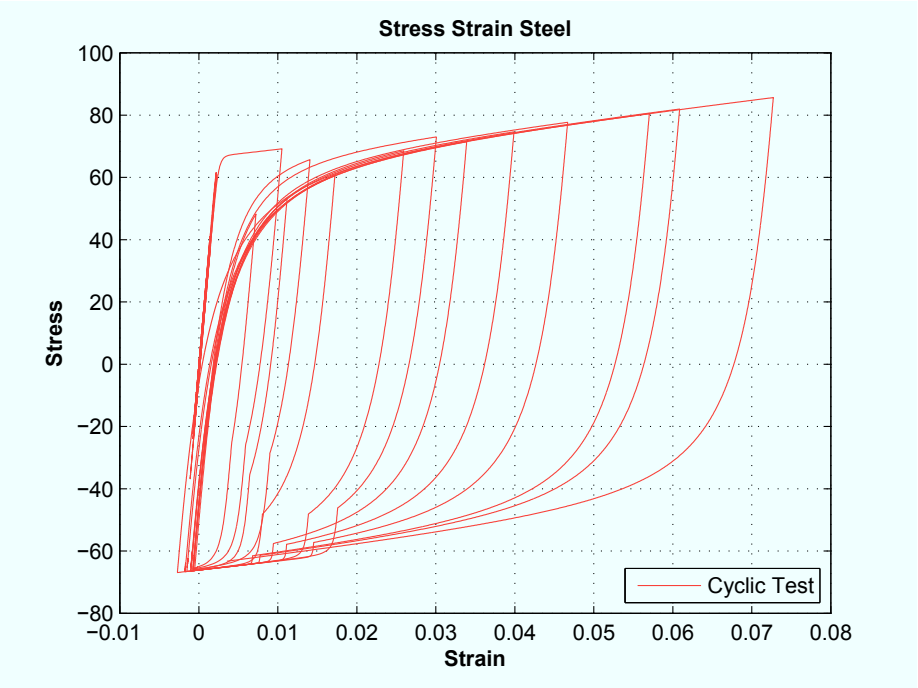

Figure 9.6: Traditional frame, model

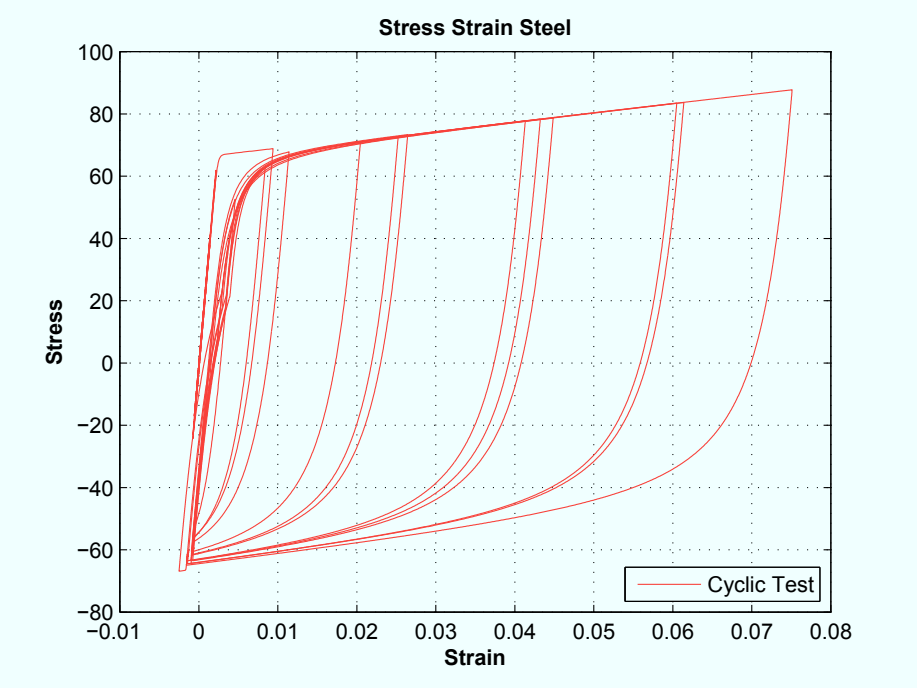

Figure 9.7: Traditional frame, model

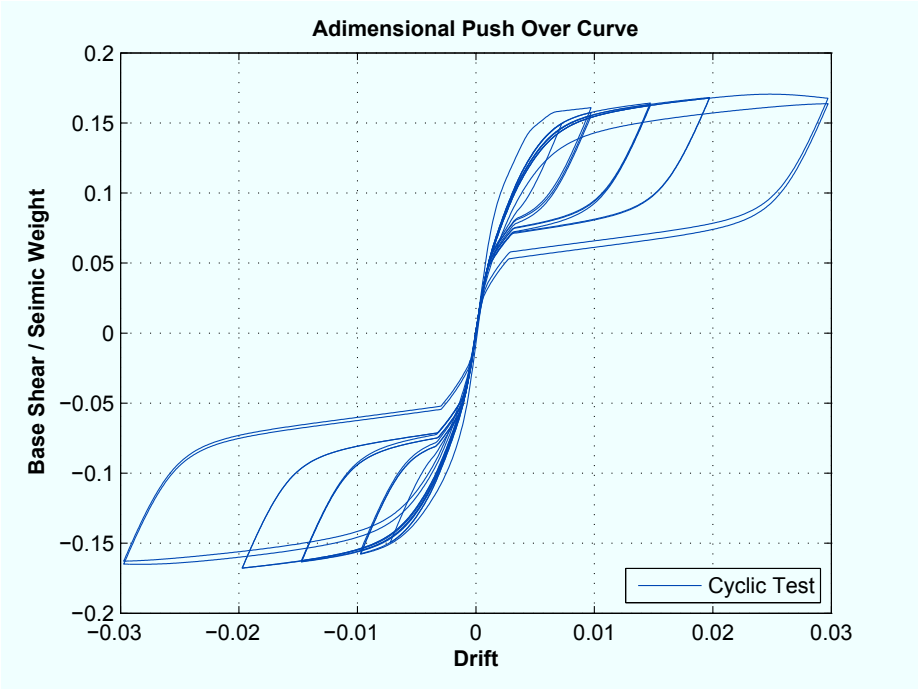

Figure 9.8: Innovative frame, model

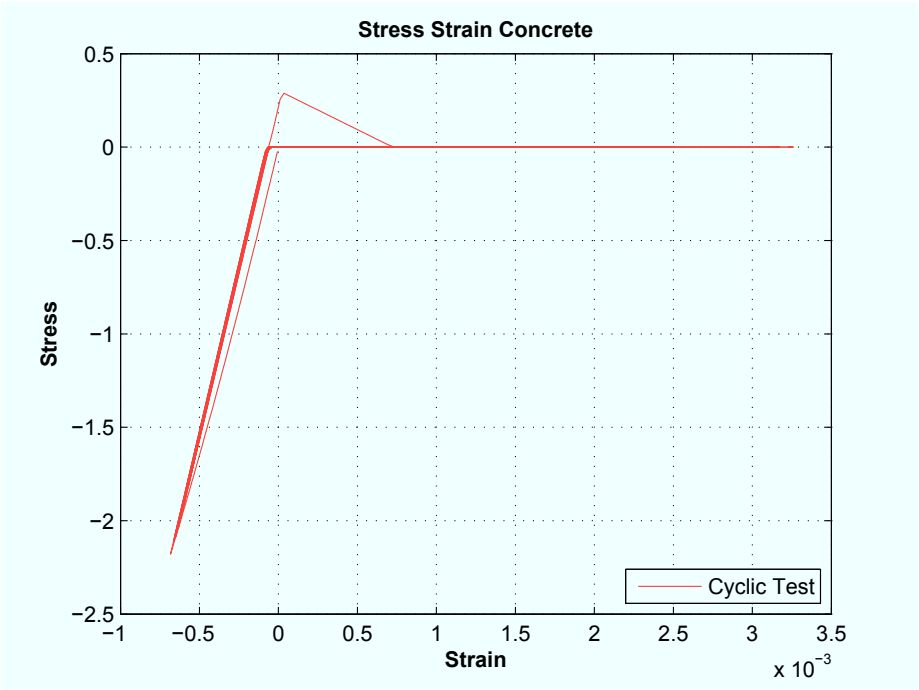

Figure 9.9: Innovative frame, model

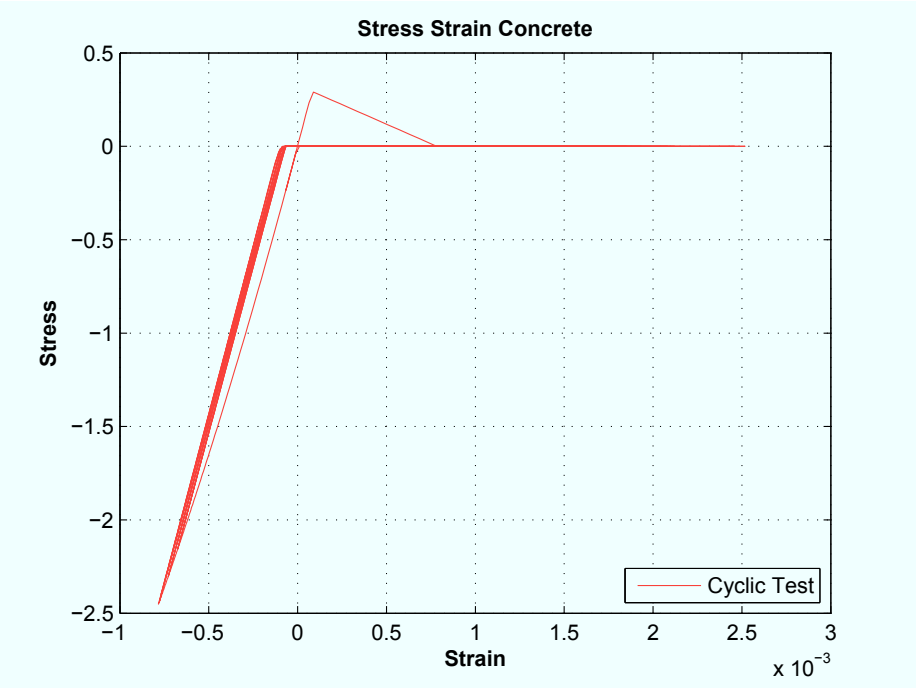

Figure 9.10: Innovative frame, model

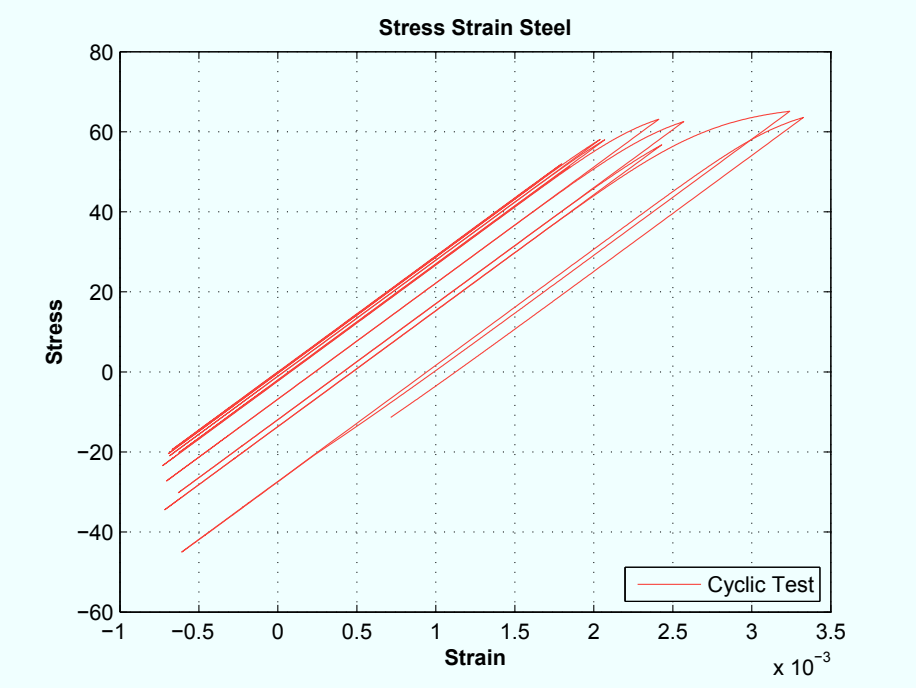

Figure 9.11: Innovative frame, model

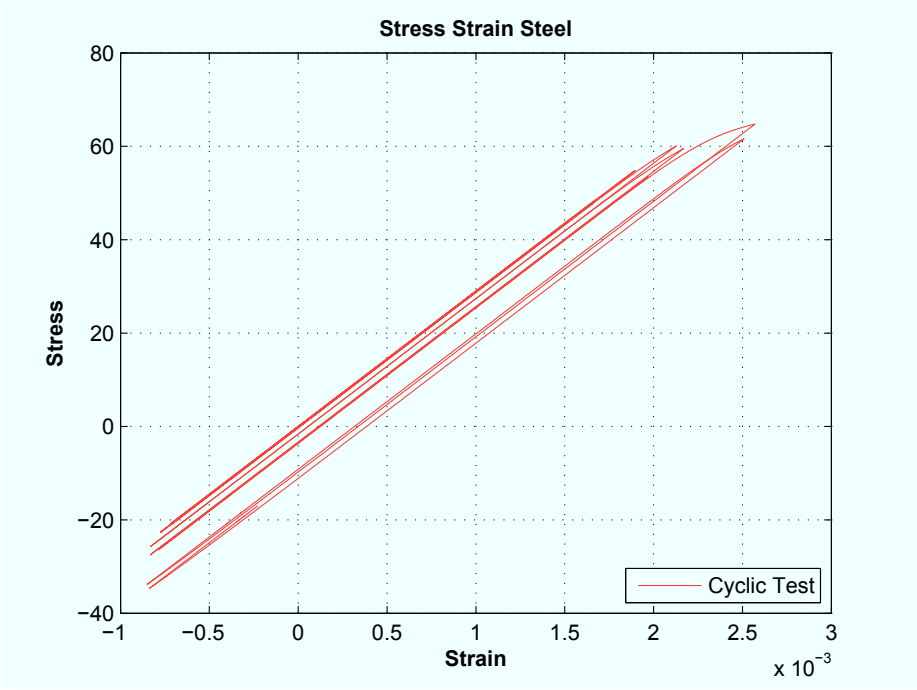

Figure 9.12: Innovative frame, model

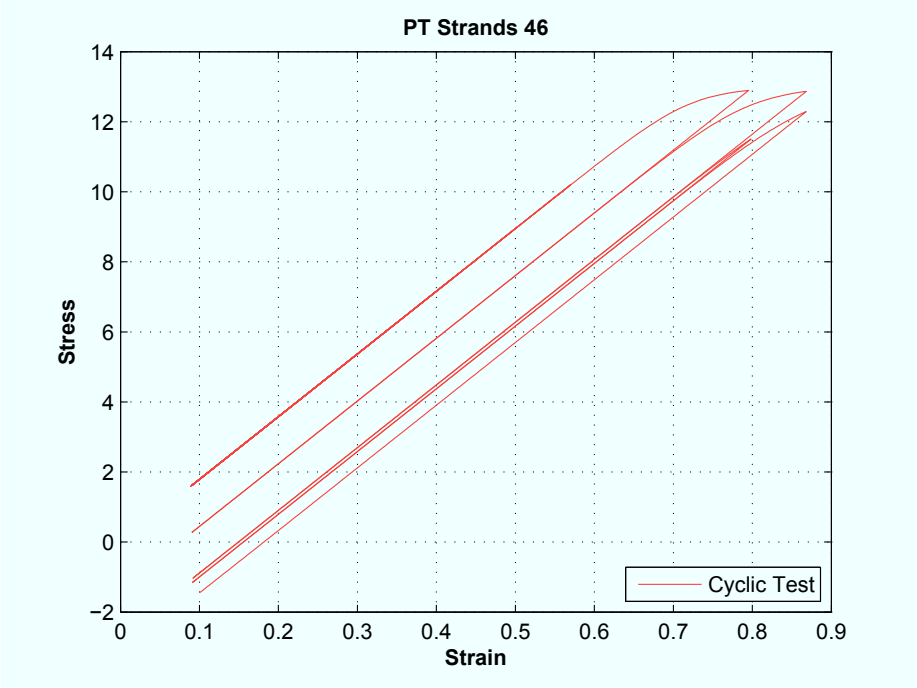

Figure 9.13: Innovative frame, model

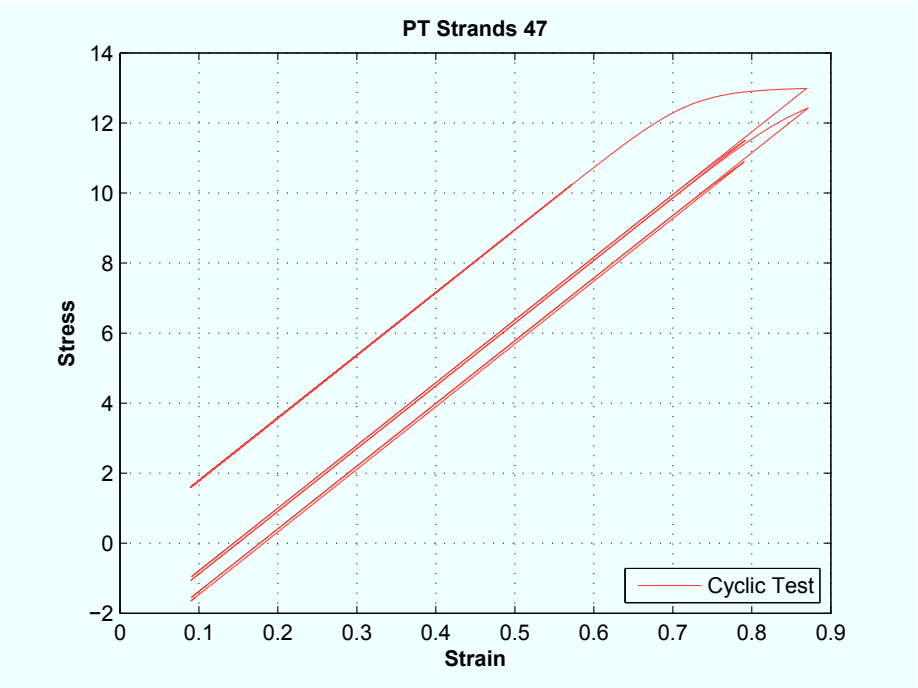

Figure 9.14: Innovative frame, model

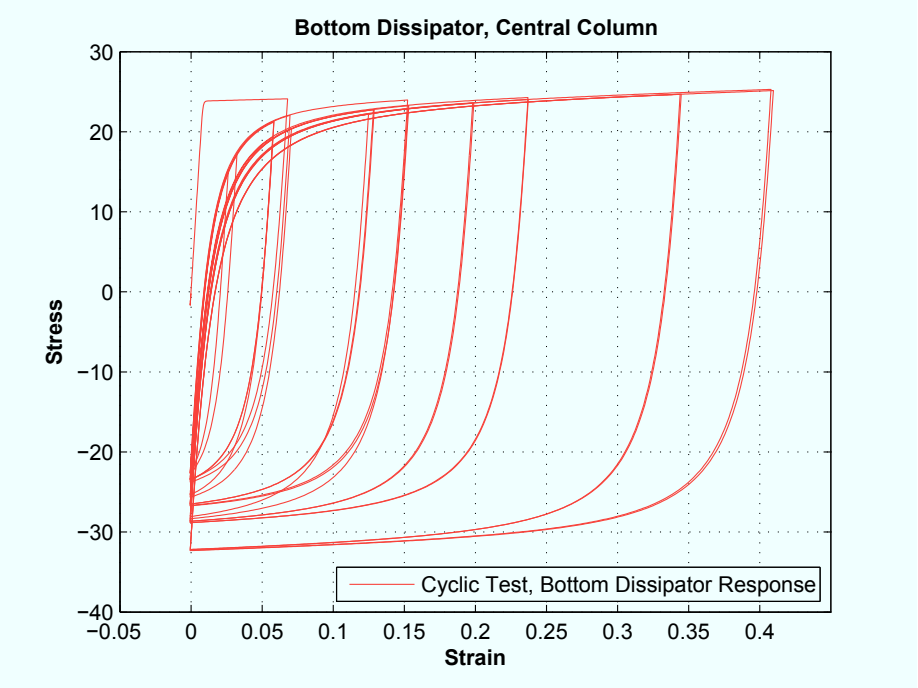

Figure 9.15: Innovative frame, model

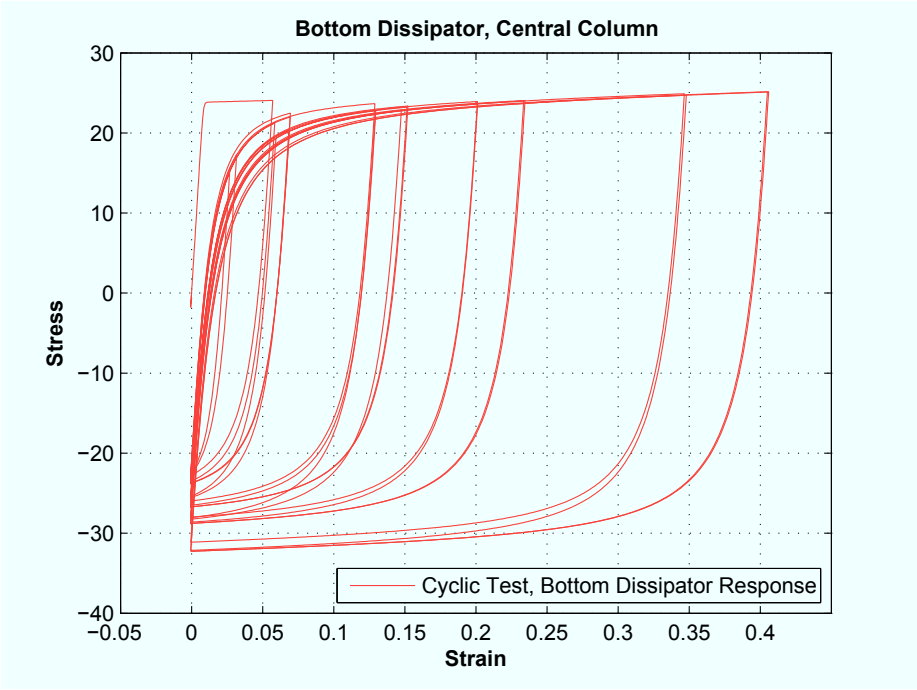

Figure 9.16: Innovative frame, model

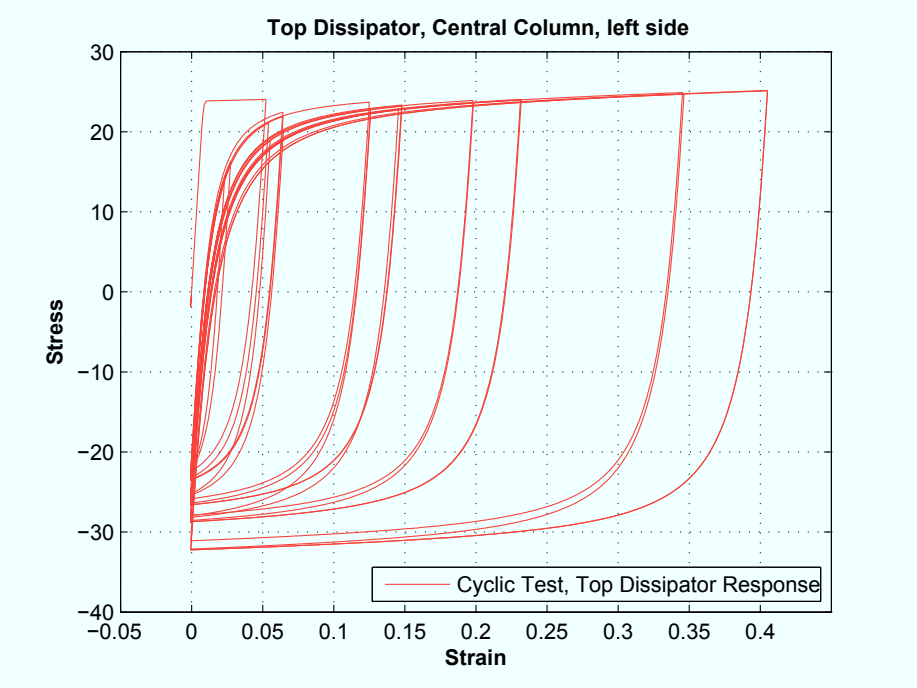

Figure 9.17: Innovative frame, model

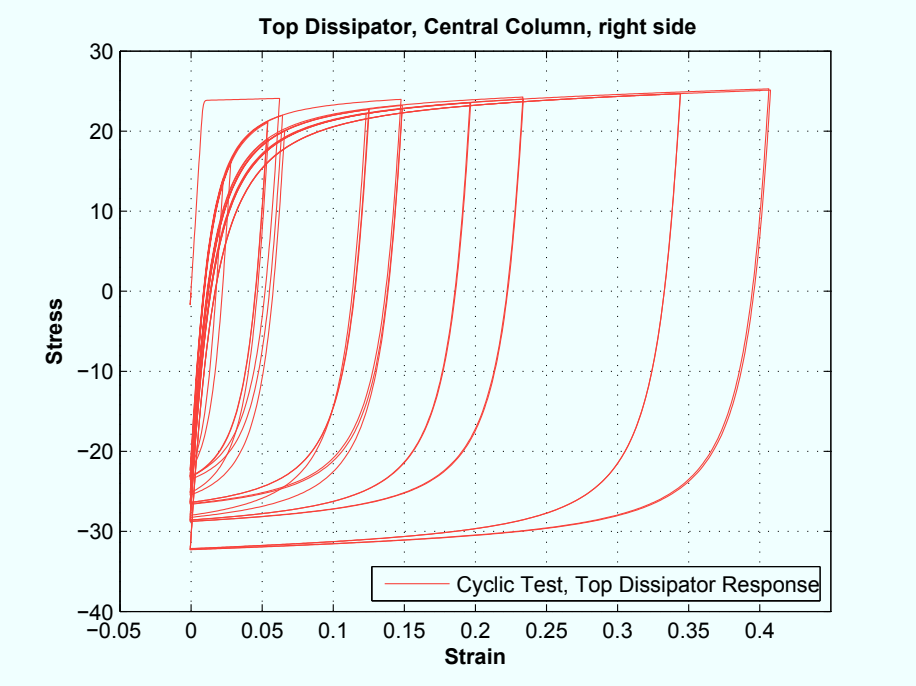

Figure 9.18: Innovative frame, model

9.4 Performance Comparison

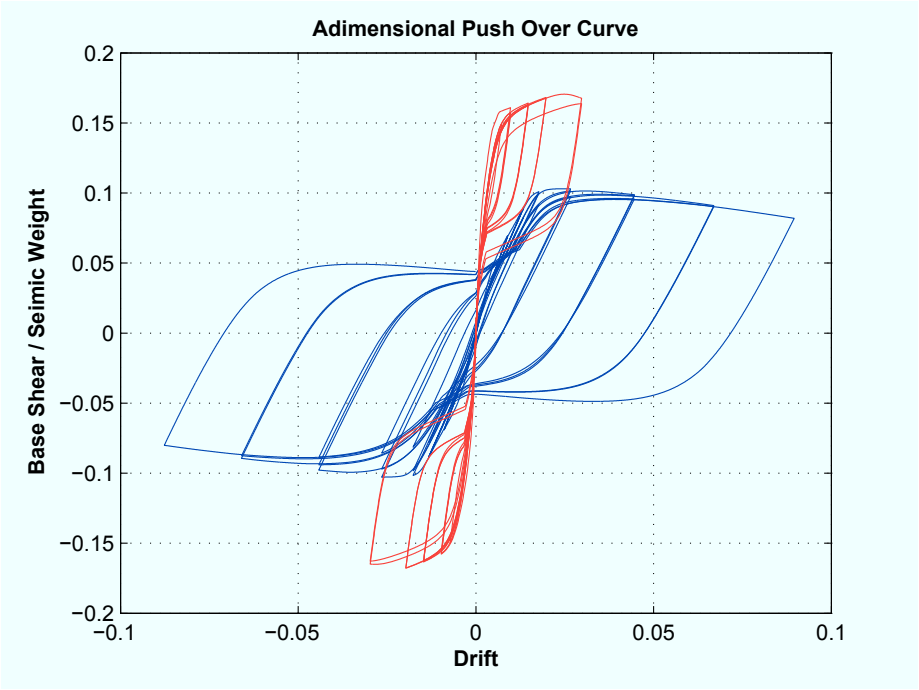

Figure 9.19: Performance Comparison

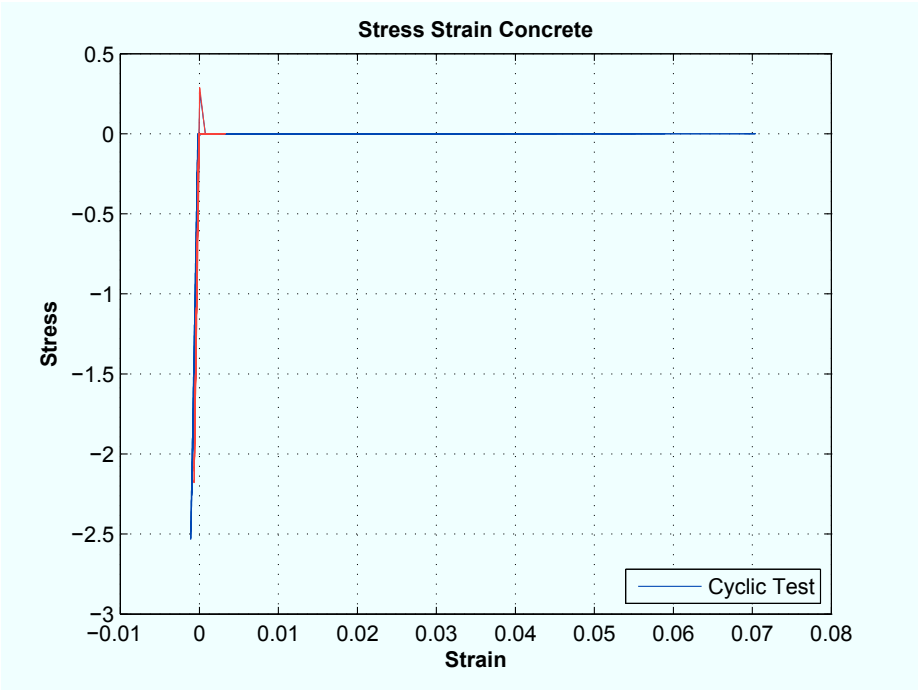

Figure 9.20: Performance Comparison

Figure 9.21: Performance Comparison

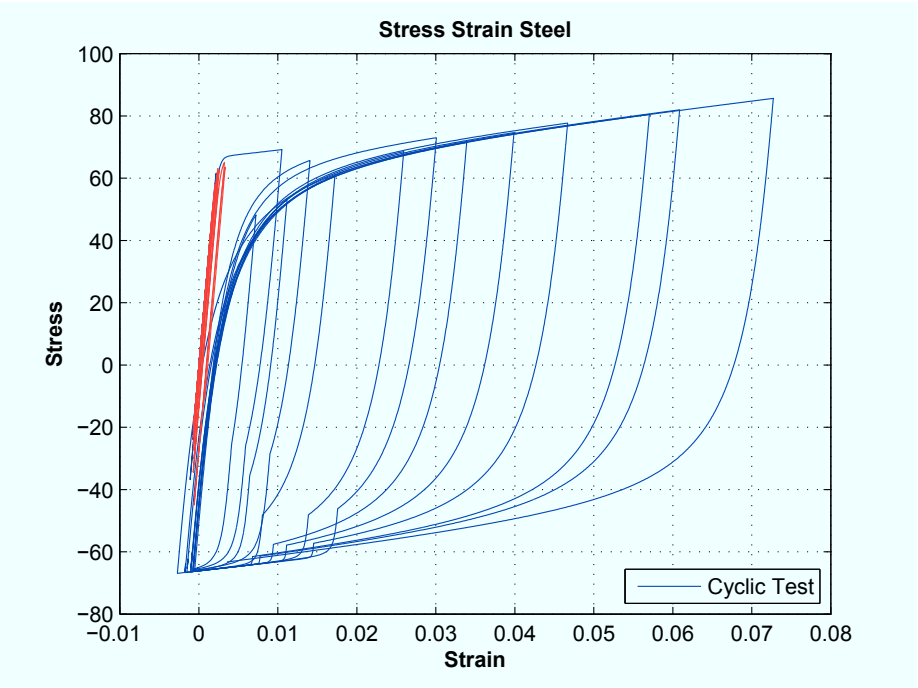

Figure 9.22: Performance Comparison

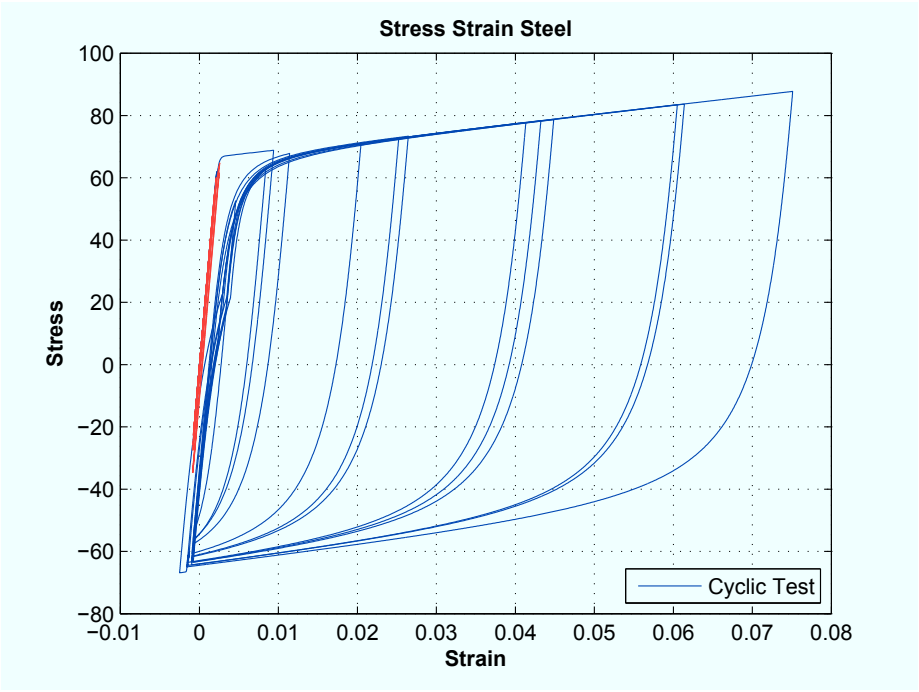

Figure 9.23: Performance Comparison

Appendix A

Dual Shell Columns: Drawings.

Detailed drawings of the tested specimens are here provided, based on the design by Gabriele Guerrini, Graduate Student Researcher, Department of Structural Engineering, University of California, San Diego.

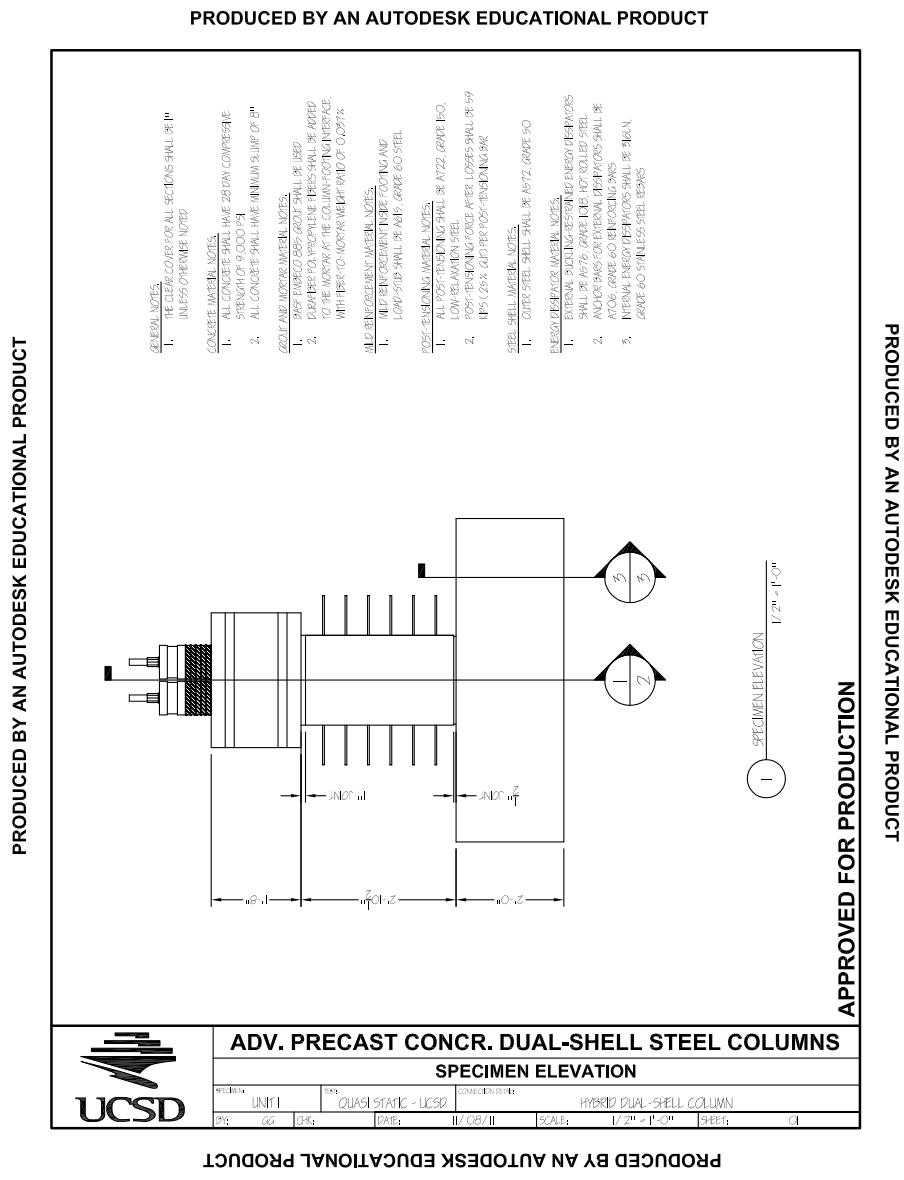

Figure A.1: Precast concrete one story industrial building

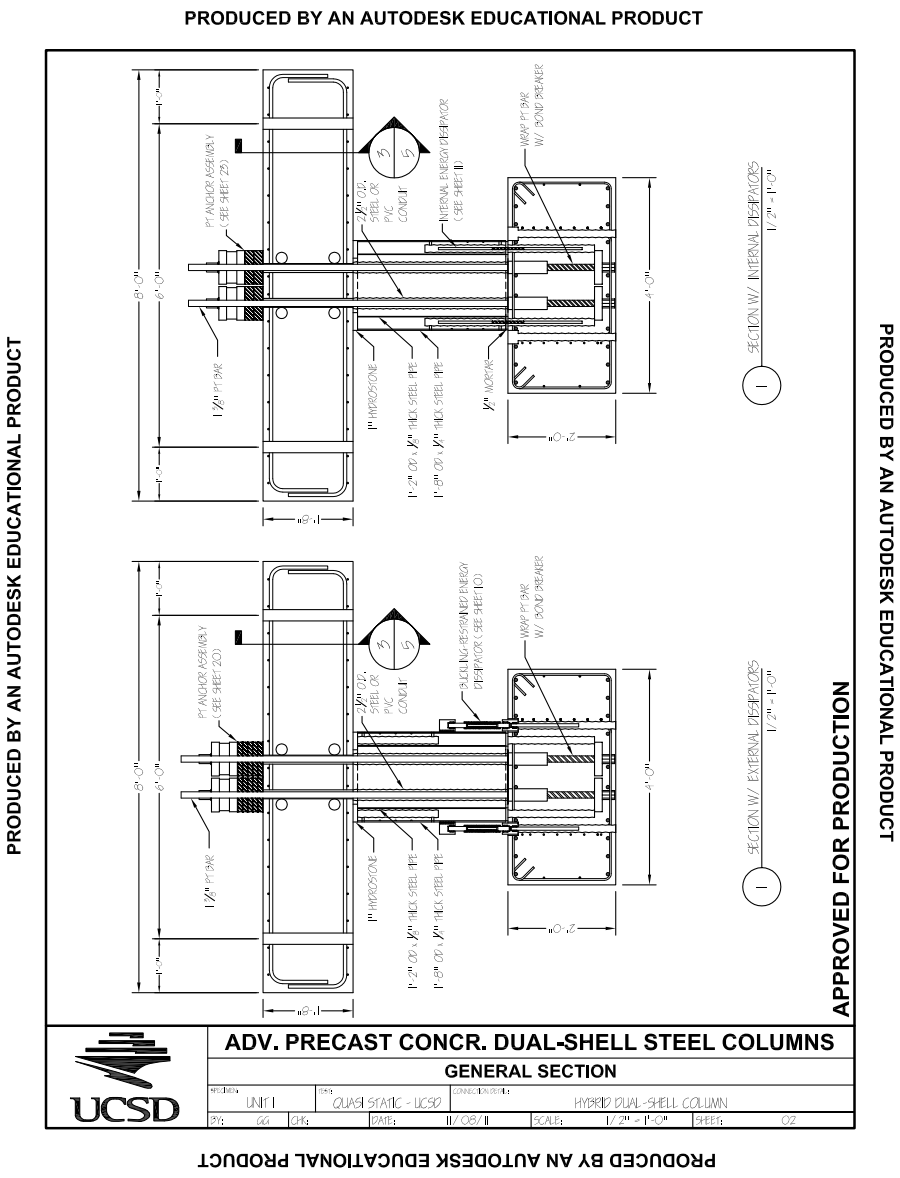

Figure A.2: Precast concrete one story industrial building

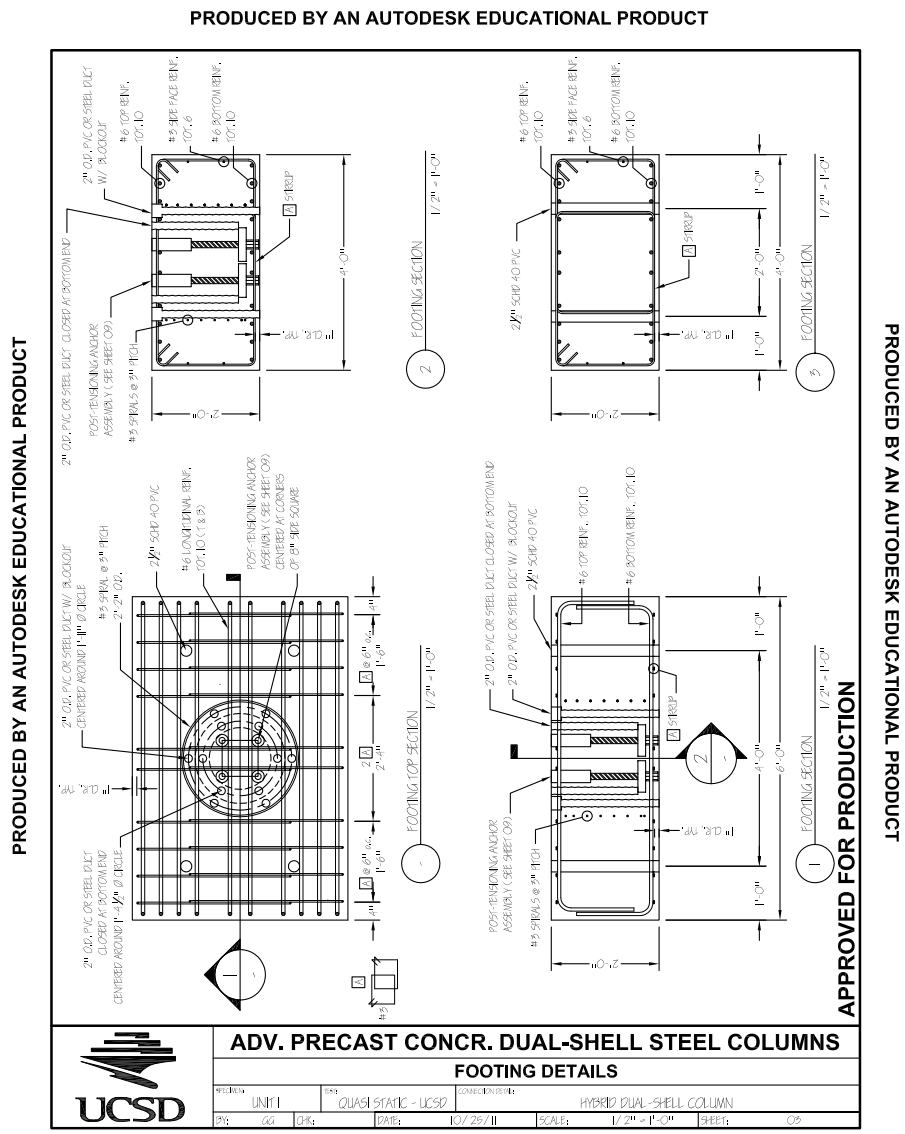

Figure A.3: Precast concrete one story industrial building

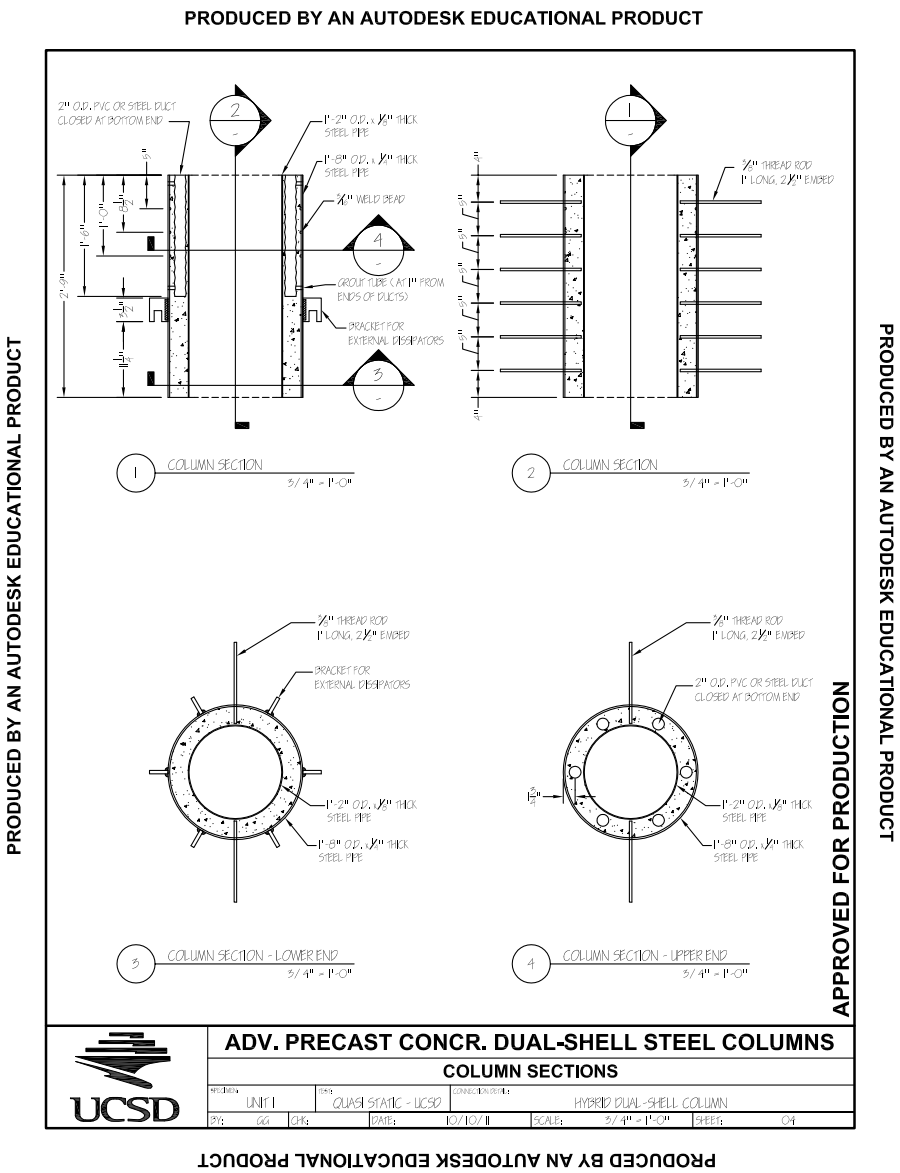

Figure A.4: Precast concrete one story industrial building

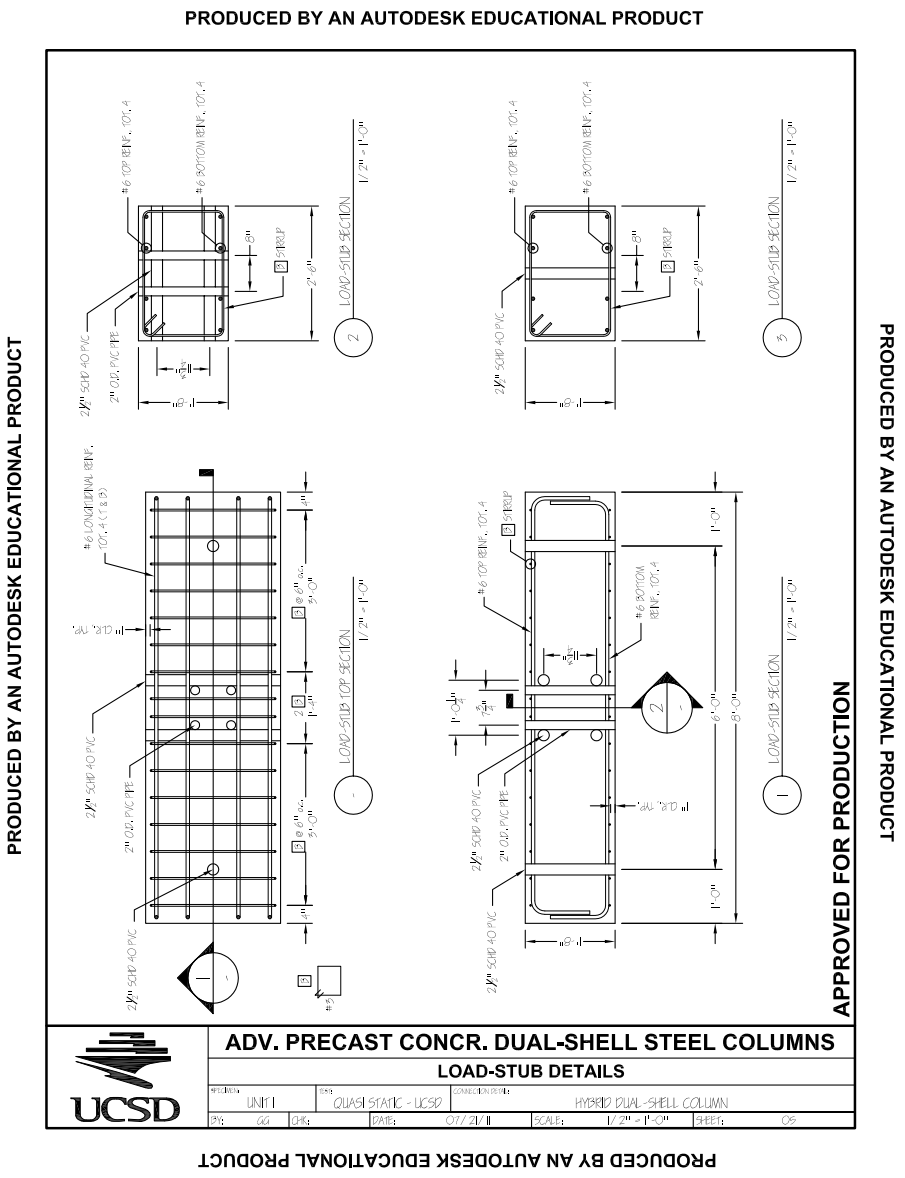

Figure A.5: Precast concrete one story industrial building

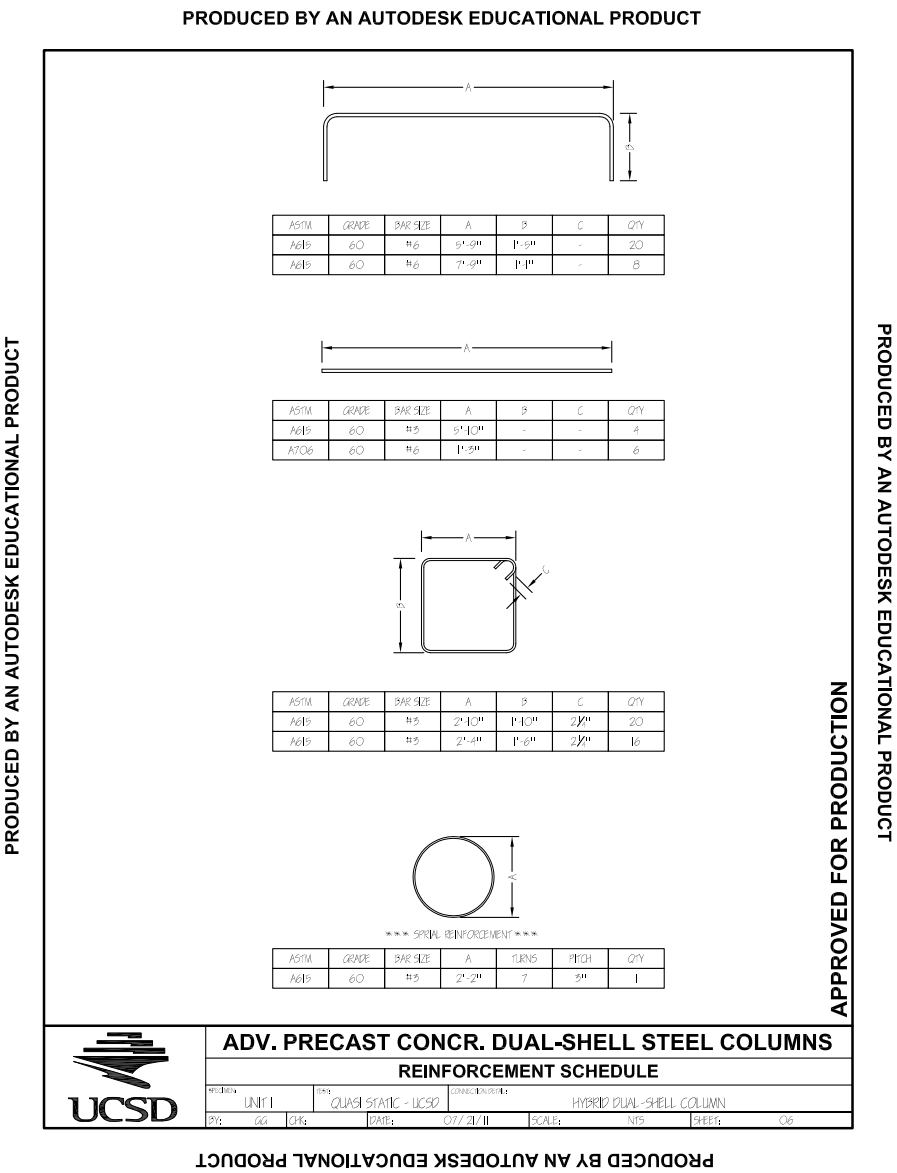

Figure A.6: Precast concrete one story industrial building

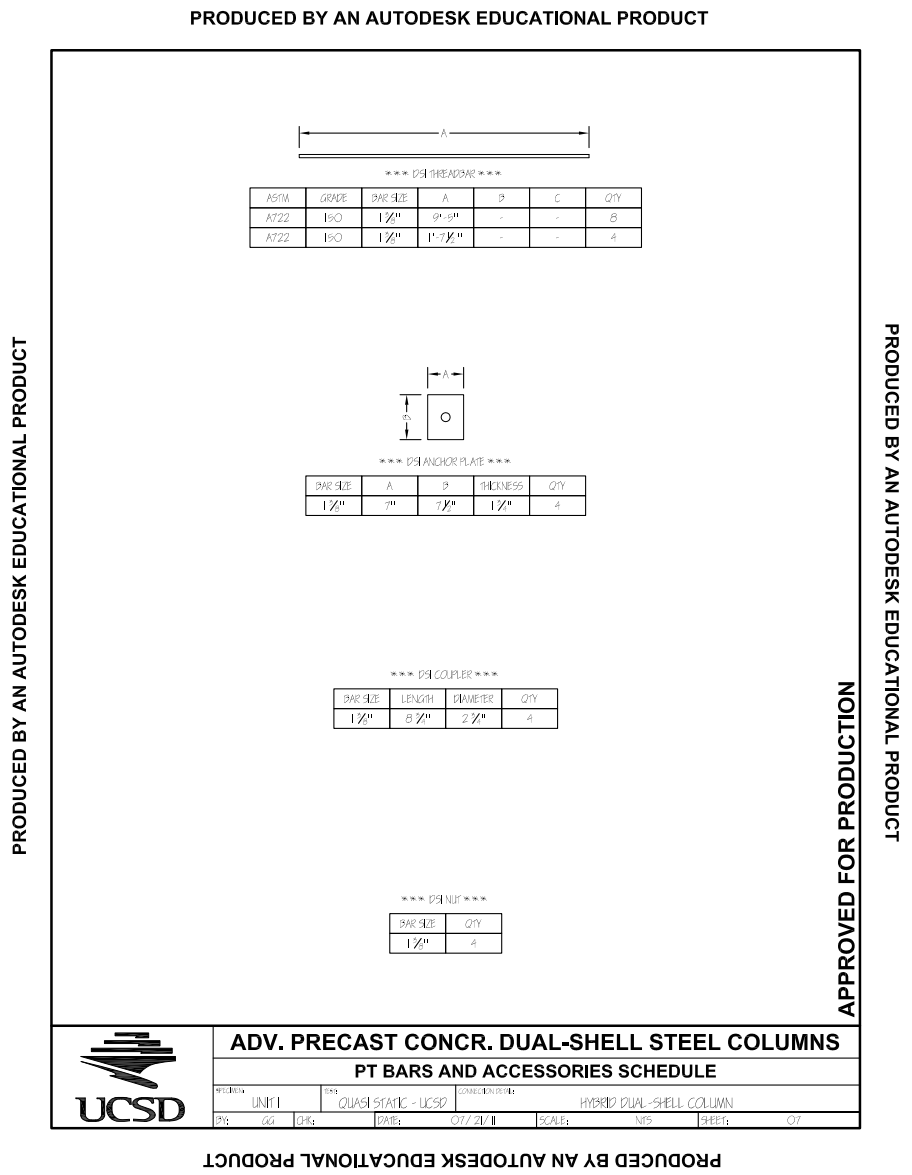

Figure A.7: Precast concrete one story industrial building

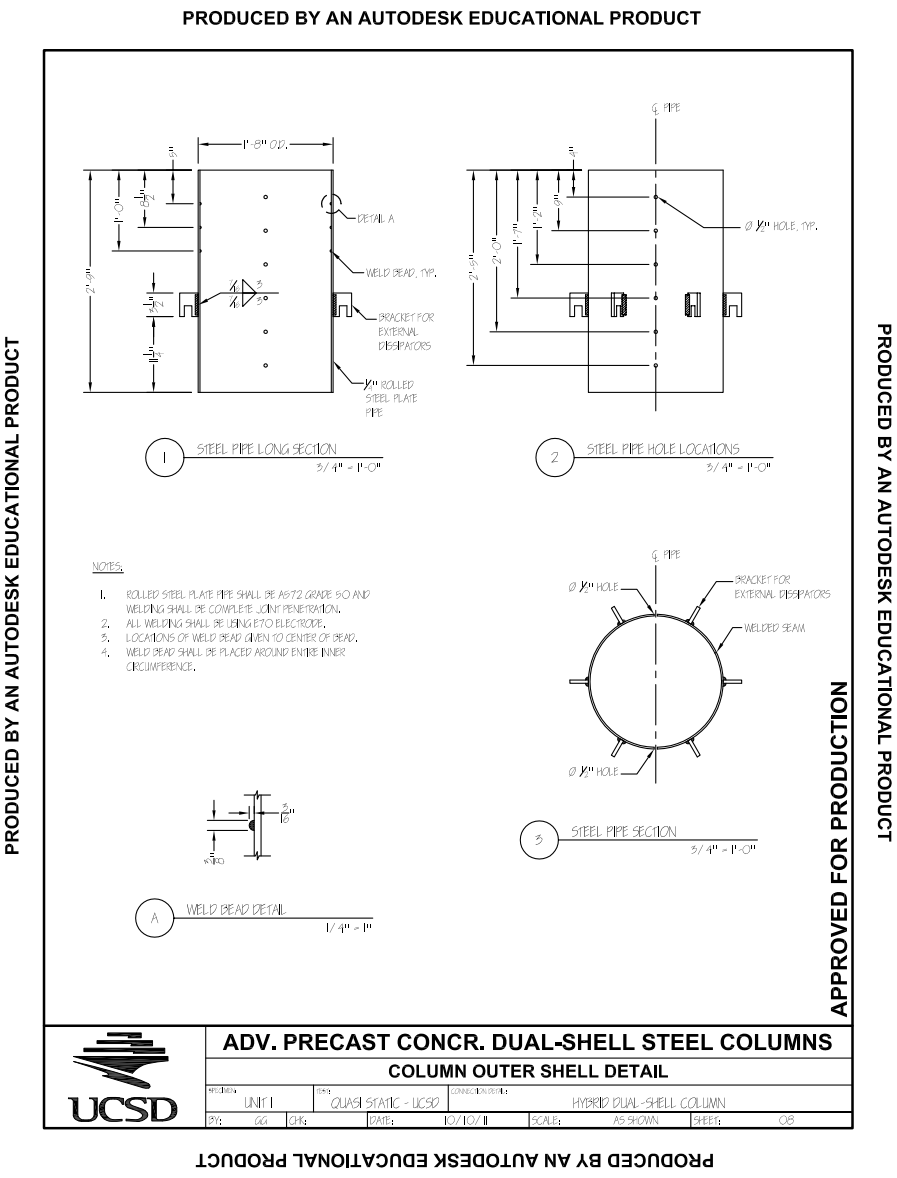

Figure A.8: Precast concrete one story industrial building

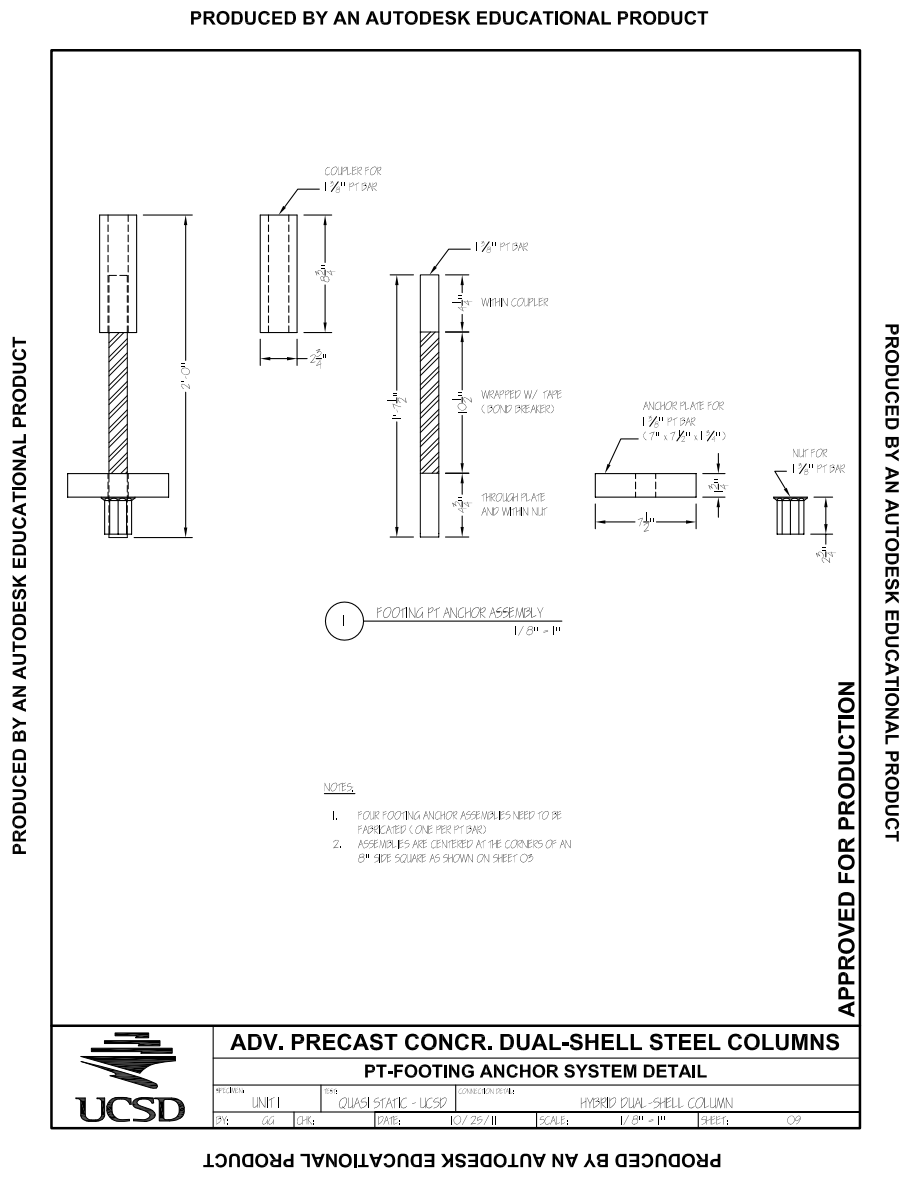

Figure A.9: Precast concrete one story industrial building

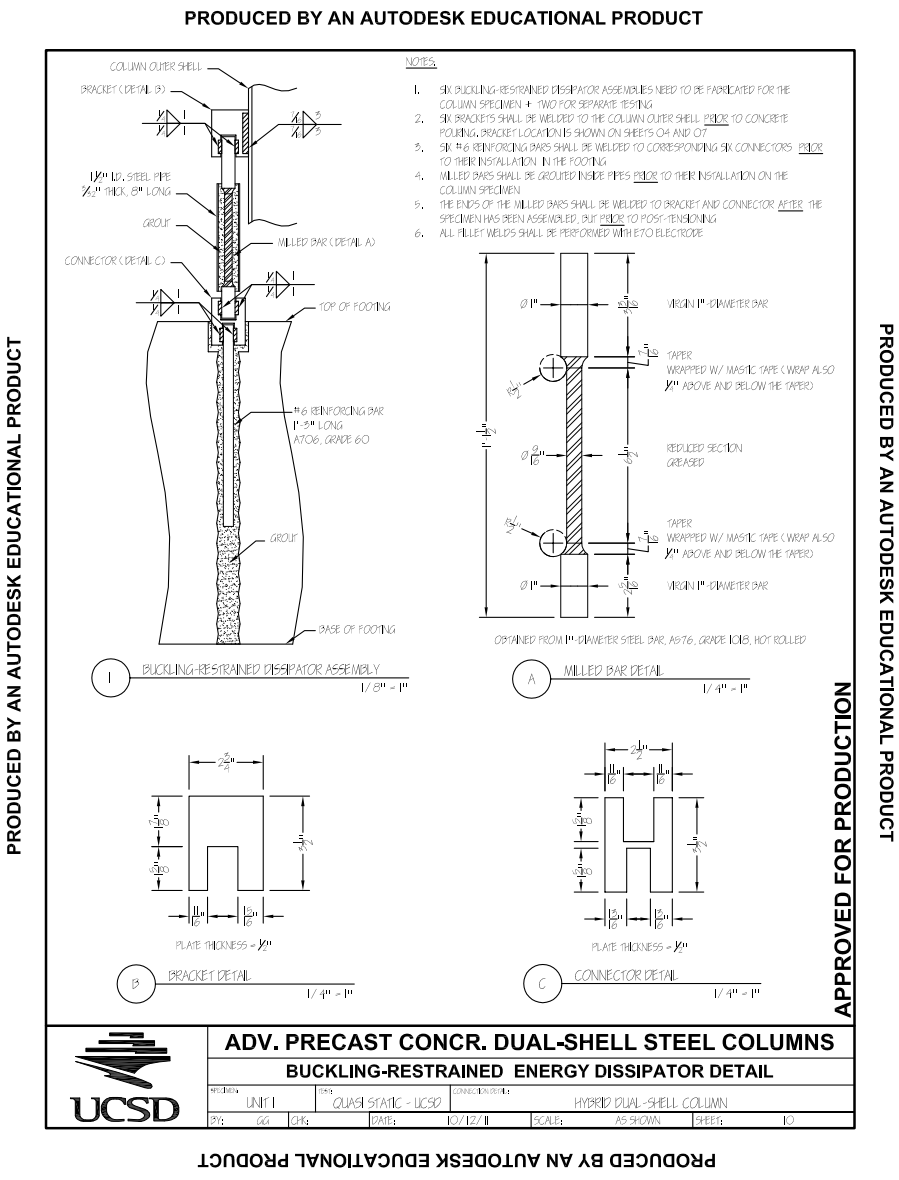

Figure A.10: Precast concrete one story industrial building

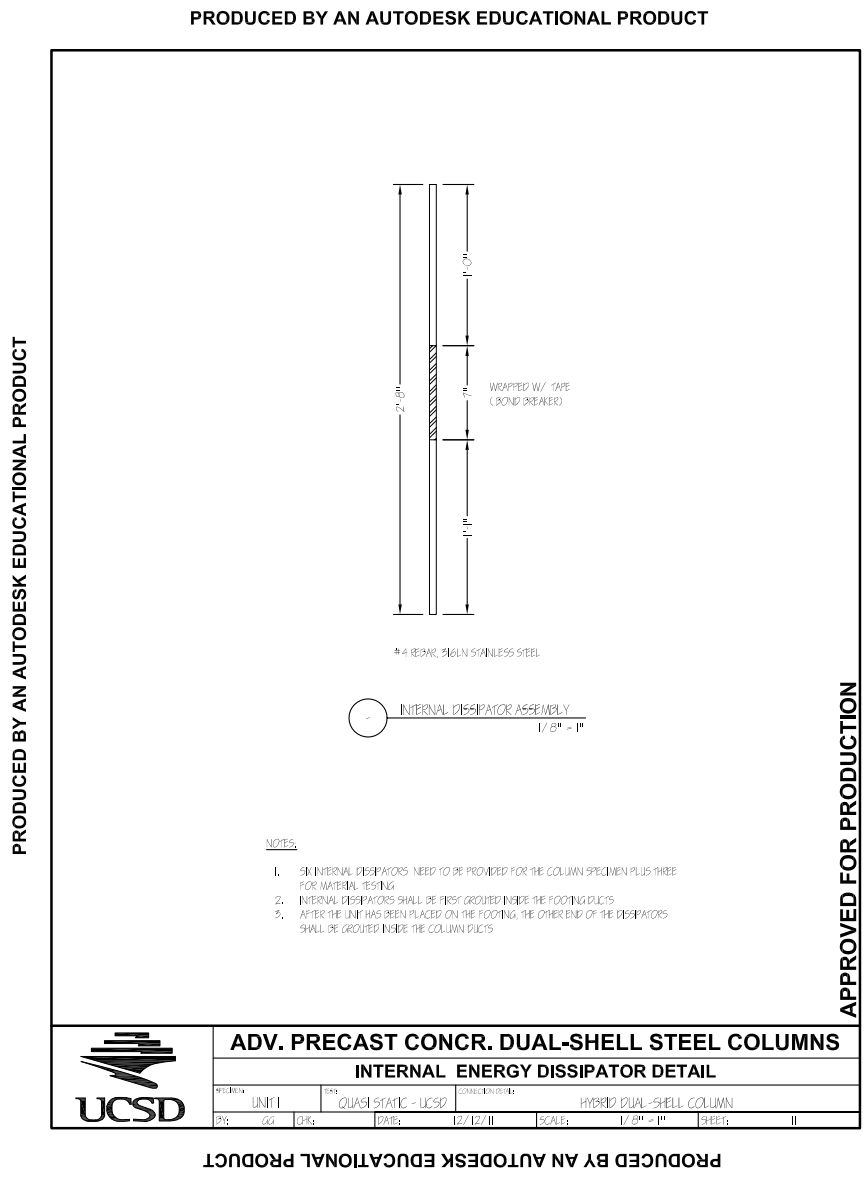

Figure A.11: Precast concrete one story industrial building

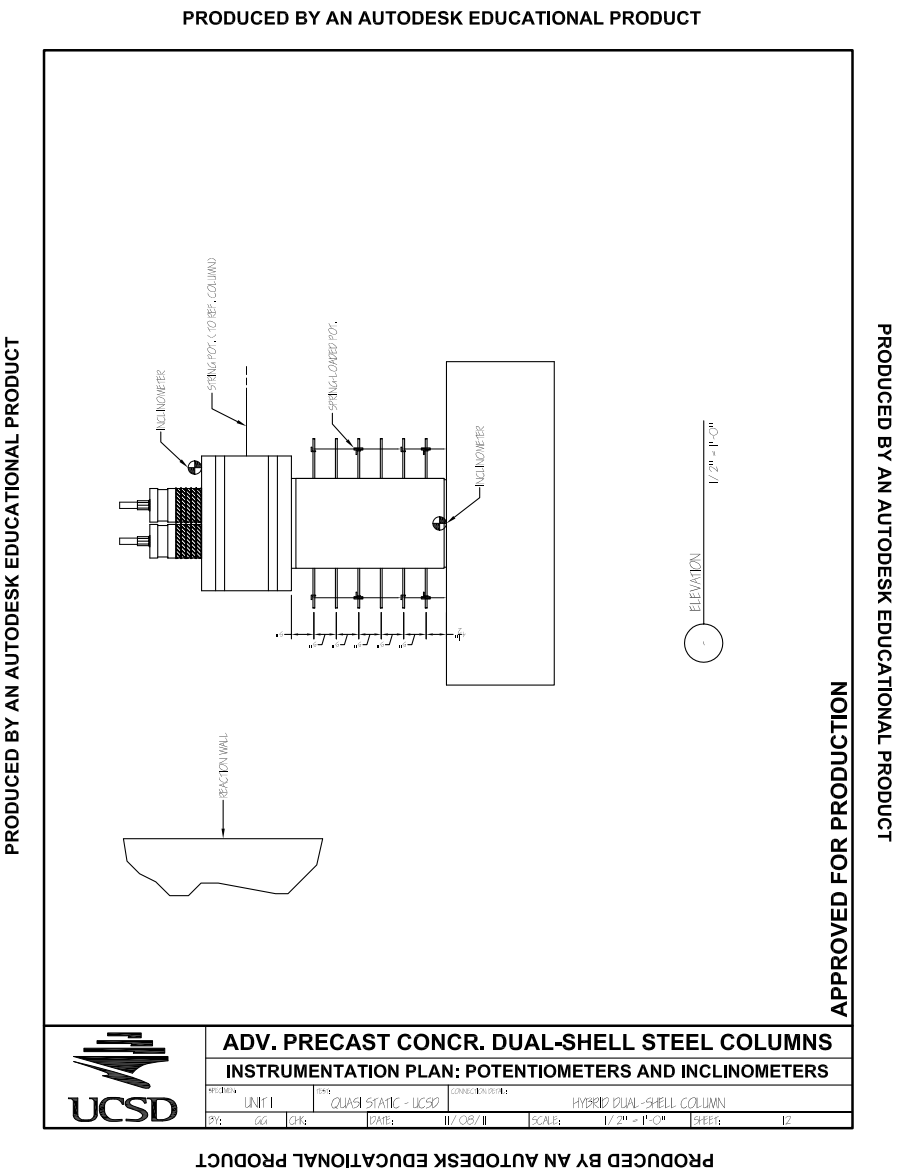

Figure A.12: Precast concrete one story industrial building

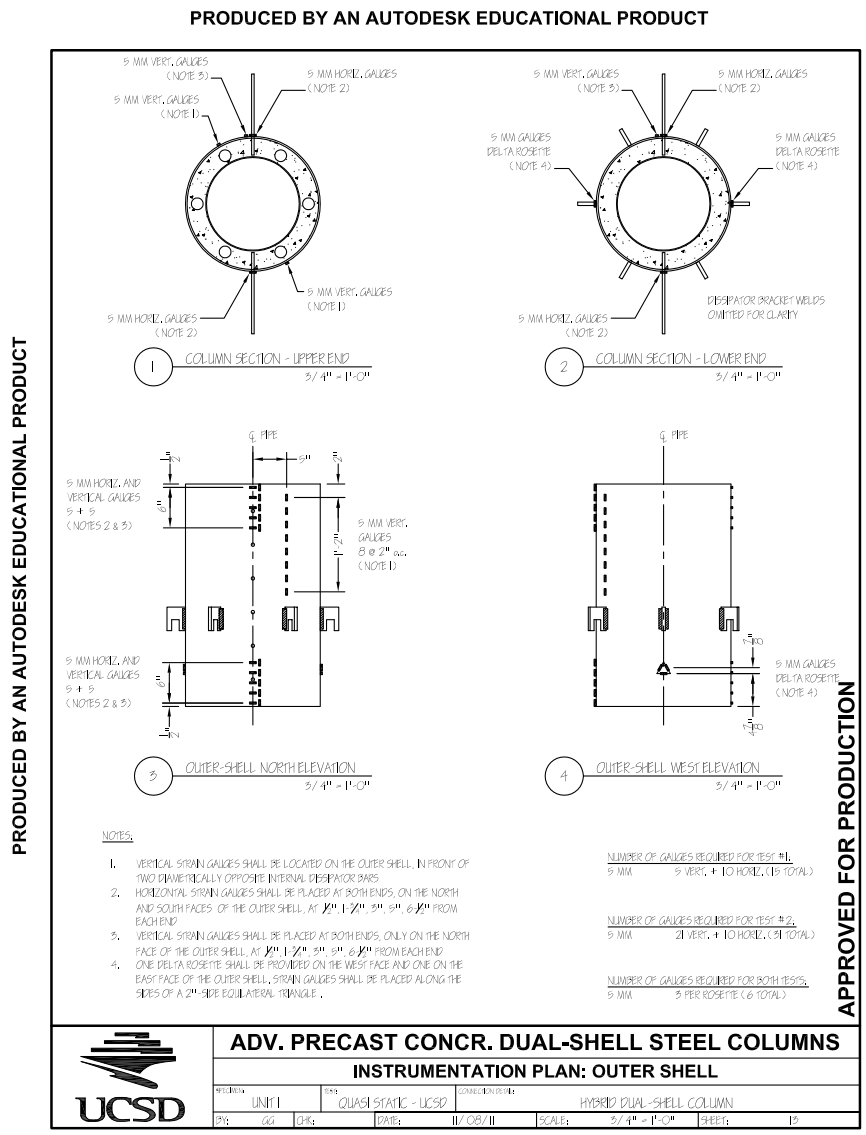

Figure A.13: Precast concrete one story industrial building

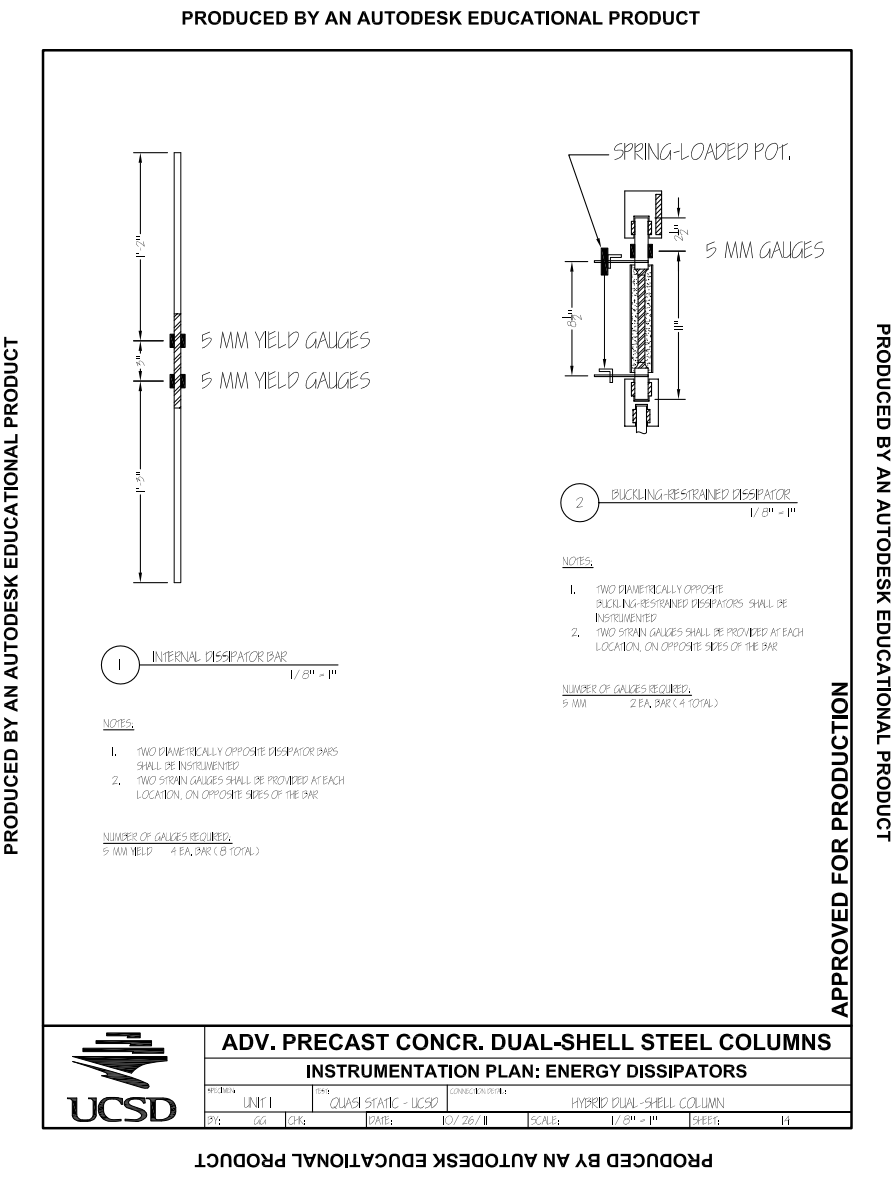

Figure A.14: Precast concrete one story industrial building

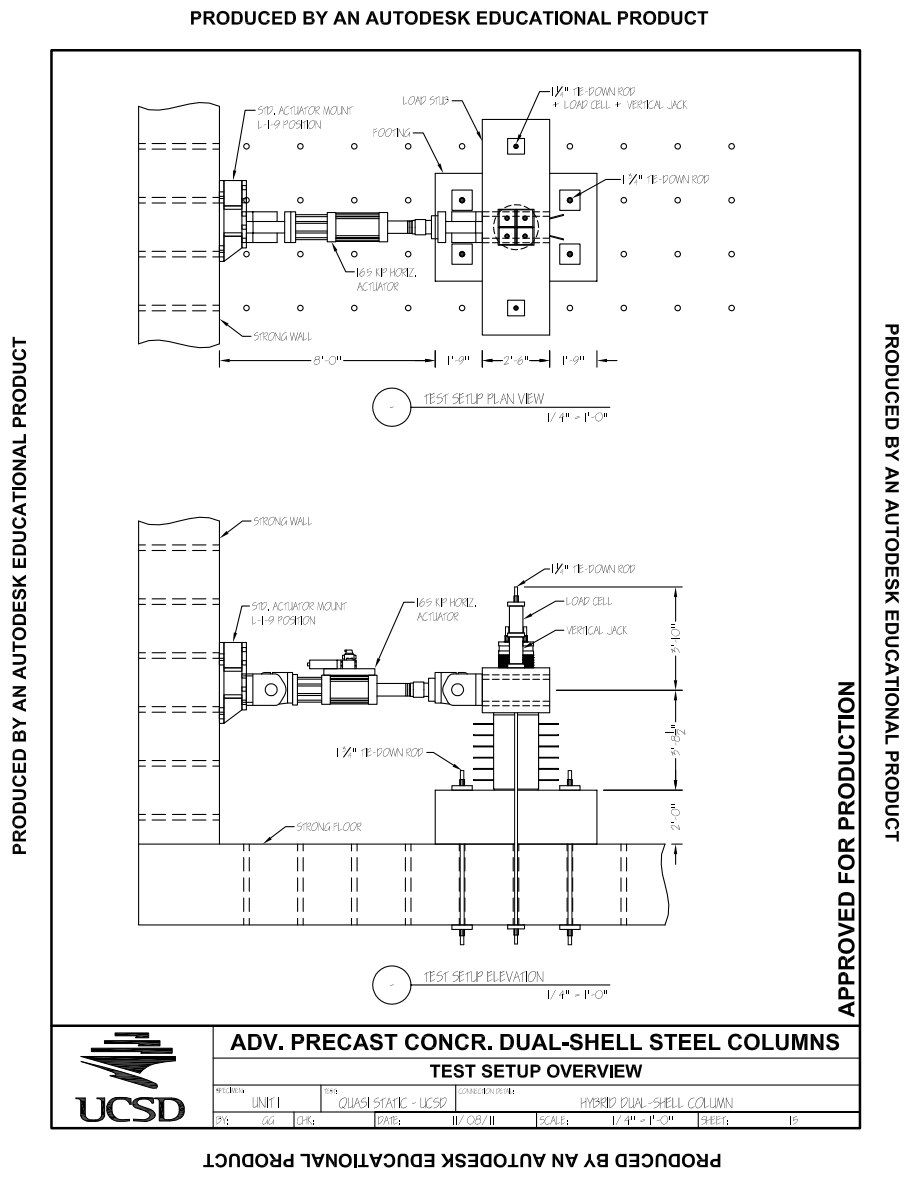

Figure A.15: Precast concrete one story industrial building

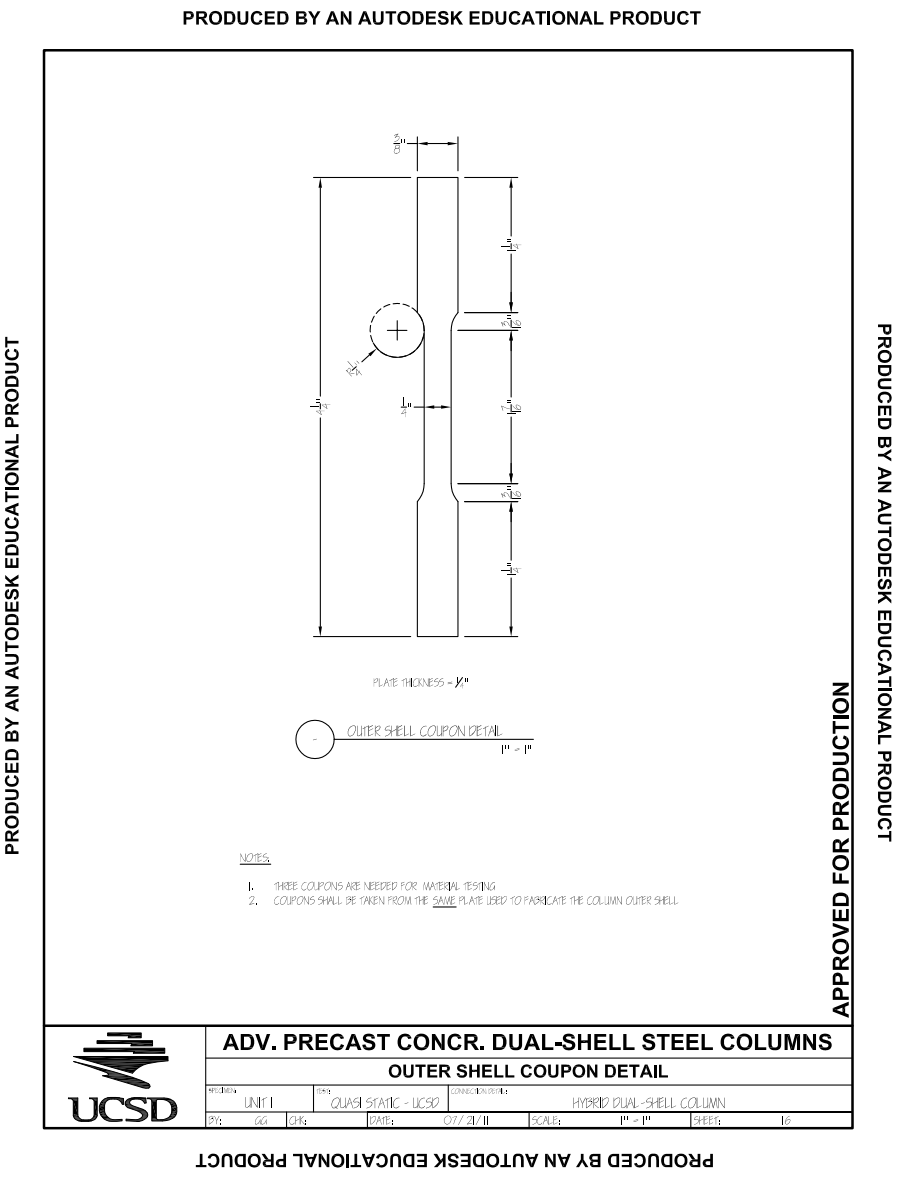

Figure A.16: Precast concrete one story industrial building

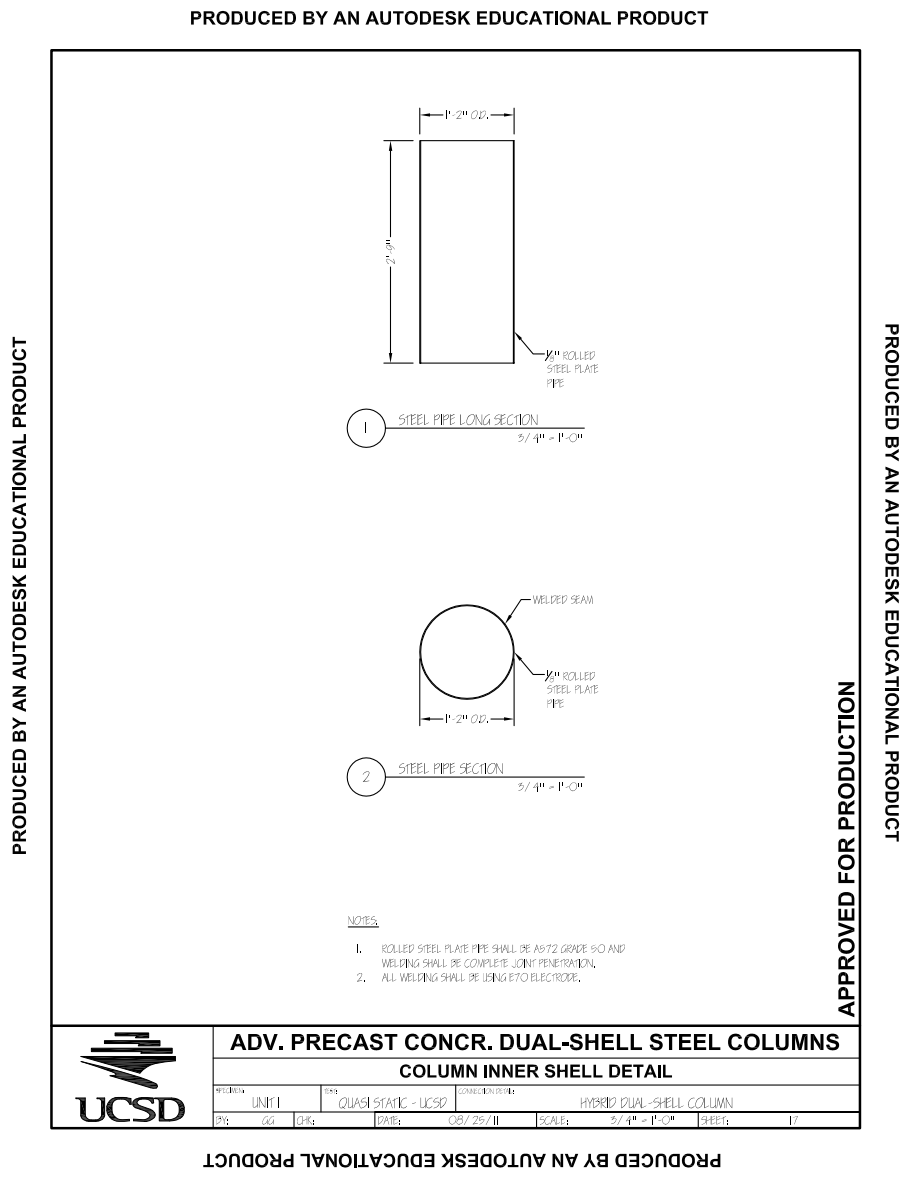

Figure A.17: Precast concrete one story industrial building

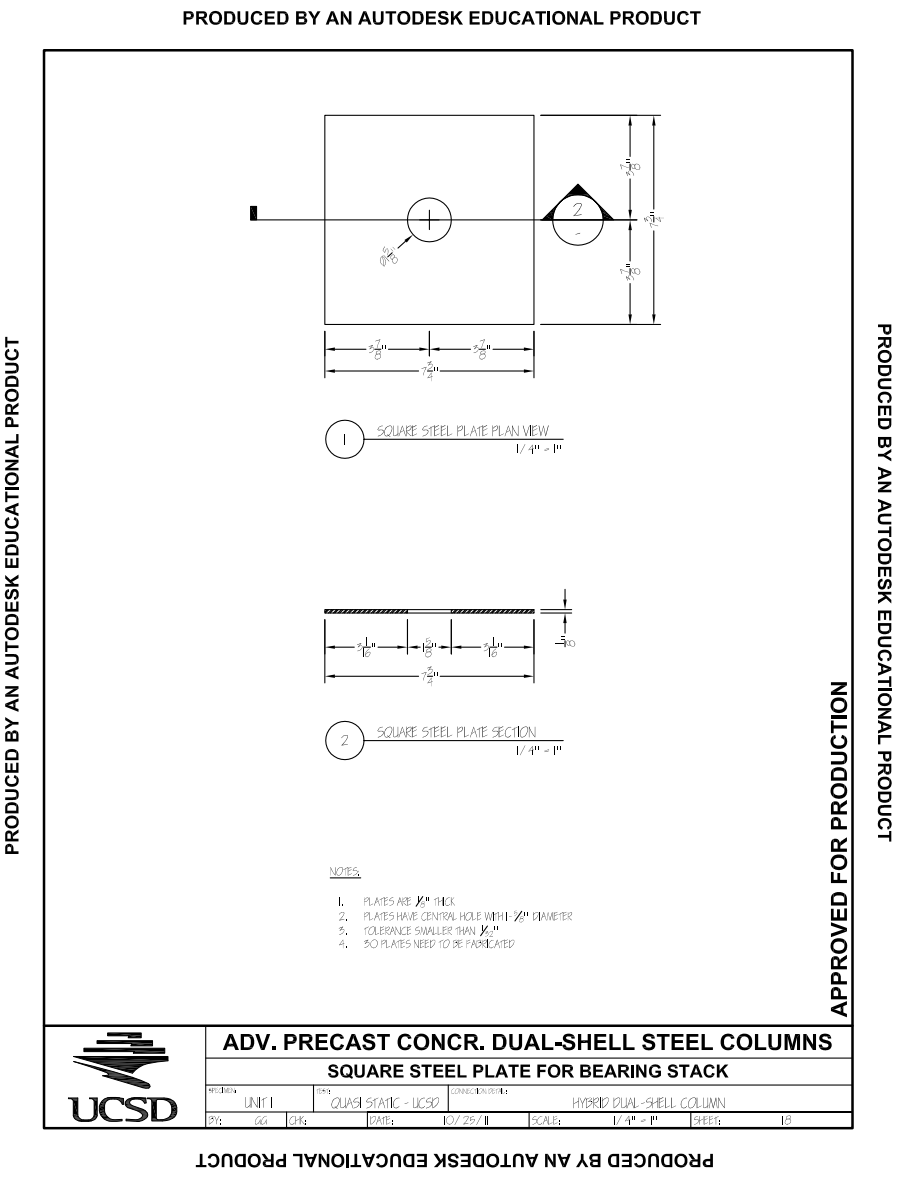

Figure A.18: Precast concrete one story industrial building

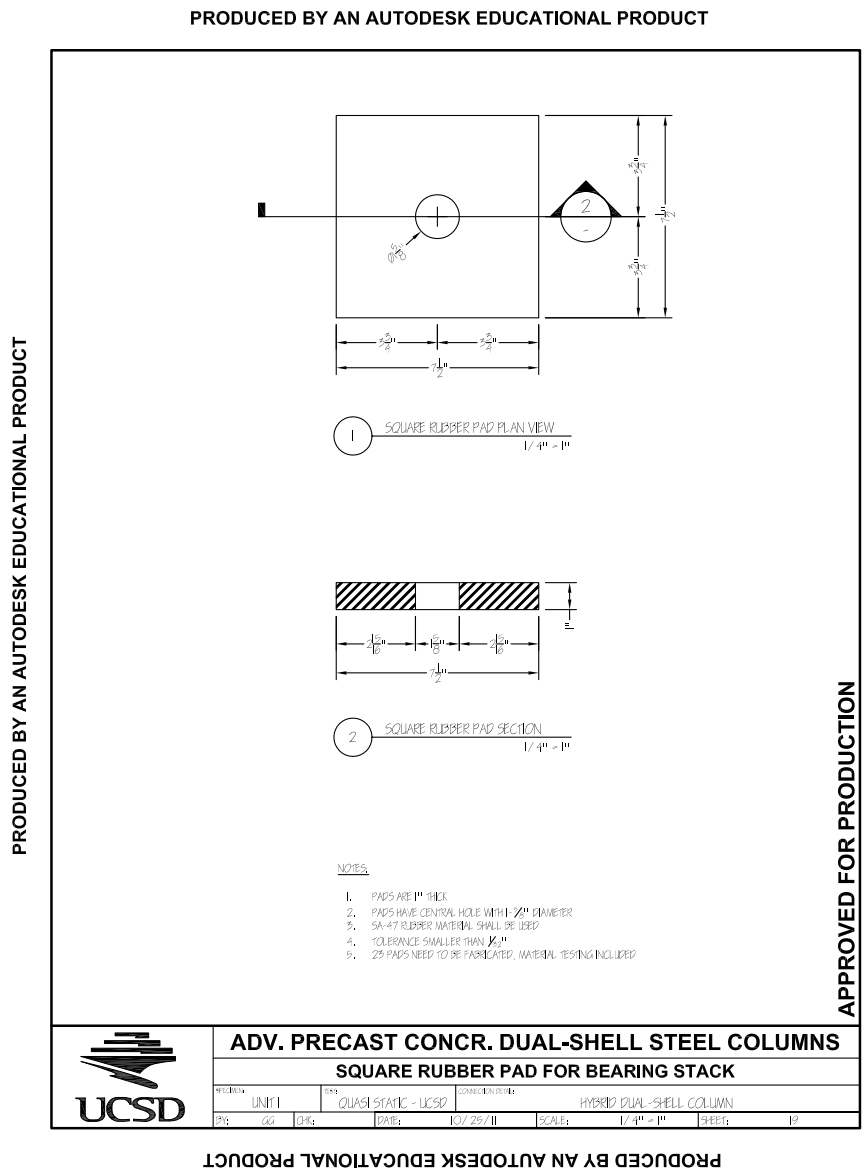

Figure A.19: Precast concrete one story industrial building

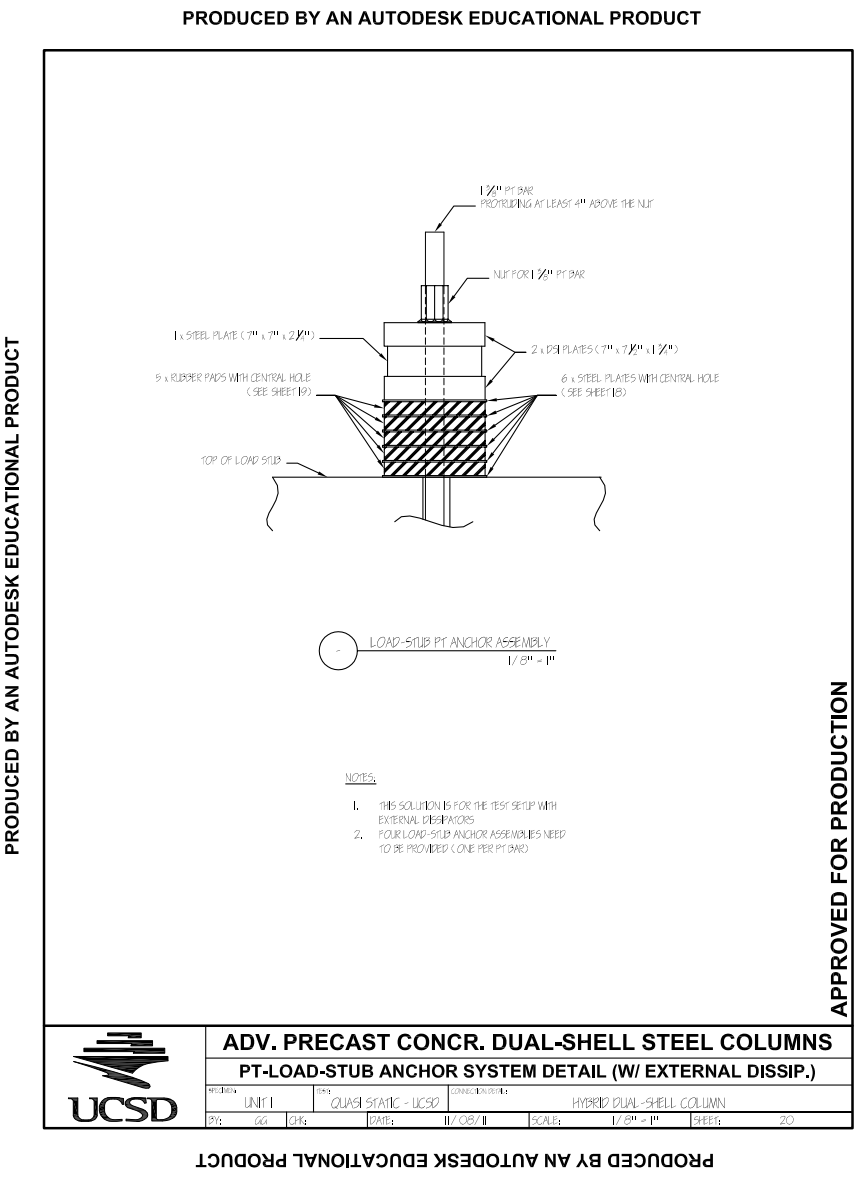

Figure A.20: Precast concrete one story industrial building

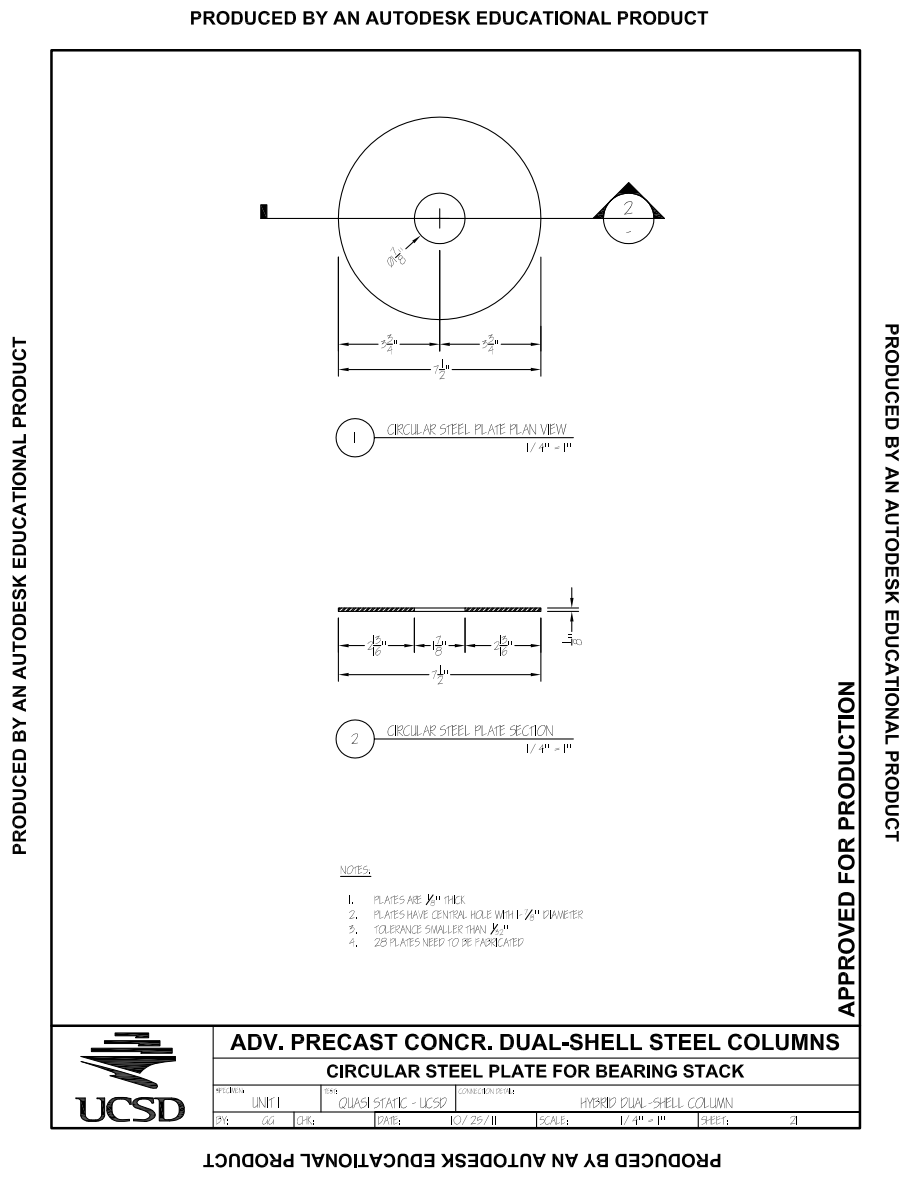

Figure A.21: Precast concrete one story industrial building

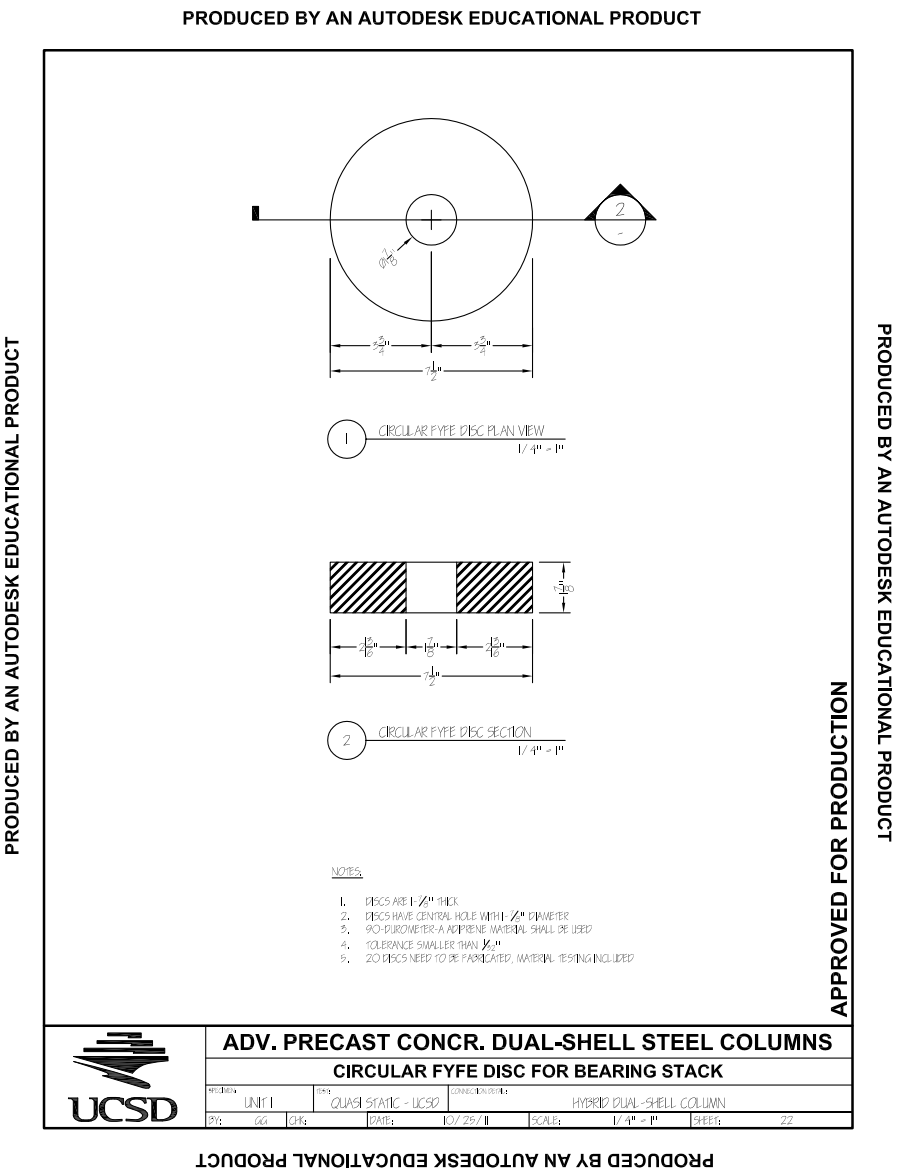

Figure A.22: Precast concrete one story industrial building

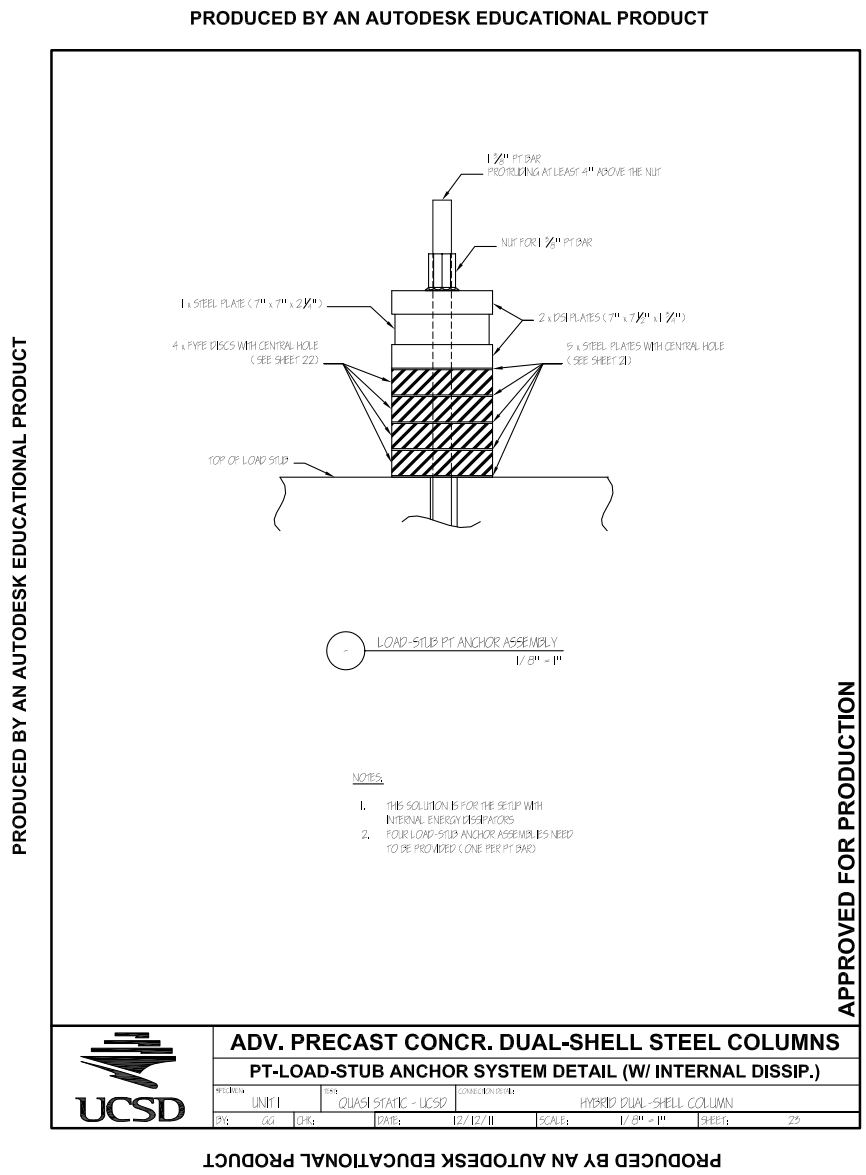

Figure A.23: Precast concrete one story industrial building

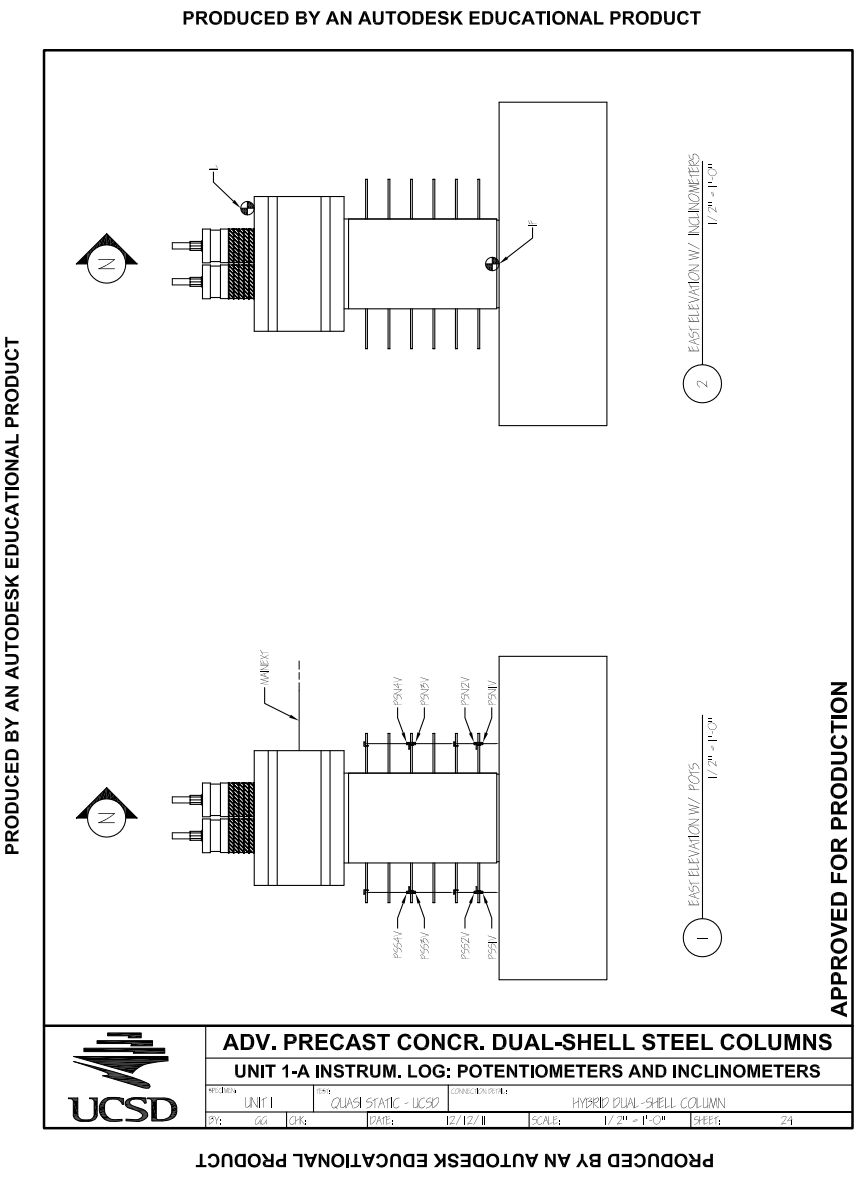

Figure A.24: Precast concrete one story industrial building

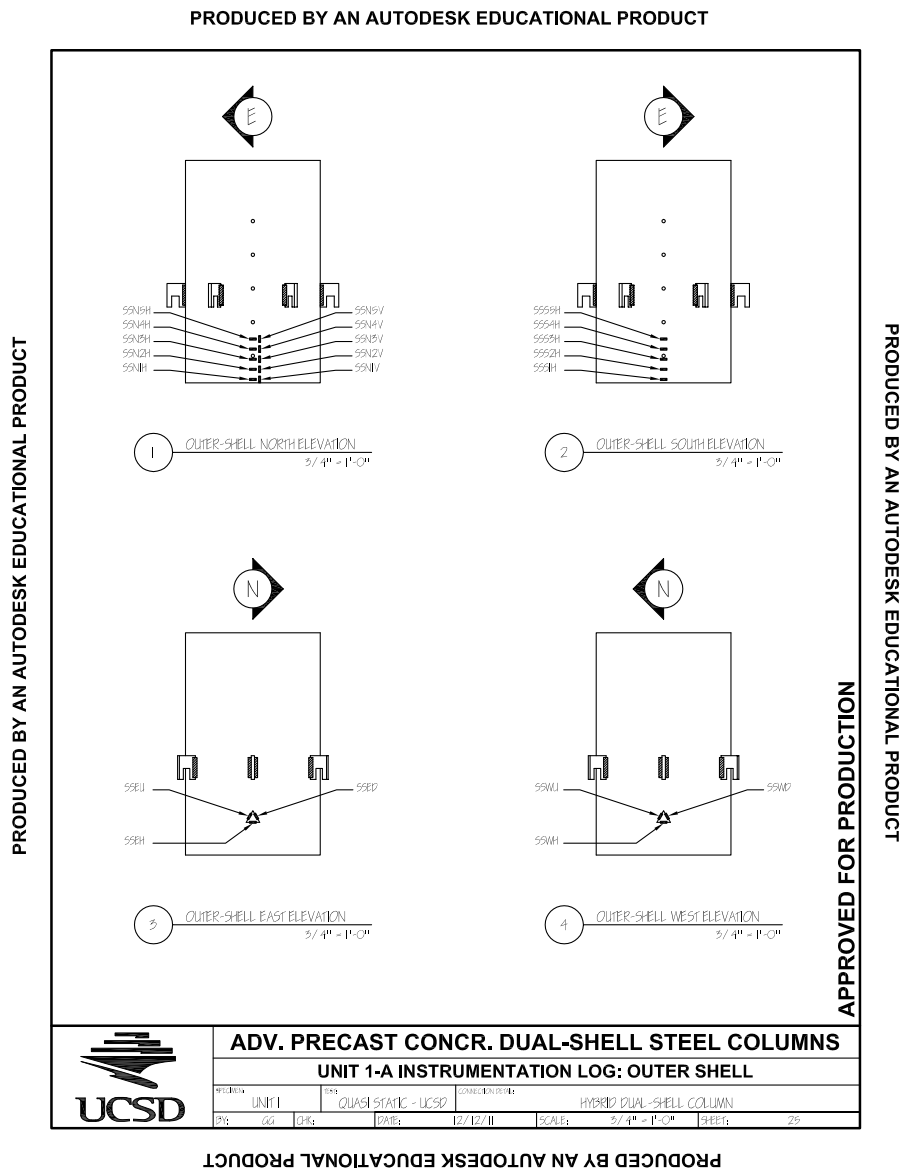

Figure A.25: Precast concrete one story industrial building

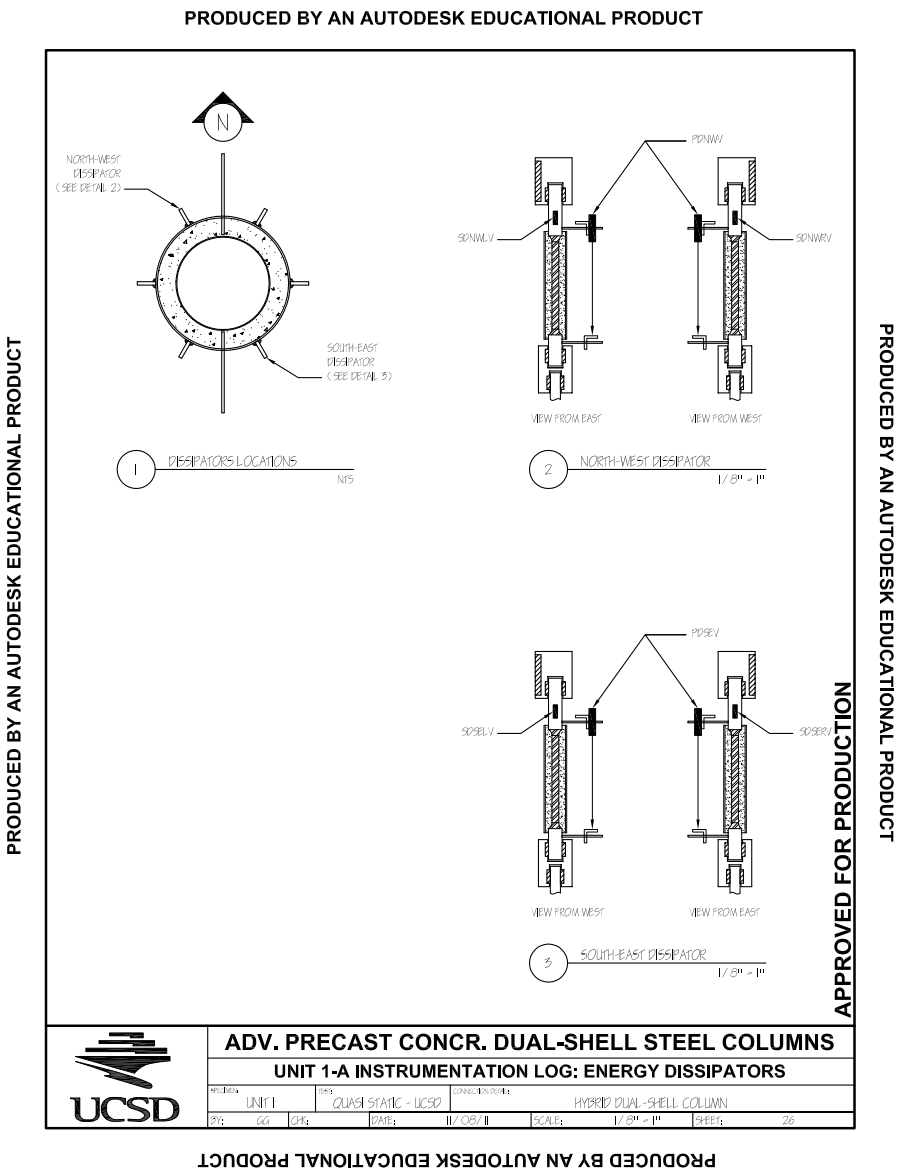

Figure A.26: Precast concrete one story industrial building

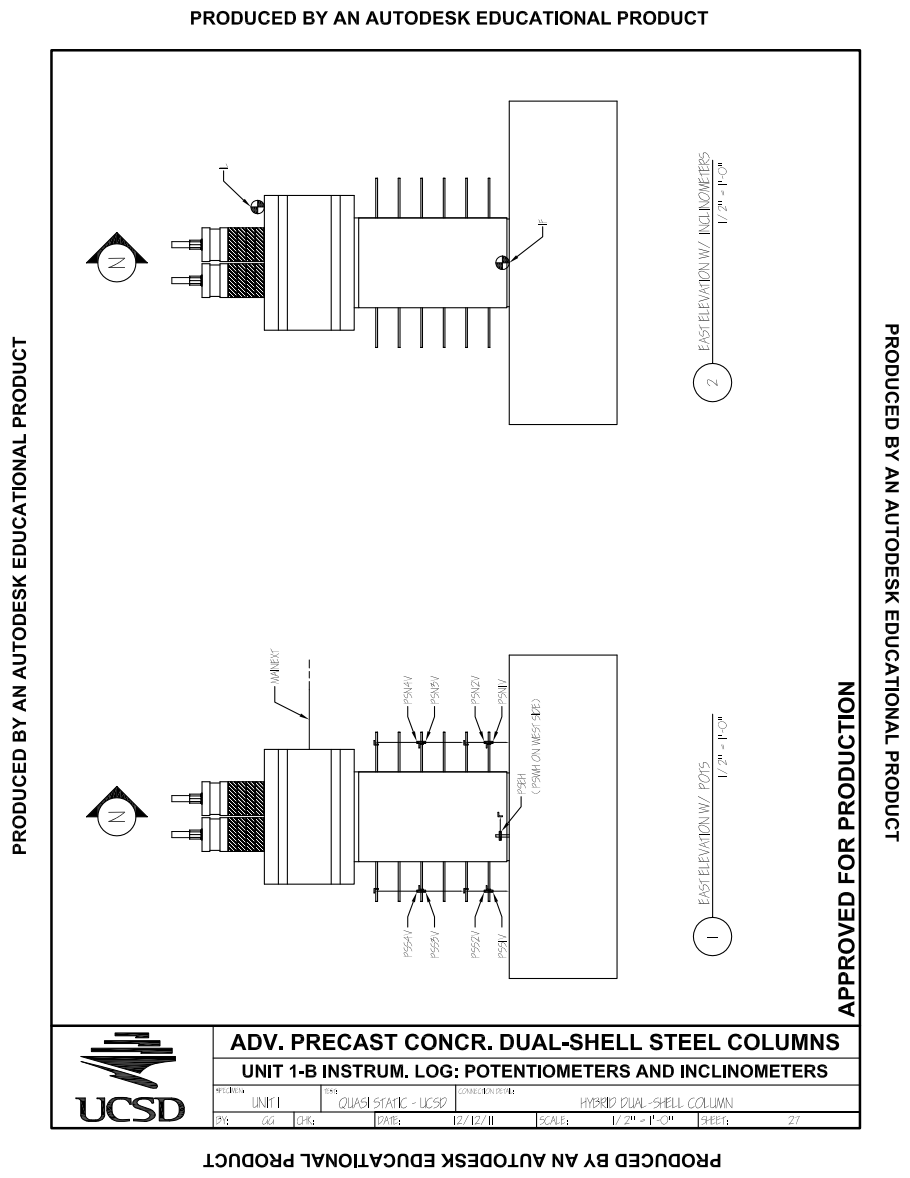

Figure A.27: Precast concrete one story industrial building

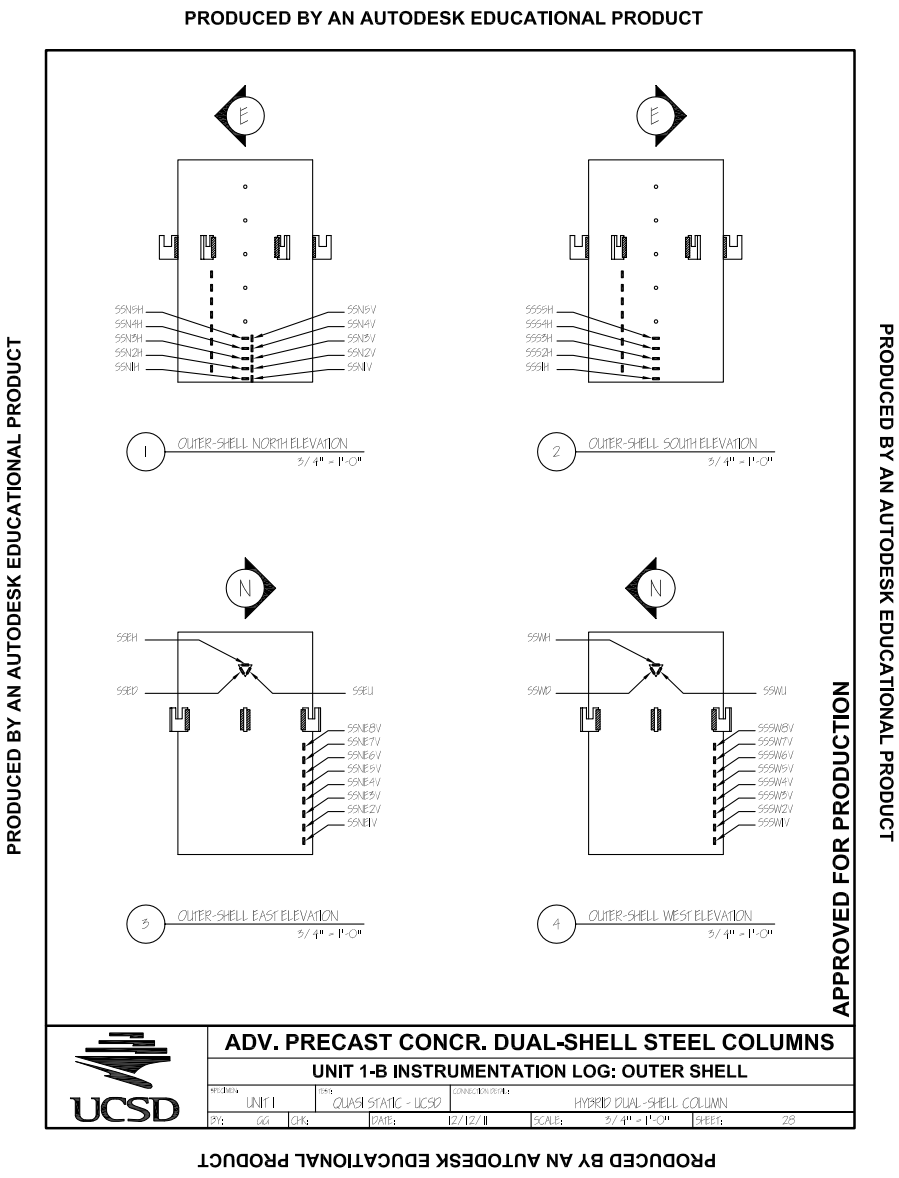

Figure A.28: Precast concrete one story industrial building

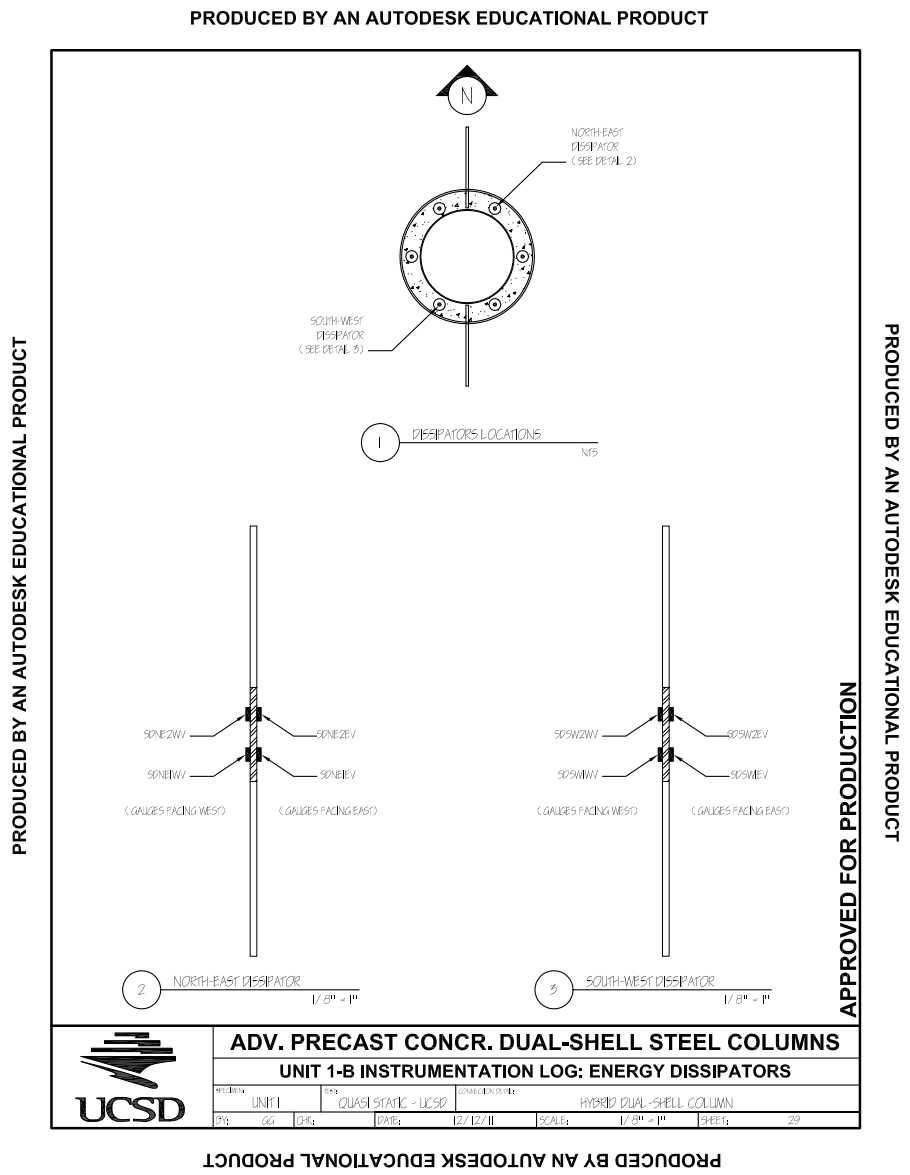

Figure A.29: Precast concrete one story industrial building

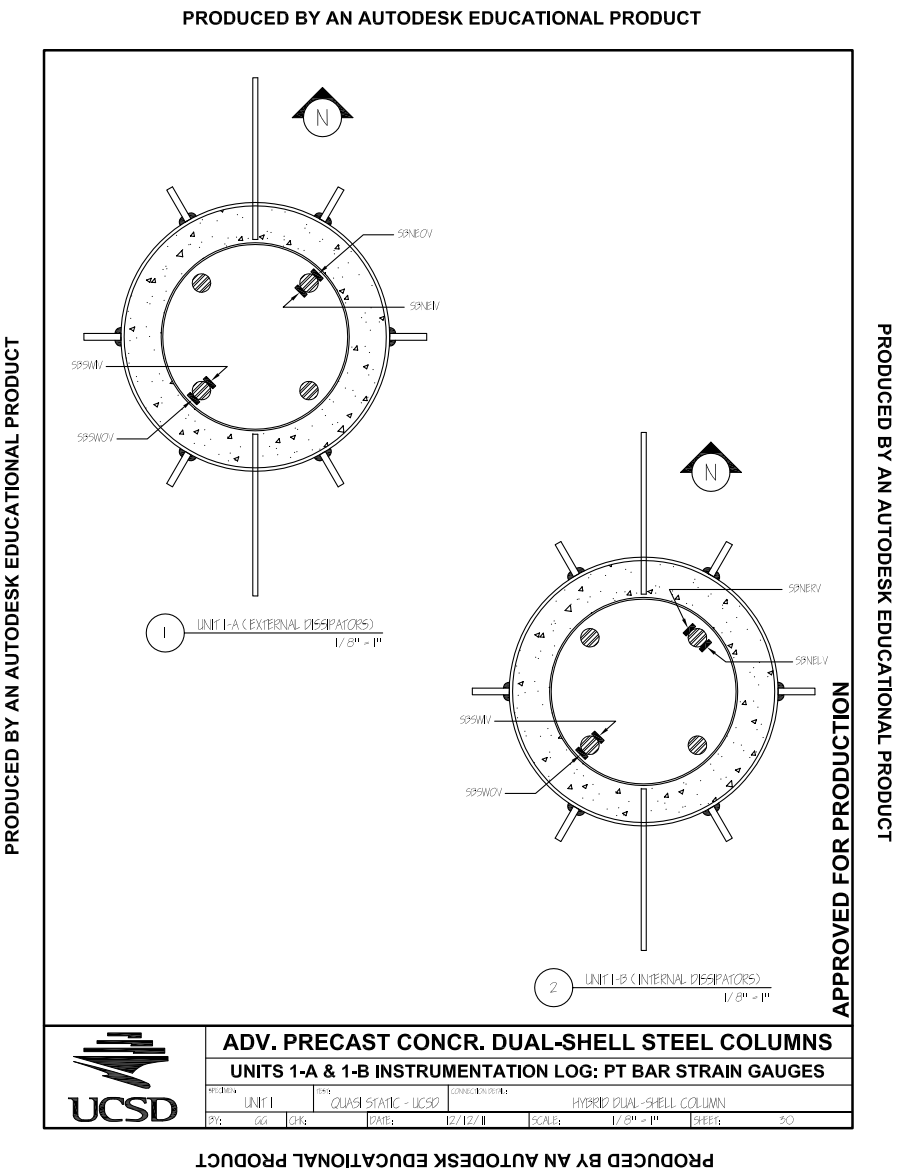

Figure A.30: Precast concrete one story industrial building

Appendix B

Optimal Traditional Design Procedure complies with the NTC 2008 Code

In this appendix is presented a program developed to economically optimize the design of a traditional precast one story building according to the 2008 NTC Italian Code. The procedure, define the construction site and consequently the seismic hazard of the site, allow to know which design, low or high ductility class, is more convenient and for each of them determines the best combination of concrete section and longitudinal and transversal reinforcement. The analysis is based of unit costs of materials and of labor costs function of the concrete volume need. Substantially this procedure follow the steps considered in the previous design and develop a design for each combination of concrete section and longitudinal and transversal reinforcement and the related analysis of the cost. The obtained design can verified the request of the considered code or no. Between the verified design one is less expensive and is the solution. This is developed for both high and low ductility class. Finally the more economic solution between the best solution in high and low ductility class represents the objective of the procedure.

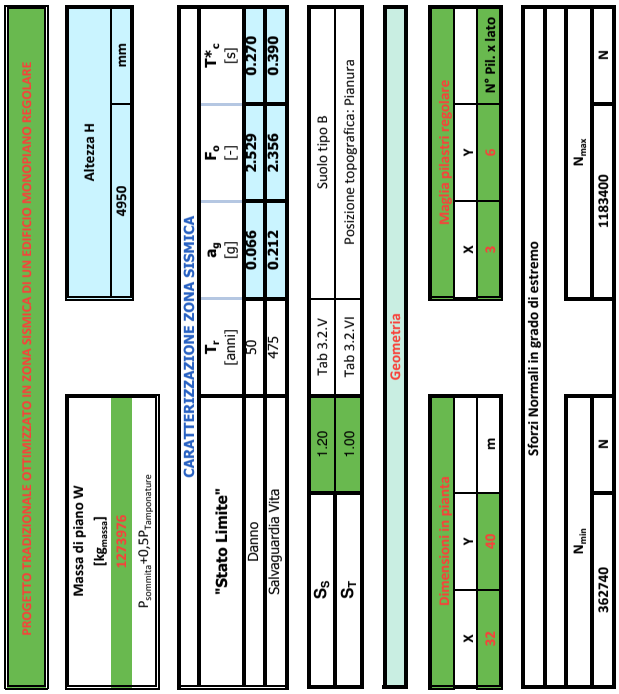

Figure B.1: Precast concrete one story industrial building

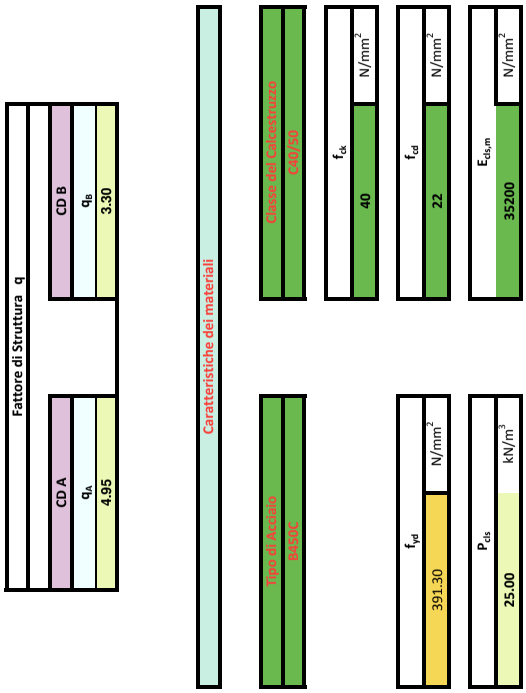

Figure B.2: Precast concrete one story industrial building

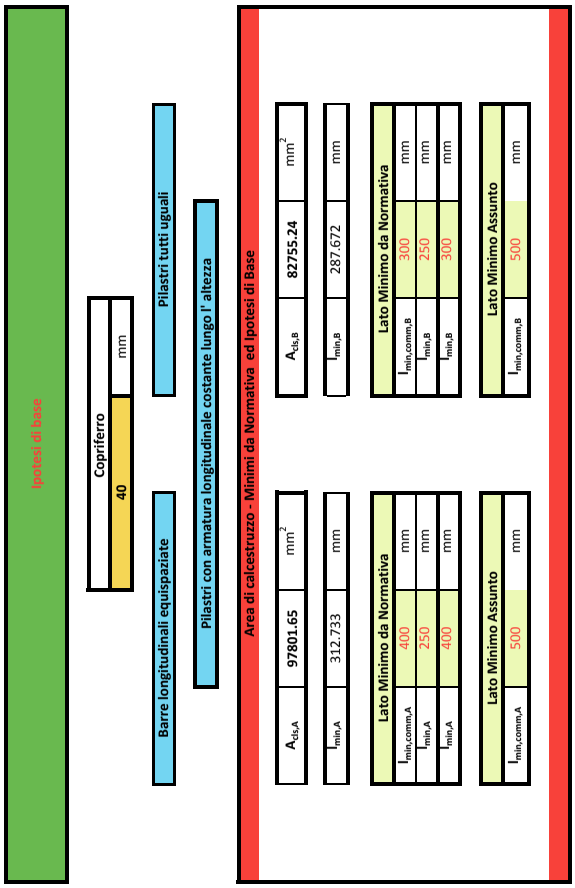

Figure B.3: Precast concrete one story industrial building

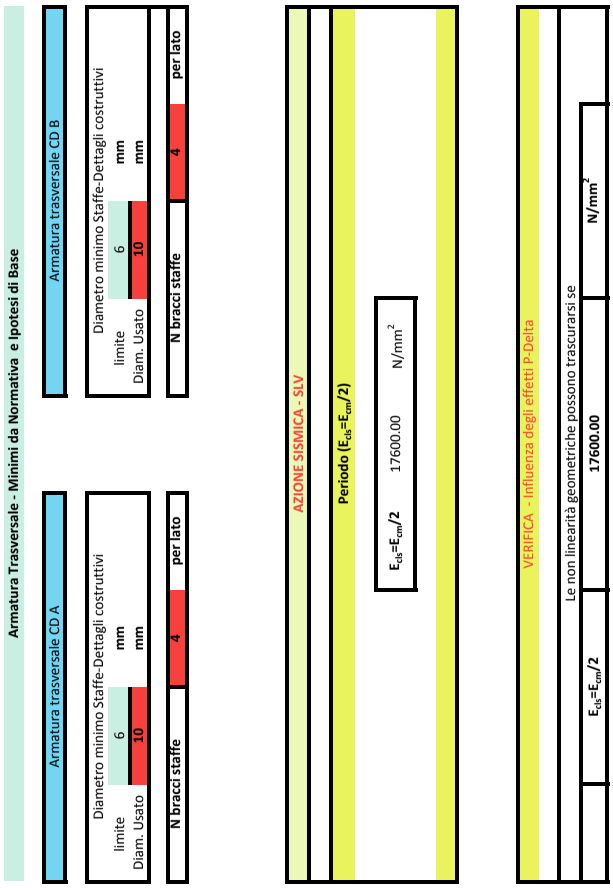

Figure B.4: Precast concrete one story industrial building

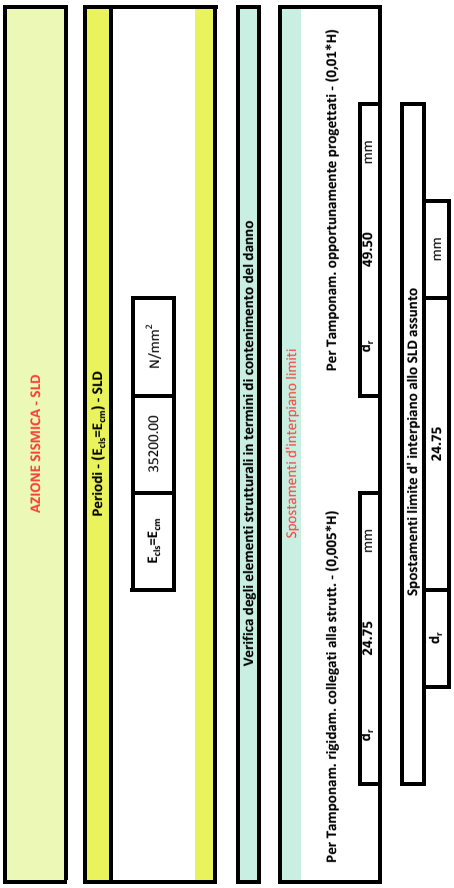

Figure B.5: Precast concrete one story industrial building

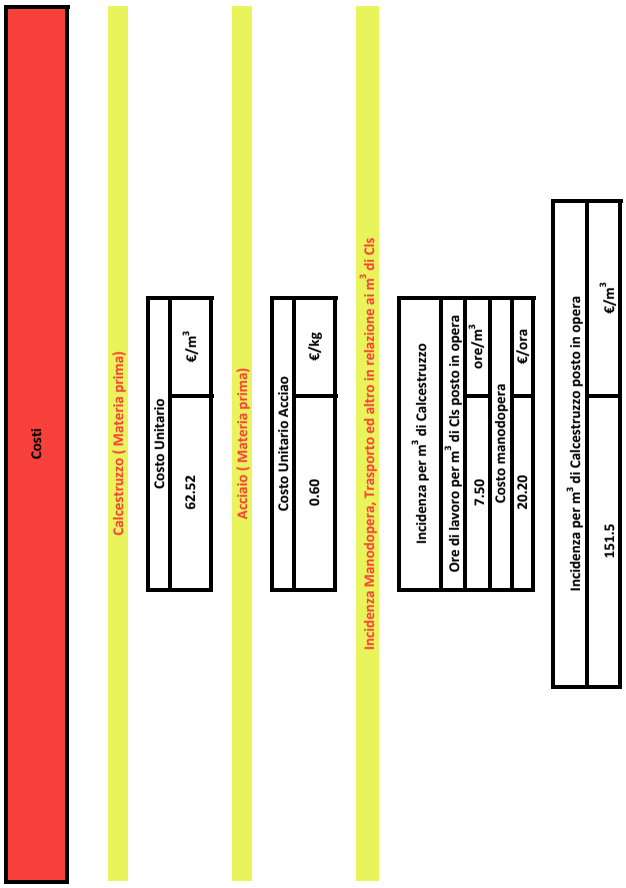

Figure B.6: Precast concrete one story industrial building

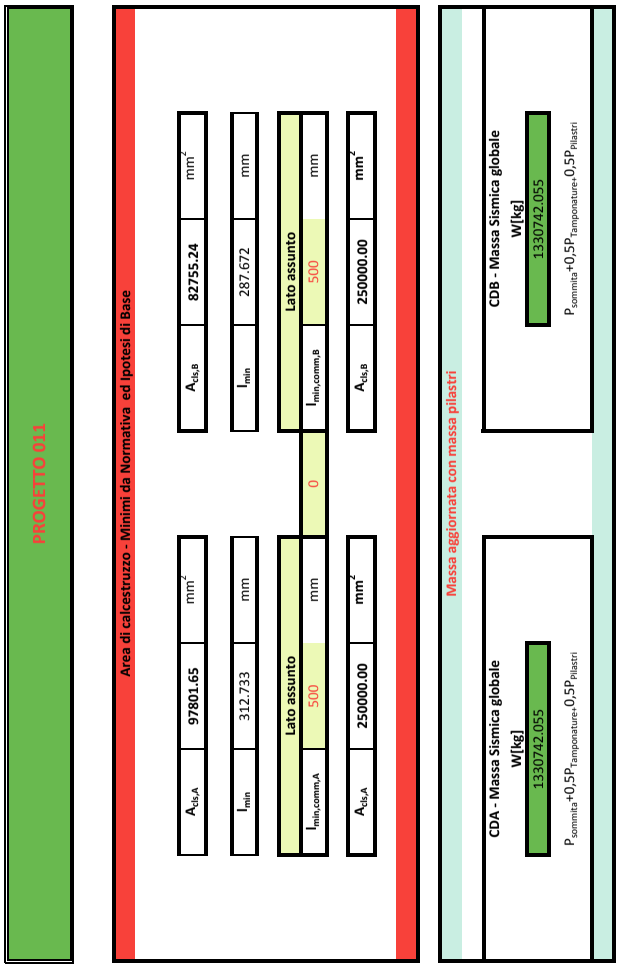

Figure B.7: Precast concrete one story industrial building

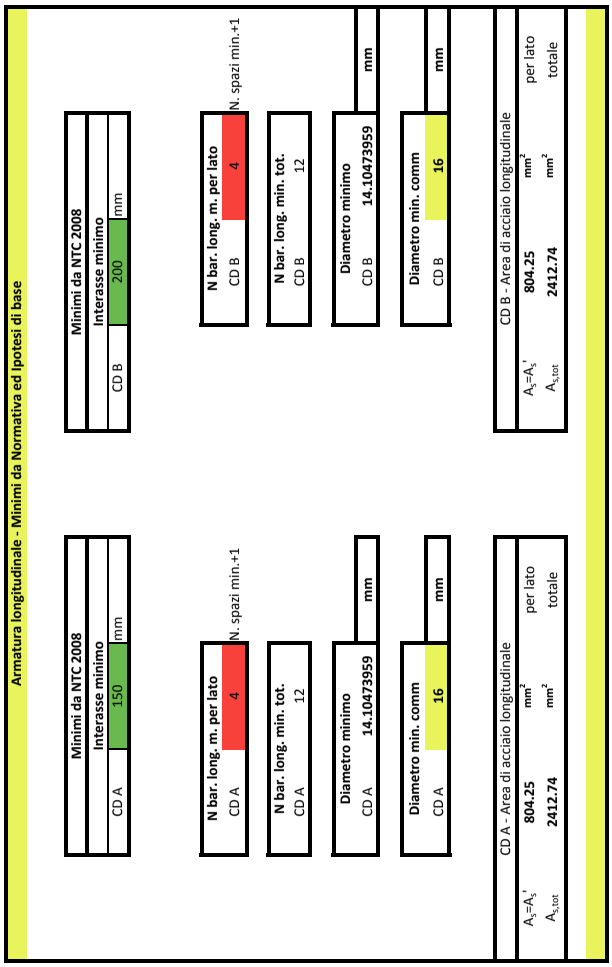

Figure B.8: Precast concrete one story industrial building

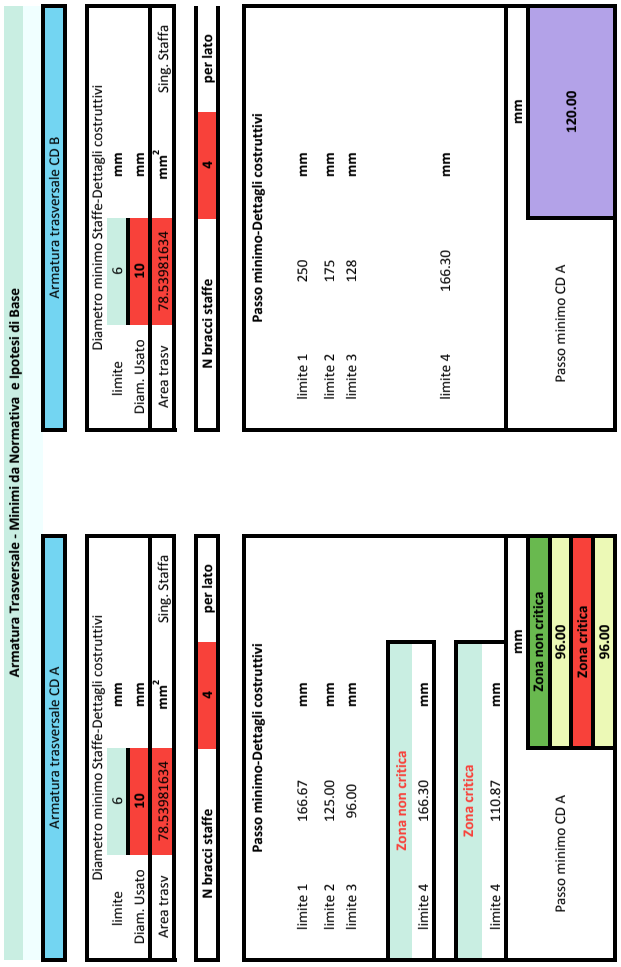

Figure B.9: Precast concrete one story industrial building

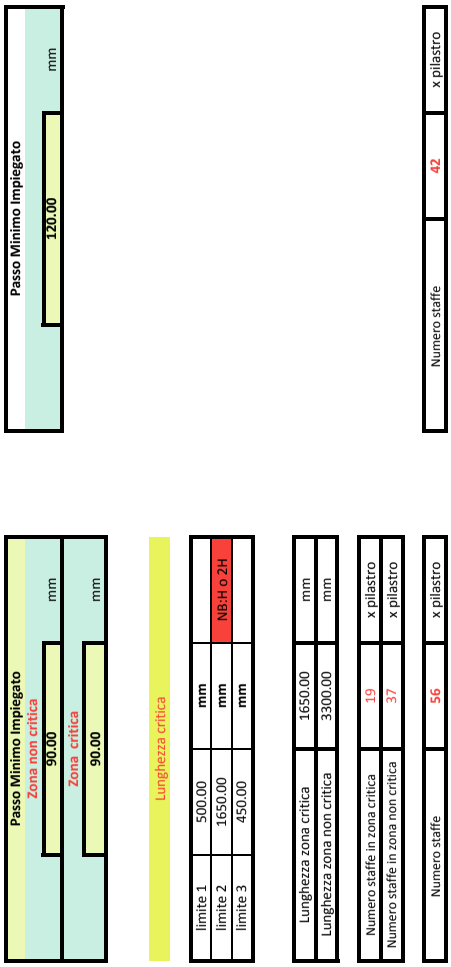

Figure B.10: Precast concrete one story industrial building

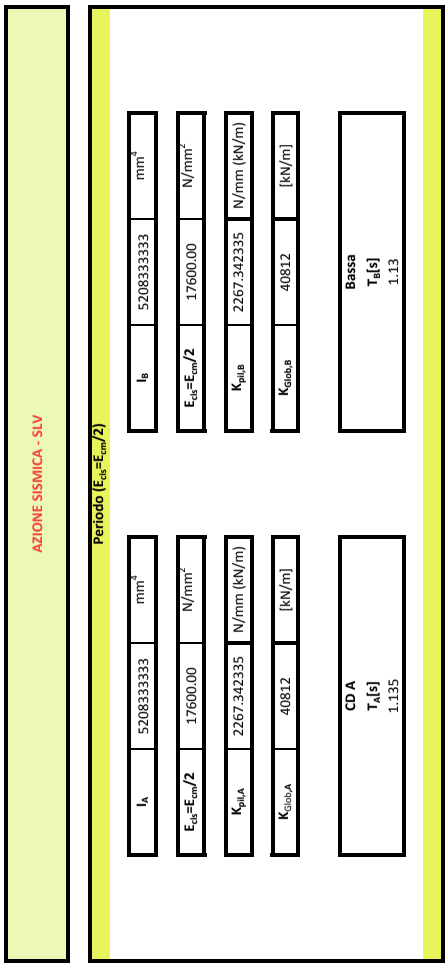

Figure B.11: Precast concrete one story industrial building

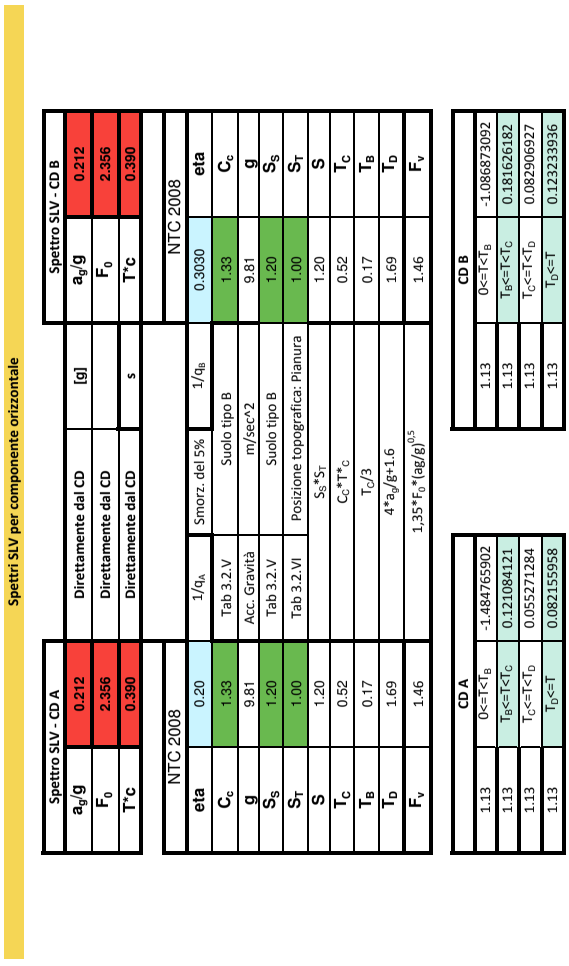

Figure B.12: Precast concrete one story industrial building

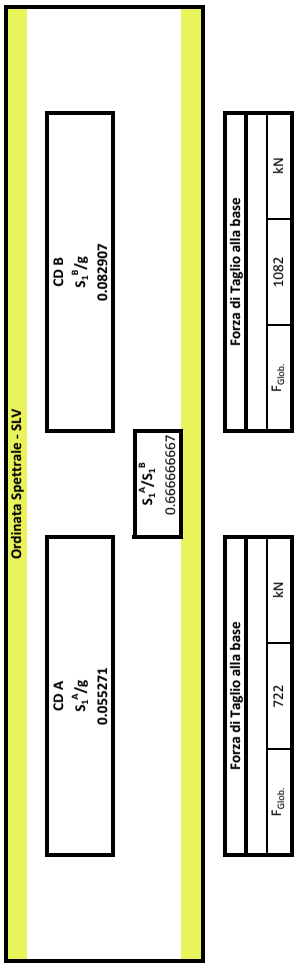

Figure B.13: Precast concrete one story industrial building

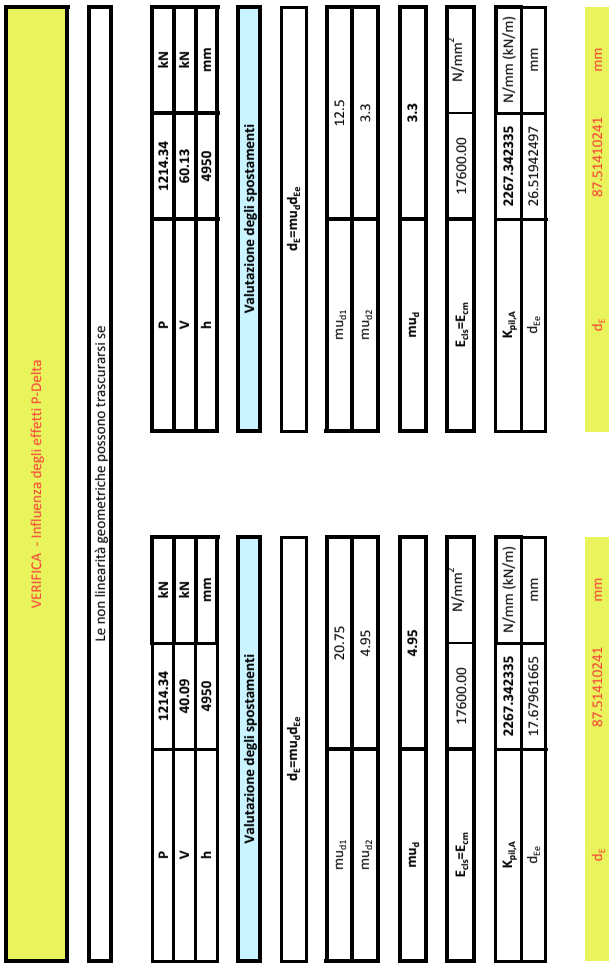

Figure B.14: Precast concrete one story industrial building

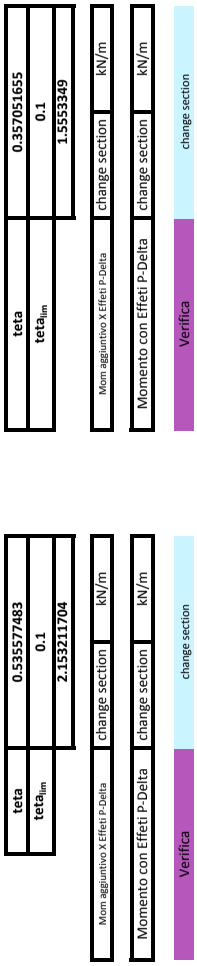

Figure B.15: Precast concrete one story industrial building

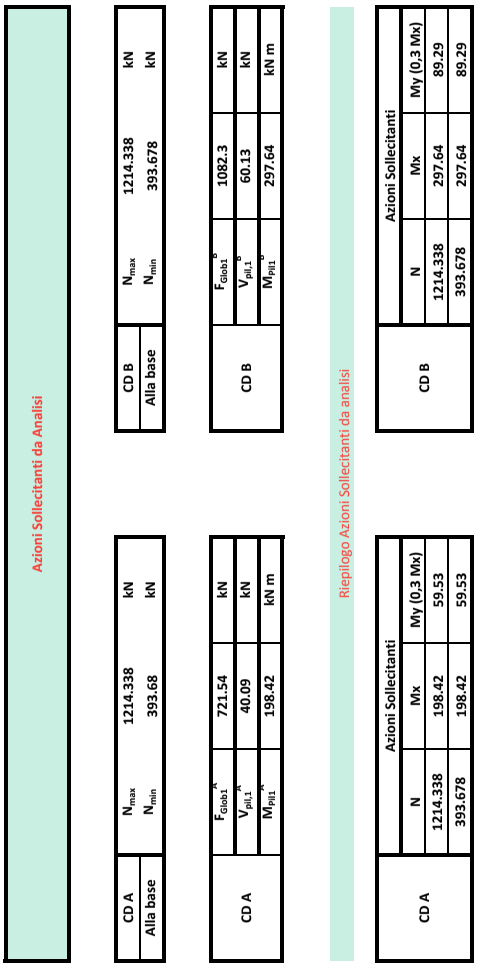

Figure B.16: Precast concrete one story industrial building

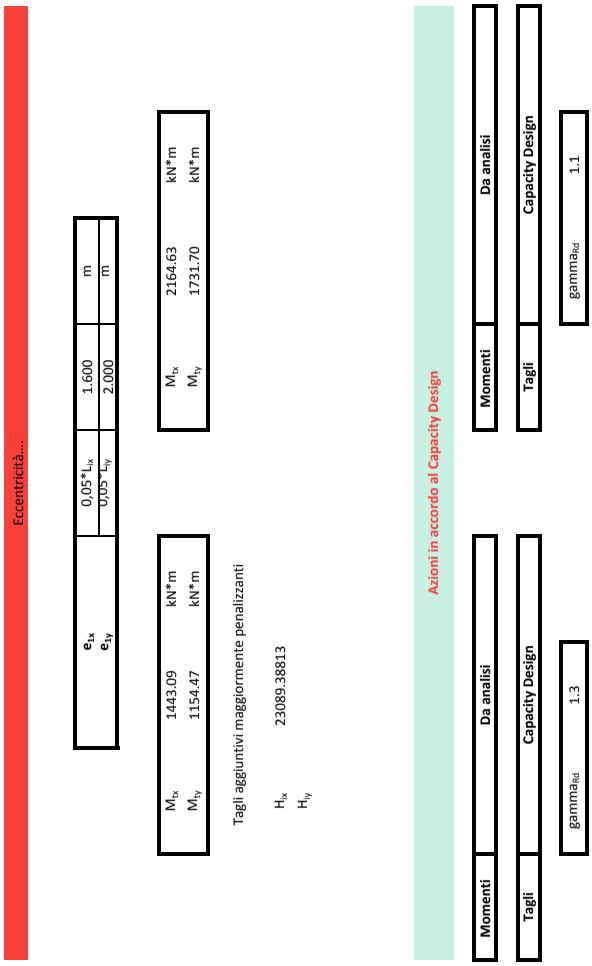

Figure B.17: Precast concrete one story industrial building

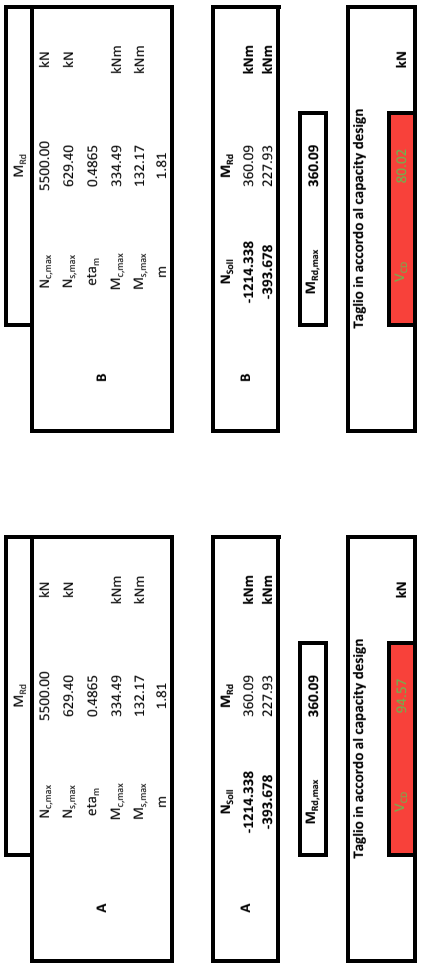

Figure B.18: Precast concrete one story industrial building

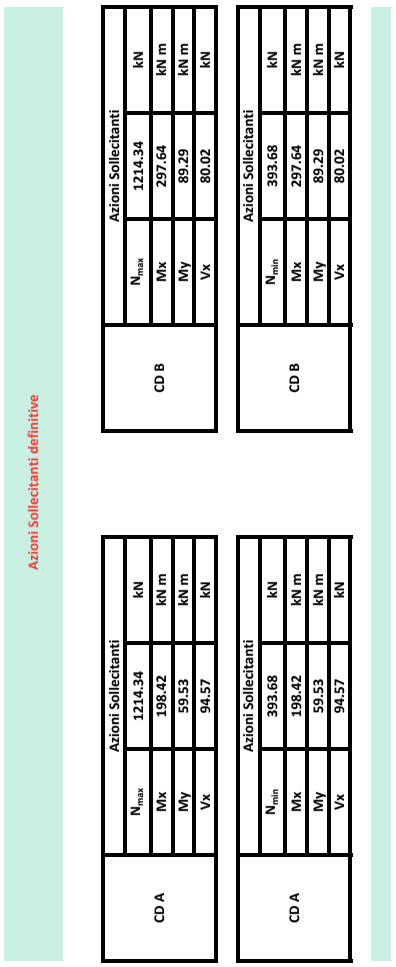

Figure B.19: Precast concrete one story industrial building

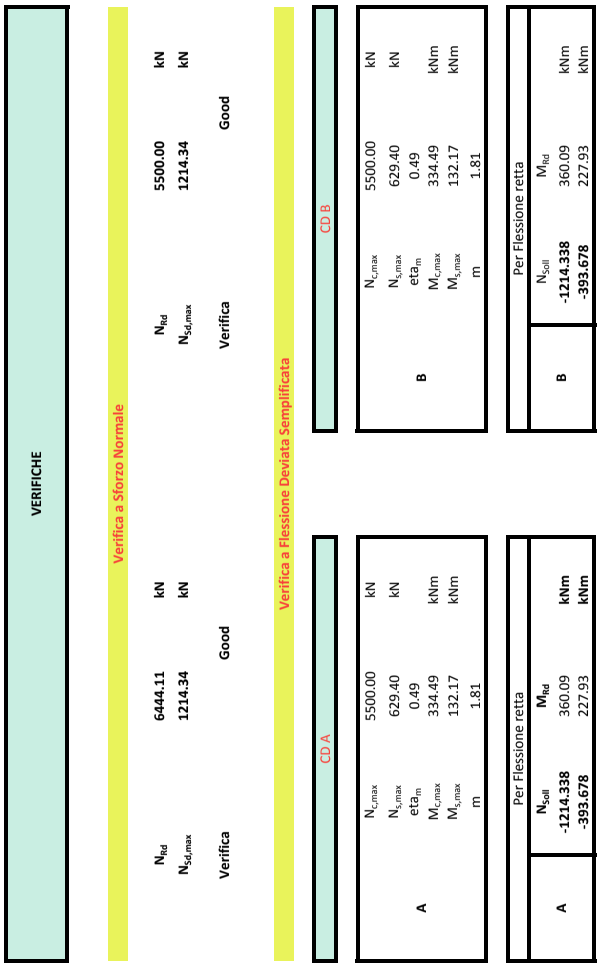

Figure B.20: Precast concrete one story industrial building

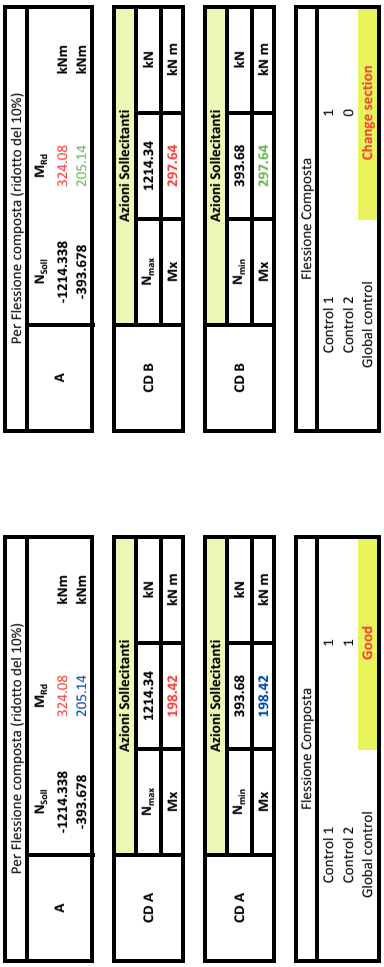

Figure B.21: Precast concrete one story industrial building

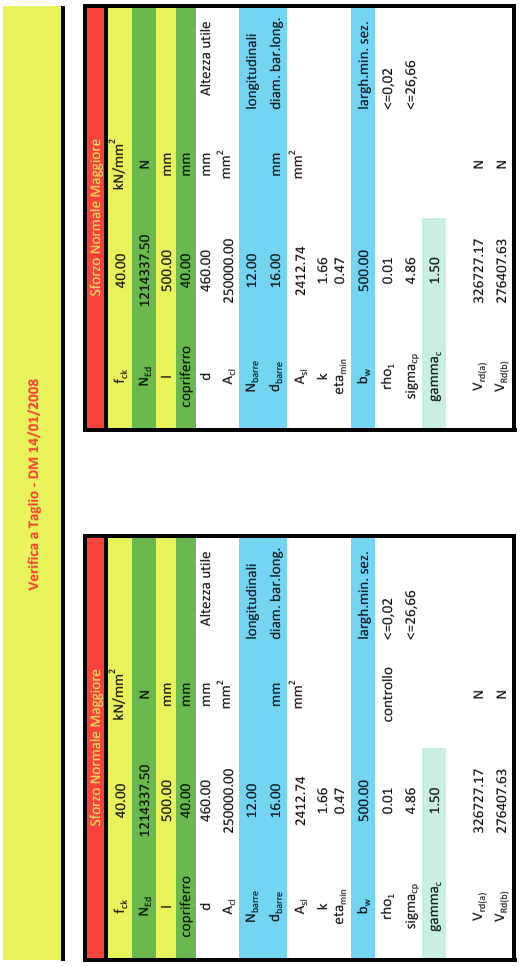

Figure B.22: Precast concrete one story industrial building

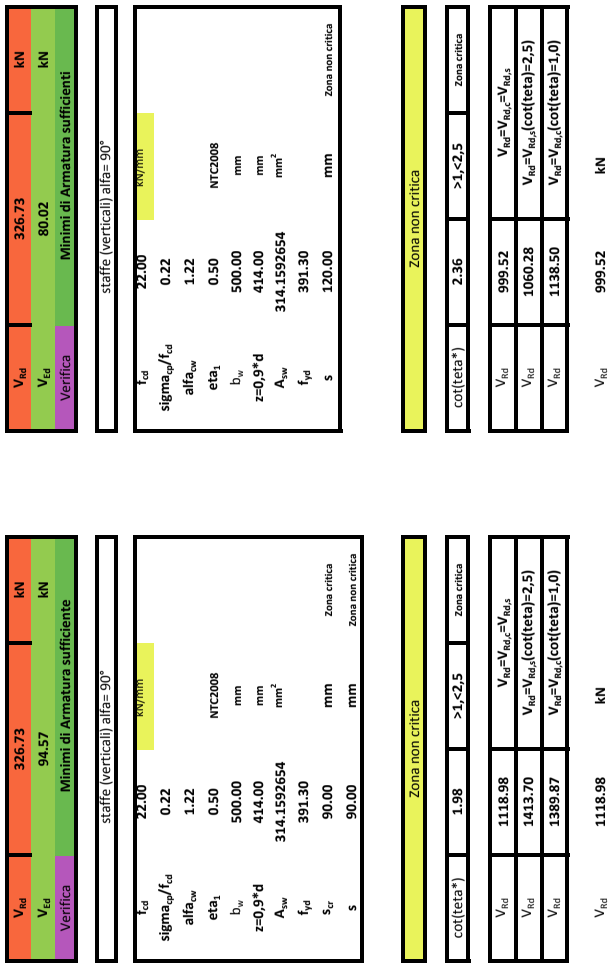

Figure B.23: Precast concrete one story industrial building

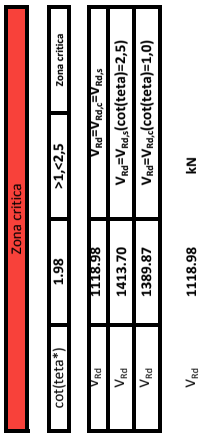

Figure B.24: Precast concrete one story industrial building

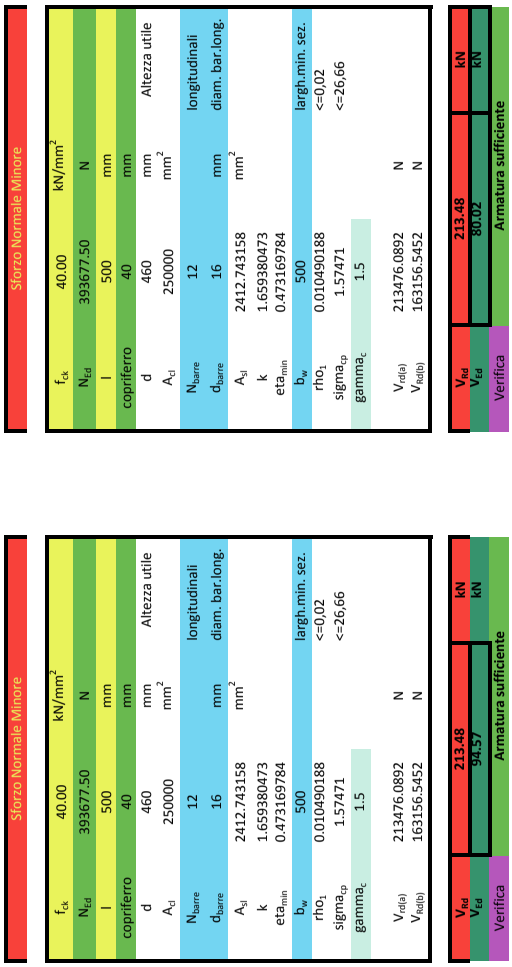

Figure B.25: Precast concrete one story industrial building

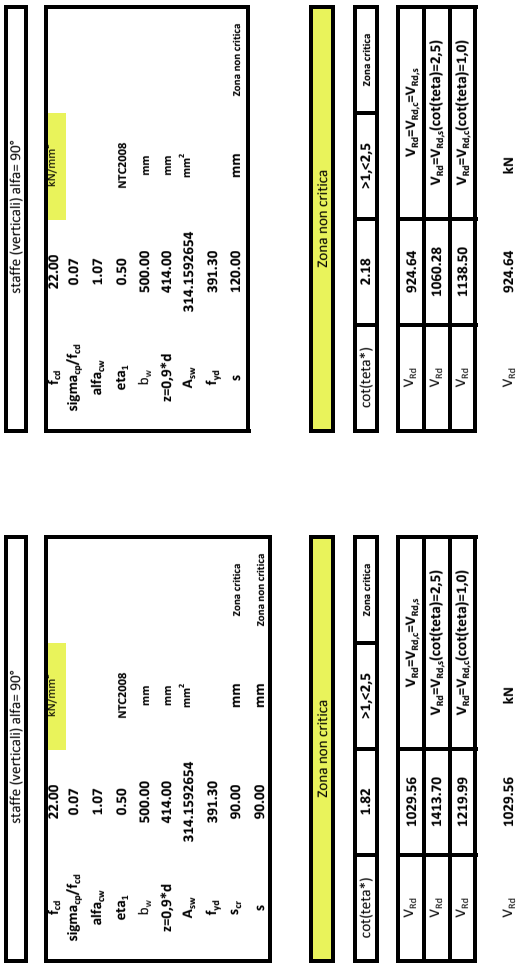

Figure B.26: Precast concrete one story industrial building

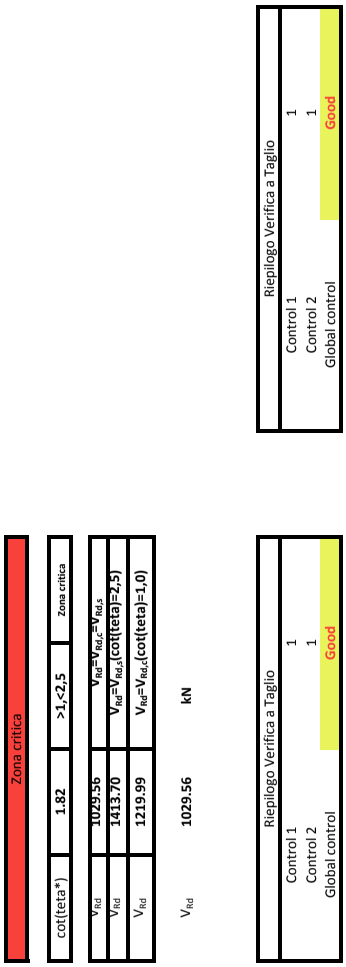

Figure B.27: Precast concrete one story industrial building

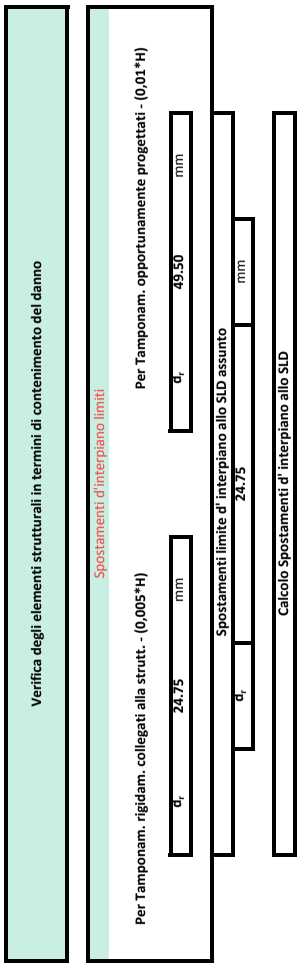

Figure B.28: Precast concrete one story industrial building

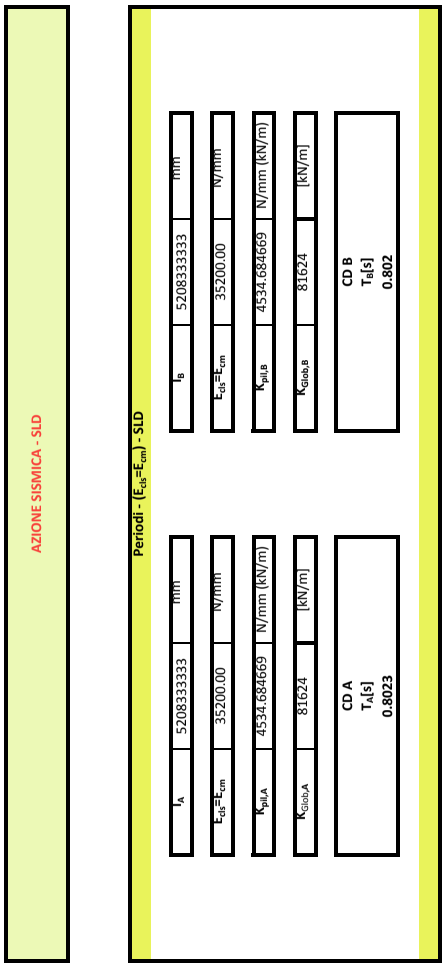

Figure B.29: Precast concrete one story industrial building

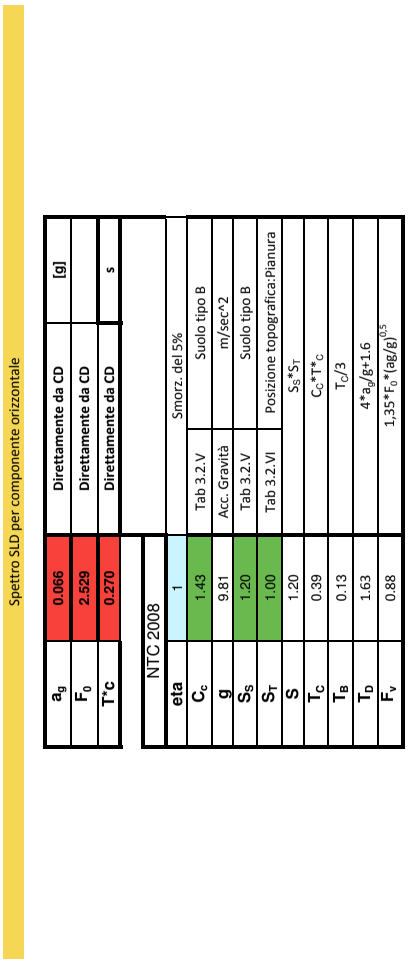

Figure B.30: Precast concrete one story industrial building

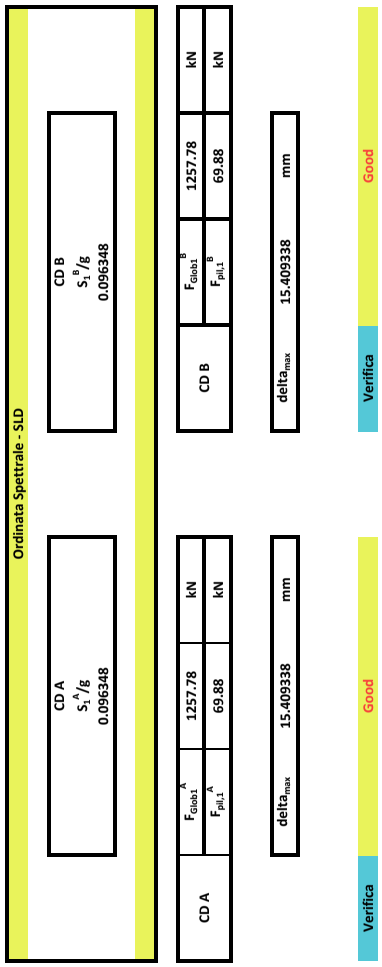

Figure B.31: Precast concrete one story industrial building

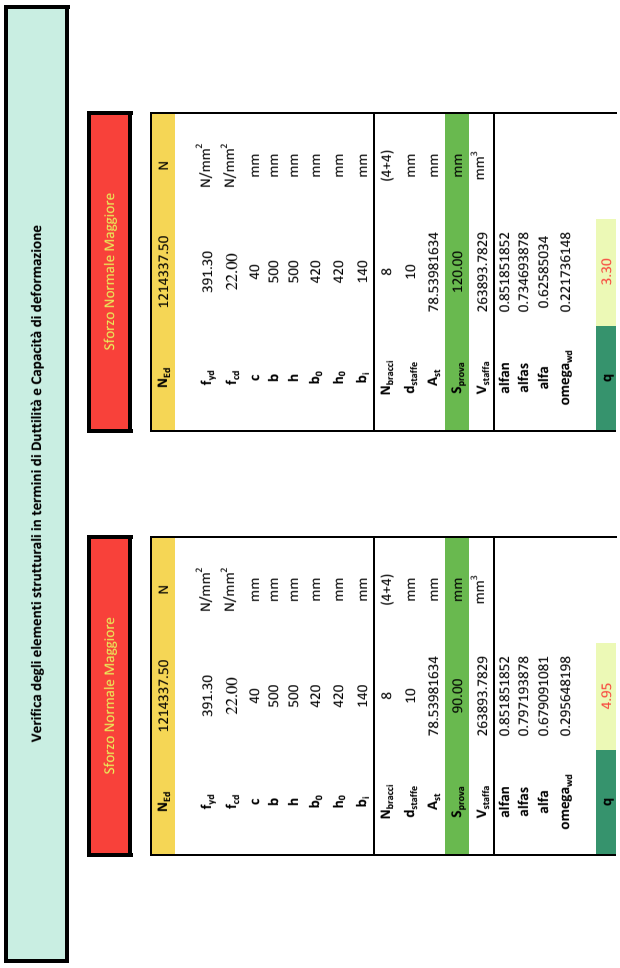

Figure B.32: Precast concrete one story industrial building

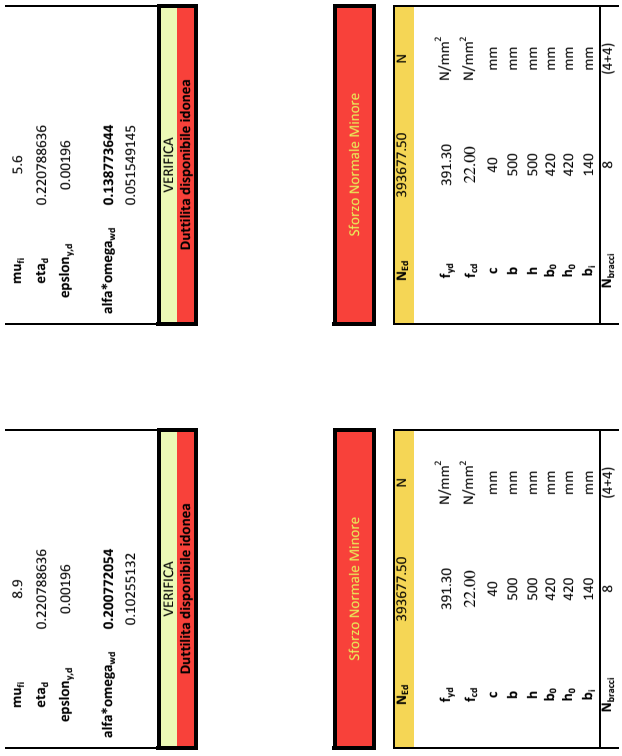

Figure B.33: Precast concrete one story industrial building

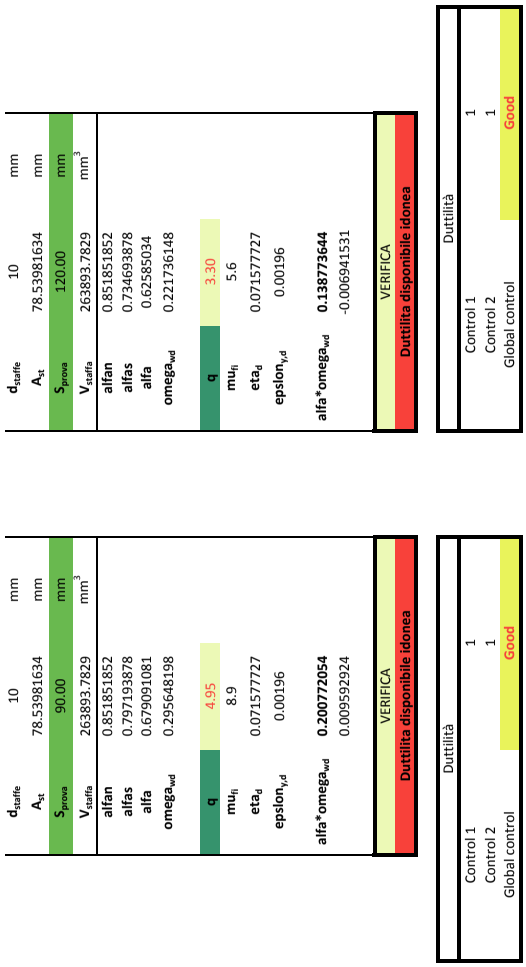

Figure B.34: Precast concrete one story industrial building

Figure B.35: Precast concrete one story industrial building

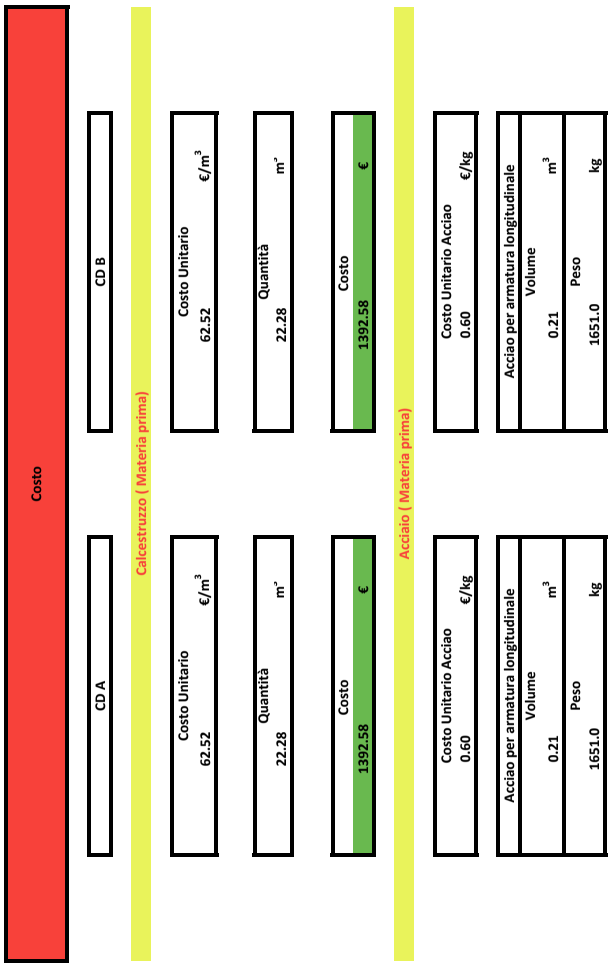

Figure B.36: Precast concrete one story industrial building

Figure B.37: Precast concrete one story industrial building

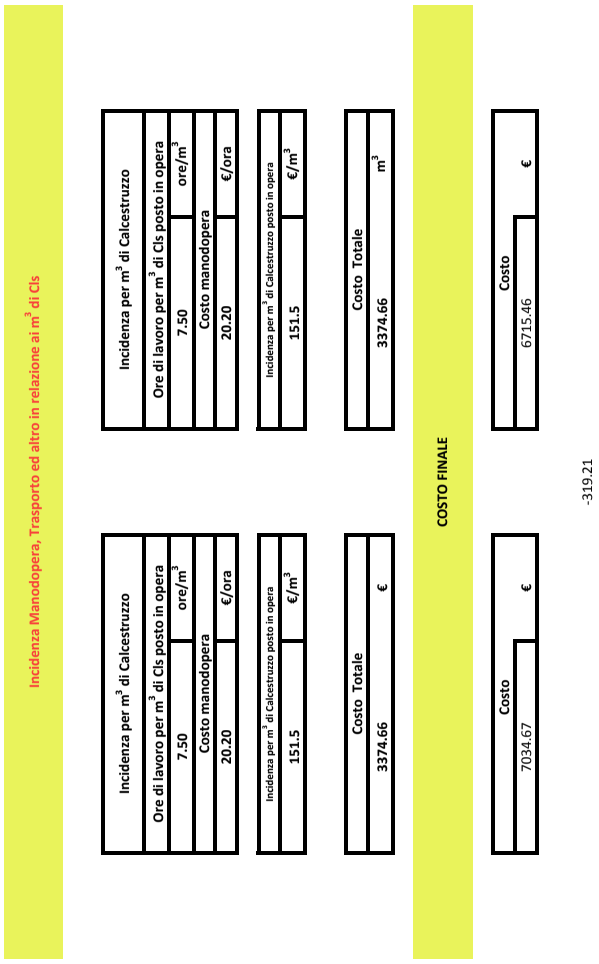

Figure B.38: Precast concrete one story industrial building

Design of Reinforced Concrete Sections

Global Design - CD A

l_{0A}	500	Φ_{bl0}	Φ_{bl1}	Φ_{bl2}	Φ_{bl3}	Φ_{bl4}	Φ_{bl5}	Φ_{bl6}	Φ_{bl7}
		16	18	20	22	24	26	28	30
n_{bl0}	4	No	No	No	No	No	No	No	No
n_{bl1}	5	No	No	No	No	No	No	No	No
n_{bl2}	6	No	No	No	No	No	No	No	No
n_{bl3}	7	No	No	No	No	No	No	No	No
n_{bl4}	8	No	No	No	No	No	No	No	No

l_{0A+1}	600	Φ_{bl0}	Φ_{bl1}	Φ_{bl2}	Φ_{bl3}	Φ_{bl4}	Φ_{bl5}	Φ_{bl6}	Φ_{bl7}
		18	20	22	24	26	28	30	32
n_{bl0}	5	No	Good	Good	Good	Good	Good	Good	Good
n_{bl1}	6	Good	Good	Good	Good	Good	Good	Good	Good
n_{bl2}	7	Good	Good	Good	Good	Good	Good	Good	Good
n_{bl3}	8	Good	Good	Good	Good	Good	Good	Good	Good
n_{bl4}	9	Good	Good	Good	Good	Good	Good	Good	Good

l_{0A+2}	700	Φ_{bl0}	Φ_{bl1}	Φ_{bl2}	Φ_{bl3}	Φ_{bl4}	Φ_{bl5}	Φ_{bl6}	Φ_{bl7}
		20	22	24	26	28	30	32	34
n_{bl0}	6	Good	Good	Good	Good	Good	Good	Good	Good
n_{bl1}	7	Good	Good	Good	Good	Good	Good	Good	Good
n_{bl2}	8	Good	Good	Good	Good	Good	Good	Good	Good
n_{bl3}	9	Good	Good	Good	Good	Good	Good	Good	Good
n_{bl4}	10	Good	Good	Good	Good	Good	Good	Good	Good

Figure B.39: Precast concrete one story industrial building

Design of Reinforced Concrete Sections

Global Design - CD B

l_{OB}	500	Φ_{bl0}	Φ_{bl1}	Φ_{bl2}	Φ_{bl3}	Φ_{bl4}	Φ_{bl5}	Φ_{bl6}	Φ_{bl7}
		16	18	20	22	24	26	28	30
n_{bl0}	4	No	No	No	No	No	No	No	No
n_{bl1}	5	No	No	No	No	No	No	No	No
n_{bl2}	6	No	No	No	No	No	No	No	No
n_{bl3}	7	No	No	No	No	No	No	No	No
n_{bl4}	8	No	No	No	No	No	No	No	No

l_{OB+1}	600	Φ_{bl0}	Φ_{bl1}	Φ_{bl2}	Φ_{bl3}	Φ_{bl4}	Φ_{bl5}	Φ_{bl6}	Φ_{bl7}
		18	20	22	24	26	28	30	32
n_{bl0}	4	No	No	No	No	No	Good	Good	Good
n_{bl1}	5	No	No	No	Good	Good	Good	Good	Good
n_{bl2}	6	No	No	Good	Good	Good	Good	Good	Good
n_{bl3}	7	No	No	Good	Good	Good	Good	Good	Good
n_{bl4}	8	No	Good	Good	Good	Good	Good	Good	Good

l_{OB+2}	700	Φ_{bl0}	Φ_{bl1}	Φ_{bl2}	Φ_{bl3}	Φ_{bl4}	Φ_{bl5}	Φ_{bl6}	Φ_{bl7}
		20	22	24	26	28	30	32	34
n_{bl0}	5	No	No	Good	Good	Good	Good	Good	Good
n_{bl1}	6	No	Good	Good	Good	Good	Good	Good	Good
n_{bl2}	7	Good	Good	Good	Good	Good	Good	Good	Good
n_{bl3}	8	Good	Good	Good	Good	Good	Good	Good	Good
n_{bl4}	9	Good	Good	Good	Good	Good	Good	Good	Good

Figure B.40: Precast concrete one story industrial building

Design of Reinforced Concrete Sections

Costs - CD A

l_{0A}	500	Φ_{bl0}	Φ_{bl1}	Φ_{bl2}	Φ_{bl3}	Φ_{bl4}	Φ_{bl5}	Φ_{bl6}	Φ_{bl7}
		16	18	20	22	24	26	28	30
n_{bl0}	4	N.P.	N.P.	N.P.	N.P.	N.P.	N.P.	N.P.	N.P.
n_{bl1}	5	N.P.	N.P.	N.P.	N.P.	N.P.	N.P.	N.P.	N.P.
n_{bl2}	6	N.P.	N.P.	N.P.	N.P.	N.P.	N.P.	N.P.	N.P.
n_{bl3}	7	N.P.	N.P.	N.P.	N.P.	N.P.	N.P.	N.P.	N.P.
n_{bl4}	8	N.P.	N.P.	N.P.	N.P.	N.P.	N.P.	N.P.	N.P.
		Nessuna soluzione soddisfa i requisiti di progetto							

l_{0A+1}	600	Φ_{bl0}	Φ_{bl1}	Φ_{bl2}	Φ_{bl3}	Φ_{bl4}	Φ_{bl5}	Φ_{bl6}	Φ_{bl7}
		18	20	22	24	26	28	30	32
n_{bl0}	5	N.P.	10269	10703	11177	11693	12250	12849	13489
n_{bl1}	6	10459	10785	11327	11920	12565	13262	14010	14810
n_{bl2}	7	10877	11301	11951	12663	13437	14273	15171	16130
n_{bl3}	8	11295	11817	12576	13406	14309	15284	16332	17451
n_{bl4}	9	11713	12333	13200	14149	15181	16295	17492	18772
		10269							

l_{0A+2}	700	Φ_{bl0}	Φ_{bl1}	Φ_{bl2}	Φ_{bl3}	Φ_{bl4}	Φ_{bl5}	Φ_{bl6}	Φ_{bl7}
		20	22	24	26	28	30	32	34
n_{bl0}	6	13679	14221	14814	15459	16156	16904	17703	18555
n_{bl1}	7	14195	14845	15557	16331	17167	18065	19024	20046
n_{bl2}	8	14711	15469	16300	17203	18178	19225	20345	21537
n_{bl3}	9	15227	16094	17043	18075	19189	20386	21666	23028
n_{bl4}	10	15743	16718	17786	18947	20201	21547	22987	24519
		13679							

Figure B.41: Precast concrete one story industrial building

Design of Reinforced Concrete Sections

Costs - CD B

l_{OB}	500	Φ_{bl0}	Φ_{bl1}	Φ_{bl2}	Φ_{bl3}	Φ_{bl4}	Φ_{bl5}	Φ_{bl6}	Φ_{bl7}
		16	18	20	22	24	26	28	30
n_{bl0}	4	N.P.	N.P.	N.P.	N.P.	N.P.	N.P.	N.P.	N.P.
n_{bl1}	5	N.P.	N.P.	N.P.	N.P.	N.P.	N.P.	N.P.	N.P.
n_{bl2}	6	N.P.	N.P.	N.P.	N.P.	N.P.	N.P.	N.P.	N.P.
n_{bl3}	7	N.P.	N.P.	N.P.	N.P.	N.P.	N.P.	N.P.	N.P.
n_{bl4}	8	N.P.	N.P.	N.P.	N.P.	N.P.	N.P.	N.P.	N.P.
		Nessuna soluzione soddisfa i requisiti di progetto							

l_{OB+1}	600	Φ_{bl0}	Φ_{bl1}	Φ_{bl2}	Φ_{bl3}	Φ_{bl4}	Φ_{bl5}	Φ_{bl6}	Φ_{bl7}
		18	20	22	24	26	28	30	32
n_{bl0}	4	N.P.	N.P.	N.P.	N.P.	N.P.	10966	11414	11894
n_{bl1}	5	N.P.	N.P.	N.P.	10904	11420	11977	12575	13215
n_{bl2}	6	N.P.	N.P.	11053	11647	12292	12988	13736	14536
n_{bl3}	7	N.P.	N.P.	11678	12390	13164	13999	14897	15857
n_{bl4}	8	N.P.	11543	12302	13133	14035	15011	16058	17178
		10904							

l_{OB+2}	700	Φ_{bl0}	Φ_{bl1}	Φ_{bl2}	Φ_{bl3}	Φ_{bl4}	Φ_{bl5}	Φ_{bl6}	Φ_{bl7}
		20	22	24	26	28	30	32	34
n_{bl0}	5	N.P.	N.P.	13784	14300	14857	15456	16095	16776
n_{bl1}	6	N.P.	13934	14527	15172	15868	16616	17416	18267
n_{bl2}	7	13908	14558	15270	16044	16880	17777	18737	19759
n_{bl3}	8	14424	15182	16013	16916	17891	18938	20058	21250
n_{bl4}	9	14940	15806	16756	17788	18902	20099	21379	22741
		13784							

Figure B.42: Precast concrete one story industrial building

Optimal Design of a precast one-story insustrial building

Optimal Design - CD A

I_{0A}	500	Φ_{bl0}	Φ_{bl1}	Φ_{bl2}	Φ_{bl3}	Φ_{bl4}	Φ_{bl5}	Φ_{bl6}	Φ_{bl7}
		16	18	20	22	24	26	28	30
n_{bl0}	4								
n_{bl1}	5								
n_{bl2}	6								
n_{bl3}	7								
n_{bl4}	8								

I_{0A+1}	600	Φ_{bl0}	Φ_{bl1}	Φ_{bl2}	Φ_{bl3}	Φ_{bl4}	Φ_{bl5}	Φ_{bl6}	Φ_{bl7}
		18	20	22	24	26	28	30	32
n_{bl0}	5								
n_{bl1}	6		10269						
n_{bl2}	7								
n_{bl3}	8								
n_{bl4}	9								

I_{0A+2}	700	Φ_{bl0}	Φ_{bl1}	Φ_{bl2}	Φ_{bl3}	Φ_{bl4}	Φ_{bl5}	Φ_{bl6}	Φ_{bl7}
		20	22	24	26	28	30	32	34
n_{bl0}	6								
n_{bl1}	7								
n_{bl2}	8								
n_{bl3}	9								
n_{bl4}	10								

Figure B.43: Precast concrete one story industrial building

Optimal Design of a precast one-story insustrial building

Optimal Design - CD B

l_{OB}	500	Φ_{bl0}	Φ_{bl1}	Φ_{bl2}	Φ_{bl3}	Φ_{bl4}	Φ_{bl5}	Φ_{bl6}	Φ_{bl7}
		16	18	20	22	24	26	28	30
n_{bl0}	4								
n_{bl1}	5								
n_{bl2}	6								
n_{bl3}	7								
n_{bl4}	8								

l_{OB+1}	600	Φ_{bl0}	Φ_{bl1}	Φ_{bl2}	Φ_{bl3}	Φ_{bl4}	Φ_{bl5}	Φ_{bl6}	Φ_{bl7}
		18	20	22	24	26	28	30	32
n_{bl0}	4								
n_{bl1}	5								
n_{bl2}	6				10904				
n_{bl3}	7								
n_{bl4}	8								

l_{OB+2}	700	Φ_{bl0}	Φ_{bl1}	Φ_{bl2}	Φ_{bl3}	Φ_{bl4}	Φ_{bl5}	Φ_{bl6}	Φ_{bl7}
		20	22	24	26	28	30	32	34
n_{bl0}	5								
n_{bl1}	6								
n_{bl2}	7								
n_{bl3}	8								
n_{bl4}	9								

Figure B.44: Precast concrete one story industrial building

Bibliography

[1] Anil K. Chopra. *Dynamics of Structures: Theory and Applications to Earthquake Engineering*. Prentice Hall, 2000.

[2] Ray W. Clough and Joseph Penzien. *Dynamics of Sructures*. McGraw-Hill, 1993.

[3] J.L. Humar. *Dynamics of Sructures*. Prentice Hall, 1990.

[4] R. Park and T. Paulay. *Reinforced Concrete Structures*. John Wiley & Sons, 1975.

[5] James K. Wight and James G. MacGregor. *Reinforced Concrete*. Prentice Hall, 2009.